Oxidant, Particle and Photochemical Processes in the Atmosphere above a Southeast Asian Rain Forest.

Simon Malpass

PhD

University of York

Environment Department

December 2011

A major source of radical species in the atmosphere is through the oxidation reactions of biogenic volatile organic compounds that are emitted from vegetation. Tropical rainforests are responsible for over half of such biogenic species that are emitted into the atmosphere and the local, regional and global impacts of their subsequent oxidation mechanisms are currently not well understood. Further, with tropical forests being removed to make way for new land uses (such as oil palm plantations), the subsequent change in the quantity and type of biogenic emissions into the atmosphere could have far-reaching impacts.

The Oxidant, Particle and Photochemical Processes (OP3) field campaign conducted at Bukit Atur in Malaysian Borneo in 2008, aimed to address some of the uncertainties that currently exist surrounding the impact of forested regions on atmospheric chemistry. In particular, this project aims to predict the concentrations of OH, HO_2 and RO_2 radicals at Bukit Atur in Borneo during April and July of 2008, using a near-explicit photochemical box model with 15,000 reactions and 7,200 species. The model is constrained using observations made during the two experimental campaigns, and used to compare with radical measurements.

In agreement with previous studies involving tropical forests, it was found that the standard model based on the Master Chemical Mechanism (MCM v3.1) underestimates the observed concentrations of OH by a factor of 0.5 on average and overestimates HO_2 concentrations by a factor of 2. The results for RO_2 were mixed with some days over-predicted and some under-predicted. The implementation of some new theoretically derived reaction pathways without the isoprene degradation scheme improved the predicted OH concentration (modelled:measured ratio improved to 0.3), but did not improve the HO_2 estimation (modelled: measured ratio changed to 2.5). It was found that the modelled: measured discrepancy was better on days when the VOC:NOX ratio was lower, suggesting that even with the updated isoprene scheme, days with high biogenic concentrations are not well represented in the model. A rate of production analysis also confirmed that days where modelled OH agreed best with measurements were dominated more by NOX reactions, and less by for instance, Criegee biradical reactions, the latter an indication of biogenic influence.

It seems likely from the results from this study (and others) that the suggested alterations to the isoprene chemistry scheme are incomplete, as they do not completely remove the model discrepancy in the predicted OH and HO_2 concentrations. This work provides a useful contribution to the understanding of radical species production in tropical forests and provides more data in this area of research. However, this project also identifies that more research is required, particularly in the elucidation of isoprene degradation in the atmosphere, but also with issues such as the dry deposition rates of key intermediates in the model mechanism.

Table of Contents

1. Introduction……..24
1.1 Overview……...24
1.2 Radical Chemistry……...25
1.3 Previous Studies……...28
1.4 Updated Isoprene Degradation……...33
1.5 Structure of Thesis……...36
2. Experimental…….37
2.1 Modelling……...37
2.1.1 Introduction……...37
2.1.2 Box Models…….38
2.1.3 Master Chemical Mechanism……...38
2.1.4 Model Construction……...43
2.1.5 Input Data……..50
2.2 Measurements……...55
2.2.1 Introduction……...55
2.2.2 OH and HO_2 Measurements. Detection Limits and Accuracy……56
2.2.3 Measurement of $\Sigma RO_2 + HO_2$……..57
2.3 Site Description…….58
3. Model Validation……...61
3.1 Introduction……..61
3.2 Model Run Time……...65
3.3 Frequency of Constrained Data……..67
3.4 Photolysis Rate…….70
3.5 Dry Deposition Velocities…….79
3.6 HO_2 Uptake Rate……..84
3.7 Peeters Mechanism……...87
3.8 Summary……...90
4. OP3 July Campaign……..94
4.1.1 Introduction……...94
4.1.2 Data Coverage……94

4.1.3 Implications of air mass characteristics for OH, NO_3 and O_3 reactions with VOCs……95
4.2 Results……..101
4.2.1 Day 190 (9th July 2008)……101
4.2.2 Day 191 (10th July 2008)……..109
4.2.3 Day 192 (11th July 2008)……..118
4.2.4 Day 193 (12th July 2008)……..125
4.2.5 Day 194 (13th July 2008)……..133
4.2.6 Day 195 (14th July 2008)……..140
4.2.7 Day 198 (17th July 2008)……..146
4.2.8 Day 199 (18th July 2008)……..152
4.2.9 Summary of individual day data.....158
4.3.1 Rate of Production Analysis (ROPA) for Phase 2……169
5. OP3 April Campaign……...174
5.1.1 General Summary……...174
5.1.2 Data Coverage……..174
5.2 Results……..176
5.2.1 Day 111 (11th April 2008)……176
5.2.2 Day 112 (12th April 2008)……182
5.2.3 Day 113 (13th April 2008)……188
5.2.4 Day 114 (14th April 2008)……194
5.2.5 Day 115 (15th April 2008)……200
5.2.6 Day 116 (16th April 2008)……206
5.2.7 Day 117 (17th April 2008)……212
5.2.8 Day 120 (20th April 2008)……218
5.2.9 Summary of individual day data.....224
5.3 Rate of Production Analysis (ROPA) for Phase 1……...226
6. Comparisons and Conclusions……...230
6.1 Summary of Modelled Results from the Two Field Campaigns……230
6.2 Impact of new model mechanism and results from the AEROBIC campaign……...231
6.3 Previous Campaign Comparisons of VOC : NO_x vs. OH Model : Measured Results.....235
6.4 Sensitivity Analysis.....237

6.5 Conclusions.....244

7. References.....246

List of Figures

Figure 1.1.1. Key atmospheric reactions of OH, HO2 and RO2 radicals in the atmosphere**……26**

Figure 1.4.1 Isoprene molecule showing the 5 carbon atoms**……34**

Figure 2.1.. A step-by-step break down of how the MCM processes and simulates reactions of species that are used in the model**.....42**

Figure 2.2. Diurnal variation in isoprene and limonene for average concentrations in the second phase of the field campaign**……46**

Figure 2.3. Comparison between the measured data for isoprene and the interpolated values for isoprene during the second phase of the campaign**……51**

Figure 2.4. Comparison between the measured data for α-pinene and the interpolated values for α-pinene during the second phase of the campaign**……52**

Figure 2.5. Comparison between the measured data for NO and the averaged values for NO during the second phase of the campaign**……52**

Figure 2.6. Comparison between the measured data for NO_2 and the averaged values for NO_2 during the second phase of the campaign**……...53**

Figure 2.7. Comparison between the measured data for $J(O^1D)$ and the averaged values for $J(O^1D)$ during the second phase of the campaign**……...53**

Figure 3.1 Average diurnal profile of isoprene during the 2nd phase of the campaign, from 22nd June 2008 until 30th July 2008 at Bukit Atur field site**……62**

Figure 3.2 Average diurnal profile of $J(O^1D)$ during the 2nd phase of the campaign, from 22nd June 2008 until 30th July 2008 at Bukit Atur field site**……....62**

Figure 3.3 Comparison of measured OH and modelled OH using average data set for the second phase of the field campaign, from 22nd June 2008 until 30th July 2008 at Bukit Atur field site**……63**

Figure 3.4 Comparison of measured HO_2 and modelled HO_2 using average data set for the second phase of the field campaign, from 22nd June 2008 until 30th July 2008 at Bukit Atur field site**……63**

Figure 3.5 Comparison of measured RO_2 and modelled RO_2 using average data set for the second phase of the field campaign, from 22nd June 2008 until 30th July 2008 at Bukit Atur field site**……64**

Figure 3.6 Diurnal OH concentrations over each day of the model run to steady state conditions**…….65**

Figure 3.7 Diurnal HO_2 concentrations over each day of the model run to steady state conditions**…….66**

Figure 3.8 Diurnal RO_2 concentrations over each day of the model run to steady state conditions**…….66**

Figure 3.9. OH concentration predictions for day 190 in campaign 2nd phase with constrained data at 1, 5, 15 and 60 minutes**……..69**

Figure 3.10. Comparison between photolysis rates from the model containing the MCM and the TUV for four photolysis reactions in the model mechanism**……77**

Figure 3. 11. OH predictions using different vegetation types for the average day conditions during second phase of field study**…….80**

Figure 3. 12. HO_2 predictions using different vegetation types for the average day conditions during second phase of field study**…….81**

Figure 3. 13. RO_2 predictions using different vegetation types for the average day conditions during second phase of field study**…….81**

Figure 3.14 MVK predictions using different vegetation types for average day conditions during second phase of field study**…….83**

Figure 3.15 MACR predictions using different vegetation types for average day conditions during second phase of field study**…….83**

Figure 3.16. Output predictions of OH concentrations with different k_t values constrained in the model**……...85**

Figure 3.17. Output predictions of HO_2 concentrations with different k_t values constrained in the model**……...85**

Figure 3.18. Output predictions of RO_2 concentrations with different k_t values constrained in the model**……...86**

Figure 3.19 Comparison of measured OH and modelled OH from existing and experimental isoprene schemes using average data set for the second phase of the field campaign, from 22nd June 2008 until 30th July 2008 at Bukit Atur field site**……...87**

Figure 3.20 Comparison of measured HO_2 and modelled HO_2 from existing and experimental isoprene schemes using average data set for the second phase of the field campaign, from 22nd June 2008 until 30th July 2008 at Bukit Atur field site**……...88**

Figure 3.21 Comparison of measured RO_2 and modelled RO_2 from existing and experimental isoprene schemes using average data set for the second phase of the field campaign, from 22nd June 2008 until 30th July 2008 at Bukit Atur field site**……...88**

Figure 3.22 Comparison of measured OH and modelled OH using average data set for the second phase of the field campaign, from 22nd June 2008 until 30th July 2008 at Bukit Atur field site. Modelled data is taken from an original MCM based model, a model using new uptake and deposition values (run 1) and a model containing new uptake values, deposition values and the proposed Peeters scheme**……90**

Figure 3.23 Comparison of measured HO_2 and modelled HO_2 using average data set for the second phase of the field campaign, from 22nd June 2008 until 30th July 2008 at Bukit Atur field site. Modelled data is taken from an original MCM based model, a model using new uptake and deposition values (run 1) and a model containing new uptake values, deposition values and the proposed Peeters scheme**……91**

Figure 3.24 Comparison of measured RO_2 and modelled RO_2 using average data set for the second phase of the field campaign, from 22nd June 2008 until 30th July 2008 at Bukit Atur field site. Modelled data is taken from an original MCM based model, a model using new uptake and deposition values (run 1) and a model containing new uptake values, deposition values and the proposed Peeters scheme**……91**

Figure 4.1.1 Percentage contribution loss of oxidants through reactions with hydrocarbons a) overall OH loss, b) daytime OH loss, c) nighttime OH loss, d) overall O_3 loss, e) daytime O_3 loss, f) nighttime O_3 loss, g) overall NO_3 loss, h) daytime NO_3 loss, i) Nighttime NO_3 loss**…….100**

Figure 4.2.1 Air mass trajectory for 5 day arriving at the field site at 1200 hours (local time) on 9th July (JDay 190) The upper plot shows the path taken by the airmass travelling to the field site, for the 5 days previous to measurements being taken. The lower plot shows the altitude of the airmass for the 5 day period before arriving at the field site**…… 101**

Figure 4.2.2 NO and NO_2 concentrations recorded at Bukit Atur on JDay 190 (9th July 2008)**.....102**

Figure 4.2.3 Isoprene concentrations recorded at Bukit Atur on JDay 190 (9th July 2008)**……..103**

Figure 4.2.4 Monoterpene concentrations and temperatures recorded at Bukit Atur on JDay 190 (9th July 2008)**……103**

Figure 4.2.5 J(O^1D) observations recorded at Bukit Atur on JDay 190 (9th July 2008)**……...104**

Figure 4.2.6 Model-measurement comparison of [OH] for day 190 (9th July 2008)**105**

Figure 4.2.7 Model-measurement comparison of [HO_2] for day 190 (9th July 2008)**……...105**

Figure 4.2.8 Model-measurement comparison of [RO_2] for day 191 (9th July 2008) **…….....106**

Figure 4.2.9 Air mass trajectory for 5 day arriving at the field site at 1200 hours (local time) on 10th July (JDay 191) The upper plot shows the path taken by the airmass travelling to the field site, for the 5 days previous to measurements being taken. The lower plot shows the altitude of the airmass for the 5 day period before arriving at the field site**…… 109**

Figure 4.2.10 NO and NO_2 concentrations recorded at Bukit Atur on JDay 191 (10th July 2008)**……...110**

Figure 4.2.11 Isoprene concentrations recorded at Bukit Atur on JDay 191 (10th July 2008)**.....111**

Figure 4.2.12 Monoterpene concentrations and temperatures recorded at Bukit Atur on JDay 191 (10th July 2008)**…….111**

Figure 4.2.13 J(O^1D) observations recorded at Bukit Atur on JDay 191 (10th July 2008)**……...112**

Figure 4.2.14 Model-measurement comparison of [OH] for day 191 (10th July 2008)**……...113**

Figure 4.2.15 Model-measurement comparison of [HO_2] for day 191 (10/07/2008)**113**

Figure 4.2.16 Model-measurement comparison of [RO_2] for day 191 (10/07/2008)**114**

Figure 4.2.17 Air mass trajectory for 5 day arriving at the field site at 1200 hours (local time) on 11th July (JDay 192) The upper plot shows the path taken by the airmass travelling to the field site, for the 5 days previous to measurements being taken. The lower plot shows the altitude of the airmass for the 5 day period before arriving at the field site**……...118**

Figure 4.2.18 NO and NO_2 concentrations recorded at Bukit Atur on JDay 192 (11th July 2008) **…….....119**

Figure 4.2.19 Isoprene concentrations recorded at Bukit Atur on JDay 192 (11th July 2008) **…….....119**

Figure 4.2.20 Monoterpene concentrations recorded at Bukit Atur on JDay 192 (11th July 2008) **…….....120**

Figure 4.2.21 J(O^1D) observations recorded at Bukit Atur on JDay 192 (11th July 2008)**.....120**

Figure 4.2.22 Model-measurement comparison of [OH] for day 192 (11th July 2008)**……...121**

Figure 4.2.23 Model-measurement comparison of [HO_2] for day 192 (11th July 2008) **……121**

Figure 4.2.24 Model-measurement comparison of [RO_2] for day 192 (11th July 2008) **……121**

Figure 4.2.25 Air mass trajectory for 5 day arriving at the field site at 1200 hours (local time) on 12th July (JDay 193) The upper plot shows the path taken by the airmass travelling to the field site, for the 5 days previous to measurements being taken. The lower plot shows the altitude of the airmass for the 5 day period before arriving at the field site**……...125**

Figure 4.2.26 NO and NO_2 concentrations recorded at Bukit Atur on JDay 193 (12th July 2008)**……...126**

Figure 4.2.27 Isoprene concentrations recorded at Bukit Atur on JDay 193 (12th July 2008)**…….....126**

Figure 4.2.28 Monoterpene concentrations recorded at Bukit Atur on JDay 193 (12th July 2008))**…….127**

Figure 4.2.29 J(O^1D) observations recorded at Bukit Atur on JDay 193 (12th July 2008))**…….....127**

Figure 4.2.30 Model-measurement comparison of [OH] for day 193 (12th July 2008))**…….....129**

Figure 4.2.31 Model-measurement comparison of [HO_2] for day 193 (12th July 2008) **…….....129**

Figure 4.2.32 Model-measurement comparison of [RO_2] for day 193 (12th July 2008) **…….....130**

Figure 4.2.33 Air mass trajectory for 5 day arriving at the field site at 1200 hours (local time) on 13th July (JDay 194) The upper plot shows the path taken by the airmass travelling to the field site, for the 5 days previous to measurements being taken. The lower plot shows the altitude of the airmass for the 5 day period before arriving at the field site**……...133**

Figure 4.2.34 NO and NO_2 concentrations recorded at Bukit Atur on JDay 194 (13th July 2008)**……...134**

Figure 4.2.35 Isoprene concentrations recorded at Bukit Atur on JDay 194 (13th July 2008)**…….....134**

Figure 4.2.36 Monoterpene concentrations recorded at Bukit Atur on JDay 194 (13th July 2008)**……...135**

Figure 4.2.37 J(O^1D) observations recorded at Bukit Atur on JDay 194 (13th July 2008)**……...136**

Figure 4.2.38 Model-measurement comparison of [OH] for day 194 (13th July 2008)**……...136**

Figure 4.2.39 Model-measurement comparison of [HO_2] for day 194 (13th July 2008))**…….....137**

Figure 4.2.40 Model-measurement comparison of [RO_2] for day 194 (13th July 2008)**……...137**

Figure 4.2.41 Air mass trajectory for 5 day arriving at the field site at 1200 hours (local time) on 14th July (JDay 195) the upper plot shows the path taken by the airmass travelling to the field site, for the 5 days previous to measurements being taken. The lower plot shows the altitude of the airmass for the 5 day period before arriving at the field site**……..140**

Figure 4.2.42 NO and NO_2 concentrations recorded at Bukit Atur on JDay 195 (14th July 2008)**……...141**

Figure 4.2.43 Isoprene concentrations recorded at Bukit Atur on JDay 195 (14th July 2008)**…….....142**

Figure 4.2.44 Monoterpene concentrations and temperature recorded at Bukit Atur on JDay 195 (14th July 2008)**……..142**

Figure 4.2.45 J(O^1D) observations recorded at Bukit Atur on JDay 195 (14th July 2008)**……...143**

Figure 4.2.46 Model-measurement comparison of [OH] for day 195 (14th July 2008)**……...143**

Figure 4.2.47 Model-measurement comparison of [HO_2] for day 195 (14th July 2008)**……...144**

Figure 4.2.48 Model-measurement comparison of [RO_2] for day 195 (14th July 2008)**……...144**

Figure 4.2.49 Air mass trajectory for 5 day arriving at the field site at 1200 hours (local time) on 17th July (JDay 198) The upper plot shows the path taken by the airmass travelling to the field site, for the 5 days previous to measurements being taken. The lower plot shows the altitude of the airmass for the 5 day period before arriving at the field site**……...146**

Figure 4.2.50 NO and NO_2 concentrations recorded at Bukit Atur on JDay 198 (17th July 2008)**……...147**

Figure 4.2.51 Isoprene concentrations recorded at Bukit Atur on JDay 198 (17th July 2008)**…….....147**

Figure 4.2.52 Monoterpene concentrations recorded at Bukit Atur on JDay 198 (17th July 2008)**……...148**

Figure 4.2.53 JO^1D observations recorded at Bukit Atur on JDay 198 (17th July 2008)**……149**

Figure 4.2.54 Model-measurement comparison of [OH] for day 198 (17th July 2008)**……149**

Figure 4.2.55 Model-measurement comparison of [HO_2] for day 198 (17th July 2008)**……150**

Figure 4.2.56 Model-measurement comparison of [RO_2] for day 198 (17th July 2008)**……150**

Figure 4.2.57 Air mass trajectory for 5 day arriving at the field site at 1200 hours (local time) on 18th July (JDay 199) The upper plot shows the path taken by the airmass travelling to the field site, for the 5 days previous to measurements being taken. The lower plot shows the altitude of the airmass for the 5 day period before arriving at the field site**)…….152**

Figure 4.2.58 NO and NO_2 concentrations recorded at Bukit Atur on JDay 199 (18th July 2008**)……...153**

Figure 4.2.59 Isoprene concentrations recorded at Bukit Atur on JDay 199 (18th July 2008**)…….....153**

Figure 4.2.60 Monoterpene concentrations recorded at Bukit Atur on JDay 199 (18th July 2008)**……...154**

Figure 4.2.61 $J(O^1D)$ observations recorded at Bukit Atur on JDay 199 (18th July 2008)**……..154**

Figure 4.2.62 Model-measurement comparison of [OH] for day 199 (18th July 2008)**……...155**

Figure 4.2.63 Model-measurement comparison of [HO_2] for day 199 (18th July 2008)**……...155**

Figure 4.2.64 Model-measurement comparison of [RO_2] for day 199 (18th July 2008)**……...156**

Figure 4.2.65 Average modelled (OP3 Peeters) to measured ratios of OH from 11:00 to 15:00 plotted against the ratio of VOCs (ppbC) to total NO_x during the second phase of the field campaign at Bukit Atur. The individual days are identified by data labels**……...164**

Figure 4.2.66 Average modelled (OP3) to measured ratios of OH from 11:00 to 15:00 plotted against the ratio of VOCs (ppbC) to total NO_x during the second phase of the field campaign at Bukit Atur. The individual days are identified by data labels**…..165**

Figure 4.2.67 Modelled (Peeters) to measured ratios of OH from 11:00 to 15:00 plotted against the ratio of VOCs to total NO_x during the second phase of the field campaign at Bukit Atur**……..166**

Figure 4.2.68 Modelled (without Peeters) to measured ratios of OH from 11:00 to 15:00 plotted against the ratio of VOCs to total NO_x during the second phase of the field campaign at Bukit Atur**……..167**

Figure 4.2.69 Modeled and measured values of HO_2/OH plotted against the concentration of measured NO during the second phase of the field campaign at Bukit Atur**…….168**

Figure 4.3.1 Rate of production analysis between 11:00 and 15:00 hours for day 193 (Peeters model), *193 (OP3 model),* **192 (Peeters model)……..173**

Figure 5.2.1 Air mass back trajectory for 5 day arriving at the field site at 1200 hours (local time) on 11th April (JDay 111) The upper plot shows the path taken by the airmass travelling to the field site, for the 5 days previous to measurements being taken. The lower plot shows the altitude of the airmass for the 5 day period before arriving at the field site**……..176**

Figure 5.2.2 NO and NO_2 concentrations recorded at Bukit Atur on JDay 111 (11th April 2008)**……177**

Figure 5.2.3 Isoprene concentrations recorded at Bukit Atur on JDay 111 (11th April 2008)**……178**

Figure 5.2.4 Average monoterpene concentrations from Bukit Atur used to model JDay 111 (11th April 2008) with the recorded temperatures**.....178**

Figure 5.2.5 J(O^1D) observations recorded at Bukit Atur on JDay 111 (11th April 2008)**……...179**

Figure 5.2.6 Model-measurement comparison of [OH] for day 111 (11th July 2008)**……...180**

Figure 5.2.7 Model-measurement comparison of [HO_2 + RO_2] for day 111 (11th July 2008)**……...180**

Figure 5.2.8 Air mass back trajectory for 5 day arriving at the field site at 1200 hours (local time) on 12th April (JDay 112) The upper plot shows the path taken by the airmass travelling to the field site, for the 5 days previous to measurements being taken. The lower plot shows the altitude of the airmass for the 5 day period before arriving at the field site**……...182**

Figure 5.2.9 NO and NO_2 concentrations recorded at Bukit Atur on JDay 112 (12th April2008)**……..183**

Figure 5.2.10 Isoprene concentrations recorded at Bukit Atur on JDay 112 (12th April 2008)**……...184**

Figure 5.2.11 JO^1D observations recorded at Bukit Atur on JDay 112 (12th April 2008)**……...184**

Figure 5.2.12 Model-measurement comparison of [OH] for day 112 (12th April 2008)**……...185**

Figure 5.2.13 Model-measurement comparison of [HO_2 + RO_2] for day 112 (12th April 2008)**…….186**

Figure 5.2.14 Air mass back trajectory for 5 day arriving at the field site at 1200 hours (local time) on 13th April (JDay 113) The upper plot shows the path taken by the airmass travelling to the field site, for the 5 days previous to measurements being taken. The lower plot shows the altitude of the airmass for the 5 day period before arriving at the field site**…….....189**

Figure 5.2.15 NO and NO_2 concentrations recorded at Bukit Atur on JDay 113 (13th April 2008)**…….190**

Figure 5.2.16 Isoprene concentrations recorded at Bukit Atur on JDay 113 (13th April 2008)**……..191**

Figure 5.2.17 J(O^1D) observations recorded at Bukit Atur on JDay 113 (13th April 2008)**……..192**

Figure 5.2.18 Model-measurement comparison of [OH] for day 113 (13th April 2008)**…….193**

Figure 5.2.19 Model-measurement comparison of [HO_2 + RO_2] for day 113 (13th April 2008)**…….193**

Figure 5.2.20 Air mass back trajectory for 5 day arriving at the field site at 1200 hours (local time) on 14th April (JDay 114) The upper plot shows the path taken by the airmass travelling to the field site, for the 5 days previous to measurements being taken. The lower plot shows the altitude of the airmass for the 5 day period before arriving at the field site**……...194**

Figure 5.2.23 NO and NO_2 concentrations recorded at Bukit Atur on JDay 114 (14th April 2008)**…….195**

Figure 5.2.22 Isoprene concentrations recorded at Bukit Atur on JDay 114 (14th. April 2008)**……...196**

Figure 5.2.23 J(O^1D) observations recorded at Bukit Atur on JDay 114 (14th April 2008)**……...196**

Figure 5.2.24 Model-measurement comparison of [OH] for day 114 (14th April 2008)**……...197**

Figure 5.2.25 Model-measurement comparison of [HO_2 + RO_2] for day 114 (14th April 2008)**…….198**

Figure 5.2.26 Air mass back trajectory for 5 days arriving at the field site at 1200 hours (local time) on 15th April (JDay 115) The upper plot shows the path taken by the airmass travelling to the field site, for the 5 days previous to measurements being taken. The lower plot shows the altitude of the airmass for the 5 day period before arriving at the field site**……...200**

Figure 5.2.27 NO and NO_2 concentrations recorded at Bukit Atur on JDay 115 (15th April 2008)**…….201**

Figure 5.2.28 Isoprene concentrations recorded at Bukit Atur on JDay 115 (15th April 2008)**……...202**

Figure 5.2.29 J(O^1D) observations recorded at Bukit Atur on JDay 115 (15th April 2008)**……...202**

Figure 5.2.30 Model-measurement comparison of [OH] for day 115 (15th April 2008)**……...203**

Figure 5.2.31 Model-measurement comparison of [HO_2 + RO_2] for day 115 (15th April 2008)**…….204**

Figure 5.2.32 Air mass back trajectory for 5 day arriving at the field site at 1200 hours (local time) on 16th April (JDay 116) The upper plot shows the path taken by

the airmass travelling to the field site, for the 5 days previous to measurements being taken. The lower plot shows the altitude of the airmass for the 5 day period before arriving at the field site**……...206**

Figure 5.2.33 NO and NO_2 concentrations recorded at Bukit Atur on JDay 116 (16^{th} April 2008)**…….207**

Figure 5.2.34 Isoprene concentrations recorded at Bukit Atur on JDay 116 (16^{th} April 2008)**……..208**

Figure 5.2.35 J(O^1D) observations recorded at Bukit Atur on JDay 116 (16^{th} April 2008)**……..209**

Figure 5.2.36 Model-measurement comparison of [OH] for day 116 (16^{th} April 2008)**……...210**

Figure 5.2.37 Model-measurement comparison of [RO_2 + HO_2] for day 116 (16^{th} April 2008)**…….210**

Figure 5.2.38 Air mass back trajectory for 5 day arriving at the field site at 1200 hours (local time) on 17^{th} April (JDay 117) The upper plot shows the path taken by the airmass travelling to the field site, for the 5 days previous to measurements being taken. The lower plot shows the altitude of the airmass for the 5 day period before arriving at the field site**……...212**

Figure 5.2.39 NO and NO_2 concentrations recorded at Bukit Atur on JDay 117 (17^{th} April 2008)**…….213**

Figure 5.2.40 Isoprene concentrations recorded at Bukit Atur on JDay 117 (17^{th} April 2008)**……...214**

Figure 5.2.41 J(O^1D) observations recorded at Bukit Atur on JDay 117 (17^{th} April 2008)**……..215**

Figure 5.2.42 Model-measurement comparison of [OH] for day 117 (17/04/2008)**……...216**

Figure 5.2.43 Model-measurement comparison of [RO_2 + HO_2] for day 117 (17/04/2008)**……...216**

Figure 5.2.44 Air mass trajectory for 5 day arriving at the field site at 1200 hours (local time) on 20^{th} April (JDay 120) The upper plot shows the path taken by the airmass travelling to the field site, for the 5 days previous to measurements being taken. The lower plot shows the altitude of the airmass for the 5 day period before arriving at the field site**……...218**

Figure 5.2.45 NO and NO_2 concentrations recorded at Bukit Atur on JDay 120 (20^{th} April 2008)**……219**

Figure 5.2.46 Isoprene concentrations recorded at Bukit Atur on JDay 120 (20^{th} April 2008)**…….220**

Figure 5.2.47 Average monoterpene concentrations from Bukit Atur used to model JDay 120 (20^{th} April 2008) with the recorded temperatures**…….220**

Figure 5.2.48 J(O^1D) observations recorded at Bukit Atur on JDay 120 (20^{th} April 2008)**…….221**

Figure 5.2.56 Model-measurement comparison of [HO_2 + RO_2] for day 120 (20/04/2008)**……...222**

Figure 5.3.1 ROPA study of day 120 (11:00 to 15:00) for the OP3 Peeters model and OP3 model**……228**

Figure 6.2.1 NO and NO_2 concentrations for an average day during the AEROBIC field campaign**……232**

Figure 6.2.2 VOC concentrations for an average day during the AEROBIC field campaign**……232**

Figure 6.2.3 OH concentration from the AEROBIC average data predicted using the AEROBIC, OP3 and OP3 Peeters models**……..233**

Figure 6.2.4 HO_2 concentration from the AEROBIC average data predicted using the AEROBIC, OP3 and OP3 Peeters models**……233**

Figure 6.2.5 RO_2 concentration from the AEROBIC average data predicted using the AEROBIC, OP3 and OP3 Peeters models**……234**

Figure 6.3.1. Modelled/Measured OH against VOC:NO_x ratios for OP3, TORCH, AEROBIC and SOAPEX field campaigns averages for 11:00 to 15:00**……236**

Figure 6.4.1 Predicted average OH profile from second phase of the OP3 field campaign at Danum Valley introducing increased VOC and NO concentrations to represent missing chemical species using the OP3 model**……238**

Figure 6.4.2 Predicted average HO_2 profile from second phase of the OP3 field campaign at Danum Valley introducing increased VOC and NO concentrations to represent missing chemical species using the OP3 model**……238**

Figure 6.4.3 Predicted average RO_2 profile from second phase of the OP3 field campaign at Danum Valley introducing increased VOC and NO concentrations to represent missing chemical species using the OP3 model**……239**

Figure 6.4.4 Predicted average OH profile from second phase of the OP3 field campaign at Danum Valley introducing increased VOC and NO concentrations to represent missing chemical species using the OP3 model**…….239**

Figure 6.4.5 Predicted average HO_2 profile from second phase of the OP3 field campaign at Danum Valley introducing increased VOC and NO concentrations to represent missing chemical species using the OP3 model**…….240**

Figure 6.4.6 Predicted average RO_2 profile from second phase of the OP3 field campaign at Danum Valley introducing increased VOC and NO concentrations to represent missing chemical species using the OP3 model**…….240**

List of Tables

Table 2.1 Photolysis calculations set in the MCM**……..40**

Table 2.2. Current rate coefficients used in the MCM for reactions between VOCs and OH**…….42**

Table 2.3. Percentage loss of measured VOCs from reactions with OH during the campaign 2nd phase. Daytime is defined as the period from 07:00 to 19:00 h and nighttime is defined as the period from 19:00 to 07:00 h**……44**

Table 2.4. Percentage loss of measured VOCs from reactions with O_3 during the campaign 2nd phase. Daytime is defined as the period from 07:00 to 19:00 h and nighttime is defined as the period from 19:00 to 07:00 h**……44**

Table 2.5. Percentage loss of measured VOCs from reactions with NO_3 during the campaign 2nd phase. Daytime is defined as the period from 07:00 to 19:00 h and nighttime is defined as the period from 19:00 to 07:00 h**……45**

Table 2.6. Ten most reactive organic species from reactions with OH during the first phase of the campaign**……..47**

Table 2.7. Comparison between camphene, γ-terpinene and potential analogues that can be used in the OP3 Model**……48**

Table2.8. Percentage Difference between averaged measured and processed data for the first and second phase of the campaign. A positive value denotes that the averaged data were larger than the measured data**…… 54**

Table 2.9. Overview of measurements made during OP3 that are included in the model**……57**

Table 3.1 Average, maximum and minimum concentrations for constrained species during the second phase of the field campaign, from 22nd June 2008 until 30th July 2008 at Bukit Atur field site**……64**

Table 3.2 Concentrations of the three radical species at midday when running the model over a 5 day period to achieve steady state**……...67**

Table 3.3. Predicted concentrations of radical species from input file frequency testing averaged over the 2 hour period**……...68**

Table 3.4. Percentage difference at 12:00 between 15 minute interval test and other time intervals**……68**

Table 3.5: Quantified differences between the TUV and MCM photolysis models for the first and second phases of the field campaign at Bukit Atur**……..78**

Table 3.6 Dry-deposition velocities taken from the MCM and two modeled scenarios containing different types of vegetation**.....80**

Table 3.7 Midday concentrations of radical species for an average condition day during second phase of field campaign using different deposition velocities**……..82**

Table 3.8 Mean values of OH, HO_2 and RO_2 predictions from 3 different model runs (the original MCM based model using values of k_t at 0, 0.05 and 1 supplied by Manchester) using average data set for the second phase of the field campaign, from 22nd June 2008 until 30th July 2008 at Bukit Atur field site**……86**

Table 3.9 Mean values of OH, HO_2 and RO_2 predictions from 2 different model runs (original baseline MCM model and the same model but including the Peeters scheme) using average data set for the second phase of the field campaign, from 22nd June 2008 until 30th July 2008 at Bukit Atur field site**……89**

Table 3.10 Mean values of OH, HO_2 and RO_2 predictions from 3 different model runs (original baseline MCM model, run 1 and run 2) using average data set for the second phase of the field campaign, from 22nd June 2008 until 30th July 2008 at Bukit Atur field site**……92**

Table 4.1.1 Data coverage for the second phase of the field campaign. ✓ indicates species that have a full days worth of cover and x indicates species where a whole days worth of data coverage is not present**……95**

Table 4.2.1 Average concentrations of OH, HO_2 and RO_2 at Bukit Atur on JDay 190 (09/07/2008) for the whole day, daytime (06:00 – 18:00), nighttime (00:00 – 06:00 and 18:00 – 24:00) and midday (11:00 -15:00)**……107**

Table 4.2.2 Average concentrations of OH, HO_2 and RO_2 at Bukit Atur on JDay 191 (10/07/2008) for the whole day, daytime (06:00 – 18:00), nighttime (00:00 – 06:00 and 18:00 – 24:00) and midday (11:00 -15:00)**…….114**

Table 4.2.3 Average concentrations of OH, HO_2 and RO_2 at Bukit Atur on JDay 192 (11^{th} July 2008) for the whole day, daytime (06:00 – 18:00), nighttime (00:00 – 06:00 and 18:00 – 24:00) and midday (11:00 -15:00)**……123**

Table 4.2.4 Average concentrations of OH, HO_2 and RO_2 at Bukit Atur on JDay 193 (12^{th} July 2008) for the whole day, daytime (06:00 – 18:00), nighttime (00:00 – 06:00 and 18:00 – 24:00) and midday (11:00 -15:00)**……..131**

Table 4.2.5 Average concentrations of OH, HO_2 and RO_2 at Bukit Atur on JDay 194 (13^{th} July 2008) for the whole day, daytime (06:00 – 18:00), nighttime (00:00 – 06:00 and 18:00 – 24:00) and midday (11:00 -15:00)**……..138**

Table 4.2.6 Average concentrations of OH, HO_2 and RO_2 at Bukit Atur on JDay 195 (14^{th} July 2008) for the whole day, daytime (06:00 – 18:00), nighttime (00:00 – 06:00 and 18:00 – 24:00) and midday (11:00 -15:00)**……..145**

Table 4.2.7 Average concentrations of OH, HO_2 and RO_2 at Bukit Atur on JDay 198 (17^{th} July 2008) for the whole day, daytime (06:00 – 18:00), nighttime (00:00 – 06:00 and 18:00 – 24:00) and midday (11:00 -15:00)**……..151**

Table 4.2.8 Average concentrations of OH, HO_2 and RO_2 at Bukit Atur on JDay 199 (18^{th} July 2008) for the whole day, daytime (06:00 – 18:00), nighttime (00:00 – 06:00 and 18:00 – 24:00) and midday (11:00 -15:00)**……..156**

Table 4.2. 9 Average modelled and measured values between 11:00 and 15:00 during the second phase of the OP3 campaign**……..159**

Table 4.2.10 Average modelled and measured values between 11:00 and 15:00 during the second phase of the OP3 campaign**……..161**

Table 4.2.11 Average modelled and measured values between 11:00 and 15:00 during the second phase of the OP3 campaign**……..163**

Table 4.3.1. A summary of the rate of production analysis for radicals being predicted by the OP3 Peeters Model during the second phase of the campaign at Bukit Atur, July 2007 between 11:00 and 15:00 hours**……169**

Table 4.3.2. A summary of the rate of production analysis for radicals being predicted by the OP3 Model during the second phase of the campaign at Bukit Atur, July 2007 between 11:00 and 15:00 hours**…….170**

Table 5.1.1 Data coverage for the second phase of the field campaign. ✓ indicates species that have a full days worth of cover and x indicates species where a whole days worth of data coverage is not present**…….174**

Table 5.2.1 Average concentrations of OH and $RO_2 + HO_2$ at Bukit Atur on JDay 111 (11^{th} July 2008) for the whole day, daytime (06:00 – 18:00), nighttime (00:00 – 06:00 and 18:00 – 24:00) and midday (11:00 -15:00)**……..181**

Table 5.2.2 Average concentrations of OH and $RO_2 + HO_2$ at Bukit Atur on JDay 112 (12^{th} April 2008) for the whole day, daytime (06:00 – 18:00), nighttime (00:00 – 06:00 and 18:00 – 24:00) and midday (11:00 -15:00)**……186**

Table 5.2.3 Average concentrations of OH and $RO_2 + HO_2$ at Bukit Atur on JDay 113 (13^{th} April 2008) for the whole day, daytime (06:00 – 18:00), nighttime (00:00 – 06:00 and 18:00 – 24:00) and midday (11:00 -15:00)**……193**

Table 5.2.4 Average concentrations of OH and $RO_2 + HO_2$ at Bukit Atur on JDay 114 (14/04/2008) for the whole day, daytime (06:00 – 18:00), nighttime (00:00 – 06:00 and 18:00 – 24:00) and midday (11:00 -15:00)**……..199**

Table 5.2.5 Average concentrations of OH and $RO_2 + HO_2$ at Bukit Atur on JDay 115 (16^{th} April 2008) for the whole day, daytime (06:00 – 18:00), nighttime (00:00 – 06:00 and 18:00 – 24:00) and midday (11:00 -15:00)**……205**

Table 5.2.6 Average concentrations of OH and $RO_2 + HO_2$ at Bukit Atur on JDay 116 (16^{th} April 2008) for the whole day, daytime (06:00 – 18:00), nighttime (00:00 – 06:00 and 18:00 – 24:00) and midday (11:00 -15:00)**……211**

Table 5.2.7 Average concentrations of OH and $RO_2 + HO_2$ at Bukit Atur on JDay 117 (17/04/2008) for the whole day, daytime (06:00 – 18:00), nighttime (00:00 – 06:00 and 18:00 – 24:00) and midday (11:00 -15:00)**……..217**

Table 5.2.8 Average concentrations of OH and $RO_2 + HO_2$ at Bukit Atur on JDay 120 (20/04/2008) for the whole day, daytime (06:00 – 18:00), nighttime (00:00 – 06:00 and 18:00 – 24:00) and midday (11:00 -15:00)**……..223**

Table 5.2.9 Average modelled and measured values of OH between 11:00 and 15:00 during the first phase of the OP3 campaign**……...225**

Table 5.2.10 Average modelled and measured values of HO_2+RO_2 between 11:00 and 15:00 during the first phase of the OP3**…….....225**

Table 5.3.1 ROPA data from the OP3 Peeters and OP3 model between 11:00 and 15:00 for day 120**……...227**

Table 6.2.1 Radical concentrations predicted by the AEROBIC, OP3 and OP3 Peeters models and measurements between 11:00 and 15:00 (using average data from the AEROBIC campaign)**……235**

Table 6.4.1. Predicted concentrations of OH, HO_2 and RO_2 between 11:00 and 15:00 using the average day data in the second phase of the OP3 campaign, with increased concentrations of NO and VOCs**……241**

Declaration

I declare that all work contained within this thesis is my own unless otherwise stated.

Acknowledgements

Firstly, I would like to thank my supervisor Nicola Carslaw for her constant help and support throughout my undergraduate and doctorate degrees. She helped me through the hardest project that I have ever under taken and reassured me of my own abilities whenever I doubted what I was doing, despite having to face the hardest battle of her life at the same time.

The financial support of the Natural Environment Research Council (NERC) was greatly appreciated. The funding they supplied allowed me to fully take part in the OP3 project travelling to Borneo, to experience the environment I was studying at first hand.

I would also like to thank everyone connected to the OP3 project. In particular Nick Hewitt for leading and organising the project. Also Dwayne Heard and Paul Monks and their research groups at the universities of Leeds and Leicester for supplying data that was vital for the use in my models. I would also like to thanks the research group at the University of Manchester, especially Gordon McFiggans and Niall Robinson for the aerosol data they provided and calculated.

I would also like to thank everyone at the Environment Department for making my time here through out my undergraduate and doctorate so enjoyable. I would particularly like to thank Paul Ayris and Nicola Myers for being so supportive over the last 4 years, listening to my problems and keeping me sane.

Finally I would like to thank my family and friends for their unfailing support and love.

Chapter 1. Introduction

1.1 Overview

Over half the forests in the world are found in the tropics, covering an area of 1.8 billion ha (Hewitt et al., 2009). These forests account for over half of all the biogenic volatile organic carbon (VOC) emissions into the atmosphere (Hewitt et al., 2009) and are believed to have a large effect on the chemistry of the atmosphere. Biogenic emissions from tropical forests depend on climatic factors such as temperature and rainfall (Hewitt et al., 2009); a changing global climate will likely impact upon the rates of VOC emissions, so changing the atmospheric chemistry of these regions into the future (Chappell et al., 2001). At the present time, their impacts on the atmospheric chemistry, both locally and globally are not well understood.

In order to investigate the atmospheric chemistry of such a region in detail, a major instrumental field campaign was conceived where by two major ground-based field campaigns were carried out in Malaysian Borneo in 2008. The objectives of the campaigns were to understand how emissions of reactive trace gases from a tropical rain forest mediate the regional scale production and processing of oxidants and particles in the troposphere and to better understand the impact of these processes on local, regional and global scale atmospheric composition, chemistry and climate (Hewitt et al., 2009). By very close coupling of ground-based and airborne measurements of surface fluxes and atmospheric compositions of reactive trace gases, particles and modelling the project aimed to address the following questions;

- What are the rates of transfer of organic compounds emitted from the tropical forests?
- How are these organic compounds chemically processed immediately after release?
- To what extent do the regional organic emissions contribute to the atmospheric aerosol in the region, and what are the effects of the aerosol? What is the composition of the organic fraction of the aerosol?

- What are the effects of these biogenic emissions on global chemistry and climate?

The specific aim of this modelling project within the wider OP3 campaign was to investigate the photochemical processing of gas-phase species. In order to achieve this aim, ground-based measurements were to be used to constrain a detailed chemical box model to provide a detailed analysis of the chemical processes occurring in the tropical forest. In particular the role of biogenic emissions was to be a particular focus.

The region of Borneo was predicted to be perfect to study the atmospheric chemistry of forested regions. As well as the substantial natural emissions from vegetation, the high levels of sunlight and humidity were expected to provide high concentrations of radical species. Coupled with moderate concentrations of NO_X and high temperatures, ideal conditions for chemical processes were anticipated. In addition, Borneo is part of a complex system of tropical seas and islands (Hewitt et al., 2009). Due to the combination of land and sea in south east Asia there is a strong maritime effect providing much more efficient transport of materials in the boundary layer, leading to a disproportionately large effect on global atmospheric processes (Fueglistaler and Haynes, 2005).

There now follows a brief overview of radical chemistry, followed by a summary of past field campaigns where measured and modelled radical concentrations have been investigated. A thesis plan is then provided at the end of the chapter.

1.2 Radical Chemistry.

The hydroxyl radical (OH) is an important oxidising species in the atmosphere. It is a very reactive chemical species, reacting with almost all other atmospheric species initiating oxidation reactions that eventually lead to carbon dioxide and water. OH is not directly affected by transport itself, due to its short chemical lifetime (less than 1 second in the mid-latitude continental boundary layer). Consequently the concentration of OH is controlled by local influences such as the concentrations of ozone (O_3), water, volatile organic compounds (VOCs), carbon monoxide (CO), nitrogen oxides (NO_X) and the strength of the sunlight.

In areas where there are high concentrations of VOCs, such as polluted urban environments with anthropogenic VOCs, or forested regions with natural (vegaetative) VOCs, reactions with OH occur rapidly causing OH to be cycled to form hyydroperoxy (HO_2) and organic peroxy (RO_2) radicals. These radicals can undergo further reactions with NO to reform OH. Reaction of HO_2 with NO also forms NO_2, which can undergo photolysis to eventually create O_3, which in turn can further react, leading to the formation of more OH. A single OH radical can trigger a chain reaction leading to the degradation of many VOCs and trace gases, removing them from the atmosphere and forming tropospheric O_3. OH plays a vital part in photochemistry. In order to fully understand the chemistry of the atmosphere a complete understanding of sources, sinks and the cycling of OH is required. These reactions are summarised in figure 1.1.1 and a more detailed review of radical chemistry in the tropospheric boundary layer is available in the review by Monks (2005).

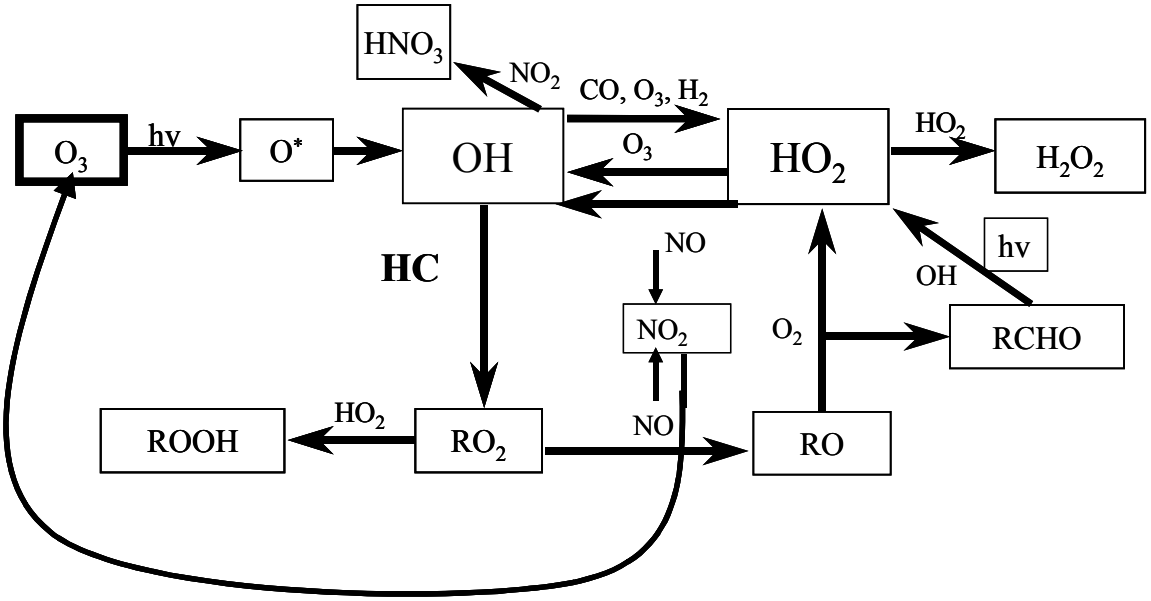

Figure 1.1.1 Key atmospheric reactions of OH, HO2 and RO2 radicals in the atmosphere (Emmerson et al., 2005)

In clean atmospheric conditions where NO_X concentrations are low, the most important source of OH is usually the photolysis of O_3 by light at wavelengths of ≤ 340 nm. This photolysis reaction produces oxygen atoms in an excited state (O^1D), which then react with water vapour to produce two OH radicals. Other photolytic reactions can yield OH radicals atmospheres. Where HONO builds up over night, in the presence of high concentrations of NO_2, photolysis occurs at wavelengths of light below 400 nm. This is important at dawn, before shorter wavelengths of light necessary to photolyse O_3 reach the lower troposphere, and can lead to an increase in early morning OH concentrations while O_3 concentrations are suppressed. Other photolysis reactions that can affect radical production are the photolysis of carbonyls, e.g. formaldehyde (HCHO) photolysis leads to the production of two HO_2 radicals. This process tends to occur more towards the end of the day when carbonyls (as secondary pollutants) have attained higher concentrations and can continue after ozone photolysis has ceased (Alicke et al., 2003).

The OH and HO_2 radicals also undergo propagation reactions leading to the creation of other radical species. For example, OH reacts with CO or O_3 to produce HO_2, but

it can also react with hydrocarbons to form RO_2. RO_2 undergoes propagation reactions when NO is present to form HO_2, which can undergo a further reaction with O_3 in clean atmospheres to reform OH. This reaction can also occur in polluted atmospheres, with HO_2 reacting with NO to form OH.

Another important radical feedback mechanism in forested environments is through the reactions of ozone with biogenic species such as monoterpenes. Monoterpenes are natural compounds emitted from many species of vegetation in forests. Important monoterpene species include alpha-pinene and beta-pinene (pine forest smell), limonene (citrus smell), camphene, carene and gamma-terpinene. These species are extremely reactive and react with both OH and O_3. However, when monoterpenes react with O_3, OH, HO_2 and RO_2 radicals are formed. Depending on the OH and O_3 concentrations, monoterpenes can be a net source or sink of radicals. For more details refer to Atkinson et al., (1994). Such reactions can also provide a important source of radicals at nighttime, when the usual photolytic sources are absent.

In clean atmospheres, the main sinks of HO_X (total of OH and HO_2) are the self-reactions and cross-reactions of peroxy and hydroperoxy radicals. However, in polluted atmospheres most of the HO_x species are lost through the reactions of OH with NO_2, leading to the formation of nitric acid (HNO_3).

1.3 Previous Studies

There have now been many studies comparing modelled to measured radical concentrations. However, this section focuses on those carried out where biogenic emissions had a large influence. For a wider review of other campaigns, the reader is referred to Heard and Pilling (2003).

PROPHET (Program for Research on Oxidants: Photochemistry, Emissions and Transport) campaigns in 1997 and 1998 used ground based samples taken at a forest site in Michigan, where the diurnal differences and night time decay of VOC's were

studied (Hurst et al., 2001). A higher than expected decay rate of isoprene and examined different explanations for the phenomena were proposed including chemical (with OH) and/or physical explanations (involving vertical mixing). The chemical explanation through reaction with isoprene require a source of OH radicals at night, also the predictions for removal by OH were often much higher than that possible from the observed rate (Hurst et al., 2001). The measurements needed to explore the vertical mixing explanation were not made during the study. Further support is given to the chemical explanation by the unusually high levels of hydroxyl radicals that were recorded at the site at night, which could potentially result from the reaction with ozone with unmeasured, but highly reactive olefinic terpenoid compound that is emitted at night (Faloona et al., 2001). A major problem with this hypothesis is that the site where the observations were made was mainly deciduous trees, whereas terpenoids are emitted by coniferous forest.

The data gathered in the PROPHET 1997 investigation were analysed in a model, which was used to predict the concentrations of radical species at the site and to investigate the diurnal variations (Mihele et al., 2003). Sillman (2002), used a 1-dimensional Langrangian model to accurately reproduce the isoprene concentrations including the night time decay. The model also predicted that the nighttime OH would only be found near the surface, linking its presence to nighttime emissions and surface processes, which agrees with the earlier prediction of its source being a terpenoid species emitted at night (Sillman, 2002). One major outcome of the PROPHET study was the conclusion that the current understanding of OH, HO_x and radical chemistry was incomplete. The flaws were further exposed when the model predictions of OH and HO_2 made with a photochemical box model are compared to the observed data from the site (Tan et al., 2001). The poorest agreement between model and observed values was seen for OH, where the mean value for the observed concentration of OH was found to be 2.6 times greater than the predicted values. The HO_2 concentrations generally showed a good level of agreement between the model and observations (Tan et al., 2001). Due to the under prediction of the concentration of OH in the model, the HO_2/OH ratio was over predicted, although this ratio was more accurately predicted by the Harvard photochemical trajectory model (PCTM) used by Sillman (2002). The PCTM used predicted levels of VOCs and NO_x, whereas the constrained photochemical box model used actual measured concentrations of

isoprene and NO_x. When the predicted values of isoprene used in the PCTM were compared with the observed values used in the box model, the predictions were found to be several times lower and the NO_x predictions to be several times higher causing doubt over the results from the PCTM (Sillman 2002).

In order to try and make the box model agree with the observations, the hypothesised unmeasured VOC's were factored into the model (Tan et al., 2001). These changes to the model created better agreement between the model and the observations, but the model still under predicted the concentrations of OH by a factor of 1.5 (Tan et al., 2001). The PROPHET campaigns indicated that atmospheric chemistry in forested areas needed further investigation.

Another project that investigated OH and HO_2 radical chemistry was the AEROBIC97 campaign, which examined a forested site in North-West Greece (Carslaw et al., 2001). The observed data showed the expected diurnal variations in OH and HO_2 and similarly to other studies of radical chemistry at forested sites, the concentration of OH was under predicted by about 50%. The modelled HO_2 also deviated from the observed values, with two days of under predicted HO_2 and then two days of significantly over predicted HO_2 (Carslaw et al., 2001).

The ORION99 (Observations at the remote island of Okinawa) study in Okinawa was disturbed by severe weather conditions, but observations were possible on several days, along with model predictions (Kanaya et al., 2001). The predictions were made using a time dependant boundary layer box model, a steady state model where predictions for OH, HO_2 and RO_2 were made every ten minutes (Kanaya et al., 2001). The ORION99 predictions for the daytime concentrations of HO_2 were in good agreement with the observed values, but again the OH predictions were underestimated. Further analysis of the results from the ORION99 project showed that there was also an over prediction of the HO_2/OH ratio. This over prediction was at its highest when NO concentrations were at their lowest (Kanaya et al., 2001).

The New England Air Quality Study 2002 (NEAQS2002) (Warneke et al, 2004) investigated the fate and lifetimes of both biogenic and anthropogenic VOCs from reactions with the three major oxidants of VOC; OH, O_3 and NO_3. The study found that the VOC's had the longest lifetime at dusk when the OH and NO_3 radicals were at their lowest concentrations (Warneke et al., 2004). However, the measurements for this study were conducted on a boat at sea, some distance away from the forests where the emissions came from; dusk was the only time at which substantial quantities of the short lived compounds could be transported in large enough quantities to be detected (Warneke et al., 2004). One other major finding of the study was that the rate at which isoprene decayed was only 30% lower at night than during the day. This was an important finding as the day time isoprene decay was mainly due to oxidation with OH, generally thought of as a daytime oxidant.

There have been several other studies conducted to investigate the relationship between OH, HO_2, NO_x, VOC's and O_3. The Southern Oxidants Study which was conducted in Tennessee made similar findings to the PROPHET study in that the observed nighttime concentrations of OH were much greater than the modelled predictions (Martinez et al., 2003). This study suggested similar reasons to the PROPHET study about the gaps in the understanding of the chemistry involved in the sources and sinks of OH and HO_2. However, Martinez et al. (2003) also questioned the sampling process. The hypothesised problem with the Laser Induced Fluorescence (LIF) technique is that the gases that are sampled are cooled and then warmed very quickly which could lead to weakly bound OH groups on other molecules "falling off" and being detected as OH radicals. OH is a difficult species to measure in the atmosphere as it has a life time of only 1 s in the atmosphere, but the FAGE (fluorescence assay by gas expansion) method is generally regarded to have excellent selectivity and sensitivity when measuring OH lifetime measurements. (Heard et al., 2003). The measured and calculated OH decay rates showed good correlation, although the calculated decay rate was significantly lower than the measured rate as was reported in the findings by Martinez et al. (2003).

Ren et al., (2005) reported modelled predictions of OH and HO_2 that agreed well with the observed values, for a campaign conducted in a semi-polluted atmosphere as

opposed to the clean air conditions of NEAQS, PROPHET and ORION. This study used the same LIF technique as the ORION and Southern Oxidants study, but also used a Chemical Ionisation Mass Spectrometry (CIMS) technique. This was used to measure the combined HO_2 and RO_2 mixing ratio. The Regional Atmospheric Chemistry Model (RACM) was used to reproduce the observed OH, HO_2 and (HO_2 + RO_2) concentrations. This study found that constant speciated VOC measurements do not have to be constantly made throughout the campaign to be able to produce the chemistry in some environments, but it can lead to better understanding of radical budgets in the atmospheric chemistry (Ren et al., 2005). Another outcome of this study was the finding that combined observed HO_2 and RO_2 concentrations does not increase as quickly as expected with increasing NO, although the measured-to-modelled ratios for both HO_2 and (HO_2 + RO_2) were significantly greater than 1 when measured NO was over 1ppbv (Ren et al., 2005).

A field campaign conducted in the Pearl River delta in China, aimed to quantify the concentrations of atmospheric OH and HO_2 through direct measurements (Hofzumahaus et al., 2009). The project reported findings of OH concentrations three to five times greater than were expected to be found. The results from this study lead to the proposition of a new reaction pathway in the production of OH, independent of reactions with NO that can degrade pollutants while not producing O_3.

In all these studies in atmospheric radical chemistry, none of them have managed to get good agreement on all the observations and predictions. Good correlation in the relationships of these species has been seen, but there are many areas where models over predict or under predict concentrations and decay rates which shows there is still a lot of atmospheric radical chemistry that needs to be discovered or understood (Monks 2005).

1.4 Updated Isoprene Mechanism

Though model to measured agreement has improved for very polluted and very clean atmosphere as more field campaigns have been held over the last 20 years, forested regions remain a particular challenge. Suggestions began to be made that in areas influenced by isoprene emissions (common in forests), deficiencies in the isoprene degradation mechanisms in the model used to investigate field campaigns were responsible (Lelieveld et al., 2008, Peeters et al., 2010, Hofzumahaus et al., 2009)

Several authors suggested that changes to the isoprene degradation mechanism were necessary. Stone et al., (2011) Summarises the 4 main suggestions that have been postulated to explain the discrepancy based on various ground-based and aircraft campaigns.

The first of these proposed changes to the production of OH radicals was the proposed idea of a reaction between $RO_2 + HO_2 \rightarrow OH$ (Hasson et al., 2004). The reactions between HO_2 and RO_2 radicals represent an important sink for HO_x radicals. The product of this reaction depends on the identity of the R-group. For more complex R-group species there is a higher branching ratio. The products from the degradation of these complex chemicals can lead to the formation of O_3, which in turn will lead to the production of more OH. This process was found to have a low impact in low NO_x conditions, but a greater effect in aged air where the NO_x concentration has built up (Lelieveld et al., 2008).

The second proposed change is the idea of an unknown species 'X' that reacts with HO_2 to form OH (Hofzumahaus et al., 2009). This idea was first proposed during the analysis of the investigation into OH and HO_2 in the Pearl River Delta campaign. The idea of the unknown species 'X' was a species that may be a direct emission from a strong source that would be required at noon and continue to be emitted through the afternoon. The current understanding of OH recycling is that OH can only be recycled through reactions of NO, or the oxidation of VOCs and CO with OH. The oxidation reactions of OH with VOCs produce one to three O_3 molecules for every OH + VOC reaction. The findings through the field campaign determined that the

unknown species 'X' would have to be able to recycle OH with forming ozone determining that the species 'X' could not be a VOC (Hofzumahaus et al., 2009).

The third OH recycling method was proposed by Paulot et al., (2009) through the formation of OH from epoxides formed from the degradation of isoprene. The proposed recycling method depended on the location on the isoprene molecule where the OH radical oxidises the isoprene. The formation of ISOPOOH molecules allows further reactions with OH forming and epoxide (IEPOX) and recycling the OH radical (Paulot et al ., 2009).

The final mechanism for the recycling of HO_x in pristine tropical conditions has been proposed by Peeters et al. (2009). New reaction pathways have been proposed for the oxidation of isoprene by OH and subsequent reactions with O_2 that would lead to a larger yield of OH than with the mechanism currently in the MCM v3.1 (Archibald et al., 2010).

The new scheme proposes that through isomerisation and oxidation of the new isomer products create a new set of intermediate products is created. It is the oxidation and reaction with O_2 of the new intermediate products that recycles and generates the new OH giving a greater yield than previous mechanisms (Archibald et al., 2010).

The newly proposed Peeters scheme for the reaction of isoprene starts with the initial step of the addition of OH. The structure-activity relationship (SAR), used to predict proportion of OH reactivity at each of the four unsaturated C-atoms (1-4 in figure 1.4.1), showed different proportions to those currently used in the MCM 3.1 (Peeters et al., 2009): [60% 1-OH, 30% 4-OH, 5% 2-OH and 5% 3-OH]

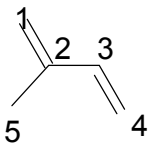

Figure 1.4.1 Isoprene molecule showing the 5 carbon atoms.

The two major adducts 1-OH and 4-OH go on to form 6 different peroxy radicals following the addition of O_2 depending on the the structure of the adduct and the site of addition. In MCMv3.1, these peroxy radicals would then react with HO_2 to form peroxides other RO_2 to form a variety of products, or NO to eventually yield HO_2. (Peeters et al., 2009)

However, Peeters et al., (2009) suggests that 4 of the peroxy radicals can undergo internal rearrangement followed by decomposition to form new products. In this way the1-OH-2-$OO^{\bullet}$ peroxy radicals yield OH, CH_2O and methylvinylketone (MVK). Similarly the 4-OH-3-$OO^{\bullet}$ yields OH, CH_2O and methacroleine (MACR) (Peeters et al., 2009). These rearrangements are competitive and perhaps even quicker than the original degradation and provide an extra route to OH formation (Peeters et al., 2009)

In addition to these reactions, the 2-1-OH-4-$OO^{\bullet}$ and 2-4-OH-1-$OO^{\bullet}$ peroxy radicals can both undergo internal rearrangement followed by decomposition to produce HO_2 radicals and unsaturated hyproperoxy-aldehydes (HPALD). These HPALDs are speculated to the dissociate and generate further OH radicals (Peeters et al., 2009)

Peeters et al., (2009) found that 70% of isoprene-oxidation chemistry passed through the new chemistry for aircraft observations over Amazonia (40 ppt NO_2 and 20 ppt NO), but note that as NO approaches 1ppb, OH and HO_2 yields from the new chemistry can decrease and other reaction routes become more competitive. This chemistry is currently speculative, based entirely on theoretical predictions. The rate coefficients are prone to uncertainty, as pointed out by Peeters et al., (2009) themselves, as well as other authors (Nguyen et al., 2010. Stavrakou et al., 2010.Stone et al., 2011). However at the present time it represents the best mechanism for isoprene degradation over rainforests at present (Stone et al., 2011) and is adapted in the current work as described in Archibald et al., (2010) detailed in subsequent chapters (Chapter 3.)

1.5 Structure of the Thesis

This thesis is set out in the following order. Chapter 2 discusses the experiment al and modelling techniques employed, whilst chapter 3 describes the model sensitivity tests. Chapters 4 and 5 provide details on the model results for the two OP3 campaigns investigated for this project. Finally chapter 6 provides a synthesis of the information in chapters 4 and 5, as well as comparing the results with previous studies, providing some recommendations for future studies and overall conclusions.

Chapter 2. Experimental

2.1 Modelling

2.1.1 Introduction

Numerical models are being used more readily to help describe complex processes across all areas of science. A numerical model uses a series of mathematical equations that attempt to describe processes that are observed in the field or under laboratory conditions. Through these equations, a simulation of a natural system can be created. The equations in the model can be changed to gain an understanding of how the system works and what effects changes on the system may have. Such understanding fills in gaps in our knowledge, where measurements are not always possible or practical.

Atmospheric models are vital tools in furthering our understanding of the chemistry in the atmosphere. They allow new ideas and concepts to be developed, tested and validated. For instance, evaluation of the kinetics of shorter lived species has permitted models to be constructed that describe the individual chemical reactions occurring in the atmosphere in great detail. These models typically contain large sets of chemical reactions to simulate the chemistry in the atmosphere to the extent that our understanding allows.

One major use of models containing such chemical mechanisms is to test and develop theories on the atmospheric chemistry of short-lived radical species such as OH. The measurement of OH in the atmosphere requires very accurate techniques due to its short lifetime, typically less than 1 second. Comparisons between measured and modelled OH concentrations provide effective tests of our understanding of fast photochemical reactions.

When studying the atmosphere there are several different types of models that can be used and for different tasks. These different tasks include diagnosis and prognosis, with diagnostic models being used to validate the understanding of a chemical system and a prognostic model being used to predict what effect changes to a system may have in the future. Once a model is validated, it can be used to monitor and evaluate the system in the future, removing the need for and expense of large amounts of analytical equipment to constantly monitor that system.

2.1.2 Box Models

There are many different types of numerical models that can be used to evaluate the understanding of a system. The selection of a different model type will depend on the spatial and temporal resolution of interest. A box model aims to simplify a complex system to provide information on the most important chemical species within it. The box model describes the atmosphere as a box within which the concentration of chemical species can be assumed to be uniform (so the air is well mixed). The concentration of each of the chemical species within the box can change over time as species are emitted into or removed from the box, or react chemically with each other to form new products. The box is assumed to be set at a specific location on the planet with the dimensions of the box being set to reflect the system being investigated. This type of model is best suited to studying the chemical systems at a fixed location, rather than the evolution of an air mass as it travels through space. However, as transport processes are not considered in such models, it is important that key species within the box are set to realistic concentrations. In this study, the concentrations of atmospheric species measured during two field campaigns in Malaysia have been used to constrain a box model, to ensure that the concentrations are representative of the local area. The degradation chemistry of these species has been represented in the model using the Master Chemical Mechanism (MCM).

2.1.3 Master Chemical Mechanism

The Master Chemical Mechanism (MCM) is a near-explicit chemical mechanism that describes the gas phase degradation of Volatile Organic Chemicals (VOCs) and the production of the resulting secondary species, including OH, HO_2, peroxy radicals, ozone and many more (Jenkin et al., 1997). The concept behind the MCM is the use of recent kinetic data relevant to the oxidation of VOCs to construct a near-explicit series of degradation mechanisms following a predefined protocol. Rate coefficients are updated regularly based on recent laboratory work. For rate coefficients and reaction pathways that remain undetermined structure-activity relationships (SARs) are used (Peeters et al., 1997).

Such a protocol allows the construction of comprehensive and continuous degradation schemes for a range of VOCs through to final products of CO_2 and water. The degradation schemes take into consideration many different types of reactions

including initiation reactions by OH and NO_3 radicals, and O_3. Initiation also includes photolysis where relevant, for example aldehydes. The subsequent reactions of intermediate organic products and peroxy radicals are also considered as defined by the protocol (Jenkin et al., 1997)

In some cases the MCM protocol dictates that product channel chemistry has been simplified to limit the number of product channels, the number of product channels is restricted to a maximum of 4. Also any channel that represents less than 5% of the overall reaction is removed, and the remaining channels are proportionally scaled up to maintain the overall mass balance.

The initial reaction of OH with VOCs follows the general patterns shown in the reaction (R2.1a, b, c)

$$C_2H_6 + OH (+ O_2) \rightarrow C_2H_5O_2 + H_2O \quad \text{(alkanes)(R2.1a)}$$

$$C_2H_4 + OH (+ UV) \rightarrow OHCH_2CH_2O_2 \quad \text{(alkenes)(R2.1b)}$$

$$CH_3CHO + OH \rightarrow CH_3CO_3 \quad \text{(aldehydes)(R2.1c)}$$

Rate coefficient data for the reactions of O_3 with VOCs in the MCM are taken from reviews by Atkinson et al., (1994) and Aschmann et al., (2003). O_3 only reacts with species containing a double bond such as alkenes and terpenes. The reaction mechanisms for O_3 follow a general pattern, with the addition of ozone to the double bond initially forming an energy-rich ozonide intermediate (Jenkin et al., 1997). The MCM protocol assumes that the ozonide degrades equally to form a Crigee biradical and a carbonyl compound (R2.2a, R2.2b).

$$O_3 + RR^1C{=}CR^2R^3 \rightarrow RC(O)R^1 + [R^2C(OO)R^3] \quad 50\% \quad \text{(R2.2a)}$$

$$O_3 + RR^1C{=}CR^2R^3 \rightarrow R^2C(O)R^3 + [RC(OO)R^1] \quad 50\% \quad \text{(R2.2b)}$$

The reaction coefficients for the reactions of NO_3 and VOCs was reviewed by Atkinson (1991, 1994) and Wayne (1991). The NO_3 reactions with alkenes also follow a general pattern (R2.3a, R2.3b), unlike the reactions with ozone there is not an equal split in the reaction channels.

$$NO_3 + CH_2{=}CHR \rightarrow CH_2(ONO_2)CHR \ (65\%) \quad \text{(R2.3a)}$$

$$NO_3 + CH_2{=}CHR \rightarrow CH_2CH(ONO_2)\ R \ (35\%) \quad \text{(R2.3b)}$$

Photolysis reactions are considered for photosensitive organic and inorganic species. Many photosensitive species are emitted into the troposphere or formed through degradation products. The photolysis rate is calculated as a function of the solar-

zenith angle and using equation (E2.1) (Table 2.1.1), by optimizing the values of the parameters l, m and n (Jenkin et al., 1997).

$$J = l(\cos x)^m \exp(-n \sec x) \quad \text{(E2.1)}$$

Table 2.1.1 Photolysis calculations set in the MCM.

Reaction code	Reaction	Equation
J1	$O_3 = O^1D$	6.073×10^{-5} *(COSX@(1.743))*EXP(0.474*SECX)
J2	$O_3 = O$	4.775×10^{-4}*(COSX@(0.298))*EXP(-0.080*SECX)
J3	$H_2O_2 = OH + OH$	1.041×10^{-5}*(COSX@(0.723))*EXP(-0.279*SECX)
J4	$NO_2 = NO + O$	1.165×10^{-2}*(COSX@(0.244))*EXP(-0.267*SECX)
J5	$NO_3 = NO$	2.485×10^{-2}*(COSX@(0.168))*EXP(-0.108*SECX)
J6	$NO_3 = NO_2 + O$	1.747×10^{-1}*(COSX@(0.155))*EXP(-0.125*SECX)
J7	$HONO = OH + NO$	2.644×10^{-3}*(COSX@(0.261))*EXP(-0.288*SECX)
J8	$HNO_3 = OH + NO_2$	9.312×10^{-7}*(COSX@(1.230))*EXP(-0.307*SECX)

The stabilised peroxy radical intermediates are treated through several different reaction processes in the mechanism. These include reactions with NO, NO_2, NO_3, HO_2 and other peroxy radicals ($R'O_2$). The reactions between NO and peroxy-radicals follow one of two channels (R2.6a, R2.6b).

$$RO_2 + NO \rightarrow RO + NO_2 \quad \text{(R2.6a)}$$

$$RO_2 + NO \rightarrow RONO_2 \quad \text{(R2.6b)}$$

The proportions of the two different reaction channels were taken from reviews of laboratory experiments (Jenkins et al., 1997). Where data were not available, values were calculated using methods recommended by Carter and Atkinson (1989). Reactions of peroxy-radicals with NO_2 produce relatively stable peroxy nitrates (R2.7). The rate parameters for the reactions of NO_2 and peroxy radicals are taken from Lightfoot *et al*. (1992):

$$RO_2 + NO_2 (+M) \leftrightarrow ROONO_2 (+M) \quad \text{(R2.7)}$$

Reactions between peroxy radicals and NO_3 are assumed to proceed through one single reaction (R2.8). The reaction coefficients for the reactions between NO_3 and peroxy radicals are taken from the data available in the review by Lightfoot *et al*. (1992).

$$RO_2 + NO_3 \rightarrow RO + NO_2 \quad \text{(R2.8)}$$

The reactions of RO_2 and HO_2 can follow one of three initial channels. Reaction coefficient data for these three channels were taken from reviews of laboratory experiments (Atkinson et al., 1997). Where experimental data are not available estimates are used which use generic analogues. The general patterns for the reaction channels are shown in (R2.9a, R2.9b, R2.9c).

$$RO_2 + HO_2 \rightarrow ROOH + O_2 \quad \text{(R2.9a)}$$

$$RO_2 + HO_2 \rightarrow ROH + O_3 \quad \text{(R2.9b)}$$

$$RO_2 + HO_2 \rightarrow R'CHO + H_2O + O_2 \quad \text{(R2.9c)}$$

The reactions between peroxy radicals (RO_2) and other peroxy radical species (RO_2 or $R'O_2$) produce reactions that produce a large number of reaction channels. (R2.10 a-e).

$$RO_2 + RO_2 \rightarrow RO + RO + O_2 \quad \text{(R2.10a)}$$

$$RO_2 + RO_2 \rightarrow R'CHO + ROH + O_2 \quad \text{(R2.10b)}$$

$$RO_2 + R'O_2 \rightarrow RO + R'O + O_2 \quad \text{(R2.10c)}$$

$$RO_2 + R'O_2 \rightarrow R''CHO + R'O + O_2 \quad \text{(R2.10d)}$$

$$RO_2 + R'O_2 \rightarrow R''CHO + R'OH + O_2 \quad \text{(R2.10e)}$$

Due to the large number of possible RO_2 radicals that would be generated in a detailed chemical mechanism, it is important to be able to simplify these reactions as it would be unrealistic to represent all these reactions in full detail. In order to achieve such a simplification a single "RO_2" parameter is defined, which is the sum of all the peroxy radical concentrations, excluding HO_2. The different permutations of the reactions of "RO_2" are simplified to three main reaction channels (R2.11a-c). The branching ratios of these reactions are determined according to the structure of the radical. An example of this for CH_3O_2 is shown in R2.12 also showing the branching ratios.

$$RO_2 \rightarrow RO \quad \text{(R2.11a)}$$

$$RO_2 \rightarrow R'CHO \quad \text{(R2.11b)}$$

$$RO_2 \rightarrow ROH \quad \text{(R2.11c)}$$

$$CH_3O_2 \rightarrow CH_3OH \quad 33\% \text{ (R2.12a)}$$

$$CH_3O_2 \rightarrow CH_3O \quad 33\% \text{ (R2.12b)}$$

$$CH_3O_2 \rightarrow CH_3O^{\cdot} \quad 33\% \text{ (R2.12c)}$$

Table 2.1.2. Current rate coefficients used in the MCM for reactions between VOCs and OH**.**

VOC	Generic rate coefficient (VOC + OH)
Isoprene	2.54×10^{-11}*EXP(410/Temperature)
Alpha-pinene	1.20×10^{-11}*EXP(444/ Temperature)
Camphene	5.33×10^{-11}
Gamma-terpinene	1.7×10^{-11}
Limonene	4.28×10^{-11}*EXP(401/ Temperature)
Ethene	7.00×10^{-29}*(TEMP/ Temperature)
Ethanal	5.55×10^{-12}*EXP(311/ Temperature)
Methanol	6.01×10^{-18}*TEMP@2*EXP(170/ Temperature)

Through the initial reactions of the VOCs by photolysis and oxidation and the subsequent reactions of the peroxy radicals, a large number of intermediate products are formed that must be included in the degradation process. These intermediates include: carbonyl compounds, organic nitrates ($RONO_2$), peroxy nitrates ($ROONO_2$) carboxylic acids (RC(O)OH), percarboxylic acids (RC(O)OOH) and alcohols (ROH).

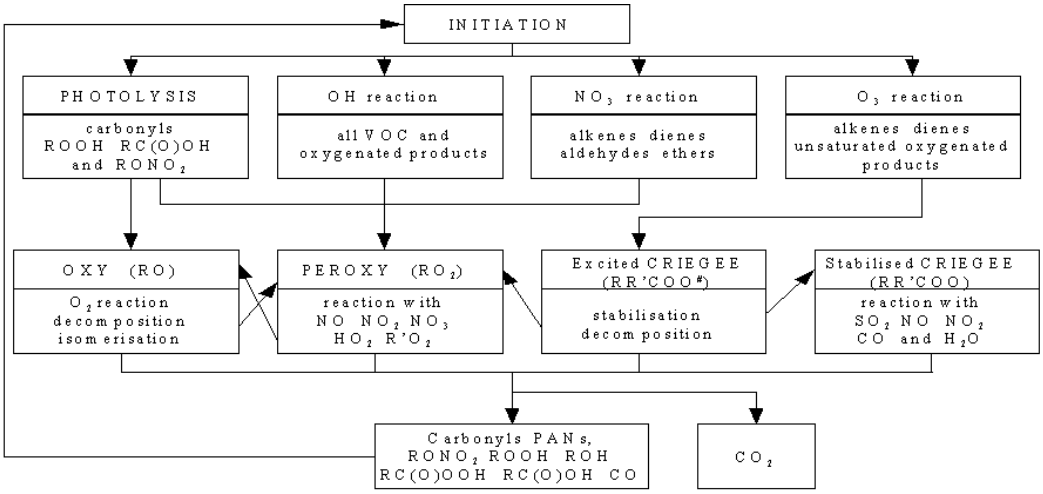

Figure 2.1.1. A step-by-step break down of how the MCM processes and simulates reactions of species that are used in the model.

To simulate the degradation of a "relatively simple" VOC such as butane the mechanism required contains 538 reactions and 178 species to fully explain its complete degradation (Pinho et al., 2005). For larger and more complicated species such as aromatics and monoterpenes even more steps are needed to completely

explain the full oxidation of the species. The total oxidation of α and β pinene requires over 1550 reactions involving approximately 520 species (Jenkin et al., 2004). As with the simpler VOCs the oxidation is initialised through the reactions of OH, O_3 and NO_3 then propagated through the reactions of oxy and peroxy radicals with the reactions being terminated by forming stable organic species or CO_2. However, larger VOCs will produce a larger number of and more complex intermediate products.

2.1.4 Model Construction

In the process of constructing the model, it was decided to only include the most important VOCs measured during the field campaigns in the model. By not including the complete set of all 20 measured VOCs, the computing power needed to run the model is reduced, shortening the time it takes to run and improve the efficiency. All rate coefficients have been updated with the most recently available literature according to the NIST and IUPAC (2006) reports.

The importance of each VOC measured at the study site in terms of reactions with the oxidising species OH, O_3 and NO_3 was quantified for each campaign. By using mean values of the concentrations of the VOCs measured at the site, and reaction rates for the measured VOCs with the relevant oxidising species, it was possible to calculate the percentage loss of oxidant owing to each individual VOC during the campaign. Such a process permits identification of the most reactive organic species. Such species can then be included in a tailored model, which means only a subset of the MCM is required.

The reactions with OH show that the most important loss route is through reaction with isoprene (Table 2.3). Isoprene is over three times more reactive with OH than the next VOC species (γ-terpinene) during the daytime and of similar reactivity during the night (Table 2.3). This indicates that isoprene reactions are likely to dominate the oxidising chemistry of the area, from the VOC species that were measured at the site. The ten most reactive species reactions accounted for 98% of the OH loss through reaction with measured VOCs. Out of these ten species three are not currently included in the MCM; gamma-terpinene, camphene and limonene.

Table 2.3. Percentage loss of measured VOCs from reactions with OH during the campaign 2nd phase. Daytime is defined as the period from 07:00 to 19:00 h and nighttime is defined as the period from 19:00 to 07:00 h.

Ranked Importance	VOC Species	Overall Loss	Daytime Loss	Nighttime Loss
1	Isoprene	60.2	66.5	30.9
2	γ-terpinene	17.8	15.0	32.6
3	Limonene	8.2	7.4	10.7
4	Iso-butene	4.9	3.6	10.2
5	Camphene	2.3	2.3	2.3
6	Methanol	1.4	1.2	2.7
7	Acetaldehyde	1.0	0.8	2.2
8	Propene	1.0	0.9	1.8
9	α-pinene	0.9	0.7	1.0
10	Ethene	0.6	0.4	1.6
11	Iso-butane	0.5	0.4	1.1
12	δ-3-carene	0.3	0.2	0.6
13	n-butane	0.3	0.2	0.6
14	Propane	0.2	0.1	0.3
15	Iso-pentane	0.1	0.1	0.4
16	n-pentane	0.1	0.1	0.3
17	Acetylene	0.1	0.1	0.2
18	Ethane	0.1	0.1	0.2
19	Acetone	0.1	0.1	0.1
20	Cyclopentane	0.0	0.0	0.0

The oxidising reactions of the VOCs with O_3 and NO_3 show different results to the reactions with OH. In the reactions with O_3 and NO_3 it is γ-terpinene that is the most reactive species during daytime and nighttime, being over 7 times more reactive with NO_3 (Table 2.5), and almost twice as reactive with O_3 as isoprene (Table 2.4).

Table 2.4. Percentage loss of measured VOCs from reactions with O_3 during the campaign 2nd phase. Daytime is defined as the period from 07:00 to 19:00 h and nighttime is defined as the period from 19:00 to 07:00 h.

Ranked Importance	VOC Species	Overall Loss	Daytime Loss	Nighttime Loss
1	γ-terpinene	40.2	37.0	53.9
2	Limonene	27.3	27.1	26.2
3	Isoprene	23.1	27.9	8.6
4	α-pinene	4.0	3.5	3.5
5	Iso-butene	3.2	2.6	4.9
6	Propene	1.0	1.0	1.4
7	Ethene	0.3	0.2	0.6
8	δ-3-carene	0.3	0.2	0.5
9	Camphene	0.1	0.1	0.1

Table 2.5. Percentage loss of measured VOCs from reactions with NO_3 during the campaign 2nd phase. Daytime is defined as the period from 07:00 to 19:00 h and nighttime is defined as the period from 19:00 to 07:00 h.

Ranked Importance	VOC Species	Overall Loss	Daytime Loss	Nighttime Loss
1	γ-terpinene	59.1	57.2	65.9
2	Acetone	16.8	16.2	18.6
3	Limonene	11.8	12.3	9.5
4	Isoprene	8.4	10.7	2.6
5	*a*-pinene	2.0	1.8	1.4
6	Iso-butene	0.6	0.6	0.8
7	δ-3-carene	0.6	0.5	0.8
8	Camphene	0.6	0.7	0.3

Gamma-terpinene is shown to be the most important VOC with all three oxidising species during the nighttime, with a greater percentage loss occurring compared to the daytime. Isoprene is responsible for a lower percentage loss at nighttime for all three oxidising species. The release of many biogenic species from the flora depends upon factors such as temperature and sunlight, causing a diurnal variation in the biogenic species concentrations. The daytime average concentrations for isoprene and gamma-terpinene were 1040 pptv and 132 pptv respectively, whereas the average nighttime concentrations were 140 pptv and 84 pptv, showing that the nighttime concentration of isoprene is reduced to a greater extent when compared to the gamma-terpinene concentration (figure 2.2). This diurnal cycle effect, combined with the reactivity of the VOCs with the oxidising species, indicates that the organic chemistry is not solely dominated by isoprene even though it is found in concentrations much greater than any of the other VOCs.

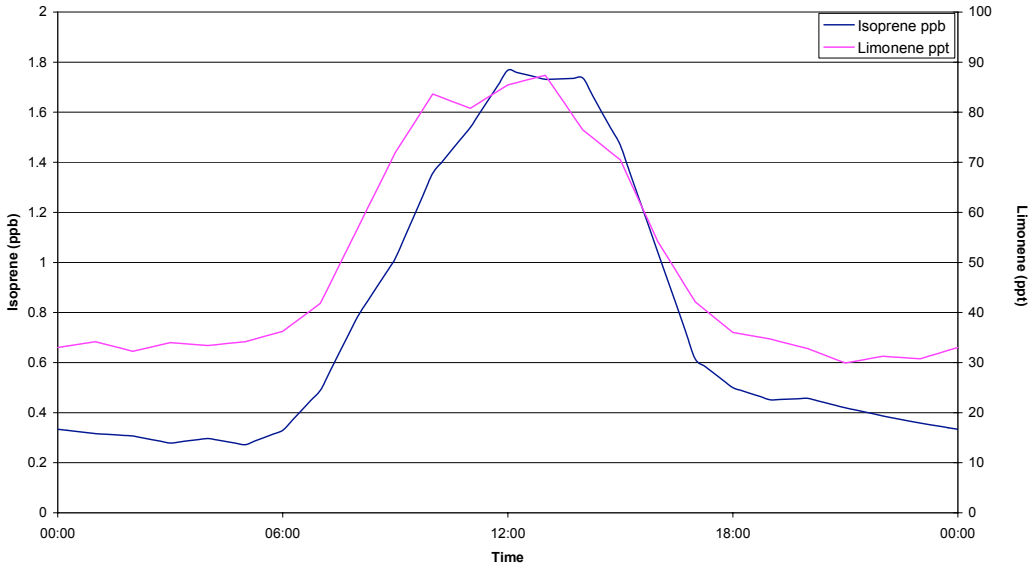

Figure 2.2. Diurnal variation in isoprene and limonene for average concentrations in the second phase of the field campaign.

A similar exercise was repeated for the first phase of the campaign, but there was much less comprehensive coverage of VOC data. From the data that were available, the ten most reactive species during the first phase of the campaign were found to be the same as the ten most reactive species in the second phase (table 2.6). The degree of reactivity seen in the VOCs in the first phase was found to be very similar with only some marginal differences in the order of the species and reactivities. Isoprene was still the most dominant species in the reactivity with OH, with γ-terpinene and limonene again the next most reactive.

Table 2.6. Ten most reactive organic species from reactions with OH during the first phase of the campaign

Ranked Importance	VOC Species	Overall Loss	Daytime Loss	Nighttime Loss
1	Isoprene	63.6	70.1	29.8
2	γ-terpinene	16.5	12.5	34.6
3	Limonene	7.0	6.7	11.7
4	Iso-butene	4.5	3.2	10.2
5	Camphene	2.0	2.3	2.3
6	Methanol	1.6	1.2	2.5
7	Propene	0.9	0.8	2.0
8	Acetaldehyde	0.8	0.9	1.4
9	α-pinene	0.7	0.7	1.0
10	Ethene	0.6	0.3	1.3

Based on these results, it was possible to produce a tailored model for the OP3 project using a subset of the complete MCM. The selected VOCs were; isoprene, γ-terpinene, limonene, camphene, iso-butane, methanol, propene, acetaldehyde, α-pinene and ethane. The MCM website (http://mcm.leeds.ac.uk/MCM) allows the user to customise the mechanism to include selected degradation schemes as well as a comprehensive inorganic scheme and photolysis rate calculations. The user has to add relevant deposition reactions, gas to particle conversions and surface interactions if required (Emmerson et al., 2006)

Most of the required VOC degradation schemes were available in the MCM website. However schemes for limonene, gamma-terpinene and camphene are not currently available. A developmental limonene scheme was made available for this work (M. Jenkins, through personal communication). The developmental scheme was added into the customised MCM subset, including all the new species and their subsequent degradation products that were defined in the model.

Gamma-terpinene and camphene do not have degradation schemes in development, so they are represented in the model by the use of analogue species. This required VOCs with similar structures and kinetics to camphene and gamma-terpinene being identified. These analogue species needed to have existing degradation mechanisms in the MCM. This limited the choices of analogues to α-pinene, β-pinene and limonene, the terpene mechanisms that were already available. From these it was

possible see that structurally, gamma-terpinene was most similar to limonene and camphene to β-pinene (table 2.7)

The key reaction coefficients were also similar for these pairings. The similarities between these species derive from the numbers of double-bonds in the molecules and the location of these bonds in the structure of the compounds (Table 2.6).

Table 2.7. Comparison between camphene, γ-terpinene and potential analogues that can be used in the OP3 Model.

Monoterpene	**Structure**	**kOH x 10^{-10} s^{-1}**	**kO_3 x 10^{-16} s^{-1}**	**kNO_3 x 10^{-11} s^{-1}**	**OH yield from O_3 + monoterpene**
Limonene	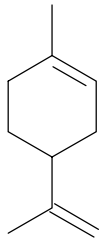	1.71	2.00	1.22	0.86
γ-terpinene	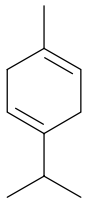	1.77	1.40	2.90	0.81 ±0.11
β-pinene	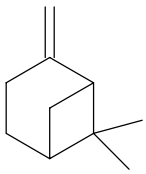	0.24	0.15	0.25	0.35
Camphene	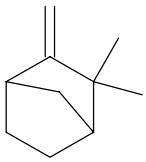	0.53	0.01	0.07	≤0.18

Values taken from Aschmann et al 2002

The analogues are adapted in the OP3 model. The first steps of the oxidation of camphene and γ-terpinene are * explicitly to form unique products using the known reaction rates for camphene and γ-terpinene with OH, NO_3 and O_3. The next step of building the analogues into the mechanism is to have these intermediate products undergo further reactions to form products that feed back into the original degradation reactions for limonene and β-pinene using the original reaction rates and pathways

for these surrogate species. Below are two parts of code from the model showing the degradation of limonene and the degradation of gamma-terpinene based on the use of limonene as an analogue.

```
*LIMONENE SCHEME;
*
*;
* DEVELOPMENTAL LIMONENE SCHEME;
*;
*;
% 4.28D-11*EXP(401/TEMP)*0.408 : LIMONENE + OH = LIMAO2              ;
% 4.28D-11*EXP(401/TEMP)*0.222 : LIMONENE + OH = LIMBO2              ;
% 4.28D-11*EXP(401/TEMP)*0.370 : LIMONENE + OH = LIMCO2              ;
% KRO2NO*0.772                 : LIMAO2 + NO = LIMAO + NO2           ;
% KRO2NO*0.228                 : LIMAO2 + NO = LIMANO3               ;
% KRO2NO3                      : LIMAO2 + NO3 = LIMAO + NO2          ;
% KRO2HO2*0.914                : LIMAO2 + HO2 = LIMAOOH              ;
% 9.20D-14*RO2*0.7             : LIMAO2 = LIMAO                      ;
% 9.20D-14*RO2*0.3             : LIMAO2 = LIMAOH                     ;
% KDEC                         : LIMAO = LIMAL + HO2                 ;

% KRO2NO*0.772                 : LIMBO2 + NO = LIMBO + NO2           ;
% KRO2NO*0.228                 : LIMBO2 + NO = LIMBNO3               ;
% KRO2NO3                      : LIMBO2 + NO3 = LIMBO + NO2          ;
% KRO2HO2*0.914                : LIMBO2 + HO2 = LIMBOOH              ;
% 8.80D-13*RO2*0.6             : LIMBO2 = LIMBO                      ;
% 8.80D-13*RO2*0.2             : LIMBO2 = LIMAOH                     ;
% 8.80D-13*RO2*0.2             : LIMBO2 = LIMBCO                     ;
% KDEC                         : LIMBO = LIMAL + HO2                 ;

% KRO2NO*0.772                 : LIMCO2 + NO = LIMCO + NO2           ;
% KRO2NO*0.228                 : LIMCO2 + NO = LIMCNO3               ;
% KRO2NO3                      : LIMCO2 + NO3 = LIMCO + NO2          ;
% KRO2HO2*0.914                : LIMCO2 + HO2 = LIMCOOH              ;
% 9.20D-14*RO2*0.7             : LIMCO2 = LIMCO                      ;
% 9.20D-14*RO2*0.3             : LIMCO2 = LIMCOH                     ;
% KDEC                         : LIMCO = LIMKET + HCHO + HO2         ;
*;
% 2.95D-15*EXP(-783/TEMP)*0.730 : LIMONENE + O3 = LIMOOA             ;
% 2.95D-15*EXP(-783/TEMP)*0.270 : LIMONENE + O3 = LIMOOB             ;
% KDEC*0.5                     : LIMOOA = LIMALAO2 + OH              ;
% KDEC*0.5                     : LIMOOA = LIMALBO2 + OH              ;
% KDEC*0.5                     : LIMOOB = LIMBOO                     ;
% KDEC*0.5                     : LIMOOB = C923O2 + CO + OH           ;
*;



* GAMMA TERPINENE SCHEME BASED ON LIMONENE SCHEME  ;
*;
* GAMMA TERPINENE + OH ;
*;
*;
% 1.7D-11*EXP *0.408           : GTERP + OH = GTERPAO2              ;
% 1.7D-11*EXP *0.222           : GTERP + OH = GTERPBO2              ;
% 1.7D-11*EXP *0.370           : GTERP + OH = GTERPCO2              ;
% KRO2NO*0.772                 : GTERPAO2 + NO = LIMAO + NO2          ;
% KRO2NO*0.228                 : GTERPAO2 + NO = LIMANO3              ;
% KRO2NO3                      : GTERPAO2 + NO3 = LIMAO + NO2         ;
```

```
% KRO2HO2*0.914                : GTERPAO2 + HO2 = LIMAOOH            ;
% 9.20D-14*RO2*0.7             : GTERPAO2 = LIMAO                    ;
% 9.20D-14*RO2*0.3             : GTERPAO2 = LIMAOH
*;
% KRO2NO*0.772                 : GTERPBO2 + NO = LIMBO + NO2         ;
% KRO2NO*0.228                 : GTERPBO2 + NO = LIMBNO3             ;
% KRO2NO3                      : GTERPBO2 + NO3 = LIMBO + NO2        ;
% KRO2HO2*0.914                : GTERPBO2 + HO2 = LIMBOOH            ;
% 8.80D-13*RO2*0.6             : GTERPBO2 = LIMBO                    ;
% 8.80D-13*RO2*0.2             : GTERPBO2 = LIMAOH                   ;
% 8.80D-13*RO2*0.2             : GTERPBO2 = LIMBCO                   ;
*;
% KRO2NO*0.772                 : GTERPCO2 + NO = LIMCO + NO2        ;
% KRO2NO*0.228                 : GTERPCO2 + NO = LIMCNO3             ;
% KRO2NO3                      : GTERPCO2 + NO3 = LIMCO + NO2        ;
% KRO2HO2*0.914                : GTERPCO2 + HO2 = LIMCOOH            ;
% 9.20D-14*RO2*0.7             : GTERPCO2 = LIMCO                    ;
% 9.20D-14*RO2*0.3             : GTERPCO2 = LIMCOH                   ;
*;
% 2.95D-15*EXP(-783/TEMP)*0.730 : GTERP + O3 = GTERPOOA             ;
% 2.95D-15*EXP(-783/TEMP)*0.270 : GTERP + O3 = GTERPOOB             ;
% KDEC*0.5                     : GTERPOOA = LIMALAO2 + OH
;
% KDEC*0.5                     : GTERPOOA = LIMALBO2 + OH            ;
% KDEC*0.5                     : GTERPOOB = LIMBOO                   ;
% KDEC*0.5*0.94                : GTERPOOB = C923O2 + CO + OH         ;
% KDEC*0.5*0.06                : GTERPOOB = C923O2 + CO ;
*;
```

In this way it was possible to see how important the initial oxidation steps for OH loss, and the specific peroxy radicals in the overall RO_2 composition.

What is constrained, explain all that enters the model.

2.1.5 Input Data

The data that are constrained in the model are input once every 15 minutes. The data are processed into a series of input files covering these 15 minute intervals. As the data for the different chemical species was measured at frequencies varying from 1-60 minutes, the measured data were interpolated or averaged to form the discrete 15 minute data files.

The inorganic species (NO, NO_2, O_3, CO) were measured at 1 minute intervals. The photolysis coefficients for O_3 and the meteorological data were also measured at 1 minute intervals. The volatile organic compounds (VOCs) were measured about once every hour.

The data were also investigated for times when technical problems lead to an absence of measurements. If the gaps in the data were an hour or less in the VOCs or 15 minutes or less for other species it was possible to interpolate through the gap. If it was a larger gap the data were not used for analysis or an averaged value was used to replace the missing data. The averaged value was taken from a diurnal plot for the species of the whole phase of the field campaign.

In order to verify the way in which the data had been processed was suitable, the averaged or interpolated data were compared to the original data set. Such a comparison was carried out for each set of input data to make sure that the data processing was valid, so peaks were in the same place and not smoothed too much.

Processed data showed good agreement with the original data (figures 2.3 to 2.7). The timing of the occurrence of peaks in the processed data was in concurrence with peaks in the measured concentrations. The averaged data showed peak heights that were similar to the originals demonstrating that the processing of the data had caused minimal loss of detail in the original measured data.

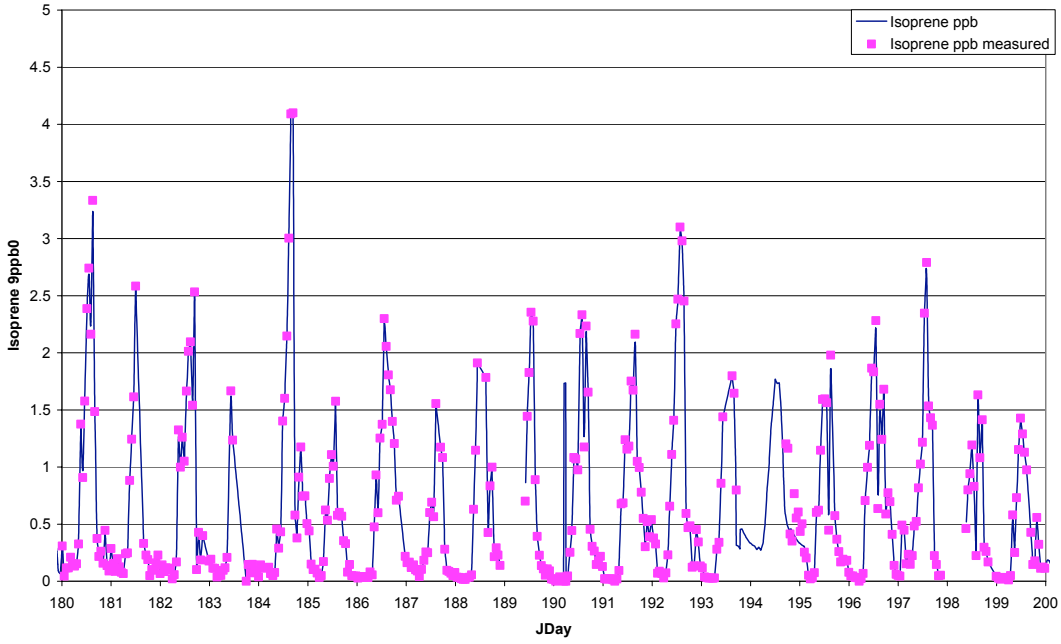

Figure 2.3. Comparison between the measured data for isoprene and the interpolated values for isoprene during the second phase of the campaign.

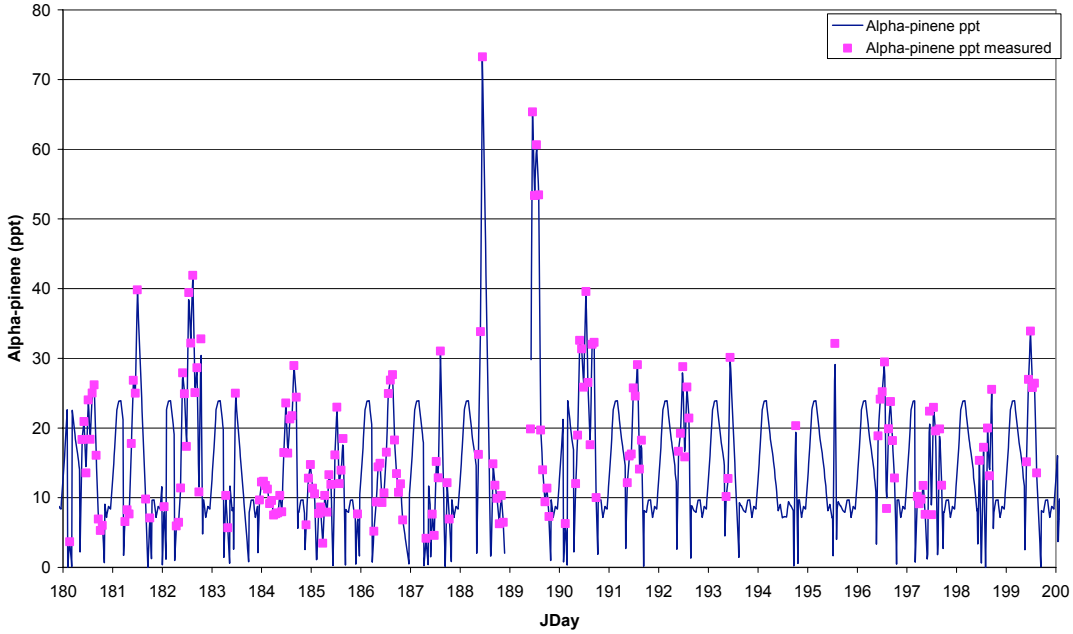

Figure 2.4. Comparison between the measured data for α-pinene and the interpolated values for α-pinene during the second phase of the campaign.

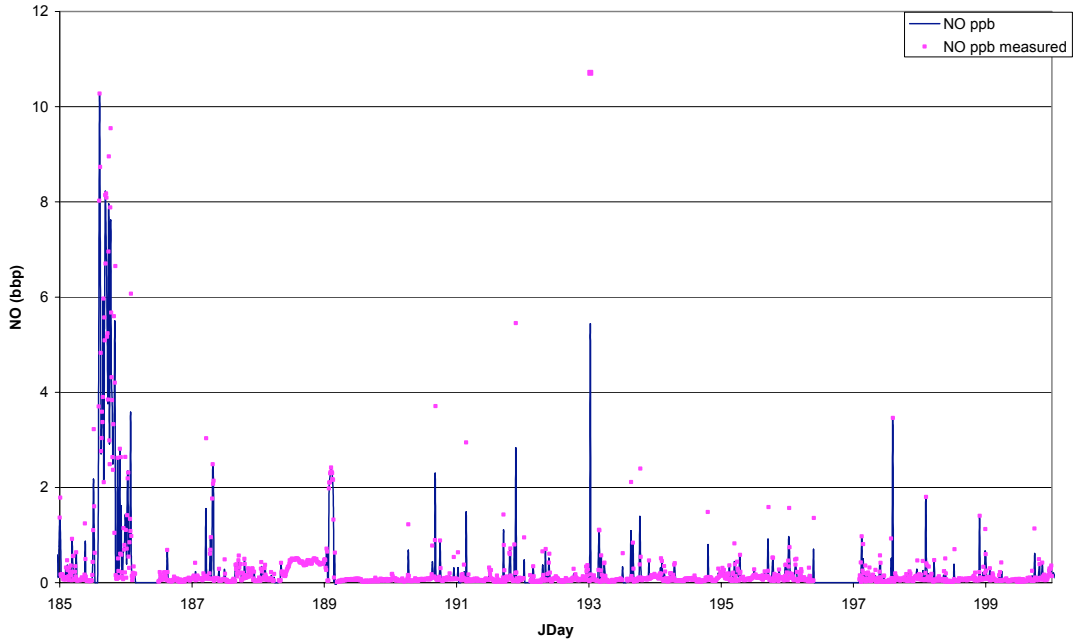

Figure 2.5. Comparison between the measured data for NO and the averaged values for NO during the second phase of the campaign.

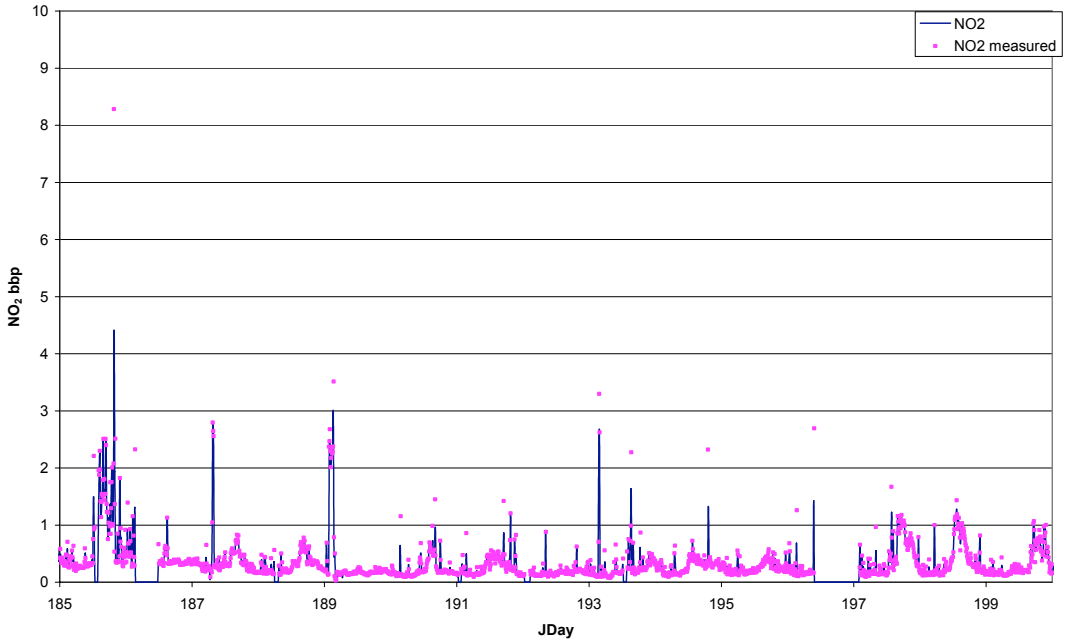

Figure 2.6. Comparison between the measured data for NO_2 and the averaged values for NO_2 during the second phase of the campaign.

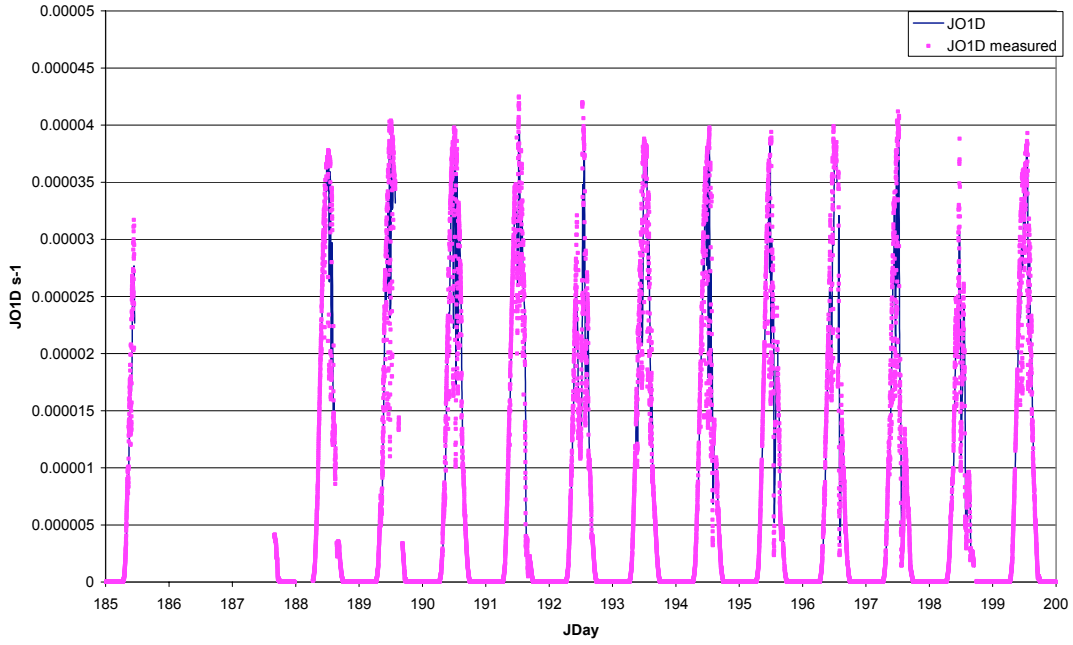

Figure 2.7. Comparison between the measured data for $J(O^1D)$ and the averaged values for $J(O^1D)$ during the second phase of the campaign.

A quantitative view of the agreement between these data sets can be found by taking an overall average value for the concentrations of species that were measured during the first and second phases of the campaign, and comparing these to an overall

averaged value for the corresponding processed data (Table 2.8). When these values are compared there is very little difference between the original values and the processed values showing again that the procedure to make the 15 minute processed data files has not lost large amounts of detail contained in the original data.

Table2.8. % Difference between averaged measured and processed data for the first and second phase of the campaign. A positive value denotes that the averaged data were larger than the measured data.

Species	Phase 1 % Difference	Phase 2 % Difference
Isoprene	9.11	8.22
α-pinene	-0.63	2.54
Camphene	0.19	3.16
δ-3-carene	-0.37	-1.59
γ-terpinene	-10.40	4.66
Limonene	0.69	1.43
Ethene	3.26	4.53
Propene	-8.98	0.00
Methanol	-14.71	1.19
Acetaldehyde	0.00	-8.14
Isobutene	1.43	-1.44
O_3	9.42	1.89
NO	-1.85	-3.62
NO_2	-4.24	1.41
CO	-1.81	-1.90
$J(O^1D)$	-0.22	-0.79

The procedure for processing the data also highlighted which days of measurements taken throughout the two phases of the campaigns would be suitable for use in the model. From the data processing it was possible to see that the first phase of the campaign contained two days worth of complete data coverage and the second phase

contained 5 days of complete data coverage. However, techniques were developed to enable further days to be investigated as discussed in chapter 4 and 5.

2.1.6 Model Assumptions

In the constructions of a model it is not possible to include every variable that is present in a system, leading to assumptions being made which can inaccuracies in the output of the model. The box model is constructed round the continuity equation of $dc/dt = F + P - L$ (Jacobs et al 2007). In this equation the inputs into the model are the terms F and P. F represents the flux of the species passing through are the box represents and P is the production of species through the reactions occurring with in the box. The term L represents the loss of species from the box through methods of deposition.

The F term in many box models will describe the flux of concentrations entering the constrained area the box model covers. In the OP3 model the model represents a fixed single point, which is not affected by a constant flux. However, the F term represents the input data that the model is constrained to at the 15 minute intervals. This F factor takes into consideration the location of the box model and the mixing height the constrained species at the site of between 300 m and 1300m. These numbers reflect the height of the boundary layer, the height of the boundary layer is varied through the model as the day progresses on a diurnal cycle, with the lowest values being calculated at night and the highest at midday. The geographical height of Bukit Atur is 426 above sea level and the position of the inlets for the measuring instruments. The model assumes that all the chemistry within the mechanism occurs at one single point; this requires all the data to be collected at one single point. This means that the boundary layer passes through the point being modelled at night. Observations of the boundary layer height were made using a LIDAR, but at the time of the model being constructed and used to predict the radical species this data was not available.

Due to the logistics of running the field campaign it is not possible have all the inputs at the same point (this difference in location is talked about in the site description

chapter 2.2). This difference could be seen to have an effect as some of the species have a very short chemical lifetime and when this is combined with distance between observation points it can not be a certainty that the concentrations of short lived species will be the same at different points at the observation site.

In the P term of the model one assumption of the model the degree of accuracy in the constants involved in the kinetics of the reactions in the mechanism. These values are reviewed on a regular basis in controlled lab experiments and field experiments and published. By using the most recently updated reaction rates and constants required by the reaction mechanism reduces uncertainty around the results of the model.

The final term in the continuity equation L represents loss in the model from dry and wet deposition. The loss due to deposition and the selection of the values, which represent loss, are discussed in sections 3.5. The potential values for loss are taken from laboratory and field experiments and assumptions have to be made while selecting the values that best represent the conditions of the field area.

Wet deposition is not a factor that is calculated by the OP3 models using the MCM3.1. The presence of wet deposition can be seen in figure 4.2.13 indicating the presence of precipitation. Any changes to the concentrations of the constrained species due to rainfall, mist or other sources of moisture are factored directly through the concentrations of constrained species. If the model was built to include larger species such as particulate mater and sulphate compounds, a wet deposition term would have to be factored into the model.

2.2 Measurements

2.2.1 Introduction

Throughout the two phases of the OP3 field campaign a large number of different chemical species were monitored as well as many other variables including photolysis and meteorological data. The instruments and measuring techniques for the species required to simulate concentrations of OH, HO_2 and RO_2 are listed in table 2.9.

Table 2.9. Overview of measurements made during OP3 that are included in the model.

Species	Method/ Analytical technique	Temporal Resolution	Detection Limit	Measurement Uncertainty	Reference
VOC, including isoprene, monoterpenes and oxygenates	Dual channel gas chromatograph with flame ionization detectors (DC-GC-FID)	1 hour	1 pptv	Variable, around 10%	(Lewis et al., 2007; Lewis et al., 2005)
OH HO_2	Fluorescence Assay by Gas Expansion (FAGE) Laser Induced Fluorescence (LIF)	10 s	(OH) $2.45x10^5$ molecule cm^{-3} (HO_2) $3.86x10^6$ molecule cm^{-3}	28% (OH and HO_2) (1σ)	(Whalley et al., 2010a, b)
$\Sigma RO_2 + HO_2$	Peroxy Radical Chemical Amplifier (PERCA) dual inlet	1 minute	0.4 pptv	38% (1σ)	(Fleming et al., 2006)
NO, NO_2, ΣNO_y, ΣNO_y-HNO_3	NO/O_3 chemi-luminescence detectors, Pho-tochemical convertor +	10 minutes	3 pptv for NO, 7 pptv for NO2	15% for NO and 20% for NO2 at 50 pptv	(Pike et al., 2009)
O_3	UV absorption	1 second	0.6 ppbv	10% ±3.4 ppbv (±1σ)	(Heard et al., 2006)
Photolysis frequencies (incl. $j(O^1D)$,$j(NO_2)$)	Calibrated filter (2π and 4π sr) radiometers and spectral-radiometer	1 second		14% and 13% 0–90◦	(Bohn et al., 2008; Edwards and Monks, 2003; Volz-Thomas, et al., 1996)
CO	Chemiluminesence				(Gerbig et al., 1999)
Meteorological parameters (Wind speed & direction, solar radiation, PAR, precipita-tion, wetness, pressure, tem-perature, RH, turbulence, sen-sible heat flux)	Standard mete-orological sen-sors (aspirated thermocouples, Vaisala WXT)	30 minutes			

More details on the different techniques employed during the field campaigns can be found in the associated references.

This wide array of analytical techniques were required to observe and record the required numbers of chemical species and physical characteristics needed to answer the key questions the OP3 project set out to investigate. Apart from the instruments noted in table 2.9, other instruments were present at Bukit Atur to record data required to answer other questions in the OP3 project. For a full list of these instrument see Hewitt et al., 2009 OP3 overiew paper.

In order to answer the questions proposed by the OP3 project more fully other modelling studies were conducted using data collected during the two phases if the OP3 project. These modelling projects included investigations simulating the composition of the atmosphere using box models and data from measurements of fluxes in key inorganinc and organic species (Pugh et al., 2010). Another model based investigations into isoprene chemistry and the formation of radicals in the tropics was investigated (Stone et al., 2010) using a similar set of instruments housed in a research aircraft which focused on the Bukit Atur research site and surrounding forest and palm plantation.

2.2.2 OH and HO_2 Measurements. Detection Limits and Accuracy.

In the OP3 field campaign OH and HO_2 were measured by the method of Fluorescence Assay by Gas Expansion (FAGE). FAGE is a form of low pressure laser-induced fluorescence (LIF). The FAGE method works by the sampled air being drawn into the instrument and the pressure of the sample being decreased, thereby expanding the volume of the sample. The change of pressure extends the lifetime of the OH molecules. OH is a very short lived species and by increasing the lifetime it is easier to detect the OH radicals. The laser, at a wavelength of 308nm, is used to energise the OH radicals to an excited state. The scattered light from the excited OH is then detected at 298nm (Heard and Piling., 2003).

In order to measure HO_2, NO is added to the sample, converting HO_2 to OH and then the OH detected using the method described above. A simultaneous measurement of

OH in a different detection cell can then be subtracted giving a value for HO_2 (Whalley et al., 2010)

The measurement of HO_2 by FAGE normally occurs simultaneously to OH, but due to difficulties in operation conditions during the OP3 campaign, only one cell was in operation meaning OH and HO_2 could not be measured simultaneously. This lead to sequential measurements of OH and HO_2. HO_2 was only measured during the second phase of the field campaign.

The FAGE technique has a detection limit for OH of 2.45 x 10^5 molecule cm^{-3} and HO_2 of 3.86 x 10^6 molecule cm^{-3}. The instrument carries a 1σ uncertainty of 28% in the measurements of OH and HO_2 (Whalley et al., 2010).

2.2.3 Measurement of $\Sigma RO_2 + HO_2$

Peroxy radical ($\Sigma RO_2 + HO_2$) measurements were made at the field site by using PEroxy Radical Chemical Amplification (PERCA) (Hewitt et al., 2009). Measurements of the total RO_2 concentrations were made by the University of Leicester using a PERCA IV instrument. The process works on the principle of HO_2 and OH catalyzed conversions of NO and CO into CO_2 and NO_2, through the addition of NO and CO to the inlet region (Fleming et al., 2006):

$$HO_2 + NO \rightarrow OH + NO_2 \quad \text{(R2.13)}$$

$$OH + CO \rightarrow H + CO_2 \quad \text{(R2.14)}$$

$$H + O_2 + M \rightarrow HO_2 + M \quad \text{(R2.15)}$$

$$\text{Overall: } NO + CO + O_2 \rightarrow NO_2 + CO_2 \quad \text{(R2.16)}$$

In the presence of NO, organic peroxy radicals are readily converted to HO_2. The HO_2 then reacts with NO yielding NO_2 (R2.13). The concentrations of NO_2 produced are equal to the organic chain length (CL) of the peroxy radicals being measured. From the recorded concentrations of NO_2 the calculation of $[NO_2]/CL$ is used to calculate $\Sigma RO_2 + HO_2$ (Fleming et al., 2006). The PERCA technique has a detection limit for $\Sigma RO_2 + HO_2$ of 0.4 pptv and the instrument carries a 1σ uncertainty of 38% in the measurements of $\Sigma RO_2 + HO_2$ (Fleming, 2006).

2.3 Site Description

The OP3 project was focused entirely on a research site called Bukit Atur (figure 2.7). Bukit Atur is located on the Malaysian side of Borneo, in the state of Sabah. The state of Sabah is located in the North East of Borneo, the world's third largest island. The island of Borneo has 257,000 km^2 of evergreen broadleaf rainforest, this covers 35% of the island. Most of the state of Sabah was once covered with rainforest (Schmitt et al., 2008). Currently 47% (36,049 km^2 of the state lies within Permanent Forest Estate (PFE). The PFE is managed and 74% is used for selective harvesting of timber and the remaining 26% is permanently protected. Within Sabah, previously clear felled areas of forest have undergone a change in land use and are mainly used for oil palm growth.

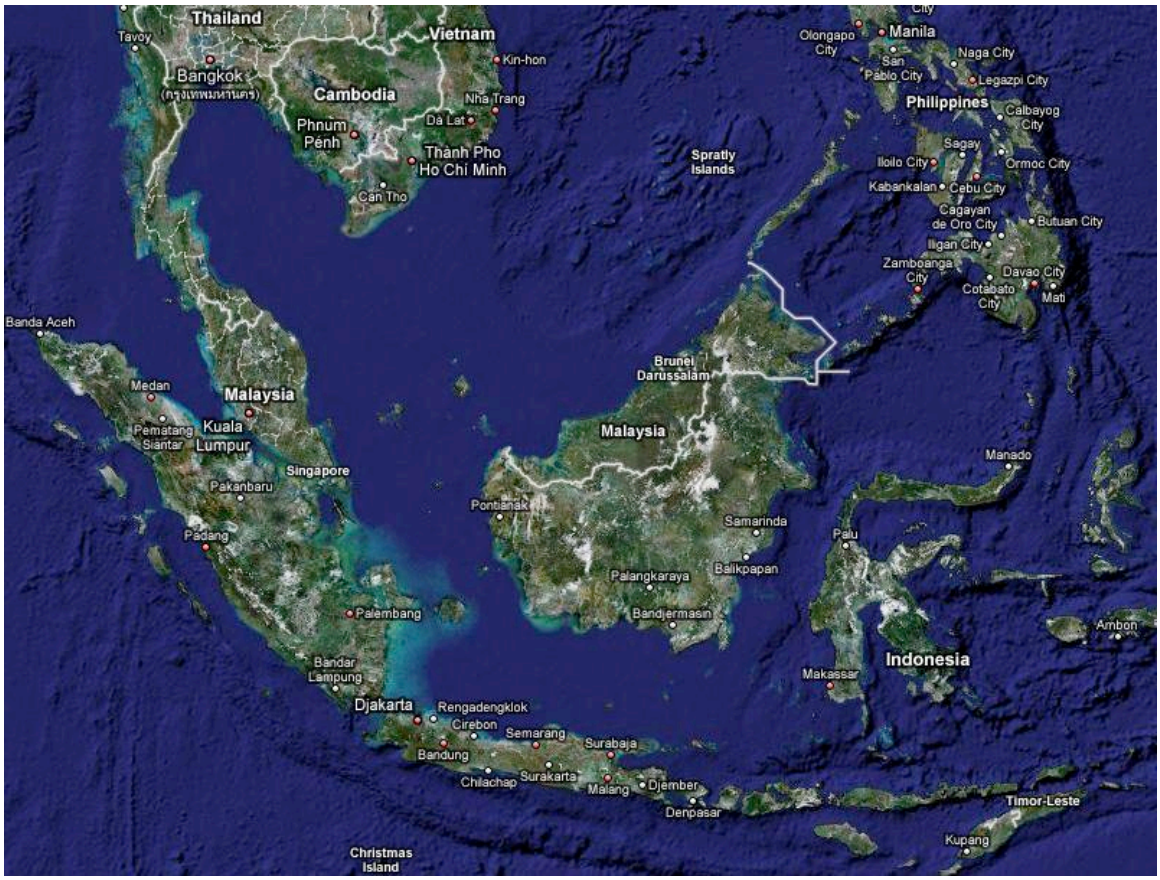

Figure 2.7 A satellite image of Malaysia and Indonesia showing the Island of Borneo. Taken from Google Earth.

Borneo is located within the tropics and as an island is heavily effected by maritime climate conditions and has a superwet climate (Hewitt et al., 2009). Most of the OP3 measurements were undertaken within the four-month period of April to July 2008. This period was 124% more wet than normal, with 1045 mm of rainfall. Notably, the driest month according to the longer-term record, April, received 170% of the normal rainfall at 263 mm. The April–July 2008 period was also cooler, with a mean temperature of 27.1 ◦ C, which was 99% of the norm for April–July 2001–2008.

The Bukit Atur field site is located 120 miles from the nearest town in the state of Sabah, Lahad Datu on the coast (figure 2.8). The exact location of Bukit Atur is 4◦ 58′ 49.33″ N, 117◦ 50′ 39.05″ E with an elevation of 426m above sea level. The Bukit Atur site is also part of the United Nations run Global Atmosphere Watch (GAW) (http://gaw.empa.ch/gawsis/). As part of the GAW program there is an existing atmospheric monitoring instruments at the field site, part of this is a 100m observation tower (figure 2.9) used for locating inlets and meteorological instruments. As well as the observation tower, a research building is also located at Bukit Atur (figure 2.10).

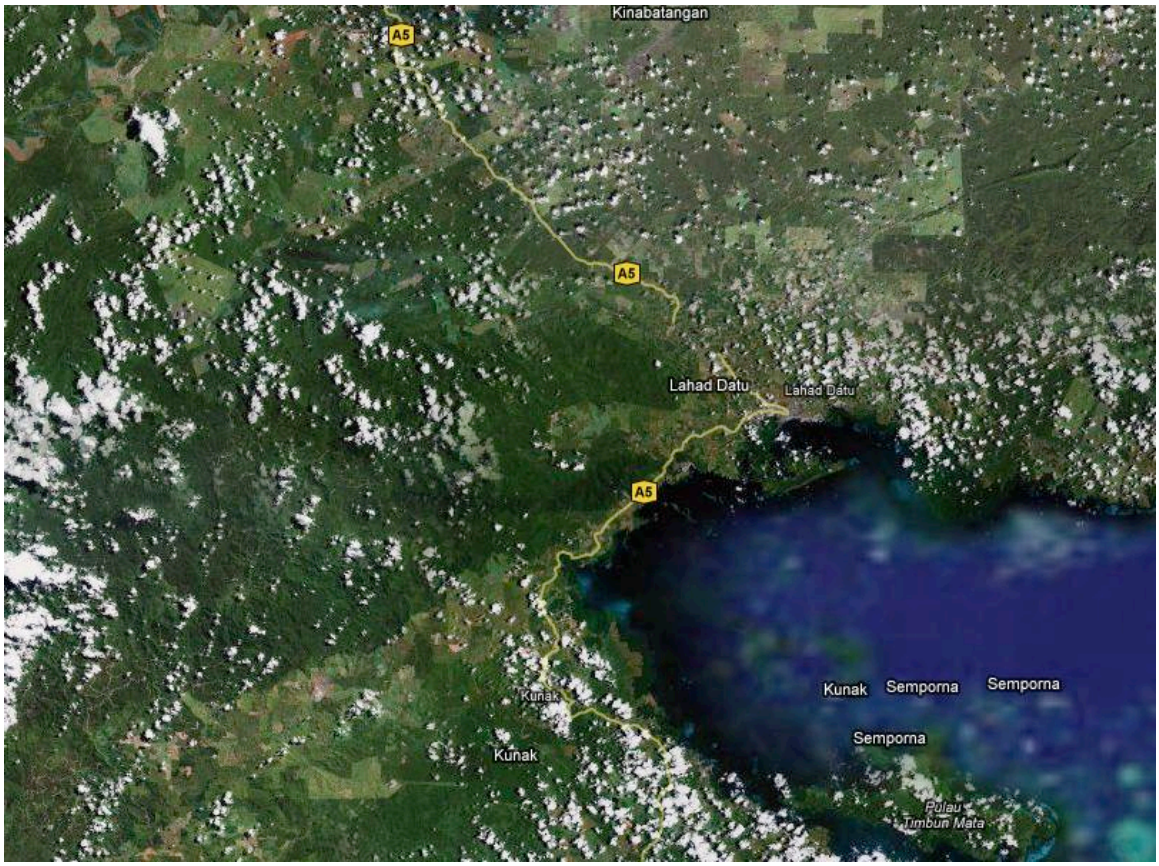

Figure 2.8. A satellite image of north east Borneo, showing the state of Sabah, the town of Lahad Datu and Bukit Atur.

Forty-seven percent of the state of Sabah is covered by Permanent Forest Estate (PFE) and of this 74% is maintained under a selective harvesting system and the remaining 26% is protected forest (Hewitt et al., 2009). The GAW site at Bukit Atur is located within a PFE Protected Forest on the Ulu-Segama reserve, in the center of a 22.6 km^2 coup that was last subjected to selective timber harvesting in 1988 (Figure 12 and 13). However, much of the east of Sabah has been clear felled and converted to palm oil cultivation (Hewitt et al., 2009).

Figure 2.9. Bukit Atur observation tower.

Figure 2.10. Bukit Atur observation tower, research building and shipping containers.

During the OP3 project the instruments were housed in a series of shipping containers brought to the field site and also place in the research building. The inlets for many of the instruments were located at various heights on the GAW tower, but many others were set at a height of 3 meters and fixed to the shipping containers. The FAGE instrument was located in the white shipping container (the right edge of figure 2.10) with its inlets located above the shipping container at a height of 3 meters. The PERCA instrument was located in the blue shipping container (centre of figure 2.10) with its inlets in the white box above the blue shipping container also set at 3 meters. The NO_x instrument and GS-MS used for detecting the organic species were located in the research building (figure 2.10) with their inlets also being located in the white box above the blue shipping container. The inlets located in the white box were a distance of approximately 10 meters away from the inlets located on the white FAGE container.

Picture 12

Picture 13

Chapter 3: Model Testing and Tuning

3.1 Introduction

In order to quantify the validity of the results from the OP3 model the sensitivity of the model needs to be tested. There are different components in the model that need to be investigated individually to see what effects changes to these components have on the overall output of the model.

To investigate these factors an average data set that represented the whole of the second phase of the field campaign was constructed. The data set was constructed by taking an average of all available data from the second phase of the campaign. 15 minute averages were then produced for each constrained species and these were used as inputs for the sensitivity tests unless otherwise indicated. The average data set was also used to fill in small gaps in data for the first and second phases of the campaign, extending the number of days in the campaigns that could be investigated through modelling studies.

The average profiles for all the species in the second campaign phase all show the same diurnal variation. Each species has lower values or concentrations during the night (19:00 to 7:00) and higher values during the day (7:00 to 19:00) with a maximum value occurring around midday or between 12:00 and 13:00. Figures 3.1 and 3.2 show examples of the average profiles and the diurnal variation in an organic species (Isoprene) and a photolysis coefficient ($J(O^1D)$).

Before any parts of the mechanism were altered, the model was run using the average data set and compared to diurnal averages of the measured radical species (figures 3.3, 3.4 and 3.5)

The average data set was used to test the model sensitivity to various input parameters as described in the following sections.

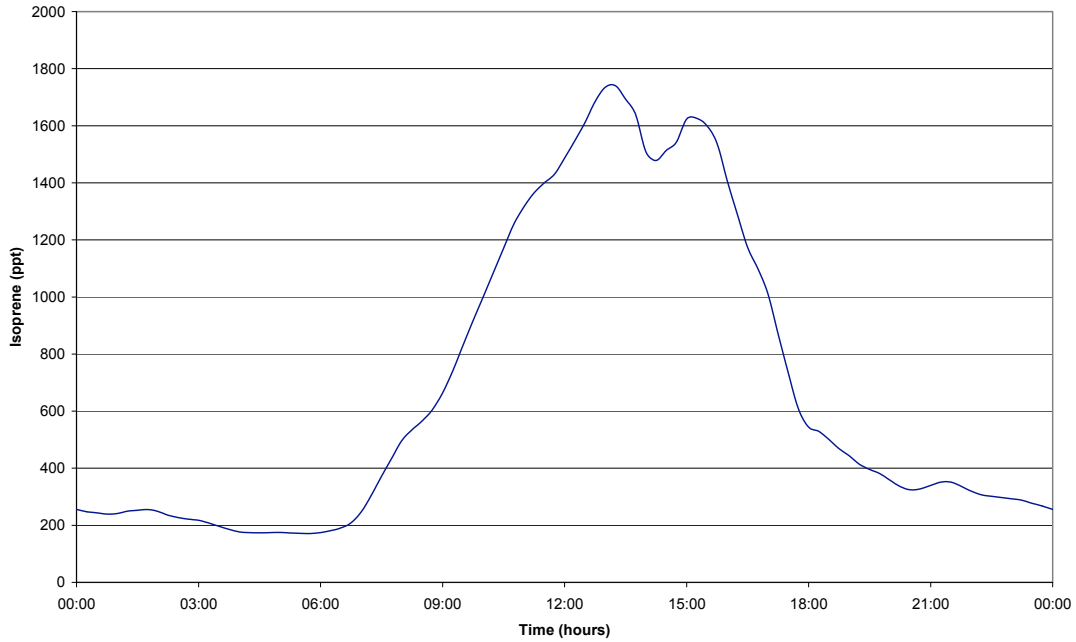

Figure 3.1 Average diurnal profile of isoprene during the 2nd phase of the campaign, from 22nd June 2008 until 30th July 2008 at Bukit Atur field site.

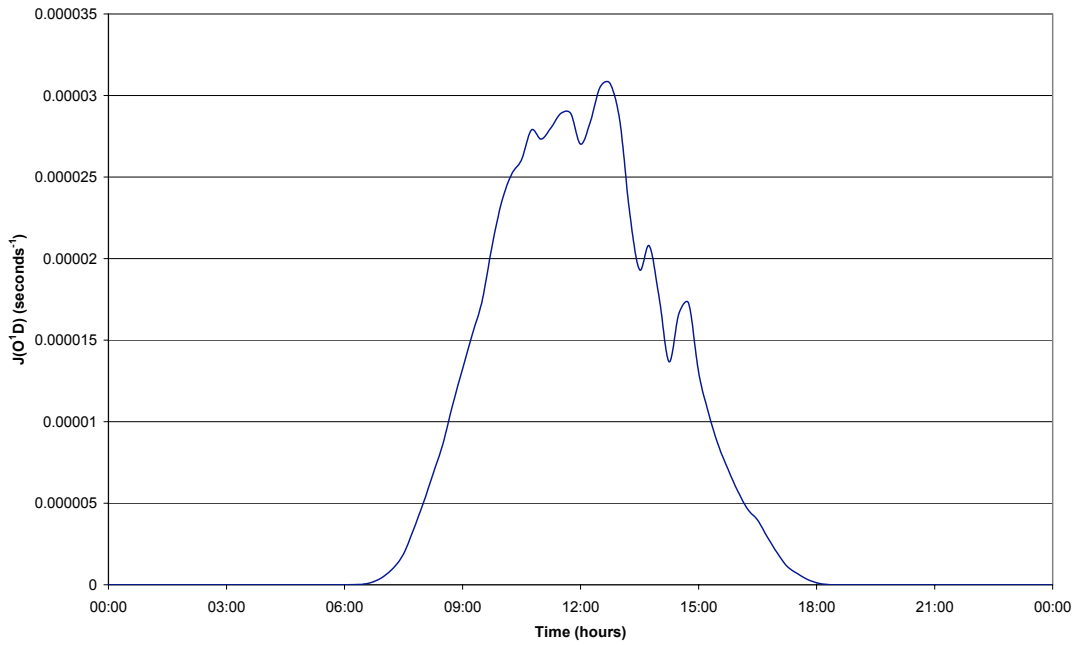

Figure 3.2 Average diurnal profile of $J(O^1D)$ during the 2nd phase of the campaign, from 22nd June 2008 until 30th July 2008 at Bukit Atur field site.

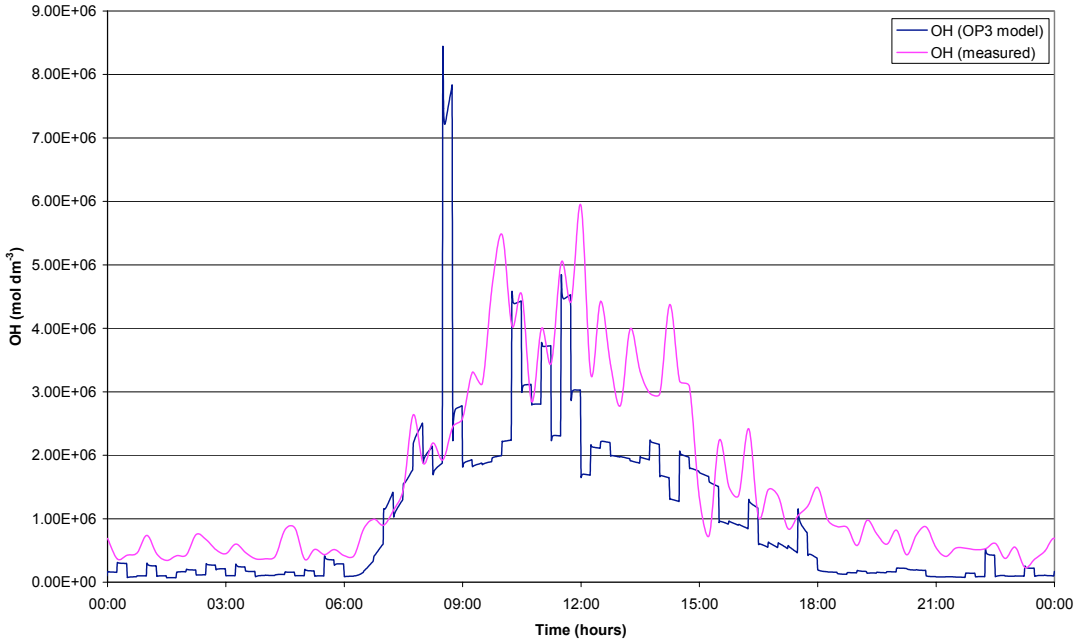

Figure 3.3 Comparison of measured OH and modelled OH using average data set for the second phase of the field campaign, from 22nd June 2008 until 30th July 2008 at Bukit Atur field site.

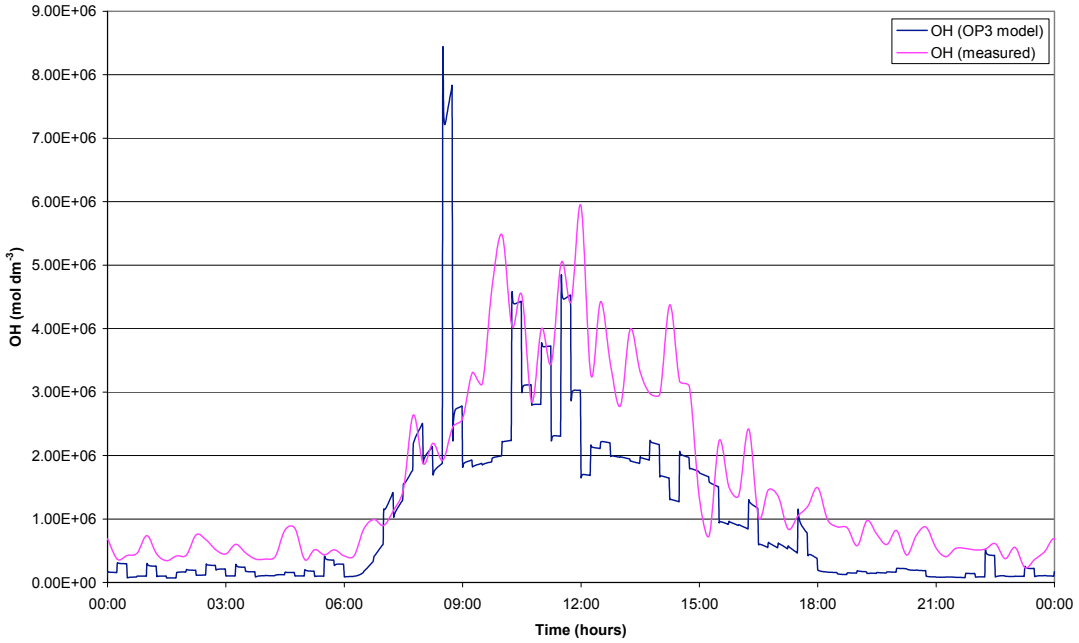

Figure 3.4 Comparison of measured HO_2 and modelled HO_2 using average data set for the second phase of the field campaign, from 22nd June 2008 until 30th July 2008 at Bukit Atur field site.

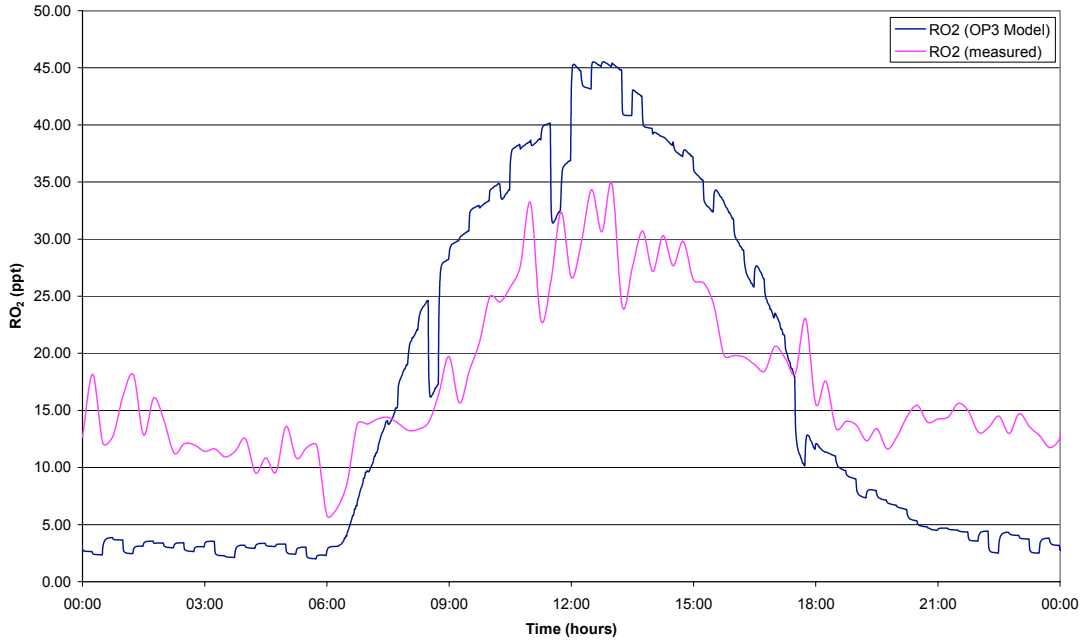

Figure 3.5 Comparison of measured RO_2 and modelled RO_2 using average data set for the second phase of the field campaign, from 22nd June 2008 until 30th July 2008 at Bukit Atur field site.

Table 3.1 Average, maximum and minimum concentrations for constrained species during the second phase of the field campaign, from 22nd June 2008 until 30th July 2008 at Bukit Atur field site.

Species	Isoprene (ppt)	Alpha-Pinene (ppt)	Camphene (ppt)	D-3-Carene (ppt)
Average	676.4	14.6	42.6	15.6
Maximum	1740.5	23.9	106.1	25.5
Minimum	171.3	7.2	15.0	6.1
Species	Gamma-Terpinene (ppt)	Limonene (ppt)	C2H4 (ppt)	CH3CHO (ppt)
Average	86.1	46.8	123.8	58.0
Maximum	150.7	89.2	157.4	66.7
Minimum	57.8	26.1	82.2	48.3
Species	NO (ppt)	NO2 (ppt)	O3 (ppb)	CO (ppb)
Average	122.7	271.1	6.4	205.0
Maximum	792.1	539.4	8.0	244.4
Minimum	41.9	128.6	3.8	187.7
Species	Temp (K)	J(O1D) (s^{-1})		
Average	297.5	6.80235E-06		
Maximum	300.1	3.07311E-05		
Minimum	296.2	0		

3.2 Model Run Time

It takes time for the model to reach steady state as many of the species included in the model are initialised at a concentration of zero. These include radical species and the intermediate products of the VOCs. The concentrations of these species predicted are by photolysis and oxidation generating them and deposition, uptake and further reactions acting as sinks for them. As the concentrations of these species start at zero it takes time for source and sink interactions to reach equilibrium. This state of equilibrium is called steady state.

The model was run for a period of 5 days using the average dataset for the second phase of the campaign. From the radical species output it was possible to quantify changes between each 24 hour run of the model to quantify how long it took for steady-state to be achieved. The three radical species all generated the lowest concentrations during the first 24 hours of the model run (figures 3.6, 3.7, 3.8). There is a large increase between day 1 and day 2 of the run, but the change between each 24 hour run becomes smaller with day 4 and 5 having a percentage change in midday value of less than 0.3% for all the radical species (table 3.2). The small change in the values between days 4 and 5 in the model runs show that the model has effectively reached steady state by the 4th day of the model run. Therefore 4-day model runs are sufficient to achieve steady-state conditions.

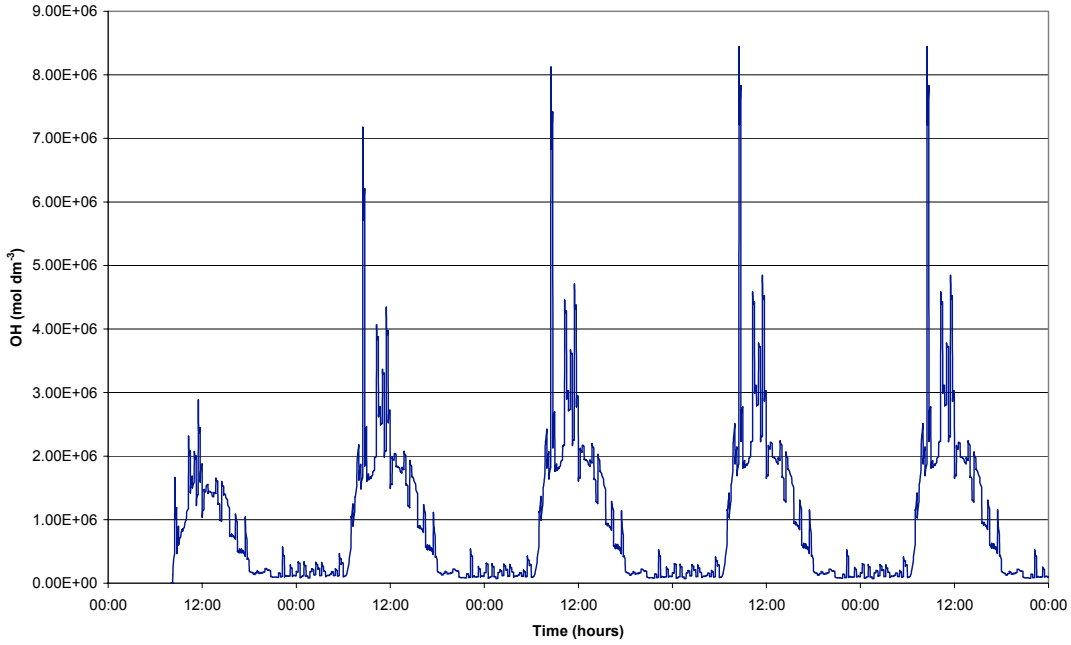

Figure 3.6 Diurnal OH concentrations over each day of the model run to steady state conditions

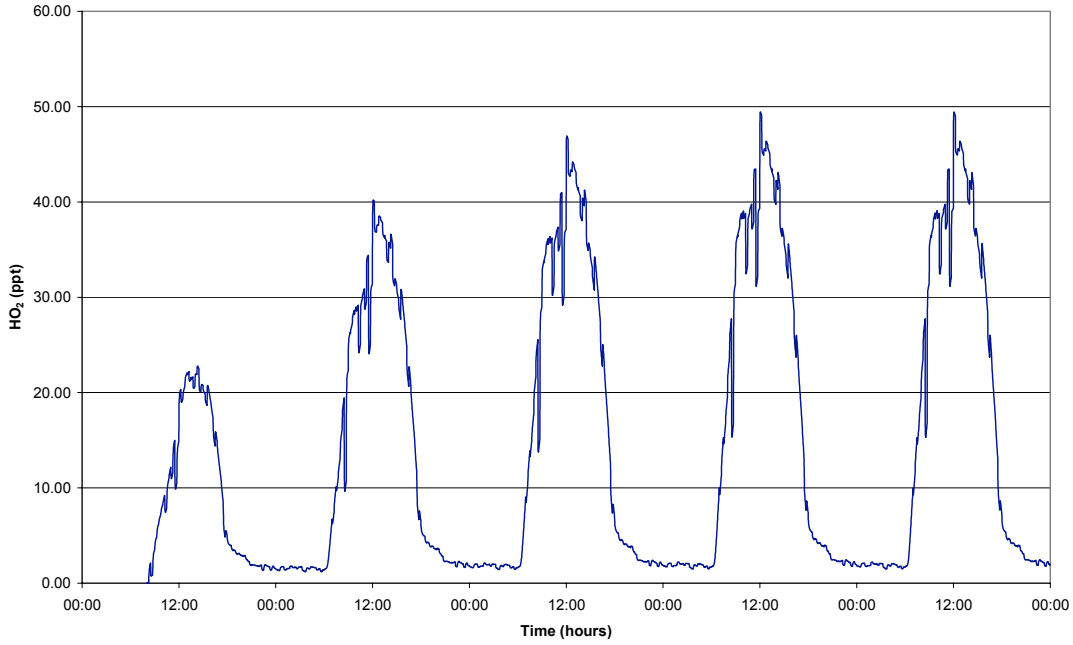

Figure 3.7 Diurnal HO_2 concentrations over each day of the model run to steady state conditions

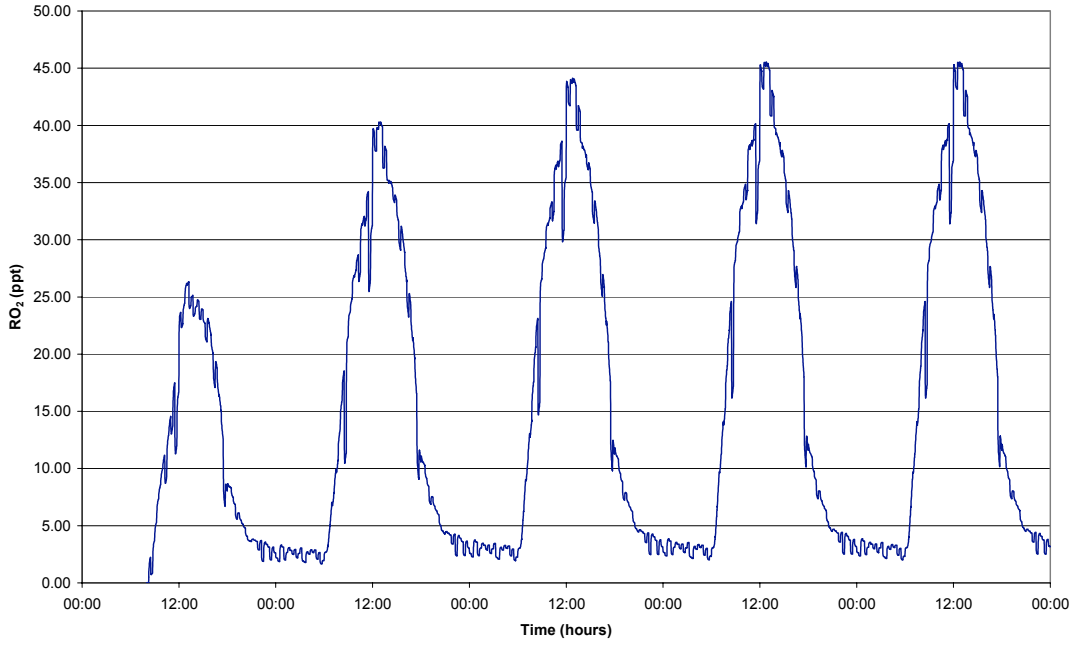

Figure 3.8 Diurnal RO_2 concentrations over each day of the model run to steady state conditions

Table 3.2 Concentrations of the three radical species at midday when running the model over a 5 day period to achieve steady state.

	OH (mol cm^{-3})		HO_2 ppt		RO_2 ppt	
	Midday Value	% Change	Midday Value	% Change	Midday Value	% Change
Day 1	1.7×10^6	0.0	17.8	0.0	23.8	0.0
Day 2	2.2×10^6	23.0	29.5	42.7	33.7	39.1
Day 3	2.4×10^6	6.4	33.5	12.8	36.8	10.5
Day 4	2.5×10^6	2.8	35.2	5.4	37.9	4.3
Day 5	2.5×10^6	0.1	35.3	0.3	38.0	0.2

The output from the models that was used to compare the model predictions to the observed values where those obtained on the fourth cycle of the model as this was when steady state with in the model was reached.

3.3 Frequency of Constrained Data

The model works by using constrained data to simulate chemical reactions over a given period. These intervals are chosen to best represent the input data, whilst not increasing the model time too much. Ideally, it would be good to input data each minute, but then the resulting models would take too long to run when compared to hourly inputs for instance.

The MCM model is constrained to a series of organic and non-organic chemical species and also physical properties. These different variables were measured at different time intervals as described in chapter 2. The organic species were measured once an hour while the non-organics were measured every minute to 15 minutes.

Currently the model is configured to read in inputs for the constrained species at 15 minute intervals. In this model, input data are interpolated or averaged to produce an input file each 15 minutes. The concentration of these input species is then held constant until new input file is used 15 minutes later. The original data were used to prepare new input files at 1, 5 and 60 minute intervals as well as the usual 15 minutes. By analysing the same 2 hours of the campaign run using the four different input time intervals for the constrained data, it was possible to assess the effect that different resolutions in time have on the model.

Table 3.3 shows that by changing the frequency at which the constrained species are read into the model, the predicted concentrations of all of the radical species. The changes in concentration have been quantified in table 3.4.

Table 3.3. Predicted concentrations of radical species from input file frequency testing averaged over the 2 hour period.

		Average concentrations of radical species over 2 hour model run			
		Data input frequency			
Jday	Radical Species	1 minute	5 minutes	15 minutes	60 minutes
190	OH (mol $cm^{-3)}$	4.2×10^6	4.3×10^6	4.5×10^6	5.0×10^6
	HO_2 ppt	23.5	23.8	24.4	26.5
	RO_2 ppt	38.7	39.2	40.5	43.3
191	OH (mol $cm^{-3)}$	5.9×10^6	5.8×10^6	6.0×10^6	5.3×10^6
	HO_2 ppt	30.4	30.0	30.6	28.3
	RO_2 ppt	57.2	56.4	57.9	55.1
Model Run Time		60 minutes	20 minutes	10 minutes	2 minutes

Table 3.4. Percentage difference at 12:00 between 15 minute interval test and other time intervals.

		% Difference to 15 minute data input		
		Data input frequency		
Jday	Species	1 minute	5 minutes	60 minutes
190	OH	- 5.6	- 2.8	+ 12.3
	HO_2	- 3.7	- 2.6	+ 8.3
	RO_2	- 4.4	- 3.3	0.0
191	OH	- 1.9	- 3.0	+ 12.0
	HO_2	- 0.9	- 2.1	+ 7.6
	RO_2	- 1.2	- 2.6	+ 4.9

Figure 3.6 shows the predictions of radical species for runs of 1, 5, 15 and 60 minute intervals for OH show. The 1, 5 and 15 minute intervals show similar trends in radical concentrations, but the 60 minute intervals show only the general variation in

the radical species; the finer details in the radical profiles are absent. The properties for HO_2 and RO_2 are similar to figure 3.9 and are not included.

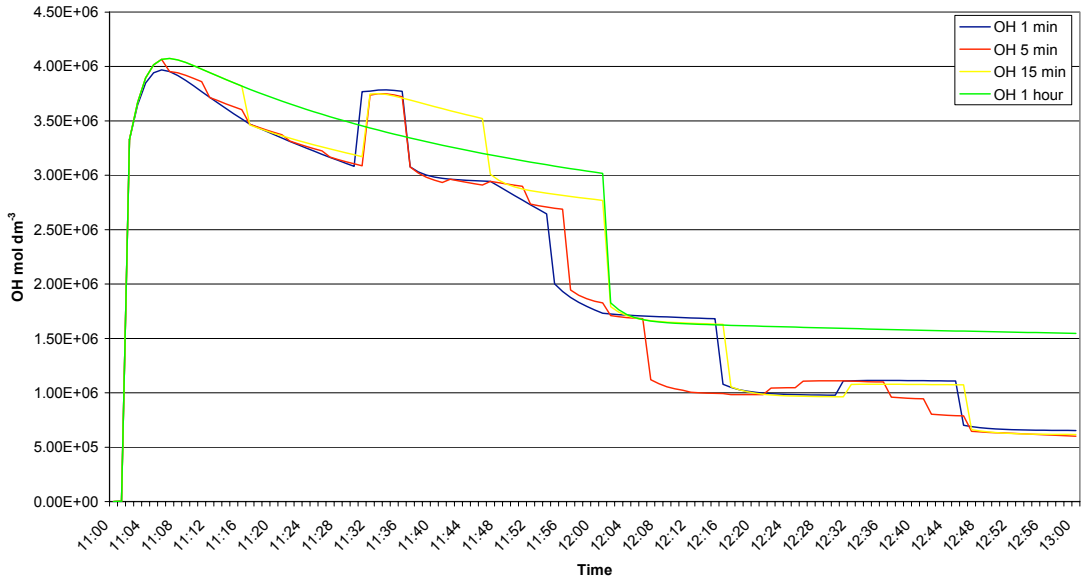

Figure 3.9. OH concentration predictions for day 190 in campaign 2nd phase with constrained data at 1, 5, 15 and 60 minutes

When the 1 minute, 5 minute and 60 minute interval constrained model runs are compared to the standard 15 minute model runs (table 3.3), the midday concentrations of the 1 and 5 minute interval tests show relatively small differences in the predicted concentrations of the radical species with the largest difference being 5.6%. However when the 15 minute and 60 minute constrained species runs are compared, there is a much larger difference with the midday OH concentration being over 10% different. Therefore the constrained data will be kept at 15 minutes as there is little change between 15 minute intervals and more frequently constrained data intervals. Also in terms of efficiency of time, 15 minute interval runs of the model take less time than 1 and 5 minute interval runs. The 15 minute interval runs, for a 2 hour period, run 6 times quicker than 1 minute intervals and twice as fast as the 5 minute interval runs. When the model is run for a 4 days instead of a 2 hour period the increase in time would make the model less efficient.

3.4 Photolysis Rates

Tropospheric ultraviolet (UV) radiation is the driving force for all tropospheric photochemical processes. In order to accurately predict the radical concentrations in the model, accurate information on photolysis reactions is needed in conjunction with concentrations of organic and inorganic chemical species. The data required to calculate the photolysis rates of the species in the model include the cross-section of the area being studied, the path length of the light entering the area (L) and the solar angle.

$$J = \int \sigma L\phi \times d\lambda \qquad \textbf{(Equation 3.1)}$$

Preferably, the model is constrained with as many measured photolysis coefficients as possible. However only the photolysis rates for O_3 to produce $O(^1D)$ ($J(O^1D)$) were made for the whole campaign, other photolysis rates were measured for small parts of the campaign. The photolysis coefficients for the remaining species are therefore calculated in the model, as described in the previous chapter. In order to assess the predictions for photolysis in the model a comparison was made with data from the Tropospheric Ultraviolet and Visible (TUV) Radiation Model (http://cprm.acd.ucar.edu/Models/TUV/index.shtml).

In order to initialise the TUV model, information for the latitude, longitude, time and date are required, along with data for the surface albedo and overhead ozone column. The TUV models can then predict the molecular photolysis rates for a wide range of photolabile species reactions. The latitude and longitude where set to the location of the field study site in Danum Valley (4.58′ 49.33″ N, 117.50′ 39.05″ E,) and the overhead ozone column was set to 300 Du.

Measured midday values for $J(O^1D)$ and other photolysis values which were available were used to compare the accuracy of the TUV model and the MCM predictions.

Comparisons between the parameterization used in the MCM model and the TUV for midday (12:00) demonstrates that both display the same general trends in the photolysis rates (figure 3.10). The values from the MCM are generated using clear skies, whereas the measurements include clouds. Therefore the model values should be the theoretical maximum value at the time in question The predictions from the MCM model are consistently lower than the values obtained from the TUV for all the photochemical reactions that were compared (table 3.5).

Phase 1

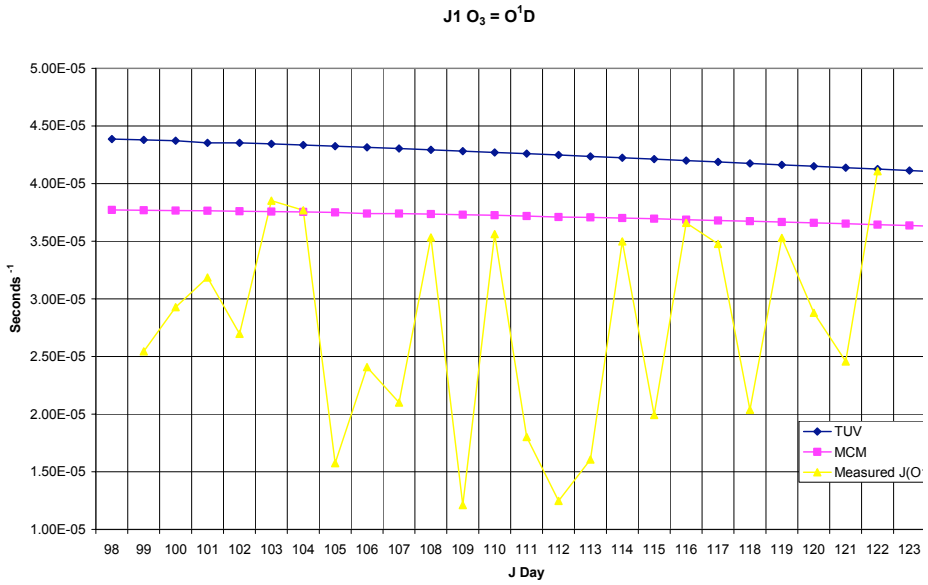

Phase 2

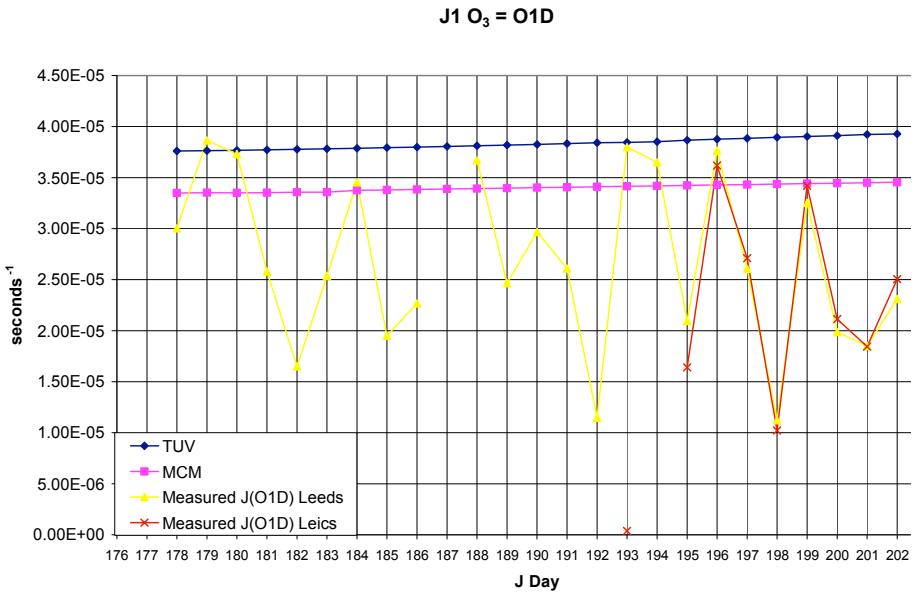

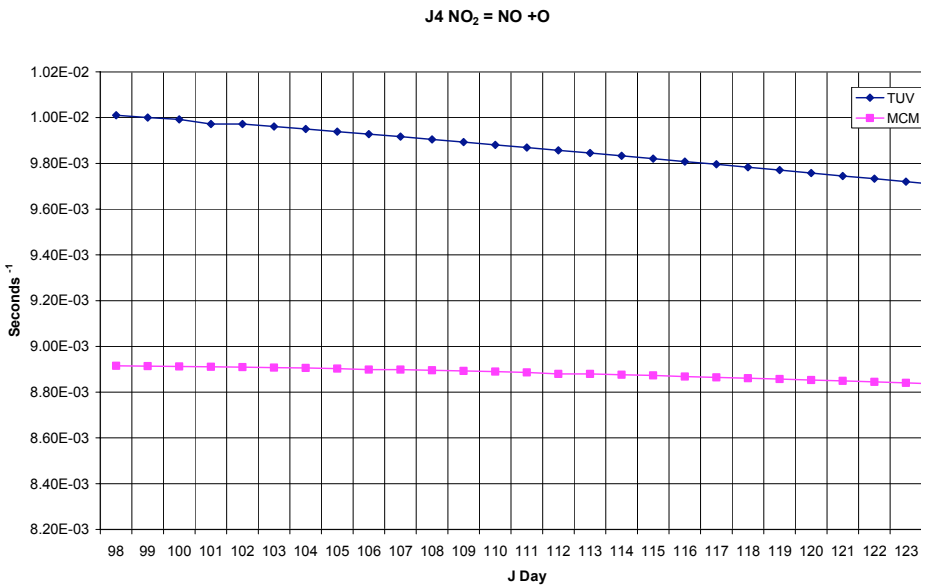
J4 NO2 = NO +O
1.02E-02
1.00E-02
9.80E-03
9.60E-03
9.40E-03
9.20E-03
9.00E-03
8.80E-03
8.60E-03
8.40E-03
8.20E-03
Seconds -1
98 99 100 101 102 103 104 105 106 107 108 109 110 111 112 113 114 115 116 117 118 119 120 121 122 123
J Day
TUV
MCM

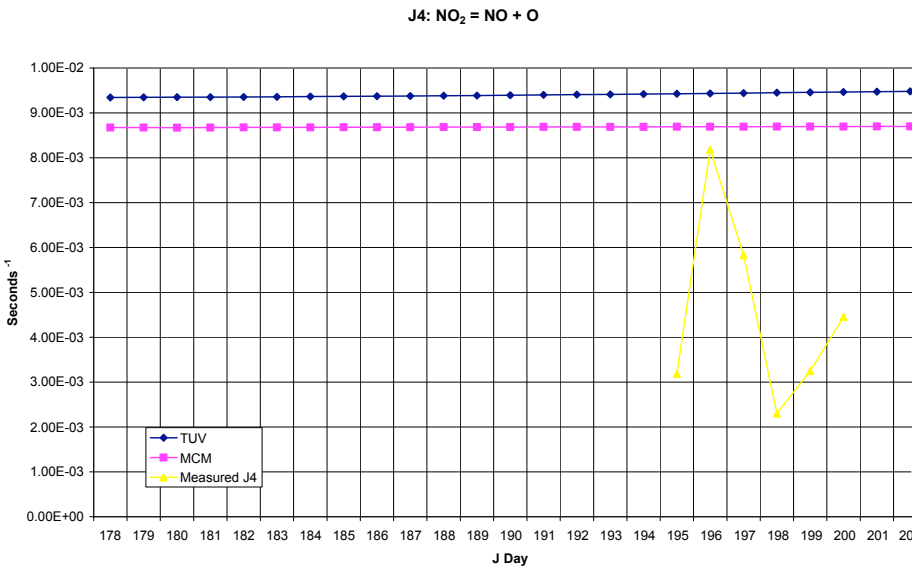
J4: NO2 = NO + O
1.00E-02
9.00E-03
8.00E-03
7.00E-03
6.00E-03
5.00E-03
4.00E-03
3.00E-03
2.00E-03
1.00E-03
0.00E+00
Seconds -1
178 179 180 181 182 183 184 185 186 187 188 189 190 191 192 193 194 195 196 197 198 199 200 201 20
J Day
TUV
MCM
Measured J4

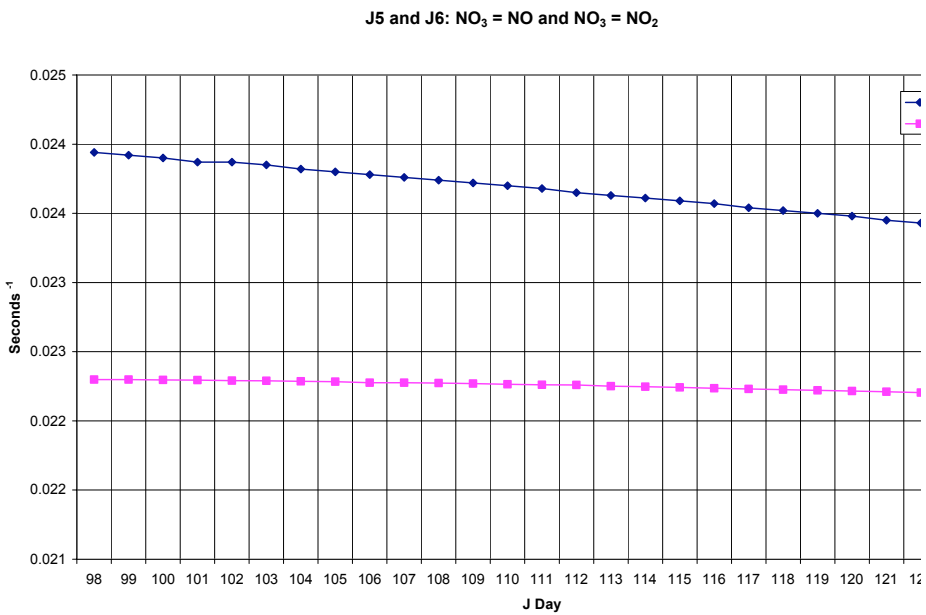
J5 and J6: NO3 = NO and NO3 = NO2
0.025
0.024
0.024
0.023
0.023
0.022
0.022
0.021
Seconds -1
98 99 100 101 102 103 104 105 106 107 108 109 110 111 112 113 114 115 116 117 118 119 120 121
J Day

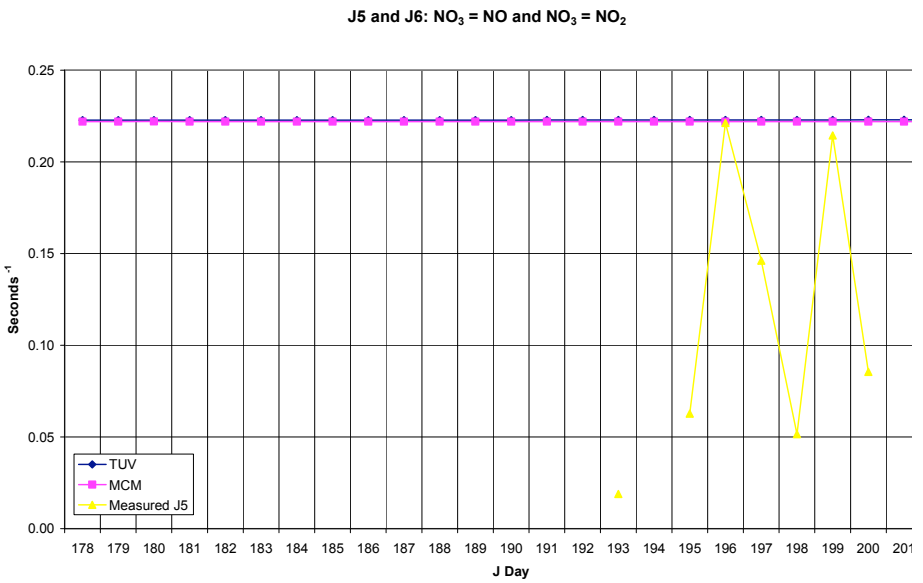
J5 and J6: NO3 = NO and NO3 = NO2
0.25
0.20
0.15
0.10
0.05
0.00
Seconds -1
TUV
MCM
Measured J5
178 179 180 181 182 183 184 185 186 187 188 189 190 191 192 193 194 195 196 197 198 199 200
J Day

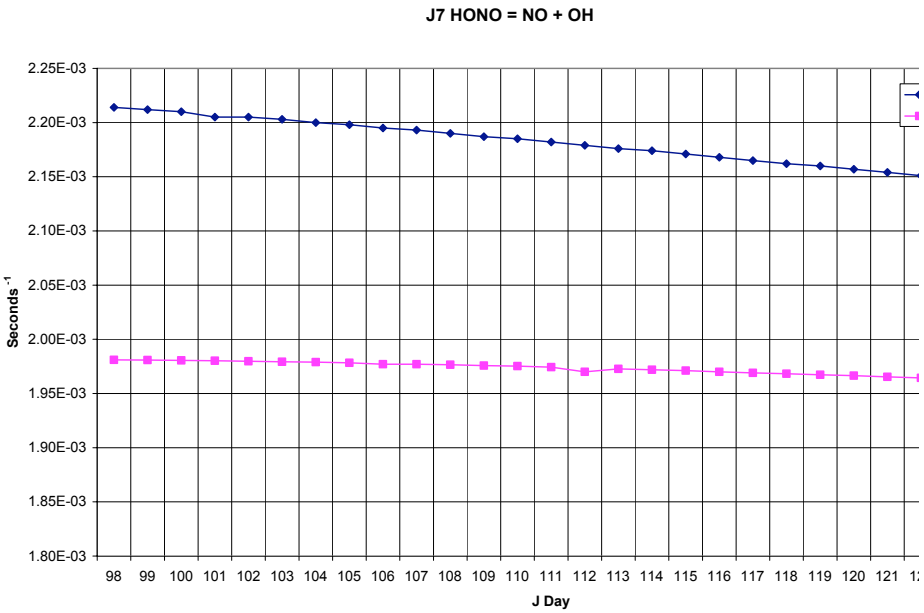
J7 HONO = NO + OH
2.25E-03
2.20E-03
2.15E-03
2.10E-03
2.05E-03
2.00E-03
1.95E-03
1.90E-03
1.85E-03
1.80E-03
Seconds -1
98 99 100 101 102 103 104 105 106 107 108 109 110 111 112 113 114 115 116 117 118 119 120 121
J Day

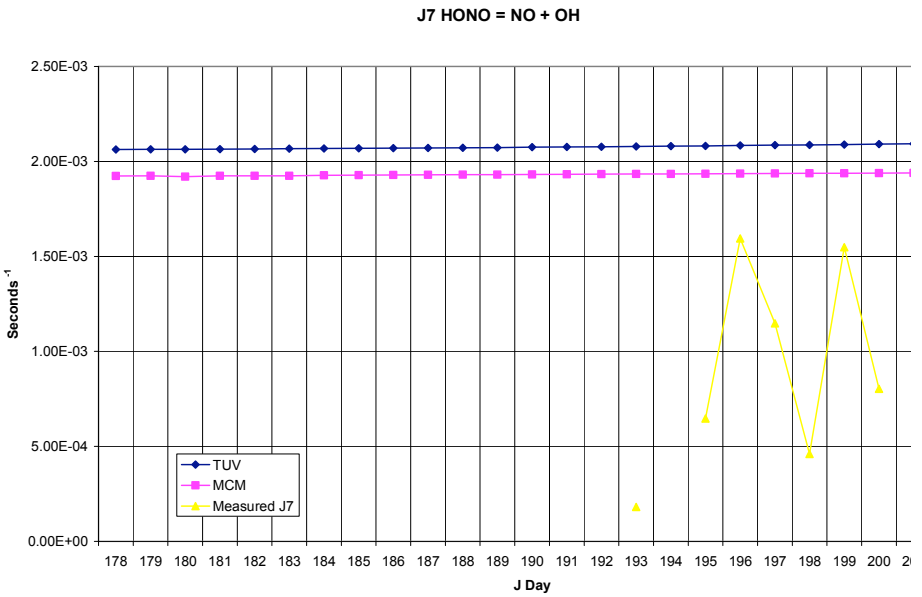
J7 HONO = NO + OH
2.50E-03
2.00E-03
1.50E-03
1.00E-03
5.00E-04
0.00E+00
Seconds -1
178 179 180 181 182 183 184 185 186 187 188 189 190 191 192 193 194 195 196 197 198 199 200
J Day
TUV
MCM
Measured J7

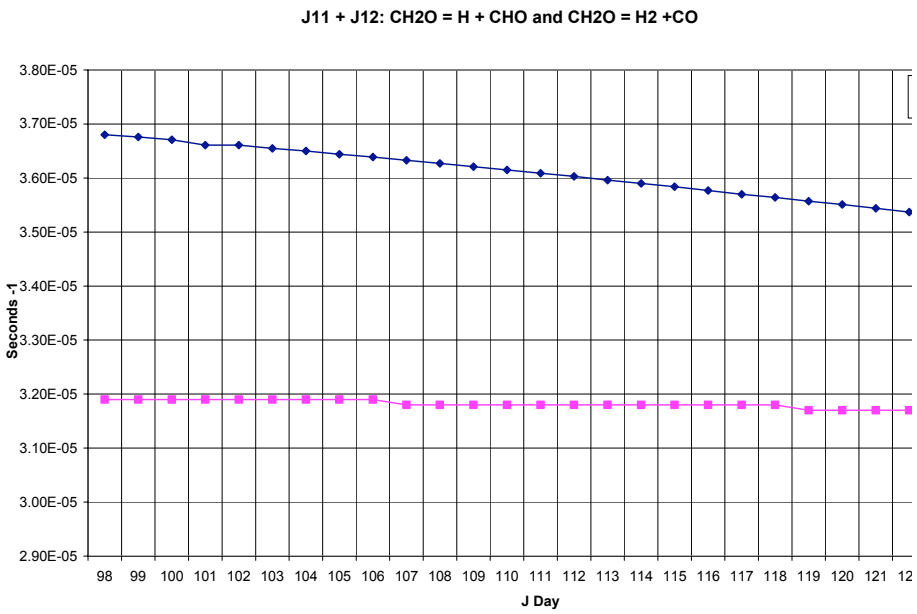
J11 + J12: CH2O = H + CHO and CH2O = H2 +CO
3.80E-05
3.70E-05
3.60E-05
3.50E-05
3.40E-05
3.30E-05
3.20E-05
3.10E-05
3.00E-05
2.90E-05
Seconds -1
98 99 100 101 102 103 104 105 106 107 108 109 110 111 112 113 114 115 116 117 118 119 120 121 12
J Day

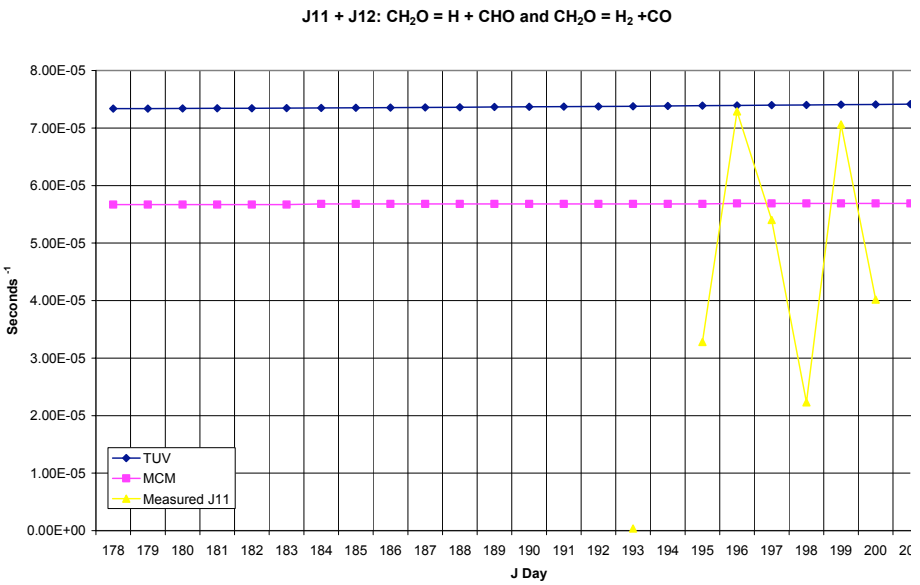
J11 + J12: CH2O = H + CHO and CH2O = H2 +CO
8.00E-05
7.00E-05
6.00E-05
5.00E-05
4.00E-05
3.00E-05
2.00E-05
1.00E-05
0.00E+00
Seconds -1
TUV
MCM
Measured J11
178 179 180 181 182 183 184 185 186 187 188 189 190 191 192 193 194 195 196 197 198 199 200
J Day

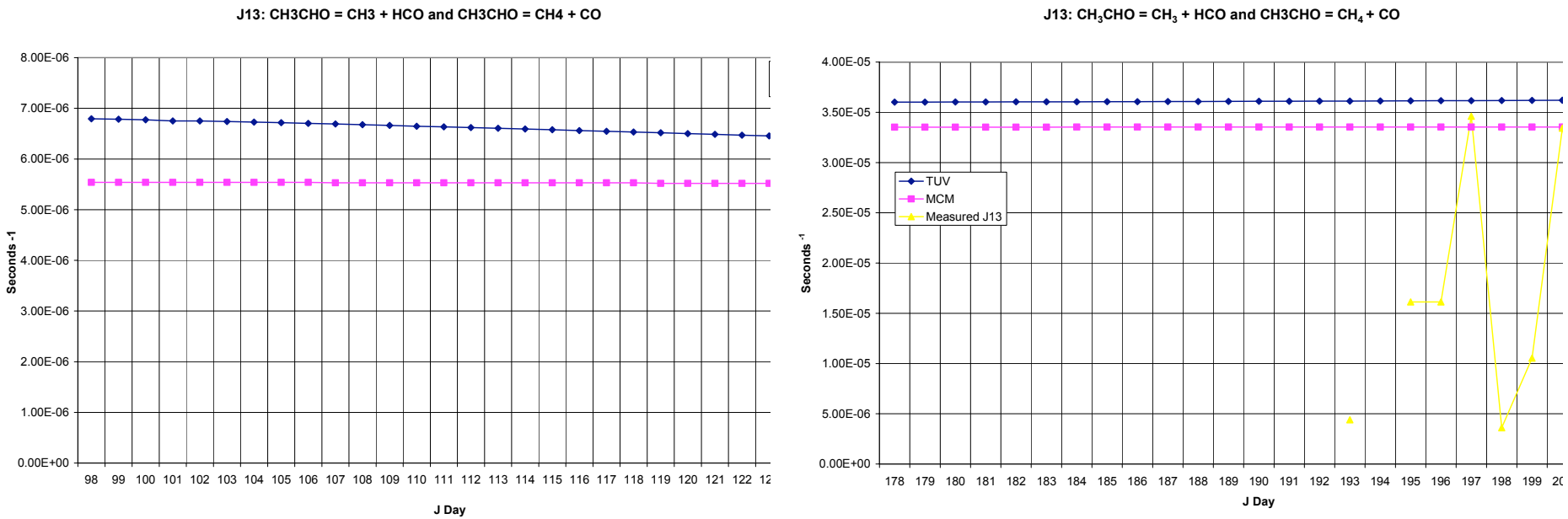

Figure 3.10. Comparison between photolysis rates from the model containing the MCM and the TUV for four photolysis reactions in the model mechanism

The comparison between the TUV and predictions of photolysis rates in the model (table 3.5) shows differences between the values for the photolysis rates of most photochemical species in the model. The differences in the photolysis rates predicted by the two models vary between species, ranging from 0.4% for JNO_3 to 23% for JCH_2O. The data from the TUV has been used in many other studies and has been found to give accurate data for the rates of photochemical reactions (Michalsky, 2008). This indicates that the photolysis predictions from the MCM model are suitable to use as they are comparable to the predictions from the TUV model.

Table 3.5: Quantified differences between the TUV and MCM photolysis models for the first and second phases of the field campaign at Bukit Atur

	Phase 1 Average s^{-1}			Phase 2 Average s^{-1}		
	TUV	MCM	Difference %	TUV	MCM	Difference %
JO^1D	$4.2x10^{-5}$	$3.7x10^{-05}$	12.7	$3.8\ x10^{-05}$	$3.4\ x10^{-05}$	11.3
JNO_2	$9.9x10^{-3}$	$8.8\ x10^{-3}$	10.0	$9.4\ x10^{-3}$	$8.6\ x10^{-3}$	7.6
JNO_3	$2.3x10^{-2}$	$2.2\ x10^{-2}$	6.0	2.210^{-2}	2.210^{-2}	0.4
JHONO	$2.2x10^{3}$	$2.0\ x10^{3}$	9.6	$2.1\ x10^{3}$	$2.0\ x10^{3}$	7.0
JCH_2O	$3.6x10^{-5}$	$1.2\ x10^{-5}$	11.8	$7.4\ x10^{-5}$	$5.7\ x10^{-5}$	23.0
JCH_3CHO	$6.6x10^{-6}$	$5.5\ x10^{-6}$	16.6	$3.6\ x10^{-5}$	$3.4\ x10^{-5}$	7.1

As the MCM and TUV models produce similar photolysis rates it was decided just to use the MCM values. These values were chosen as having to generate many photolysis values from the TUV and constraining them in the MCM would reduce the efficiency of the model.

3.5 Dry Deposition Velocities

Specific chemical, physical or biological interaction mechanisms allow many chemical species to be absorbed onto the surfaces of plants, trees, soil or other objects with large surface areas (Zhang et al., 2002). This mechanism, known as dry deposition, is factored into the model and expressed as a function of the dry deposition velocity (V_s) and the mixing height of the boundary layer (H_{mix}).

$$\mathbf{k_{dep} = V_s/H_{mix}} \qquad \textbf{(Equation 3.2)}$$

Depending on the type of vegetation in the area the deposition velocity can be affected, as different vegetation types will have different surface areas: vegetation with larger surface areas will encourage more deposition (Zhang et al., 2002). The vegetation at the study site was a mixture of deciduous broadleaf tees and needle leaf trees (Hewitt et al., 2009).

The MCM already included a baseline series of dry deposition velocities for species including HNO_3, O_3, NO_2, PANs, H_2O_2 and other large organic species (as described in chapter 2). The model was run using the baseline deposition velocities from the MCM and compared with model runs using the dry deposition velocities calculated by Zhang et al., (2000) for the vegetation types present. A further model test was carried out, setting all deposition velocities in the model to 0.1 cm s^{-1}. Table 3.6 shows the original deposition velocity values taken from the MCM compared with the values for two different environmental conditions calculated by Zhang et al., (2000). A fourth model scenario was used, where all deposition velocities in the model were set to 0.1 cm s^{-1}.

Table 3.6 Dry-deposition velocities taken from the MCM and two modeled scenarios containing different types of vegetation.

	Dry-Deposition Velocity cm s^{-1}		
Species	Original MCM Value	Broadleaf Trees	Mixed Broadleaf and Needleleaf Trees
SO_2	0.500	0.890	1.079
NO_2	0.150	0.885	1.099
O_3	0.500	0.923	1.136
H_2O_2	1.100	1.318	1.571
HNO_3	2.000	4.700	5.042
HONO	****	1.728	1.969
PAN	0.200	0.604	0.748
MPAN	0.200	0.490	0.620
HCHO	0.330	1.108	1.365
MVK	****	0.579	0.752
MACR	****	0.375	0.439

When the vegetation type is set to mixed broadleaf and needle leaf trees, which represents vegetation with larger surface areas and is the most reflective of the vegetation at the field site (Hewitt et al. 2009) more HO_2 is removed from the system (figure 3.12) (table 3.7). However, even though the mixed broadleaf and needle leaf deposition gives values of HO_2 that are closer to the measurements, they are still along way the actual measurements.

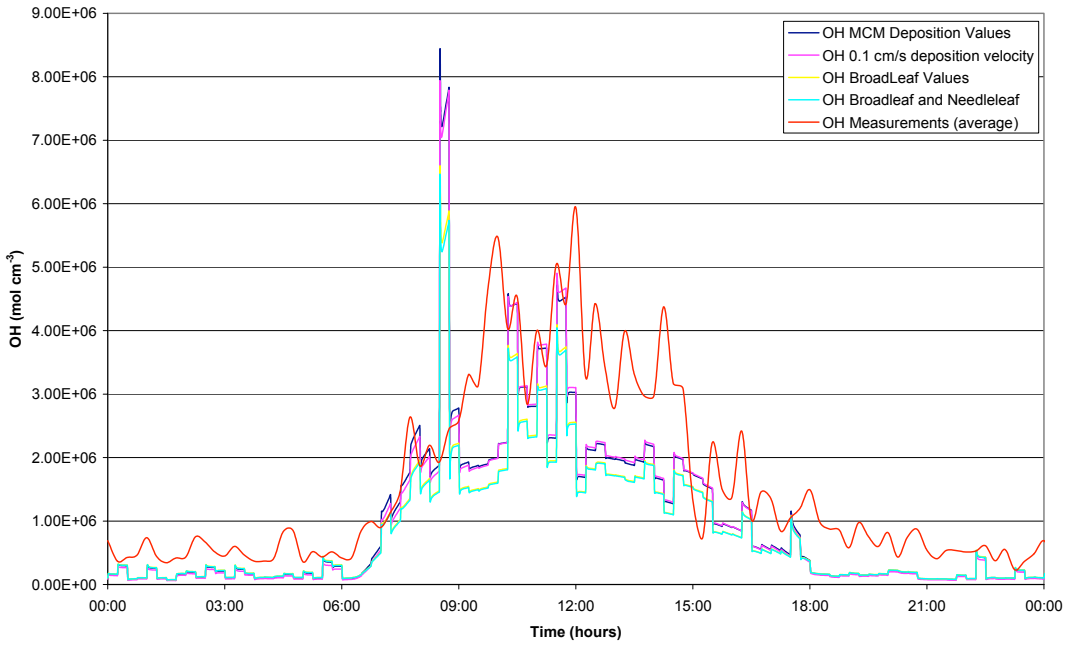

Figure 3. 11. OH predictions using different vegetation types for the average day conditions during second phase of field study.

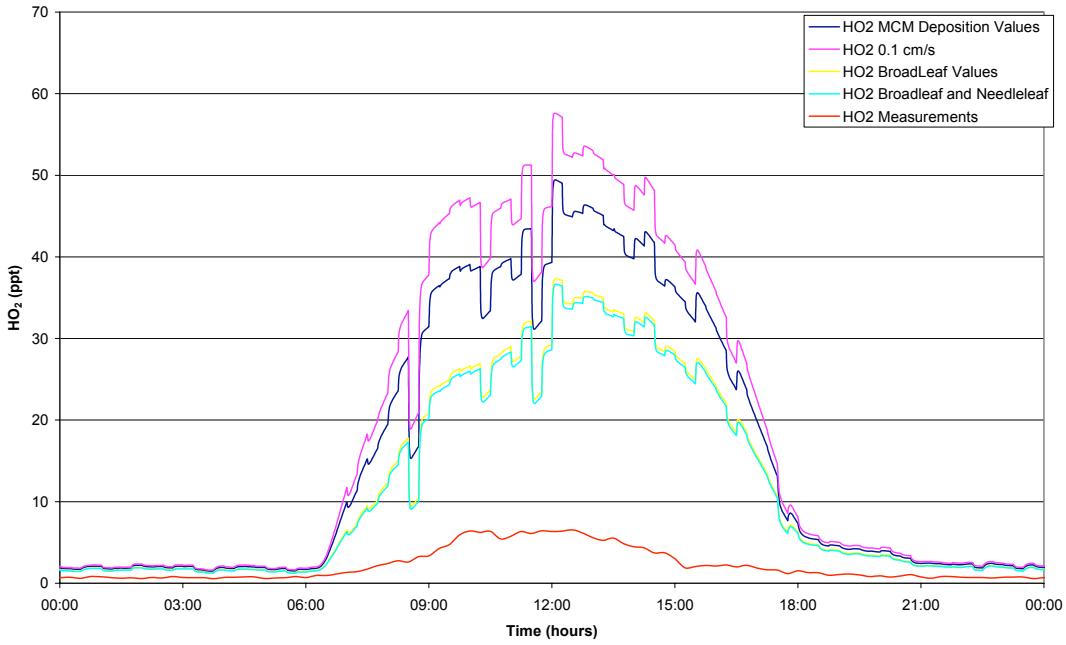

Figure 3. 12. HO_2 predictions using different vegetation types for the average day conditions during second phase of field study.

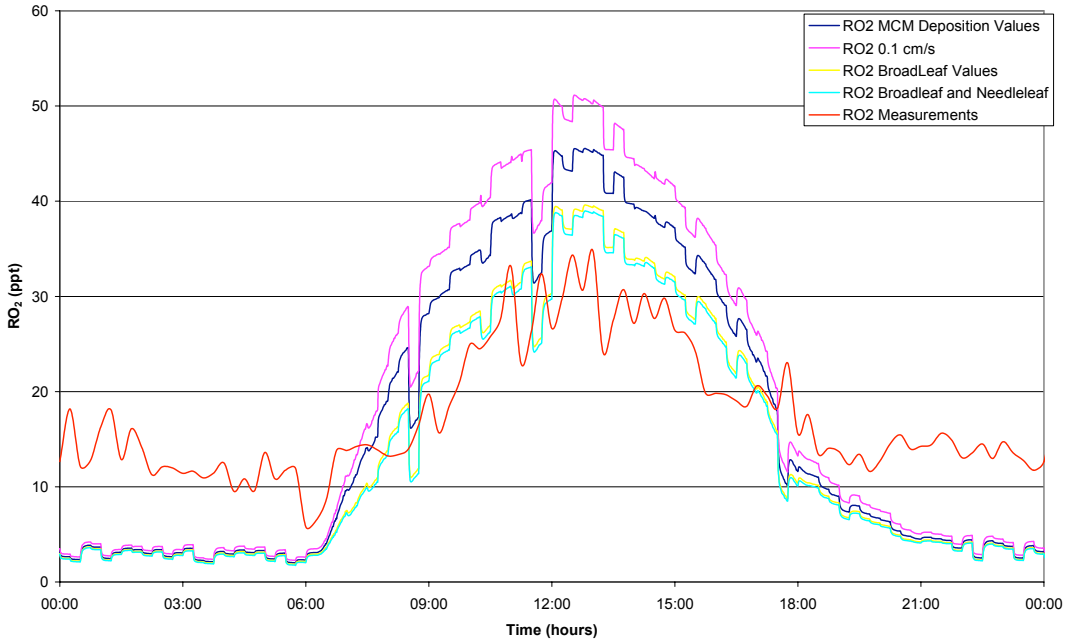

Figure 3. 13. RO_2 predictions using different vegetation types for the average day conditions during second phase of field study.

Table 3.7 Midday concentrations of radical species for an average condition day during second phase of field campaign using different deposition velocities.

Radical Concentrations at 12:00 using averaged data profiles								
OH mol cm^{-3}	MCM	$3.03x10^6$	HO2 ppt	MCM	39.32	RO2 ppt	MCM	36.90
	0.1 cm s-1	$3.10 x10^6$		0.1 cm s-1	46.19		0.1 cm s-1	41.94
	Broadleaf	$2.56 x10^6$		Broadleaf	29.52		Broadleaf	30.29
	Mixed Broadleaf and Needle leaf	$2.53 x10^6$		Mixed Broadleaf and Needle leaf	28.64		Mixed Broadleaf and Needle leaf	29.72
	Measurements	$5.92 x10^6$		Measurements	6.33		Measurements	26.63

The OP3 model is not constrained using concentrations of methyl vinyl ketone (MVK) or methacrolin (MACR) so it was used to generate concentrations of these species. One of the main sinks for these species is removal from the chemical system by dry deposition. When the model was tested with the baseline deposition and then deposition velocities for a mixed broadleaf and needle leaf forest generated predictions of MVK that were closest in concentration to observed values of MVK were obtained for the later scenario(figure 3.14). Even though the mixed leaf deposition values generated the closest values of MVK to the measurements they were still showing a general over prediction. Predicted values of MACR showed the same trend as MVK with deposition velocities for mixed leaf conditions generating the lowest predictions of MACR (figure 3.15). When the predictions of MACR were compared to the measurements, all four model scenarios show an over prediction with the mixed leaf scenario being the closest. However, at the closest point the prediction is still over 100 ppt above the measurement.

The model was tested with other theoretical values for the deposition velocity of MACR in order to discover what value would be required to force the predicted concentration of MACR to match the measured value. The theoretical deposition velocity needed would be between 2 cm s^{-1} and 4 cm s^{-1}, this is over five times greater than the value reported by Zhang et al,. (2000).

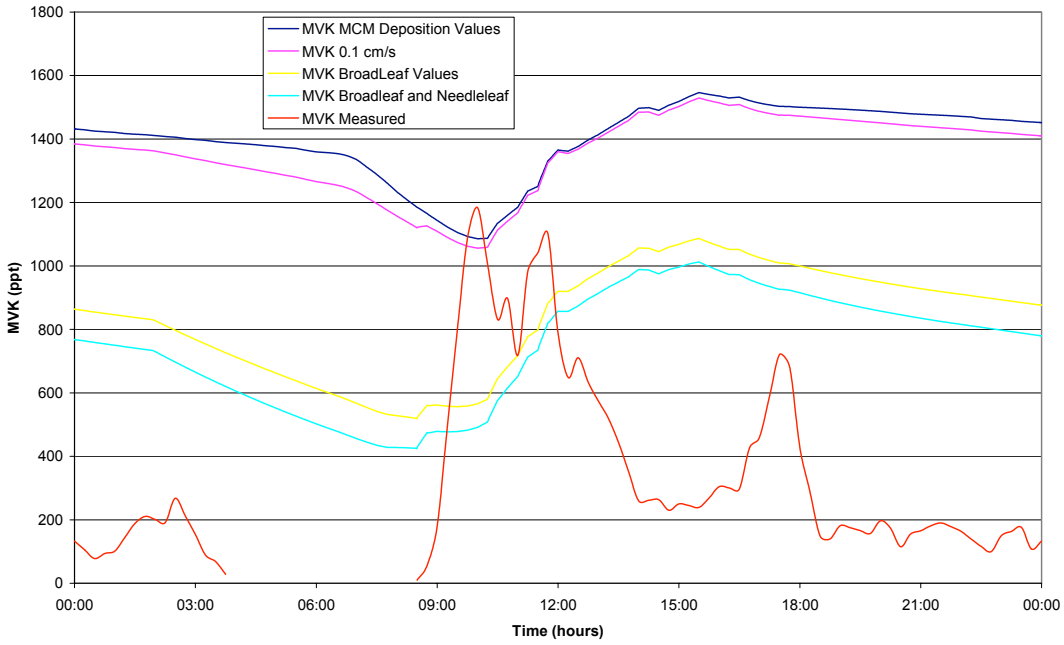

Figure 3.14 MVK predictions using different vegetation types for average day conditions during second phase of field study.

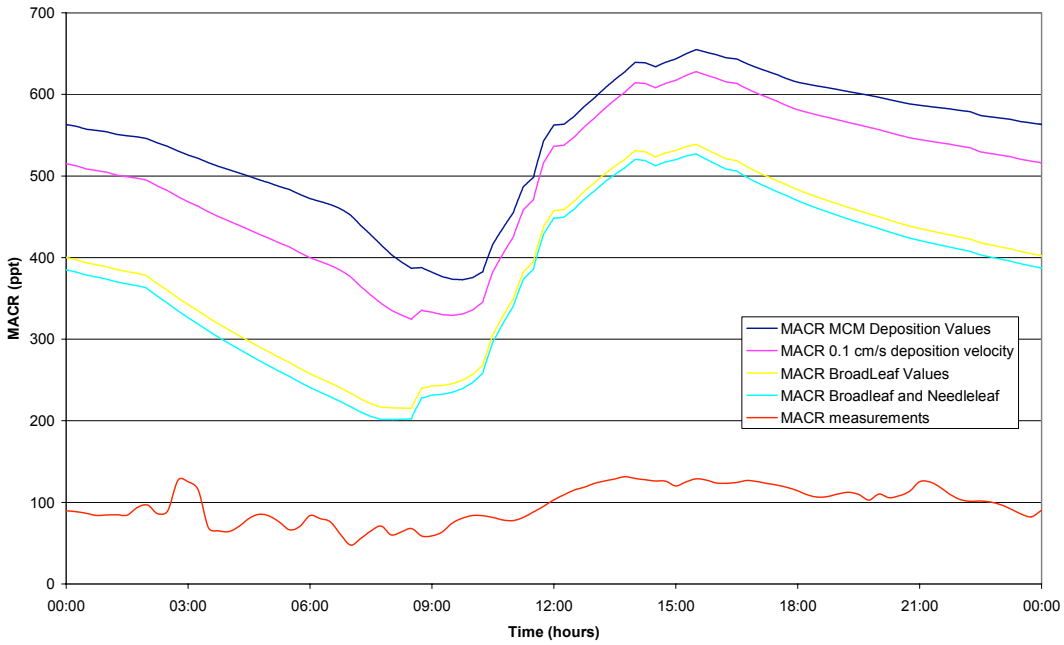

Figure 3.15 MACR predictions using different vegetation types for average day conditions during second phase of field study.

By setting the deposition velocities to those most reflective of the study site the output concentration predictions of radical species were closer in value to the observed values at the field site. The deposition velocities for the mixed broadleaf and needle leaf vegetation from Zhang et al., (2000) were chosen to be used in the OP3 model for future runs.

3.6 HO_2 Uptake Rate

As discussed in chapter 2, the OP3 model considers heterogeneous uptake of HO_2 onto aerosol surfaces. The uptake rate for HO_2 (k_t) is constrained every 15 minutes along with the other constrained input data.

The uptake rate depends upon the effective collision diameter of HO_2 in the air and the value of the uptake coefficient. The value of the uptake coefficient can range from 1 to 0. At 1 everything that comes into contact with the aerosol will stick to its surface, when the coefficient is set to 0 nothing ever sticks on collision with the aerosol.

$k_t = ¼\ c\ \gamma\ A$ **Equation 1**

The value of k_t constrained in the model was calculated using equation 1. In the equation c represents the mean velocity of the gas particles, γ is the fractional probability of reactive uptake and A represents the surface area of the aerosol. The value of A was set to a constant of 0.12 Å (1.2×10^{-9} cm^{-2}).

Data provided by Niall Robinson at the University of Manchester on 01/11/2010 was used to test the effect of changing the uptake variables in the model. It was suggested that the most likely value of the uptake rate is calculated using a γ value of 0.05.

Figure 3.17 shows the effects of altering the uptake rate of HO_2. Two of the three sets of data being compared are using uptake coefficients with γ values of 1 and 0.05. The third series of data was used where the value of k_t calculated using a γ of zero. All these model runs were compared to actual measurements of the radical species.

When the HO_2 concentration predictions using the three different values of k_t are compared, the uptake coefficient of 1 produces lower concentrations of HO_2 than a value of 0.05 (figure 3.17): The midday HO_2 concentration was 37.9 compared to 46.6 ppt respectively. The larger uptake rate lowers the midday maximum value of HO_2 by 22% when compared to the smaller uptake rates. However, the use of a larger value of k_t decreases the predicted concentration of OH (figure 3.16), causing a 20%

decrease to the midday concentration. This reduction in the predicted concentration of OH leads to an even larger under prediction of OH generation.

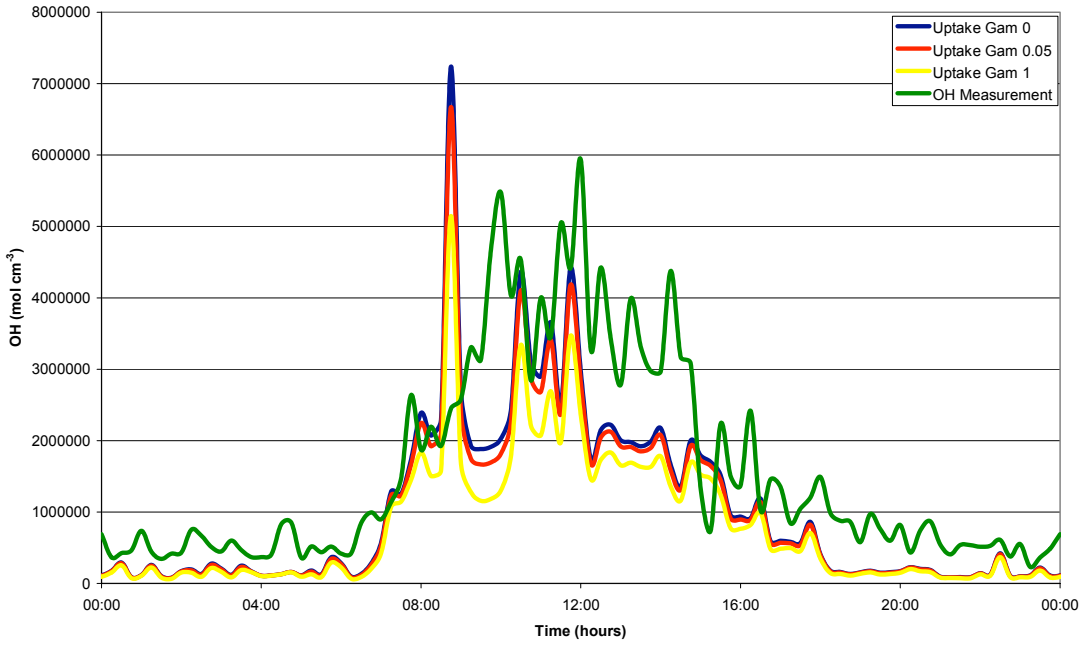

Figure 3.16. Output predictions of OH concentrations with different k_t values constrained in the model

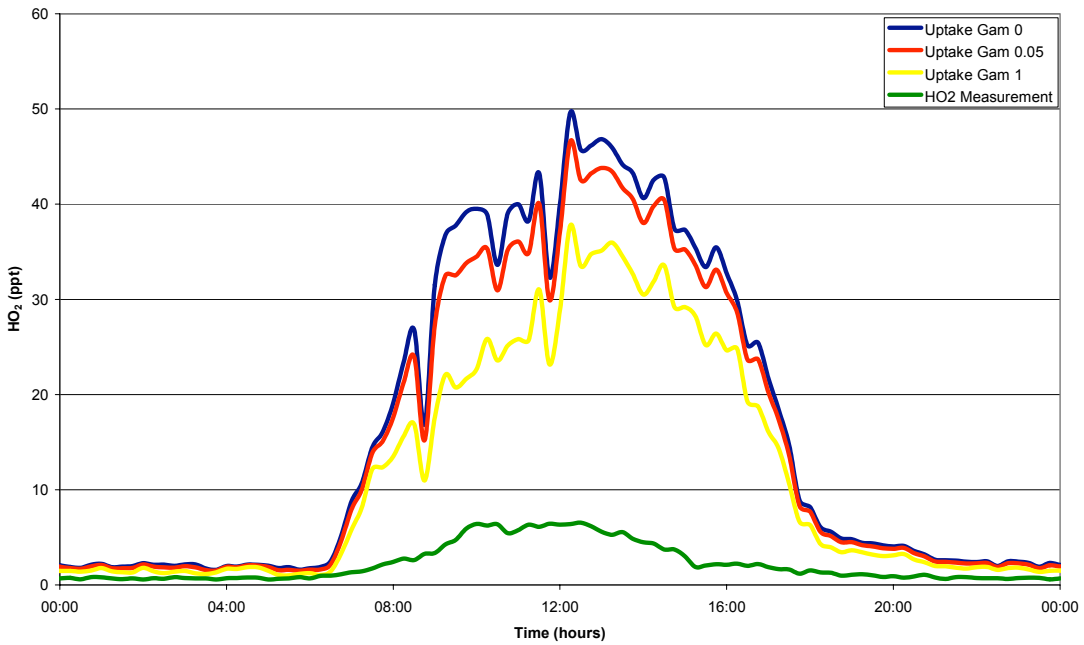

Figure 3.17. Output predictions of HO_2 concentrations with different k_t values constrained in the model

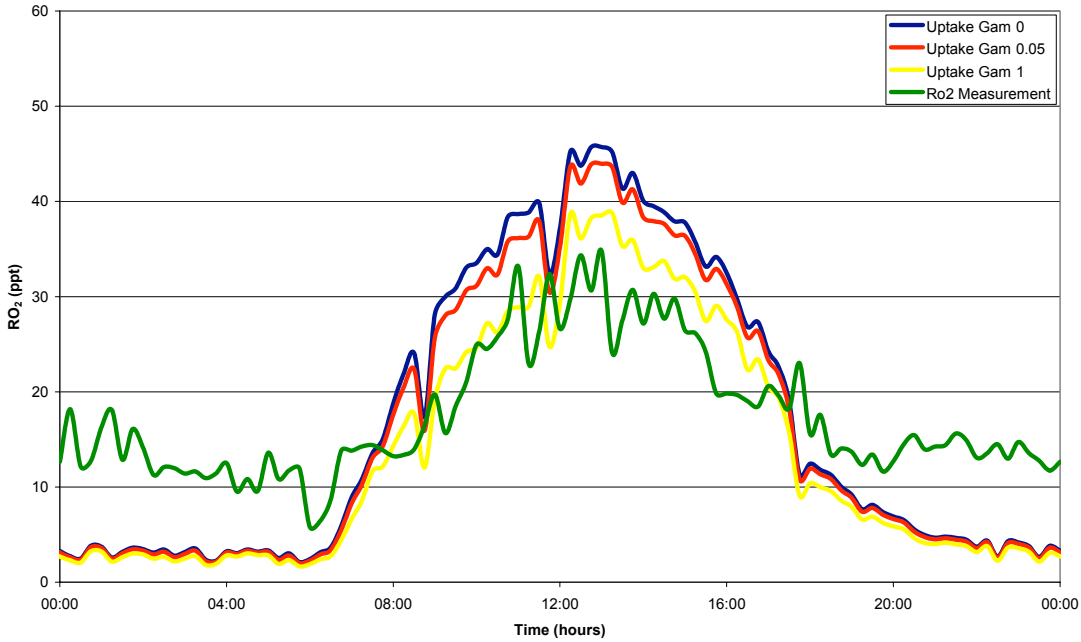

Figure 3.18. Output predictions of RO_2 concentrations with different k_t values constrained in the model

Table 3.8 Mean values of OH, HO_2 and RO_2 predictions from 3 different model runs (the original MCM based model using values of k_t at 0, 0.05 and 1 supplied by Manchester) using average data set for the second phase of the field campaign, from 22nd June 2008 until 30th July 2008 at Bukit Atur field site.

	Mean 24 Hour Value			Daytime (06:00-18:00)			Nighttime (18:00-06:00)		
	OH (mol cm-3)	HO2 (ppt)	RO2 (ppt)	OH (mol cm-3)	HO2 (ppt)	RO2 (ppt)	OH (mol cm-3)	HO2 (ppt)	RO2 (ppt)
k_t 0	1.01E+06	16	17	1.84E+06	30	29	1.69E+05	3	5
k_t 0.05	9.50E+05	15	16	1.73E+06	27	27	1.61E+05	3	4
k_t 1	7.82E+05	12	14	1.42E+06	21	23	1.41E+05	2	4
Actual Measurements	1.59E+06	2	18	2.58E+06	4	22	5.84E+05	1	13

The larger value of k_t has more of an effect on the production of HO_2 concentration from the model, bringing the predicted value the closest to the actual observed values of HO_2. However, a k_t value of 1 would be very unlikely to occur and would not be suitable to use in the model as it would not reflect realistic conditions of the uptake in the area. In the data provided by the University of Manchester and through discussion with Leeds University, it was decided that the most realistic values to use in the model would be the k_t values calculated using the γ values of 0.05.

3.7 Peeters Mechanism

The effect of adding the new isoprene scheme was compared to existing isoprene scheme by running the model with the new scheme with the average day profile data for the second phase of the campaign (figure 3.19, 3.20, 3.21).

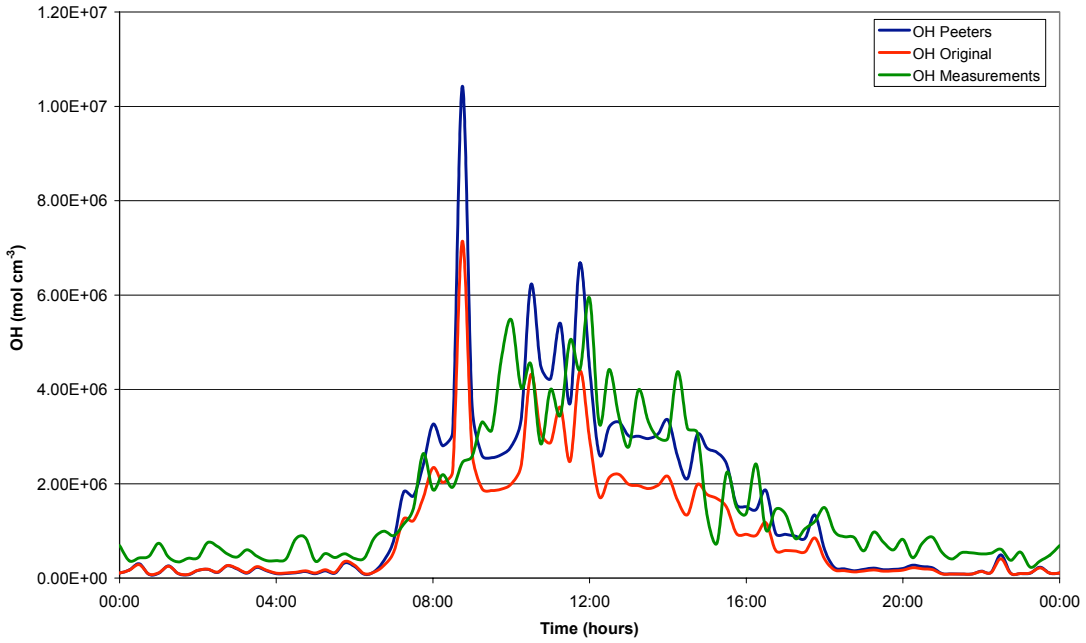

Figure 3.19 Comparison of measured OH and modelled OH from existing and experimental isoprene schemes using average data set for the second phase of the field campaign, from 22nd June 2008 until 30th July 2008 at Bukit Atur field site.

The replacement of the original MCM isoprene mechanism with the newly proposed Peeters mechanism saw an increase in the out put of OH from the model. When the outputs from the two schemes are compared both mechanisms predict the same trends with peaks in the OH concentration predicted at the same times throughout the day. However, the new mechanism predicts values of OH that are much closer to the observed values.

The average observed midday value of OH was 5.9×10^6 mol cm^{-3}. The original mechanism only predicts just over 50% of this (3.1×10^6 mol cm^{-3}), but the new mechanism with the Peeters isoprene degradation scheme was able to predict 78% of the observed values (4.6×10^6 mol cm^{-3}). When values for the whole of the daytime are used (06:00-18:00 hours) (Table 3.8) the model containing the Peeters scheme

shows an over prediction OH in this period of 4% where as the original model indicates a general under prediction of 30%

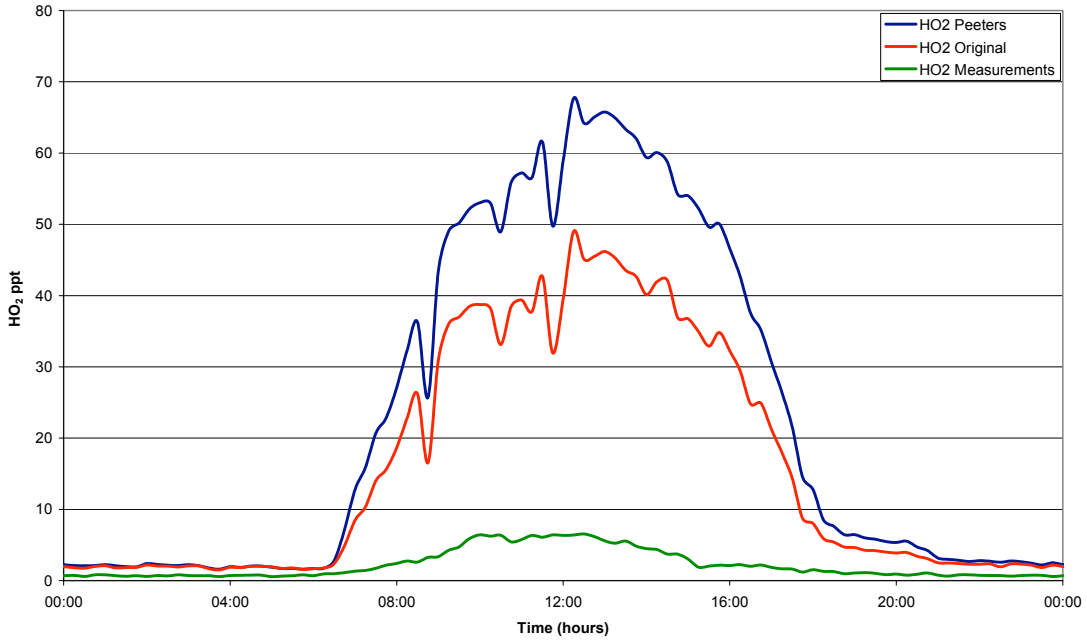

Figure 3.20 Comparison of measured HO_2 and modelled HO_2 from existing and experimental isoprene schemes using average data set for the second phase of the field campaign, from 22nd June 2008 until 30th July 2008 at Bukit Atur field site.

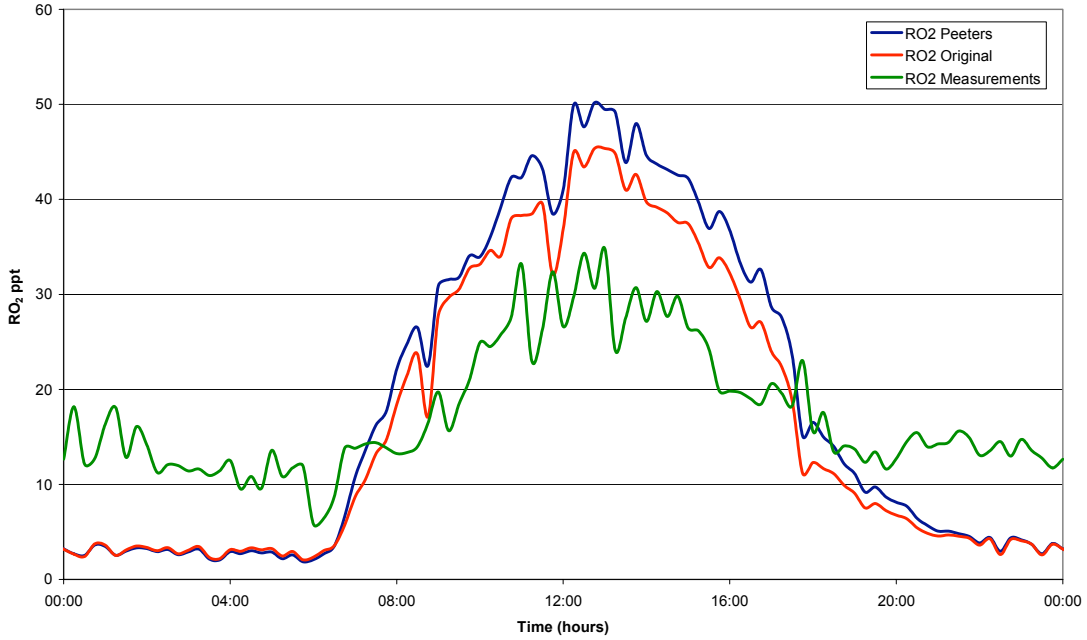

Figure 3.21 Comparison of measured RO_2 and modelled RO_2 from existing and experimental isoprene schemes using average data set for the second phase of the field campaign, from 22nd June 2008 until 30th July 2008 at Bukit Atur field site.

The addition of the new scheme also affected the production of HO_2 and RO_2 in the model. The HO_2 concentration increased in concentration, as did the RO_2. The 500% over prediction of HO_2 in creased to 700% with the addition of the new scheme and the 28% over prediction of RO_2 increased to 40%. On average the daytime prediction from the model containing the Peeters Scheme (06-00-18:00 hours) shows an over prediction of HO_2 production in the region of 10 times (table 3.9) compared to the original model where the over prediction was 7 times the observed values. Table 3.8 also shows that the introduction of the Peeters Scheme also leads to an increase in the over prediction of RO_2 in the daytime period. However, where the introduction of the Peeters scheme leads to a much larger prediction of HO_2 for the whole 24 hour period, the effect on the production of RO_2 is not as great in the 24 hour averaged period.

Table 3.9 Mean values of OH, HO_2 and RO_2 predictions from 2 different model runs (original baseline MCM model and the same model but including the Peeters scheme) using average data set for the second phase of the field campaign, from 22nd June 2008 until 30th July 2008 at Bukit Atur field site.

	Mean 24 Hour Value			Daytime (06:00-18:00)			Nighttime (18:00-06:00)		
	OH (mol cm-3)	HO2 (ppt)	RO2 (ppt)	OH (mol cm-3)	HO2 (ppt)	RO2 (ppt)	OH (mol cm-3)	HO2 (ppt)	RO2 (ppt)
Original MCM base model	9.95E+05	16	17	1.82E+06	29	28	1.63E+05	3	4
Model with new Peeters Scheme	1.44E+06	23	19	2.69E+06	42	32	1.73E+05	3	5
Average Measurements	1.59E+06	2	18	2.58E+06	4	22	5.84E+05	1	13

The increases in HO_2 and RO_2 were predicted as the yield of HO_2 as well as OH from each isoprene oxidised would increase (Peeters et al., 2009).

3.8 Summary

When each phase of the model validation process is viewed on its own, it indicates how changing one value singularly effects the working of the model. All of the validation steps must be combined to view the overall effect that the choices of parameters have had on the model as a whole.

In order to observe the effects that the changes to the mechanism have made a baseline run of the original MCM based model is compared to a run of the model containing changes to the uptake rates, deposition rates (run 1). A further comparison is made between a baseline run and a model run containing the changes to the uptake rates, deposition rates and the effect that the proposed Peeters Mechanisms has (run 2) (figure 3.22, 3.23, 3.24).

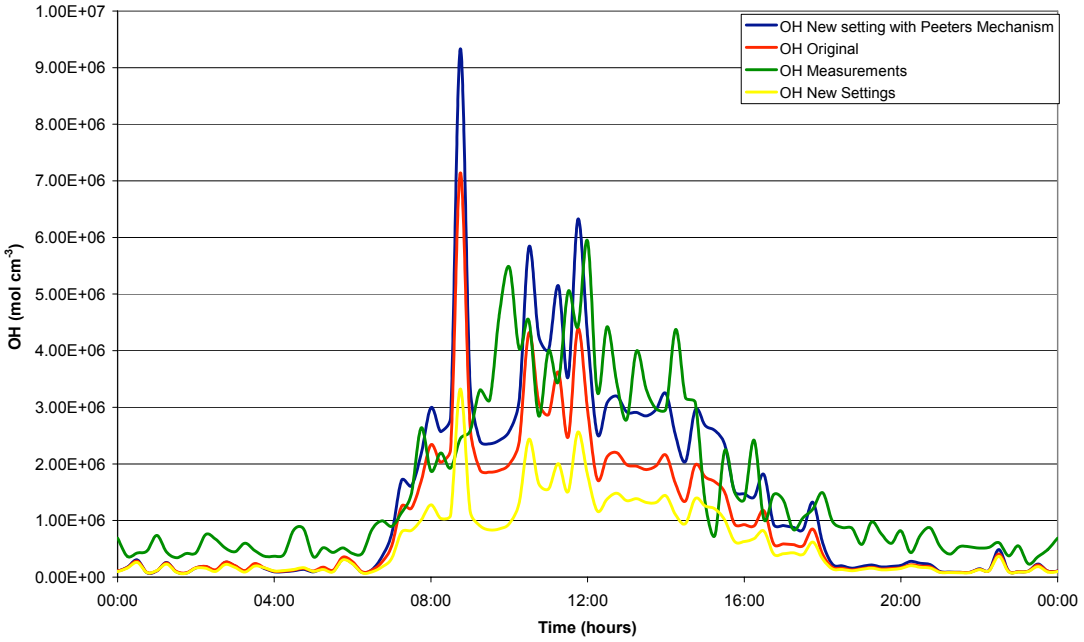

Figure 3.22 Comparison of measured OH and modelled OH using average data set for the second phase of the field campaign, from 22nd June 2008 until 30th July 2008 at Bukit Atur field site. Modelled data is taken from an original MCM based model, a model using new uptake and deposition values (run 1) and a model containing new uptake values, deposition values and the proposed Peeters scheme.

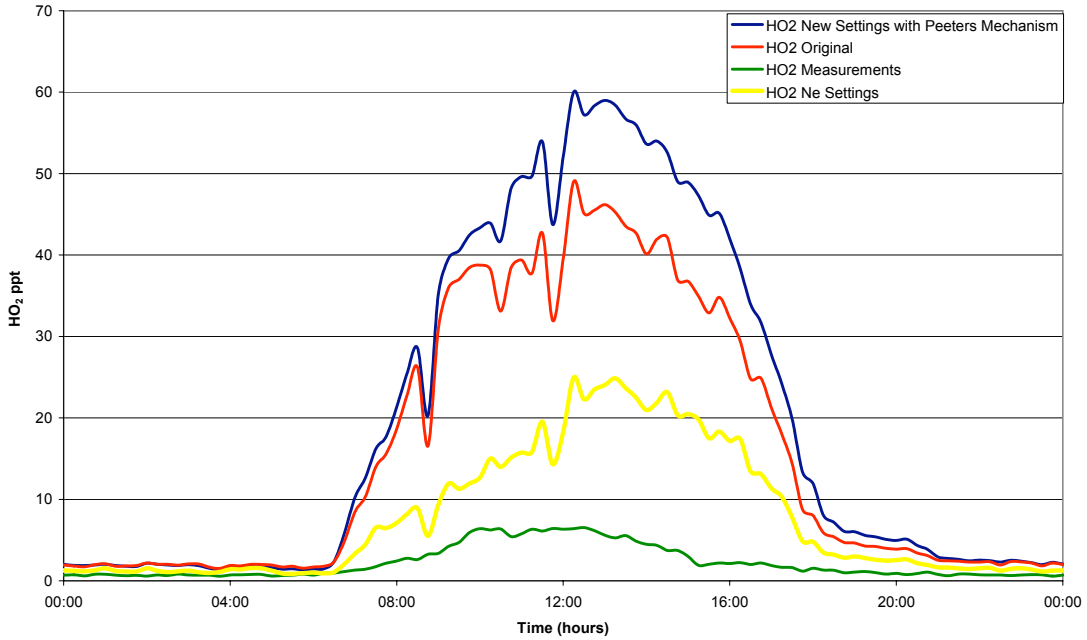

Figure 3.23 Comparison of measured HO_2 and modelled HO_2 using average data set for the second phase of the field campaign, from 22nd June 2008 until 30th July 2008 at Bukit Atur field site. Modelled data is taken from an original MCM based model, a model using new uptake and deposition values (run 1) and a model containing new uptake values, deposition values and the proposed Peeters scheme.

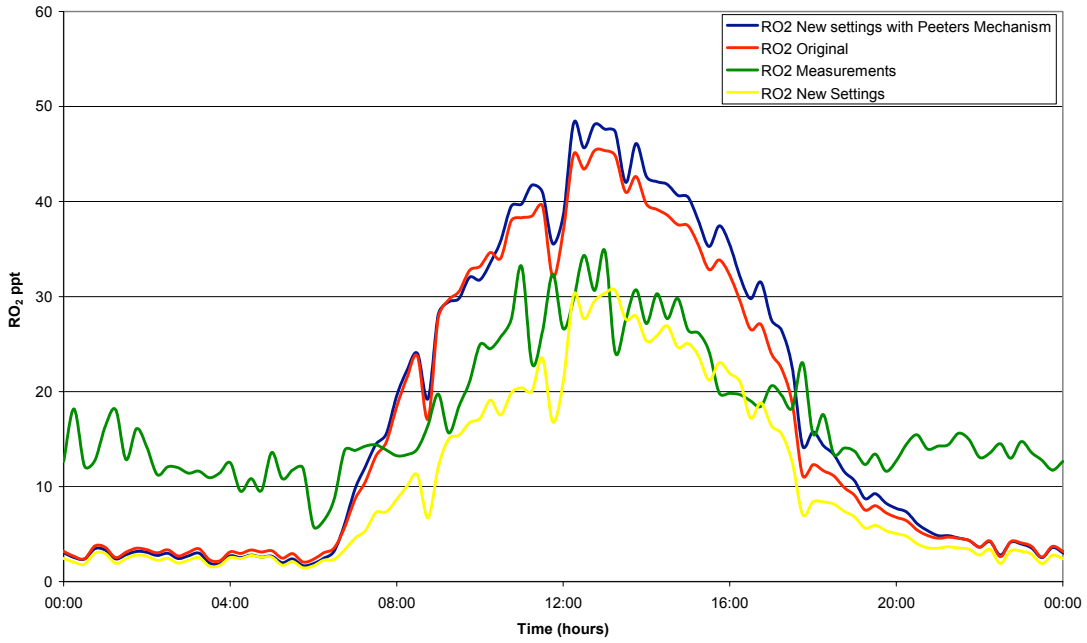

Figure 3.24 Comparison of measured RO_2 and modelled RO_2 using average data set for the second phase of the field campaign, from 22nd June 2008 until 30th July 2008 at Bukit Atur field site. Modelled data is taken from an original MCM based model, a model using new uptake and deposition values (run 1) and a model containing new uptake values, deposition values and the proposed Peeters scheme.

The results shown in figures 3.22, 3.23 and 3.24 indicates that by changing the variables in combination and then by adding in the new Peeters scheme, there are significant changes to the outputted predicted values in the concentrations of the radical species. These differences are quantified in table 3.9. The predicted values when averaged over time shows that run 1 lowers all the predicted radical values when compared to the baseline reading, but when the Peeters scheme is added to this (run 2) this increases the values of the predicted radical output.

Table 3.10 Mean values of OH, HO_2 and RO_2 predictions from 3 different model runs (original baseline MCM model, run 1 and run 2) using average data set for the second phase of the field campaign, from 22nd June 2008 until 30th July 2008 at Bukit Atur field site.

	Mean 24 Hour Value			Daytime (06:00-18:00)			Nighttime (18:00-06:00)		
	OH (mol cm^{-3})	HO_2 (ppt)	RO_2 (ppt)	OH (mol cm^{-3})	HO_2 (ppt)	RO_2 (ppt)	OH (mol cm^{-3})	HO_2 (ppt)	RO_2 (ppt)
Original MCM base model	9.95E+05	16	17	1.82E+06	29	28	1.63E+05	3	4
Model with new uptake and deposition (run 1)	6.15E+05	8	10	1.08E+06	14	17	1.46E+05	2	3
Model with new uptake, deposition, photolysis and Peeters Scheme (run 2)	1.37E+06	20	18	2.55E+06	37	30	1.75E+05	3	5
Average Measurements	1.59E+06	2	18	2.58E+06	4	22	5.84E+05	1	13

When Run 2 is compared with the average measured values the OH (Table 3.10) results show a 14% difference with the 24 hour mean and only 1 % difference with the daytime mean, compared to the original baseline run where there is a 30% difference over the 24 hour mean and 37% difference during the daytime. However, the nighttime mean for both the baseline run and Run 2 show approximately a 70% difference to the observed values.

The comparison of the predicted HO_2 and RO_2 output from the three model runs with the observed average results shows that the addition of the uptake and deposition rates (run 1) lead to an improvement of the accuracy of the HO_2 predictions, but the addition of the Peeters Scheme removed this improvement making Run 2 less accurate than the original baseline predictions.

The comparison of the mean 24 hour averaged figures illustrate that the Run 2 predictions were ten times greater than the observed values, while Run 1 was only 4 times larger. This is also observed in the daytime output when compared to the observed daytime values. The nighttime values indicate a similar trend in the comparison of modelled and measured HO_2, but there is a difference in the RO_2 values. The nighttime RO_2 is under predicted by 3 to 5 times by all three of the model runs.

In conclusion the improvements to the prediction of OH indicates that the model should include the changes to the uptake, deposition and include the Peeters scheme. However, the large over prediction of HO_2 by the model including the Peeters scheme implies that this additional mechanism has not solved all the faults in the model. Therefore, it is probably wisest to run 2 models, one containing the updated uptake and deposition variables (Run 1) and another containing these changes and the Peeters scheme.

Chapter 4. OP3 July Campaign

4.1.1 Introduction

The second phase of the OP3 field campaign was conducted from the 23rd June 2008 through to 20th July 2008 (JDay 176 to 202). During this period the climate of the area is typically strongly affected by the southwest monsoon (Hewitt et al., 2009). In this phase of the field campaign the area experienced slightly lower than average daily temperatures and higher amounts of rainfall than average. The rainfall showed a strong diurnal pattern with the main period of rainfall occurring between 1300 and 1500 hours, with a smaller peak of rainfall in the late afternoon (Hewitt et al., 2009). 2008 was the fifth wettest year in the 23-years of records, experiencing 113% of the average rainfall. The average temperature for the period from April to July was 27.1°c, 99% of the average value seen for this time of year (Hewitt et al., 2009).

4.1.2 Data Coverage

In order to replicate the measurements from the field campaign through the use of the OP3 model only day with sufficient data for each constrained variable can be used. The data were analysed and any substantial gaps of 2 hours or more in the measurements that could not be removed through interpolating the surrounding data were noted (table 4.1.1)

Table 4.1.1 Data coverage for the second phase of the field campaign. ✓ indicates species that have a full days worth of cover and x indicates species where a whole days worth of data coverage is not present.

Jday	190	191	192	193	194	195	196	197	198	199	200
Isoprene											
Alpha-Pinene											
Limonene											
Camphene											
Carene											
Gamma-Terpinene											
Ethene											
O_3											
NO							**X**	**X**			**X**
NO_2							**X**	**X**			**X**
CO											
Temperature											
H_2O											**X**
M											

This process identifies day fit for further study. No days before day 190 were chosen to use for model analysis, due to missing data in key species such as NO, NO_2 or O_3. The final eight days chosen for model assessment were days 190 to 195, then days 198 and 199.

4.1.3 Implications of air mass characteristics for OH, NO_3 and O_3 reactions with VOCs

Using the VOC data collected during the second phase of the OP3 field campaign, average concentrations of each species were calculated for each day and also for the daytime (0700 to 1900 hours) and nighttime (1900 to 0700 hours) periods. Using these average values and the rate coefficient data taken from the MCM, the loss of oxidising species OH, O_3 and NO_3 were calculated for their reactions with each VOC (chapter 2). This indicated the importance of each VOC species that had been measured, but also identified when there were significant changes in the air mass above the monitoring site.

Figures 4.6a and d show the overall importance of isoprene reacting with OH and O_3 at the monitoring site. The similarities between figures 4.6 a and b and figures 4.6 d and e show that the daytime chemistry for these species is more significant than the

nighttime chemistry. This is expected as daytime concentrations of OH and O_3 will be significantly higher than nighttime concentrations, due to photolysis being the pivital in their production. This is different to the VOC profiles of the NO_3 reactions, figure 4.6g, h and I, where the overall profile is very similar to both the daytime and nighttime profiles.

One significant difference between the OH and O_3 profiles and the NO_3 profiles is the distinct change in the air mass composition on day 192 (10/07/2008) coming three days after the distinct change in the air mass direction on day 189 (07/07/2008). At this point there is a change in O_3 and NO_3 reactivity; iso-butene, propene and ethane start to appear in the O_3 and NO_3 reactivity profiles in more significant levels (figure 4.1.1 d, e, f, g, h and i). The change in the reactivity composition is seen most strongly at night when there are fewer VOCs and monoterpenes being emitted from the forest.

This change coincides with a change in the direction of the prevailing winds. The change to a south-eastern wind potentially gave the air mass at the site a different composition, as it began to travel over an oil palm refinery before arriving at the monitoring site. The increase in anthropogenic VOCs such as acetone, acetaldehyde, propene and iso-butane indicates that new air mass is being affected anthropogenic sources (Lewis et al., 2005)

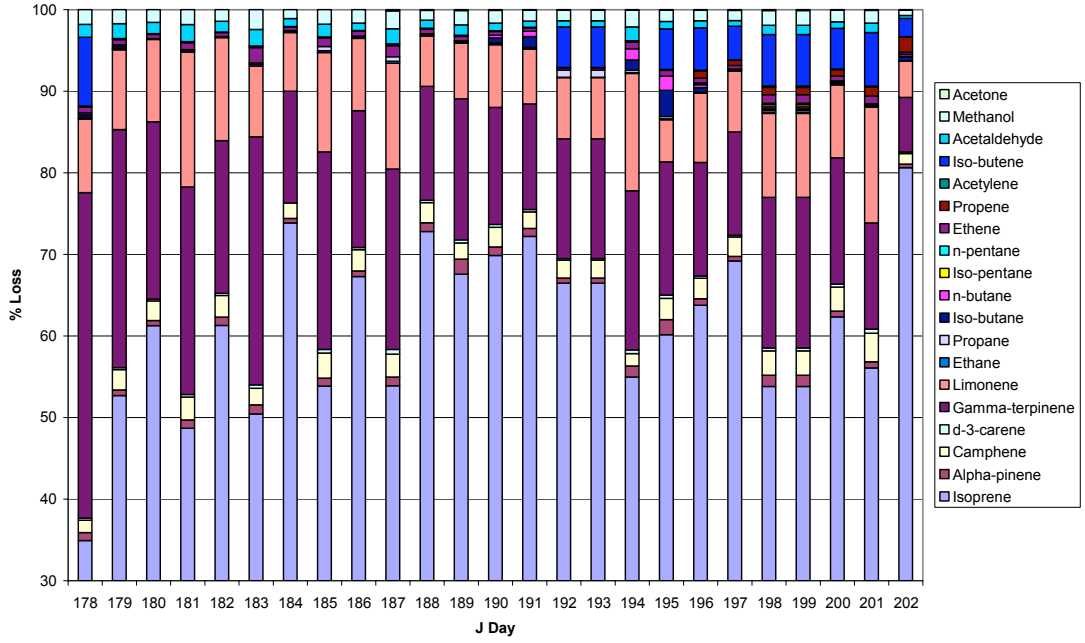

a

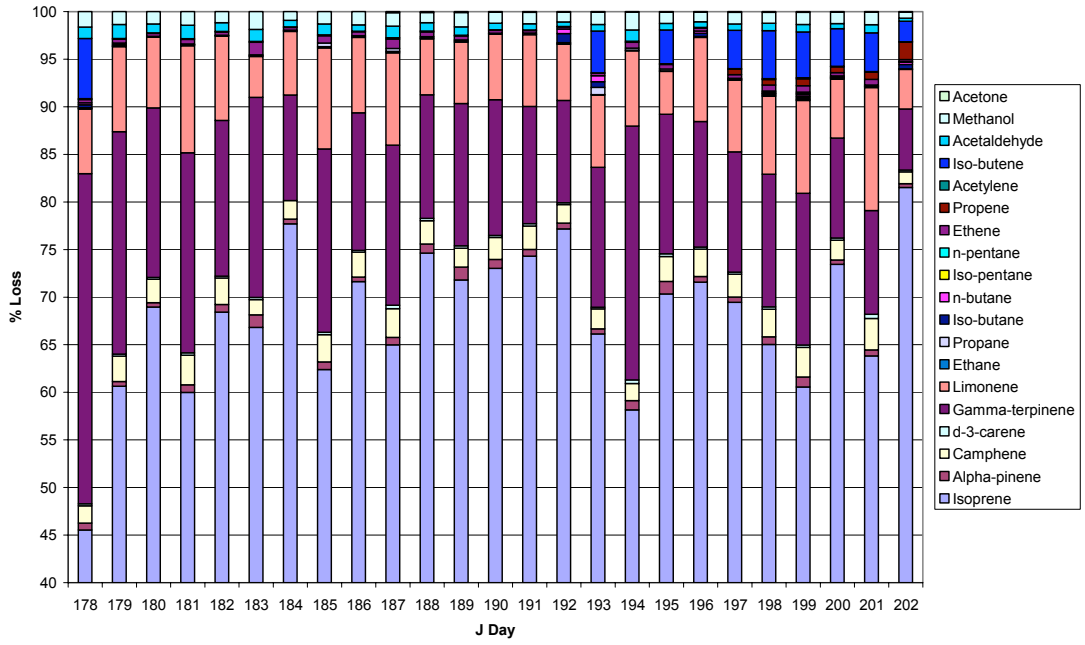
% Loss
J Day
Acetone
Methanol
Acetaldehyde
Iso-butene
Acetylene
Propene
Ethene
n-pentane
Iso-pentane
n-butane
Iso-butane
Propane
Ethane
Limonene
Gamma-terpinene
d-3-carene
Camphene
Alpha-pinene
Isoprene

b

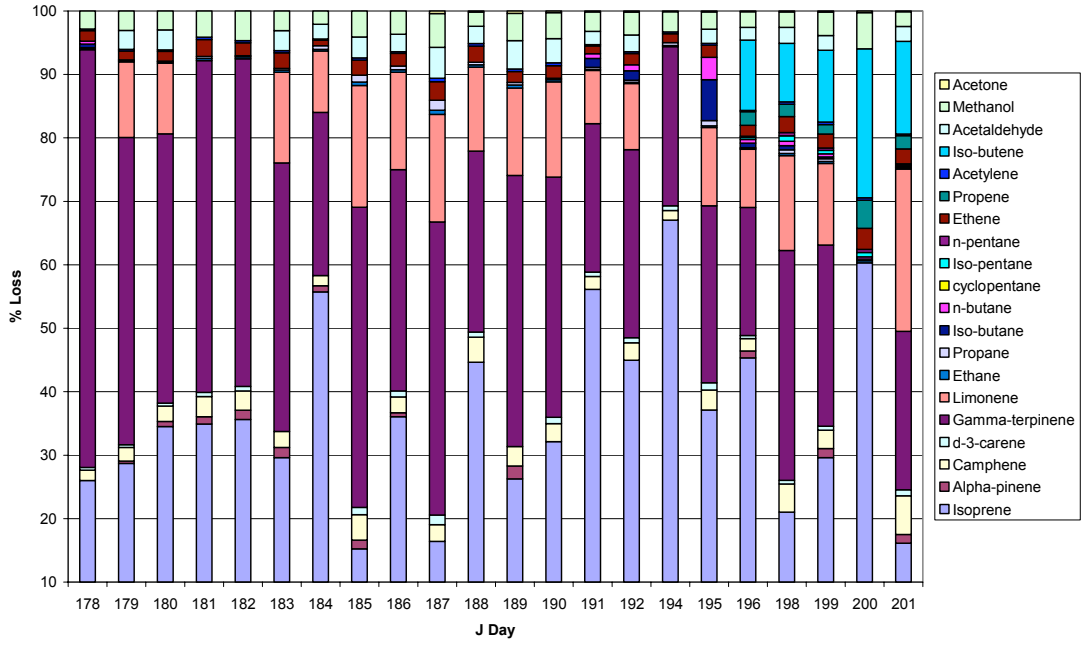
% Loss
J Day
Acetone
Methanol
Acetaldehyde
Iso-butene
Acetylene
Propene
Ethene
n-pentane
Iso-pentane
cyclopentane
n-butane
Iso-butane
Propane
Ethane
Limonene
Gamma-terpinene
d-3-carene
Camphene
Alpha-pinene
Isoprene

c

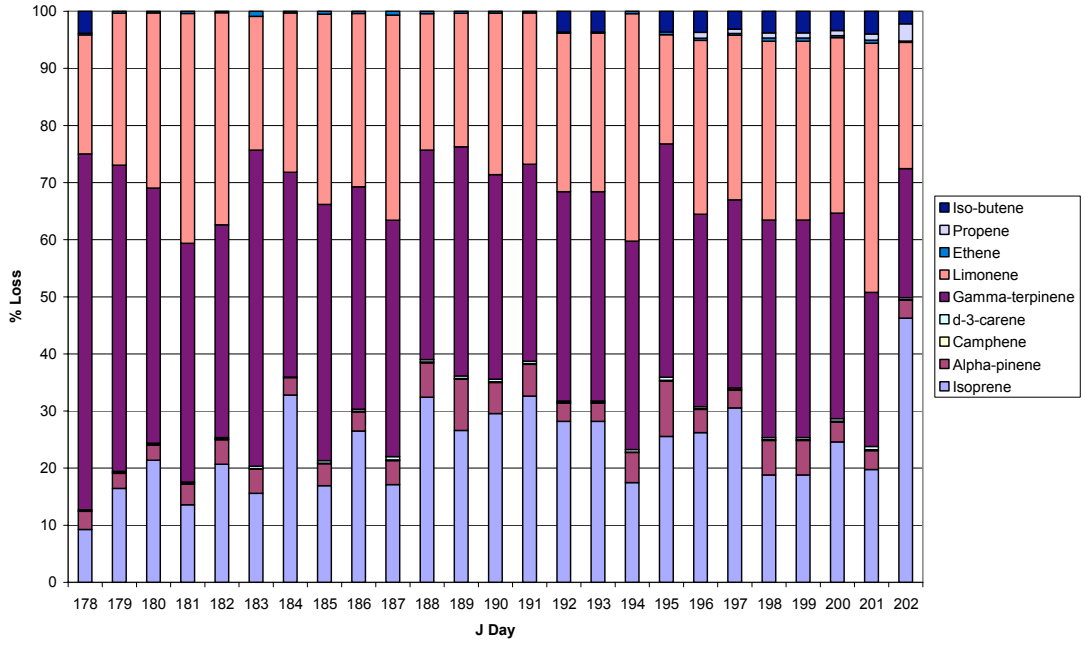
% Loss
J Day
Iso-butene
Propene
Ethene
Limonene
Gamma-terpinene
d-3-carene
Camphene
Alpha-pinene
Isoprene

d

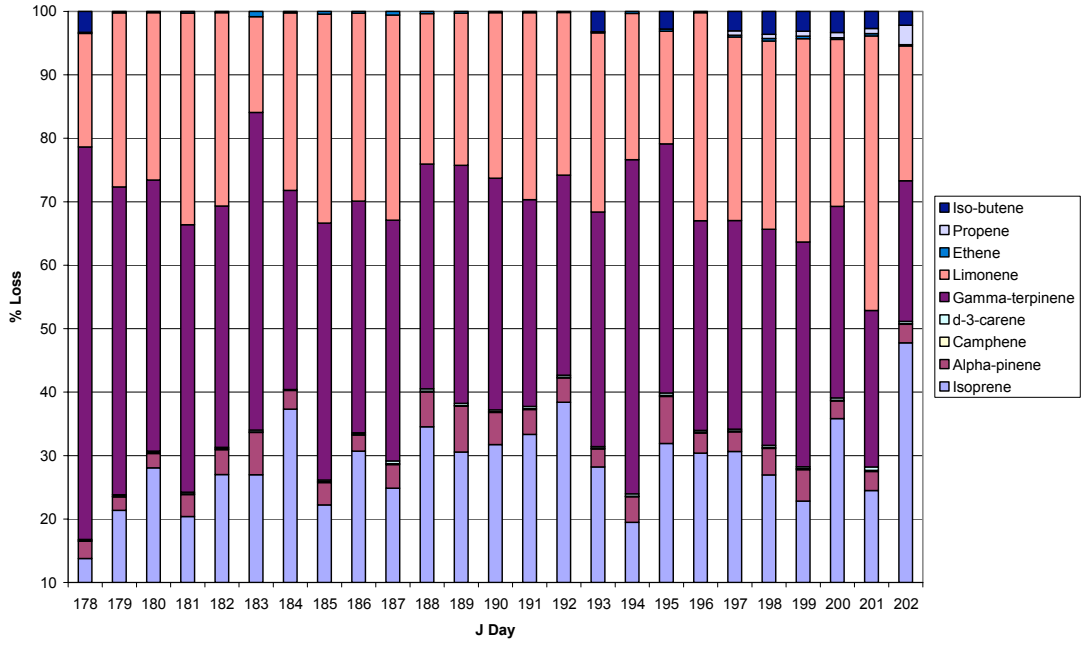
% Loss
J Day
Iso-butene
Propene
Ethene
Limonene
Gamma-terpinene
d-3-carene
Camphene
Alpha-pinene
Isoprene

e

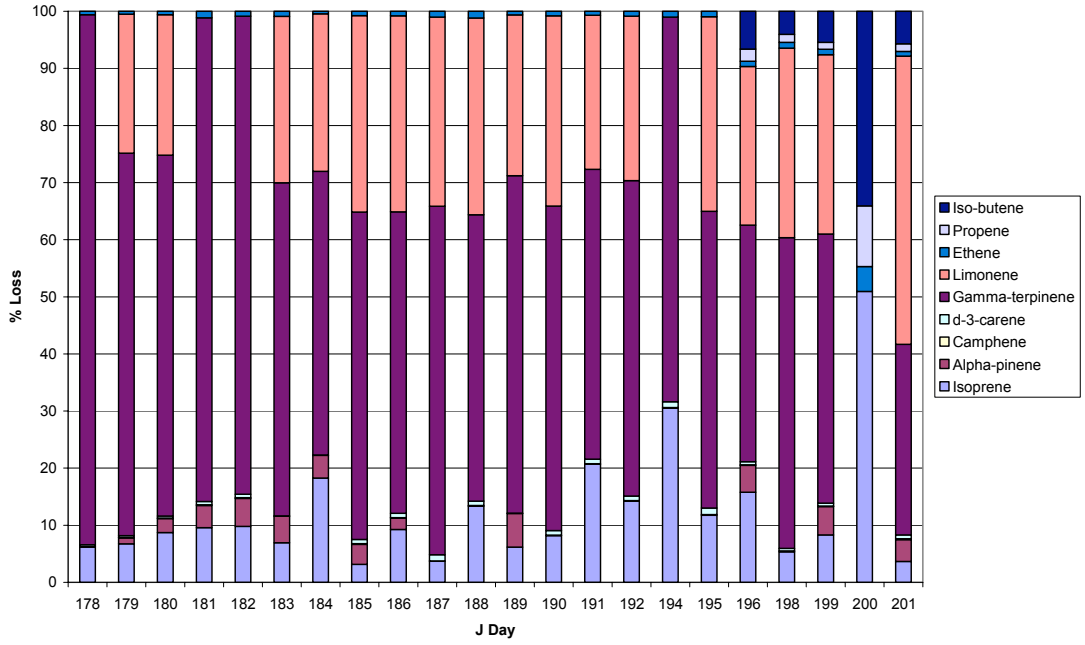
% Loss
J Day
Iso-butene
Propene
Ethene
Limonene
Gamma-terpinene
d-3-carene
Camphene
Alpha-pinene
Isoprene

f

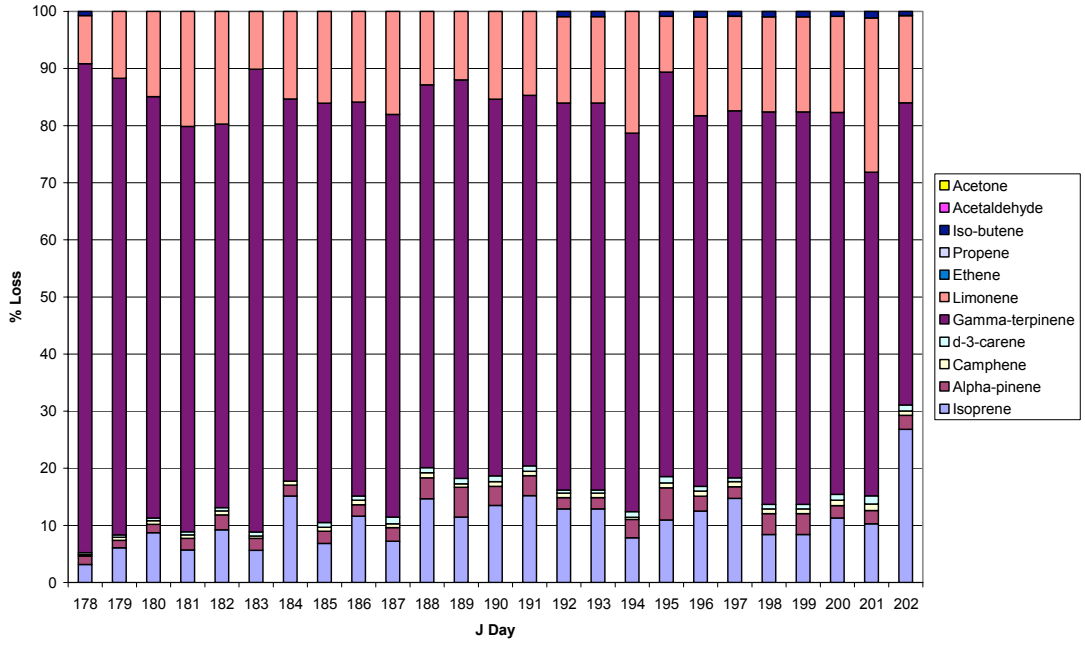
% Loss
J Day
Acetone
Acetaldehyde
Iso-butene
Propene
Ethene
Limonene
Gamma-terpinene
d-3-carene
Camphene
Alpha-pinene
Isoprene

g

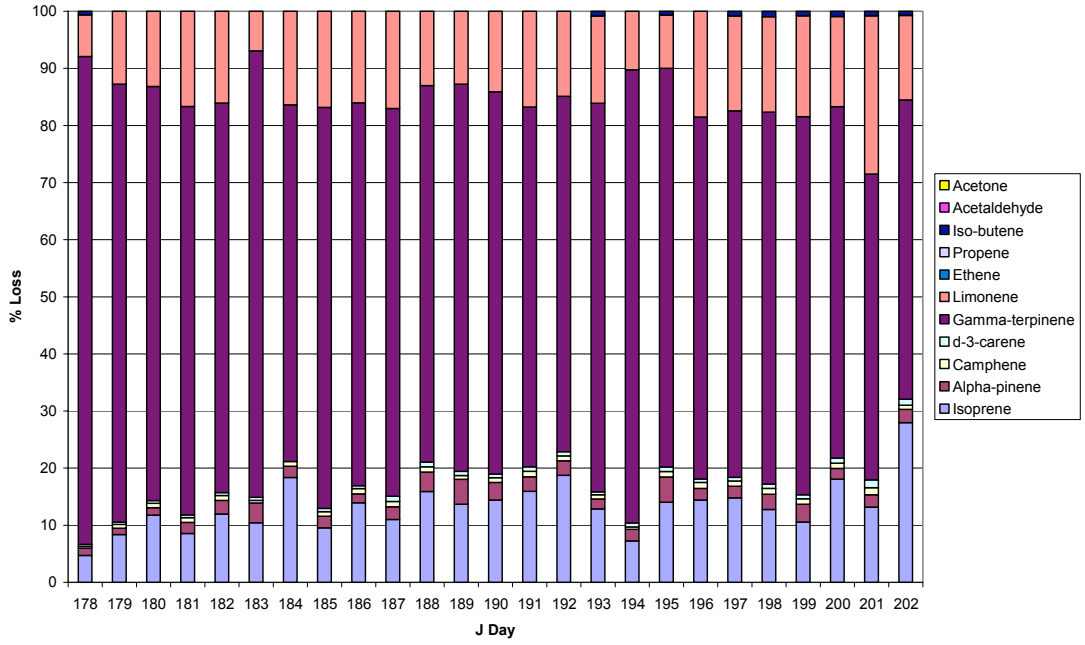

h

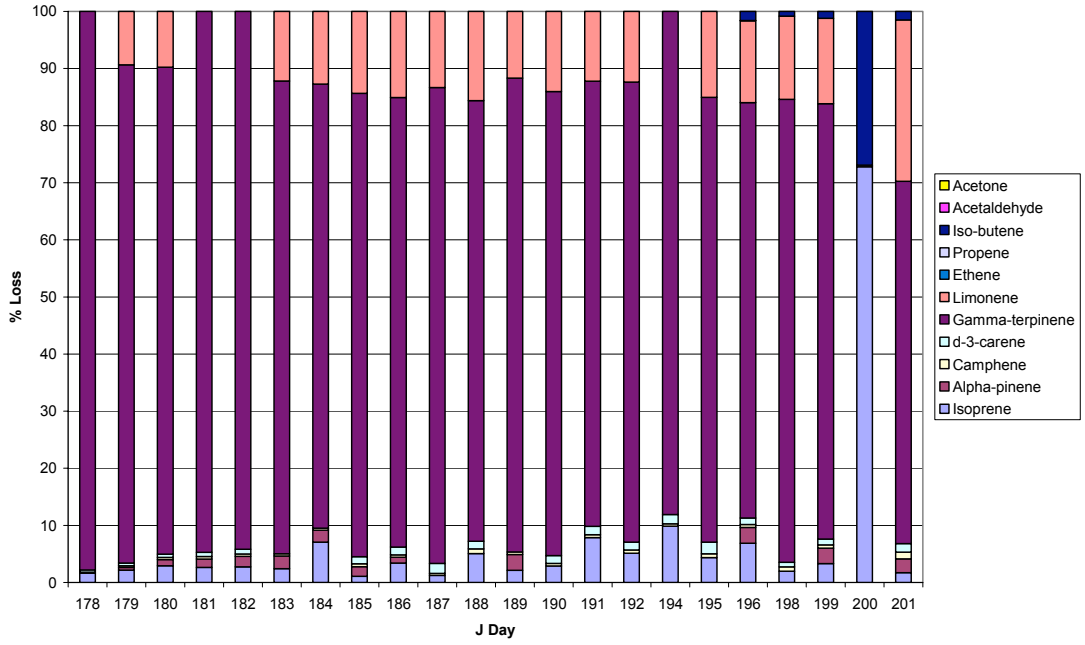

i

Figure 4.1.1 Percentage contribution loss of oxidants through reactions with hydrocarbons a) overall OH loss, b) daytime OH loss, c) nighttime OH loss, d) overall O_3 loss, e) daytime O_3 loss, f) nighttime O_3 loss, g) overall NO_3 loss, h) daytime NO_3 loss, i) Nighttime NO_3 loss.

4.2 Results

4.2.1.1 Model evaluation.

By evaluating a model it determines "how well" the model conducts the task it was designed to perform. In this modelling project the model was designed and tailored to recreate the concentrations of OH, HO_2 and RO_2 radicals. The evaluation of the model centres around the degree of accuracy to which the model recreates the observed values and changes in the concentrations of the radical species.

The OP3 and OP3 Peeters models replicate the concentrations of radicals at a single point and cover a 24 hour period. In order to evaluate the accuracy if the models the data from the two models for a 24 hour period is compared with the actual measurements of these species over the same 24 hour time frame. By conducting a graphical comparison of the model out put and recorded data for the radical species it is possible to observe where the model accurately reflects the measured concentrations and changes in the radicals.

An area of particular interest in the model is the period between 11:00 and 15:00 hours. During this period the intensity of solar radiation will be at its highest leading to a higher rate of photochemical production. To compare the degree of accuracy to which the OP3 models replicate the concentrations of radicals observed in this period, a comparison of percentage differences between observed and modelled concentrations is conducted to assess the difference between the models and the observed values. However, it is not possible to conduct this test on all days covered by the field campaign due to missing data from the FAGE or PERCA device. In the periods where the full 4 hours of data is not present the percentage comparison of the models and measurements are conducted over a smaller time period around the solar noon to ensure the model output is always being compared to measured data.

Where there is disagreement between the modelled and observed concentrations of radicals statistical testing can help determine the cause of the discrepancies. The analytical devices used for measuring the concentrations of the species constrained in the model and those that the model results are compared to, all contain a degree of error (table 2.9). By adding the level of error at each 15-minute step through a series

of error bars, to the model and instrument recording the species, it is possible to display whether discrepancy between modelled and measured values is generated as part of the error with in the recorded data or if the difference is a result of assumptions made in the construction of the model or from a lack of understanding in the chemical processes that from the mechanism with in the model.

If the model replication of the observations at Bukit Atur was conducted over a longer period of time, providing more days of data over a more periods of different climatic conditions it would be possible to conduct more rigorous statistical test on the OP3 and OP3 Peeters models to conclude the goodness of fit from the models. In order to perform a test that would determine the measure of goodness of fit, such as a correlation map or matrix, more individual days would need to be observed with more data points representing key times in the model-measurement comparisons. Other tests that can be performed on atmospheric models to provide a measure of goodness of fit include regression comparing the linear relationship between the model output and the observations (Fowell, et al., 2006). However, this method of statistical testing also would require more data over a longer period of time to justify the use in assessing this model.

4.2.1.2 Displaying the Modelled and Measured Results

The results from the model are generated by a minute-by-minute basis from sets of data that are constrained on a 15 minute basis. In order to produce results that are clearer interpret and compare to the constrained data and observations, the minute-by-minute results were converted to a single point to represent the 15-minute period for each batch of constrained data. The 15 minute results produce a smoother line on the result graphs that are easier to read than the stepped looking graphs that show the results for every minute of the day.

4.2.1 Day 190 (9th July 2008)

The air mass trajectory arriving at the Bukit Atur field site was predicted using the NOAA Hysplit model (fig 4.2.1). The NOAA model shows that the air mass arises to the South East of the field site over sea. The majority of the time the air mass is travelling to the field site is spent over sea, before it travels over the forest to the south east of the field site for the final 12 hours. The south-easterly direction of the air mass was expected, as is usual for this time of year in Borneo, and discussed in chapter 2 and Hewitt et al, (2009). Before reaching Borneo the air mass passes over two islands, first Halhahera and the Sulawasi.

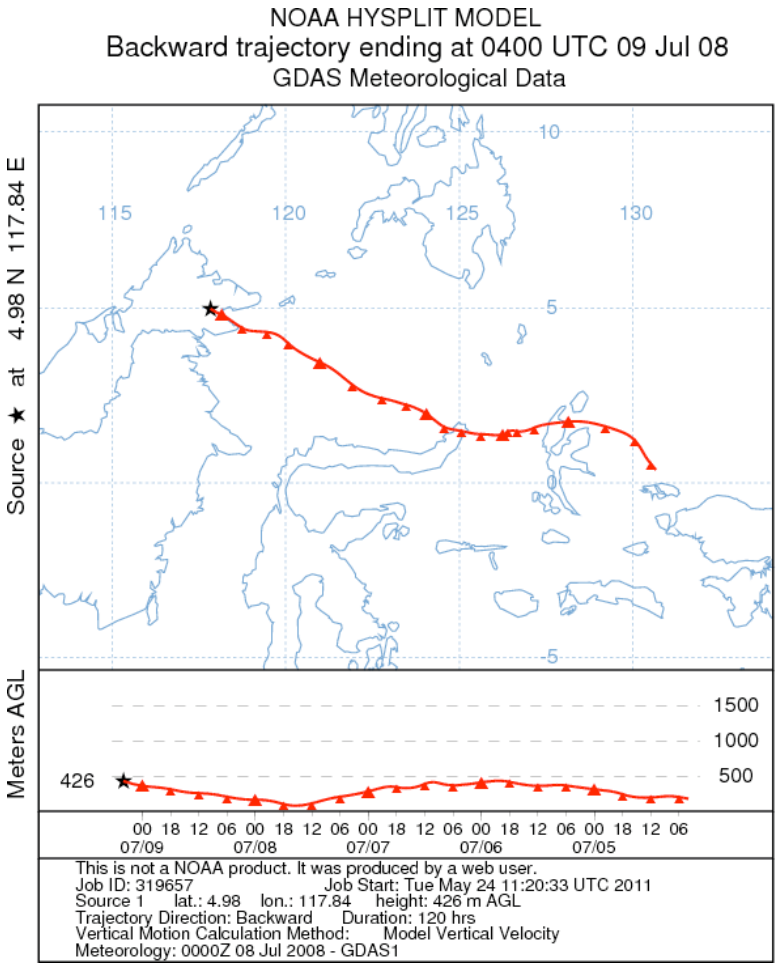

Figure 4.2.1 Air mass trajectory for 5 day arriving at the field site at 1200 hours (local time) on 9th July (JDay 190) The upper plot shows the path taken by the airmass travelling to the field site, for the 5 days previous to measurements being taken. The lower plot shows the altitude of the airmass for the 5 day period before arriving at the field site.

The air mass moves over few populated areas. There would likely be few anthropogenic organic species contained in the airmass and low concentrations of

NO_x and CO would be expected as a consequence. Figure 4.2.2 shows the concentrations of NO and NO_2 as examples. There is no uniform diurnal variation in the NO and NO_2 concentrations, which remain steady except for some peaks that can be attributed to trafficalong the logging road near to the field site. The larger peaks coincide with when vehicles were driven to the top of Bukit Atur and brought close to the observation point or when logging vehicles were observed on the road at the foot of Bukit Atur. The largest peaks occur when the vehicles were closest top the inlets at the field site.

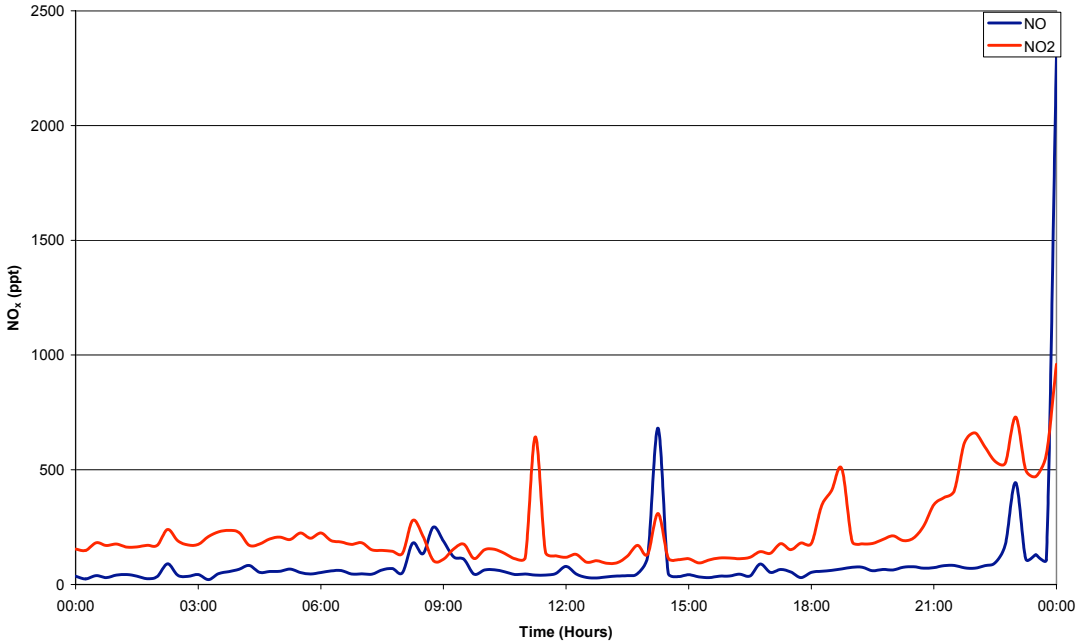

Figure 4.2.2 NO and NO_2 concentrations recorded at Bukit Atur on JDay 190 (9^{th} July 2008)

The air mass moves over the rainforest before arriving at the Bukit Atur field site, but the diurnal variation in the isoprene and monoterpene species shown in figures 4.2.3 and 4.2.4 indicates that the observed monoterpenes are generated locally at the site, by sources that are affected by temperature and sunlight levels (Hewitt et al., 2008).

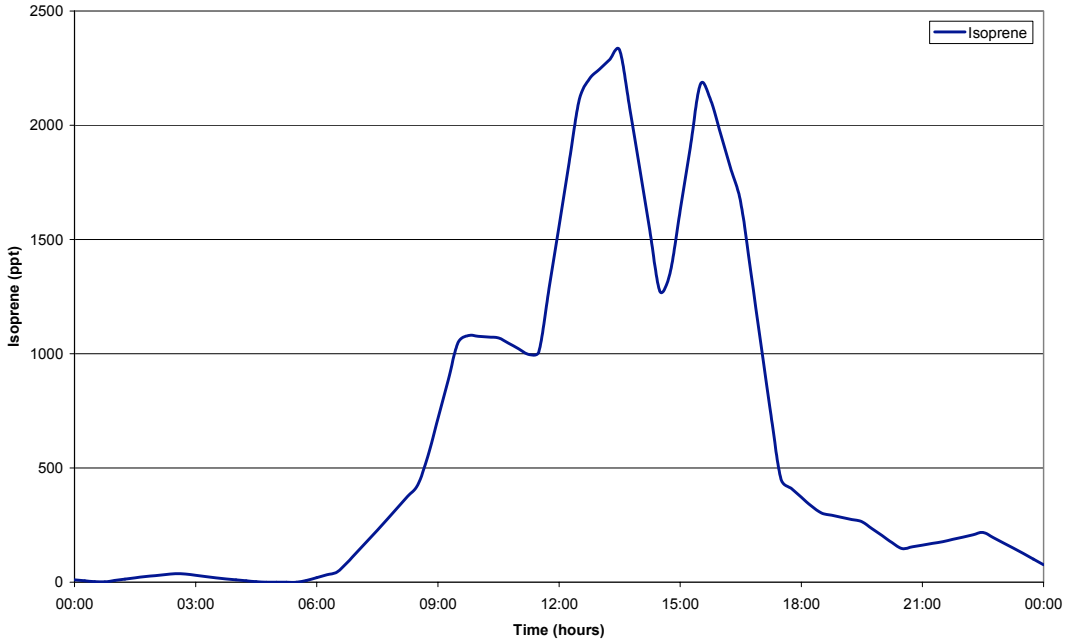

Figure 4.2.3 Isoprene concentrations recorded at Bukit Atur on JDay 190 (9th July 2008)

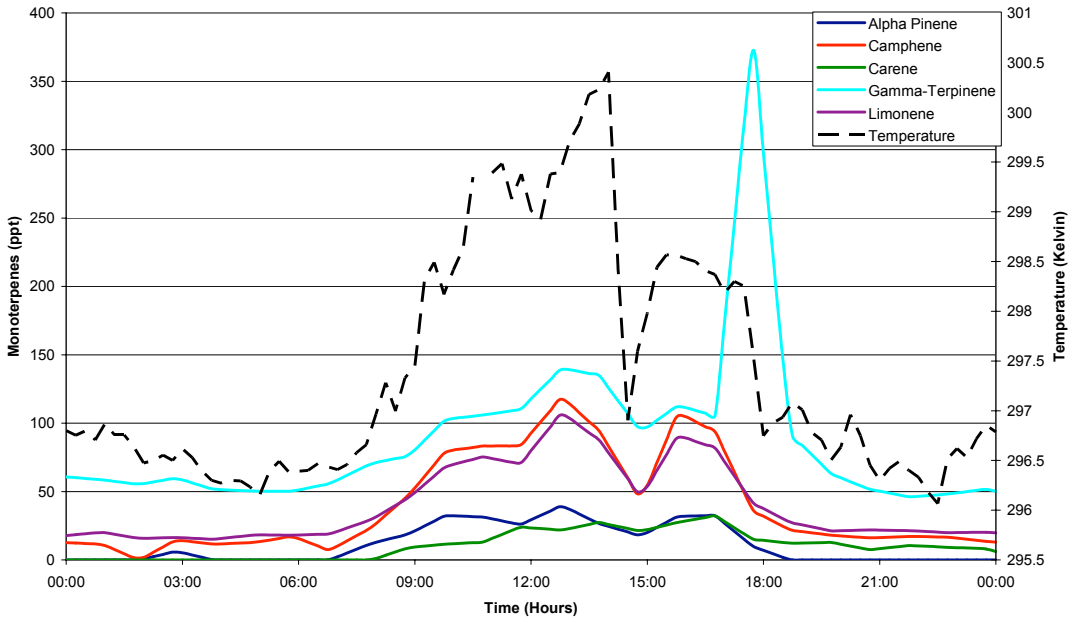

Figure 4.2.4 Monoterpene concentrations and temperatures recorded at Bukit Atur on JDay 190 (9th July 2008)

The measurements of j($O(^1D)$), the rate of the photochemical breakdown of O_3 to O_2 and an O^1D radical, were also recorded at the site on a minute by minute basis. The diurnal profile for this on JDay 190 is shown in figure 4.2.5. The diurnal plot shows that the value of j($O(^1D)$), starts to be measured at 06:00 when the sun rises at the

field site. The value continues to rise until approximately 12:00 and then begins to decline until it stops being detectable at 18:00 when the sunsets at the field site. The diurnal plot is not one smooth curve as might be expected for the change in intensity of sunlight, but there parts of the graph that shows areas where the sunlight intensity unexpectedly declines. These parts of the graph can attributed to points in the day where there was some degree of cloud cover lowering the intensity of the light reaching the photometer.

The recorded value of $j(O(^1D))$ at noon is 3.8×10^{-5} s^{-1} and the theoretical maximum value at this point calculated by the TUV and OP3 models gave $j(O(^1D))$ values of 4.0×10^{-5} and 3.6×10^{-5} respectively for day 190, as discussed in chapter 3.4. The discrepancy here could be a factor of clouds passing over the field site preventing the sunlight reaching the field site being at full intensity.

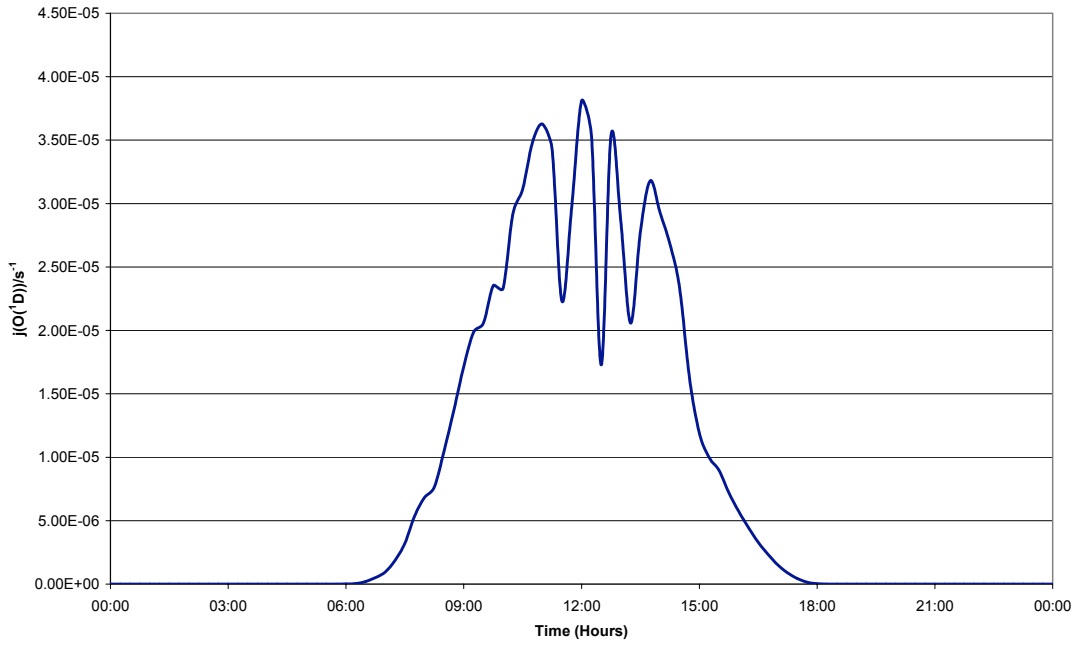

Figure 4.2.5 $J(O^1D)$ observations recorded at Bukit Atur on JDay 190 (9^{th} July 2008)

The results predicted by the OP3 model and the OP3 model containing the proposed Peeters scheme (OP3 Peeters) are displayed in figures 4.2.6, 4.2.7 and 4.2.8 along with the measured concentrations. The three species all show similar diurnal behaviour with the lowest values being predicted and measured during the nighttime periods and the highest values occurring during the daytime with maximum values tend to occur near solar noon. The OP3 Peeters model predicted higher concentrations than the OP3 model for all three species, but particularly for HO_2

(Table 4.2.1). This is to be expected given the recycling of radical discussed in chapter 3.7

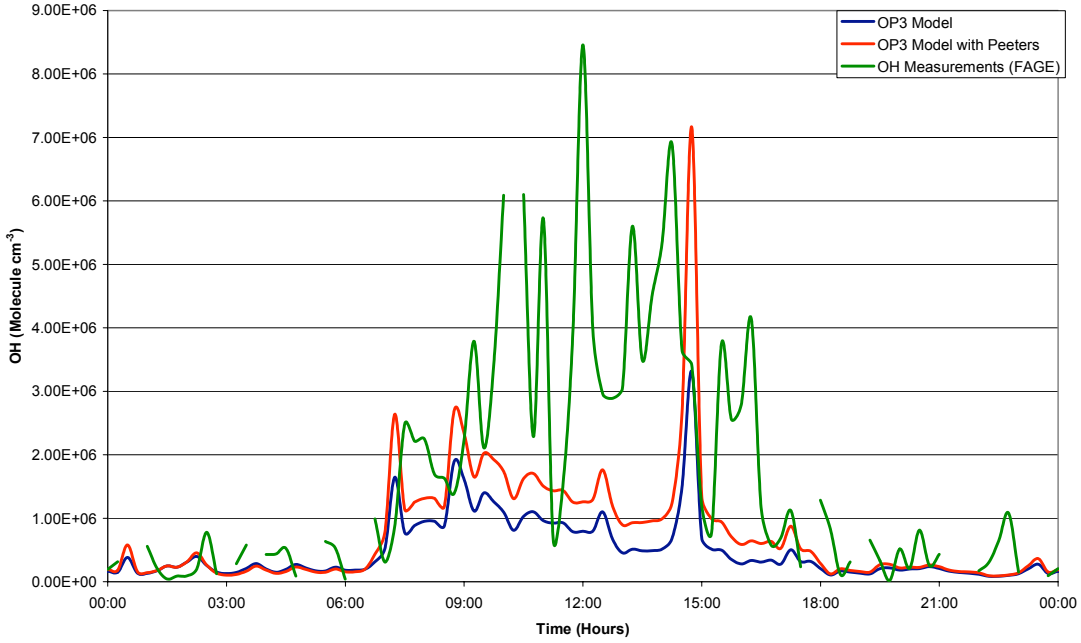

Figure 4.2.6 Model-measurement comparison of [OH] for day 190 (9th July 2008)

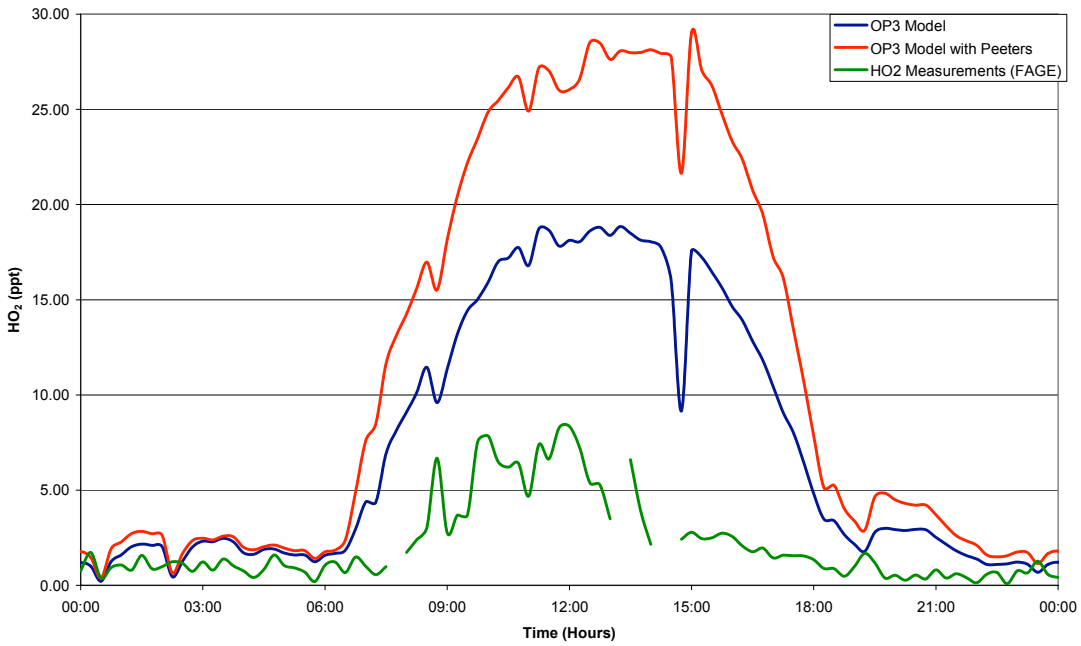

Figure 4.2.7 Model-measurement comparison of [HO_2] for day 190 (9th July 2008)

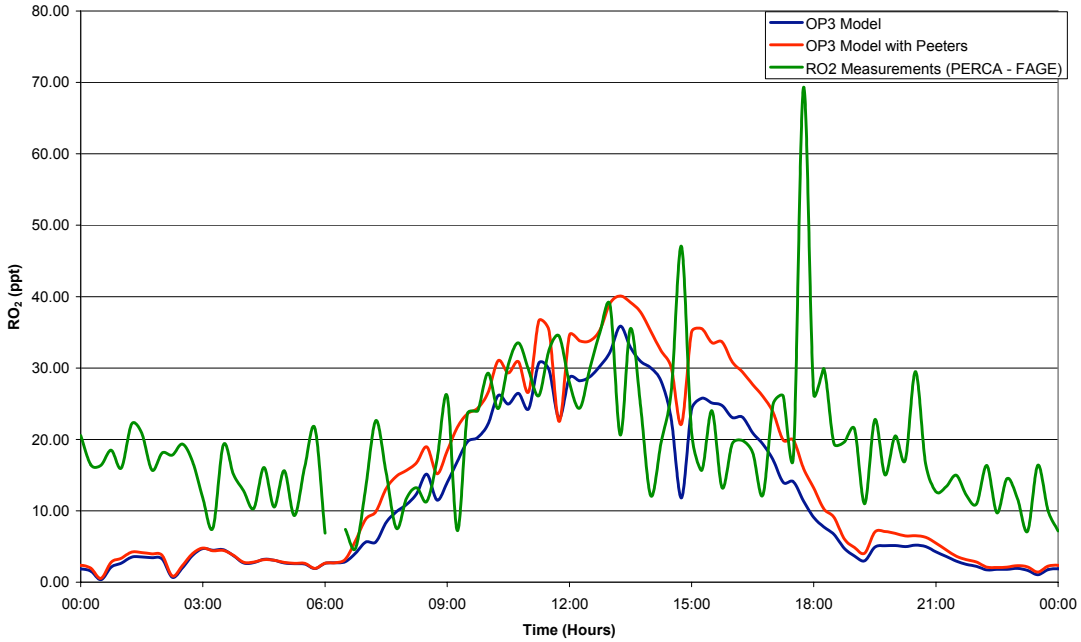

Figure 4.2.8 Model-measurement comparison of [RO_2] for day 191 (9th July 2008)

Table 4.2.1 Average concentrations of OH, HO_2 and RO_2 at Bukit Atur on JDay 190 (09/07/2008) for the whole day, daytime (06:00 – 18:00), nighttime (00:00 – 06:00 and 18:00 – 24:00) and midday (11:00 -15:00).

		OH (Molecules cm^{-3})	HO2 (ppt)	RO2 (ppt)
OP3	Daily Average	4.9×10^5	7.4	11.5
	Daytime Average	7.8×10^5	12.9	19.6
	Nighttime Average	1.8×10^5	1.9	3.2
	Average between 11:00 and 15:00	9.1×10^5	17.5	27.8
OP3 Peeters	Daily Average	7.5×10^5	11.4	14.4
	Daytime Average	1.3×10^6	20.2	24.7
	Nighttime Average	2.0×10^5	2.6	4.0
	Average between 11:00 and 15:00	1.6×10^6	27.1	33.5
Measurements	Daily Average	1.4×10^6	2.0	19.4
	Daytime Average	2.6×10^6	3.3	22.9
	Nighttime Average	2.5×10^5	0.8	15.9
	Average between 11:00 and 15:00	3.9×10^6	4.3	28.5

Despite the constant over predictions of HO_2 on this day there are several trends in the diurnal variations in the measurements and both sets of model output. One of the most noticeable trends in the HO_2 profile occurs before 15:00 (figure 4.2.7). There is

a sudden decline in the concentration in the HO_2 measurements and both sets of predicted values. This sudden decline coincides with a peak in the measurements of NO and NO_2. This sudden pulse of NO would remove HO_2 to form OH which explains the observed and predicted concentrations in HO_2 and OH at 15:00. The increase in the measurements of NO_2 at this point might be influenced by the reaction of $HO_2 + NO = OH + NO_2$. Figure 4.2.6 shows a predicted peak in OH concentrations for both models and an elevated amount of OH being measured. A similar trend is observed at 09:00 in both models predictions and the measured concentration of HO_2. There is a small peak followed by a sudden decrease in HO_2 concentrations around 09:00, this corresponds with a peak in NO and NO_2 concentrations and a peak in OH concentration at the same point.

The highest observed value of OH seen on day 190 was recorded at 12:00; at this point the models both predict a small peak in OH concentration, but under predict this peak. The input data does not show any factors in concentrations of the constrained species or the physical data as to why this large peak occurs at this point. Another distinct difference between the OH predictions and observations is at 08:45 where both models over predict a peak in OH, which coincides with a peak in NO observations. However after this peak both models then under predict a peak in the observed OH at 09:00 to 09:15.

During the nighttime (00:00 to 06:00 and 18:00 to 24:00) both models over predict the concentrations of HO_2 and under predict the concentration of OH, also the model fails to predict the fluctuations of OH in this period. This would suggest that the nighttime chemistry is incomplete and there is a factor missing from the description of the nighttime chemistry.

The values of OH from the two models show that the OP3 Peeters model shows constant higher values than the OP3 model. This is to be expected as it contains the added OH recycling system. The two models do contain the same trends in peaks in the predicted OH values. Neither model records its highest concentration around midday as might be expected, also as shown in table 4.2.1 both models predict much lower concentrations of OH between 11:00 and 15:00 than is actually observed. This

would indicate that the chemistry of both models is incomplete or information about relevant species is incomplete or missing.

The RO_2 predictions from the two models show a larger prediction from the OP3 Peeters model; this can be seen in figure 4.2.8 and table 4.2.1 where the values of RO_2 predicted by the OP3 Peeters model are much closer to the observed values than the OP3 model predictions. The average concentration values in table 4.2.1 indicate that's the OP3 Peeters model is more accurately predicting the concentrations of RO_2 than the OP3 model and that the daytime and midday predictions are much more accurate than the nighttime predictions. However, the original OP3 model gave the most accurate predictions of RO_2 during the period of 11:00 to 15:00. During this period both models predict the general shape of the pattern of concentration changes except for a sudden peak at 15:00, which corresponds with the HO_2 decrease and OH peak mentioned earlier.

In the RO_2 measurements there is a large peak in RO_2 concentrations at 18:00 which neither model predicts. At the same time there is a large peak in the concentration of Gamma-Terpinene. Reactions of Gamma-Terpinene would produce RO_2 radicals. The fact that neither model predicts this large spike in RO_2 might indicate that the gamma-terpinene reaction scheme in both models is incomplete.

4.2.2 Day 191 (10th July 2008)

The air mass trajectory arriving at the Bukit Atur field site was predicted using the NOAA Hysplit model (fig 4.2.9). The NOAA model shows that the air mass arises to the South East of the field site over sea. The majority of the time the air mass is travelling to the field site is spent over sea, before it travels over the forest to the south east of the field site for the final 18 hours. The south-easterly direction of the air mass was expected, as is usual for this time of year in Borneo, and discussed in chapter 2 and Hewitt et al. (2009). Before arriving at the island the air mass travels west over the sea for 42 hours and before that north travelling over Suluwasi.

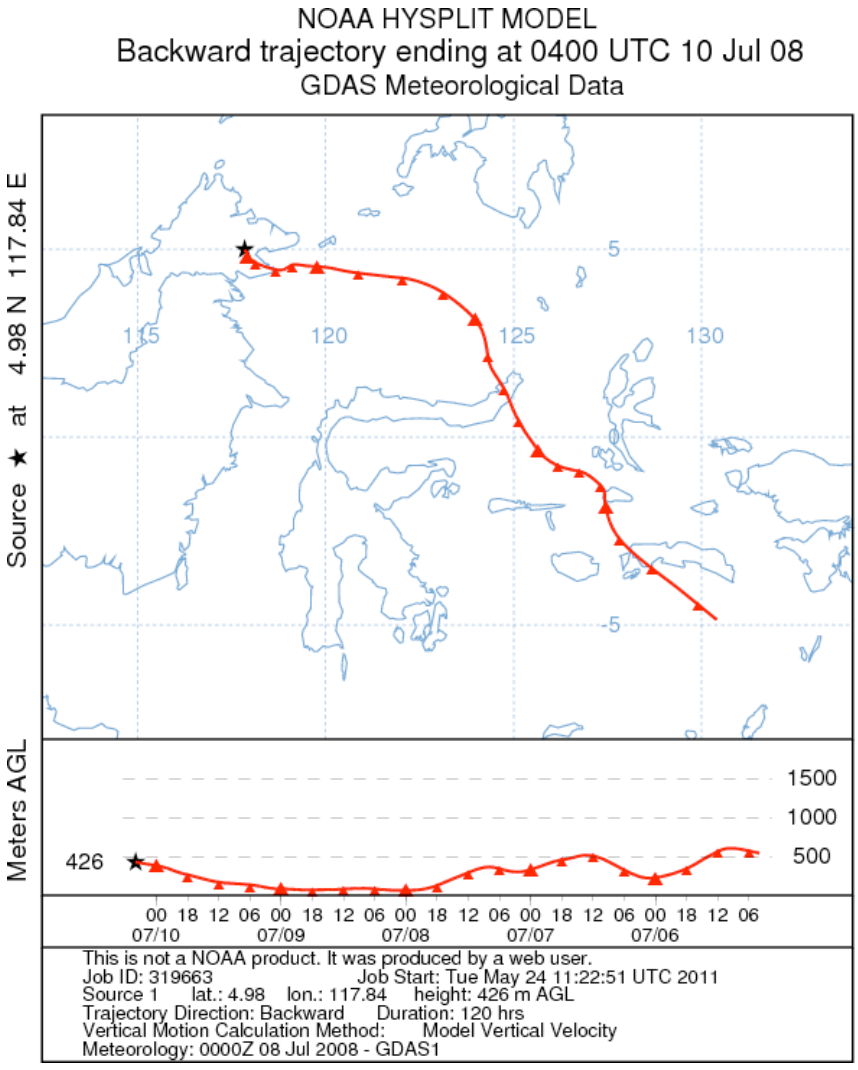

Figure 4.2.9 Air mass trajectory for 5 day arriving at the field site at 1200 hours (local time) on 10th July (JDay 191) The upper plot shows the path taken by the airmass travelling to the field site, for the 5 days previous to measurements being taken. The lower plot shows the altitude of the airmass for the 5 day period before arriving at the field site.

The air mass moves over few populated areas. There would likely be few anthropogenic organic species contained in the airmass and low concentrations of NO_x and CO would be expected as a consequence. Figure 4.2.10 shows the concentrations of NO and NO_2 as examples. There is no uniform diurnal variation in the NO and NO_2 concentrations, which remain steady except for some peaks that can be attributed to along the logging road near to the field site. The larger peaks coincide with when vehicles were driven to the top of Bukit Atur and brought close to the observation point.

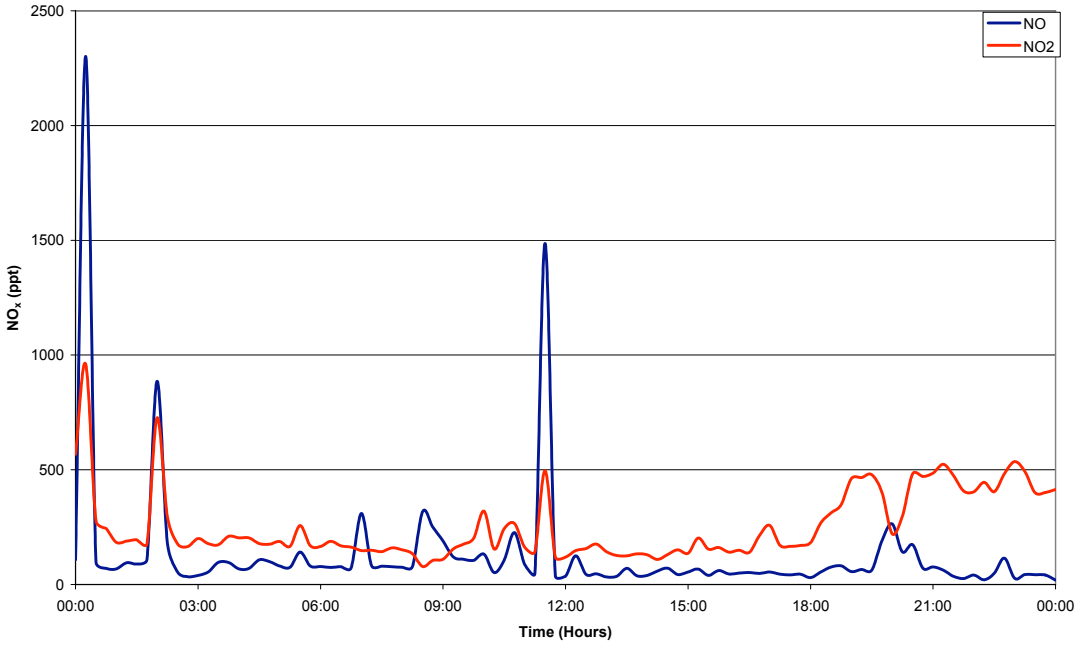

Figure 4.2.10 NO and NO_2 concentrations recorded at Bukit Atur on JDay 191 (10^{th} July 2008)

The larger peaks occurring in the NO and NO_2 profiles occurred due to exhaust emissions of vehicles occurring close to the NO_x detection inlet. When these spikes occur it is an indication that the air packet being observed and recreated through the models is les "well mixed" at these points than at other points through out the day. During these periods of the day it must be assumed that the model is not replicating an accurate picture of the mixed air at the field site, as the NO_x emissions will not be affecting the OH and HO_2 being recorded at the FAGE inlet further away from the emission point.

The air mass moves over the rainforest before arriving at the Bukit Atur field site, but the diurnal variation in the isoprene and monoterpene species shown in figures 4.2.11

and 4.2.12 indicates that the observed monoterpenes are generated locally at the site, by sources that are affected by temperature and sunlight levels (Hewitt et al., 2009).

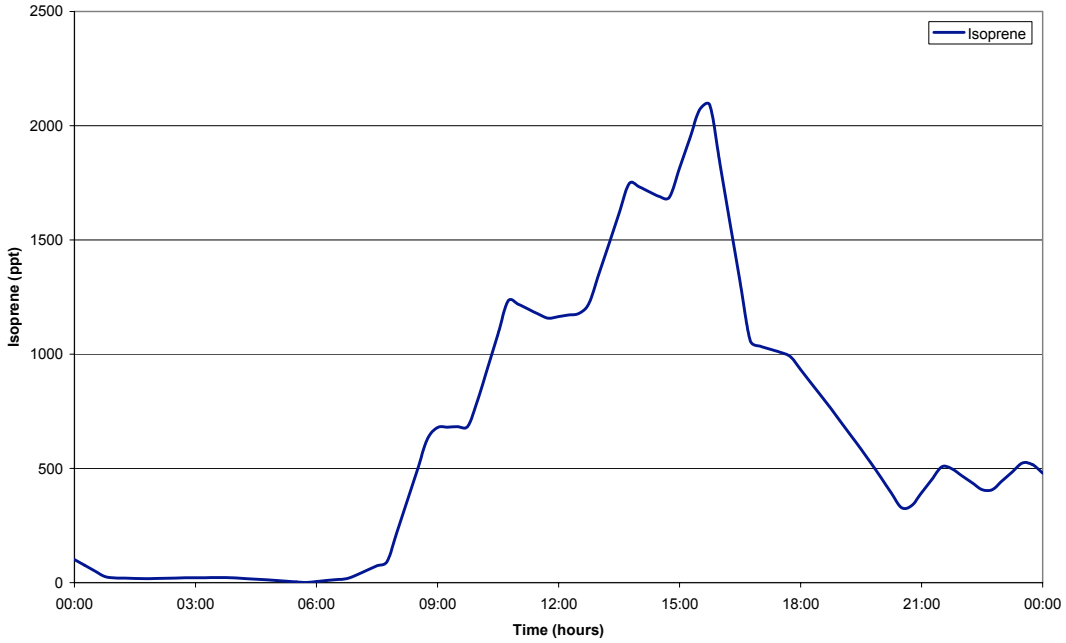

Figure 4.2.11 Isoprene concentrations recorded at Bukit Atur on JDay 191 (10th July 2008)

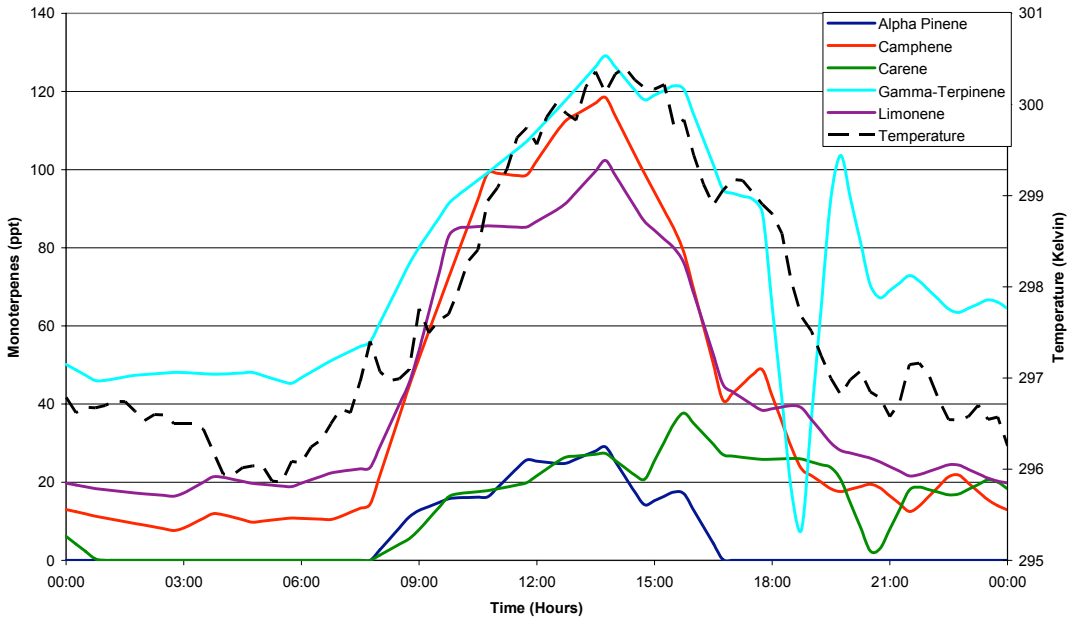

Figure 4.2.12 Monoterpene concentrations and temperatures recorded at Bukit Atur on JDay 191 (10th July 2008)

The measurements of j($O(^1D)$), the rate of the photochemical breakdown of O_3 to O_2 and an O^1D radical, were also recorded at the site on a minute by minute basis. The diurnal profile for this on JDay 191 is shown in figure 4.2.13. The diurnal plot shows that the value of j($O(^1D)$), starts to be measured at 06:00 when the sun rises at the field site. The value continues to rise until approximately 12:00 and then begins to decline until it stops being detectable at 18:00 when the sunsets at the field site. The diurnal plot is not one smooth curve as might be expected for the change in intensity of sunlight, but there parts of the graph that shows areas where the sunlight intensity unexpectedly declines. These parts of the graph can attributed to points in the day where there was some degree of cloud cover lowering the intensity of the light reaching the photometer.

The recorded value of j($O(^1D)$) at noon is 2.6 x 10^{-5} s^{-1} and the theoretical maximum value at this point is 4.0 x 10^{-5} Again, clods pass over the field site occasionally, but less so than on J191. A small rain shower was experienced at 12:00 followed by more rain showers at 14:00 through to 16:00. These periods of rain caused a reduction in the photolysis rates as the extended periods of cloud cover reduced the amount of UV light reaching the field site.

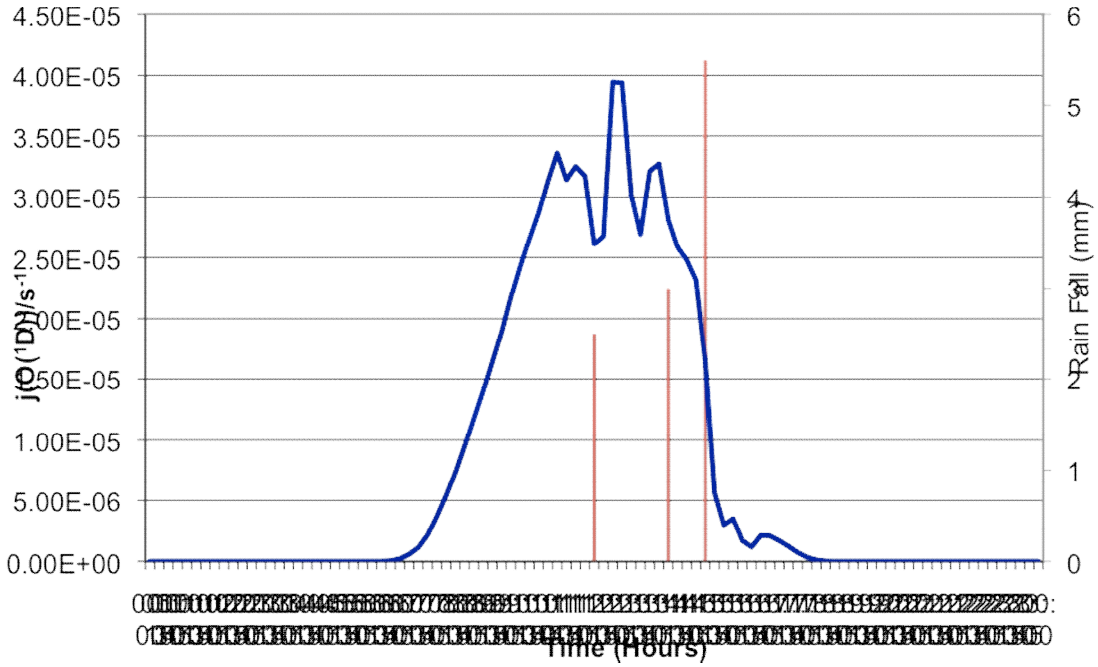

Figure 4.2.13 J(O^1D) observations recorded at Bukit Atur on JDay 191 (10^{th} July 2008)

The results predicted by the OP3 model and the OP3 model containing the proposed Peeters scheme (OP3 Peeters) are displayed in figures 4.2.14, 4.2.15 and 4.2.16 along with the measured concentrations. The three species all show similar diurnal behaviour with the lowest values being predicted and measured during the nighttime periods and the highest values occurring during the daytime with maximum values tend to occur near solar noon. The OP3 Peeters model predicted higher concentrations than the OP3 model for all three species, but particularly for HO_2 (Table 4.2.2).

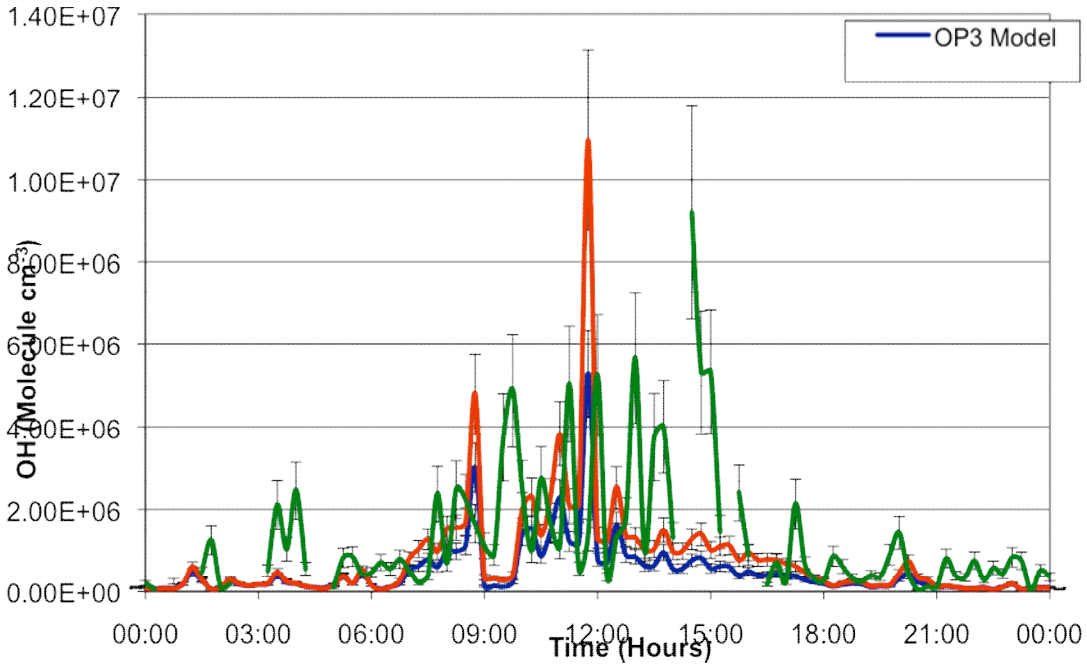

Figure 4.2.14 Model-measurement comparison of [OH] for day 191 (10th July 2008) Error bars on both models and the measuements.

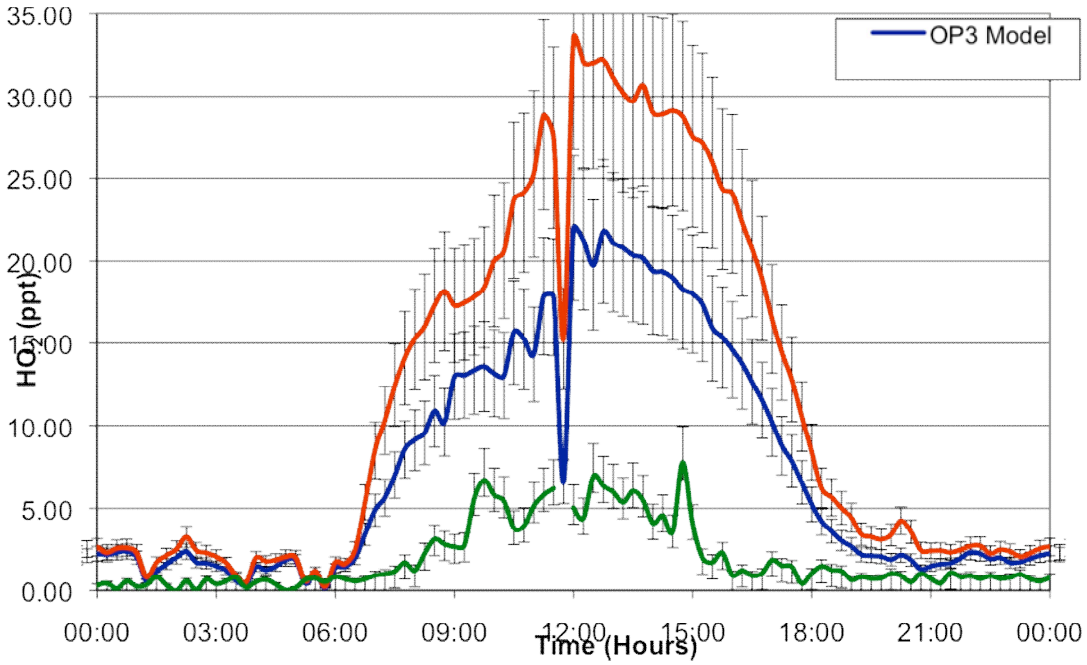

Figure 4.2.15 Model-measurement comparison of [HO_2] for day 191 (10/07/2008)

Figure 4.2.16 Model-measurement comparison of [RO_2] for day 191 (10/07/2008)

Table 4.2.2 Average concentrations of OH, HO_2 and RO_2 at Bukit Atur on JDay 191 (10/07/2008) for the whole day, daytime (06:00 – 18:00), nighttime (00:00 – 06:00 and 18:00 – 24:00) and midday (11:00 -15:00).

		OH (Molecules cm^{-3})	HO_2 (ppt)	RO_2 (ppt)
OP3	Daily Average	4.9×10^5	7.5	11.7
	Daytime Average	8.2×10^5	13.1	19.9
	Nighttime Average	1.6×10^5	1.8	3.4
	Average between 11:00 and 15:00	1.1×10^6	18.0	27.1
OP3 Peeters	Daily Average	8.0×10^5	11.5	15.0
	Daytime Average	1.3×10^6	20.4	26.0
	Nighttime Average	1.9×10^5	2.6	3.9
	Average between 11:00 and 15:00	2.1×10^6	28.9	34.1
Measurements	Daily Average	1.2×10^6	1.9	16.4
	Daytime Average	1.9×10^6	3.2	22.1
	Nighttime Average	4.8×10^5	0.6	10.6
	Average between 11:00 and 15:00	3.0×10^6	5.1	35.9

The highest observed value of OH seen on day 191 was recorded at 14:45; at this point the models both predict a small peak in OH concentration, but under predict this

peak. The input data does not show any factors in concentrations of the constrained species or the physical data as to why this large peak occurs at this point. Another distinct difference between the OH predictions and observations is at 08:45 where both models over predict a peak in OH, which coincides with a peak in NO observations. However after this peak both models then under predict a peak in the observed OH at 09:00 to 09:15.

Despite the constant over predictions of HO_2 on this day there are several trends in the diurnal variations in the measurements and both sets of model output. One of the most noticeable trends in the HO_2 profile occurs just before midday (figure 4.2.15). There is a sudden decline in the concentration in the HO_2 measurements and both sets of predicted values. This sudden decline coincides with a peak in the measurements of NO and NO_2. This sudden pulse of NO would remove HO_2 to form OH which explains the observed and predicted concentrations in HO_2 and OH at 11:45. The increase in the measurements of NO_2 at this point might be influenced by the reaction of $HO_2 + NO \rightarrow OH + NO_2$. However, this point cannot be verified as it occurs during a spike of NO_x emissions through a period of poorly mixed air.

During the nighttime (18:00 to 24:00) both models over predict the concentrations of HO_2 and under predict the concentration of OH, also the model fails to predict the fluctuations of OH in this period. This would suggest that the nighttime chemistry is incomplete and there is a factor missing from the description of the nighttime chemistry. One fluctuation that the model does predict is between 20:00 and 20:15 when there was a sudden decrease in the measured NO_2 and increase in the NO, at the same point there is an observed peak in the OH measurements and predictions. The increase in the NO allows more reaction with the HO_2 to form more OH. Even though the models both predict the peak in OH at 20:15, they both predict only half the observed concentration, with OP3 Peeters model predicting slightly more than the OP3 model. At the same point in the model the HO_2 predictions see a sudden increase, where as the HO_2 observations record temporary decrease in the concentration. Both models predict an increase in HO_2 concentration, but the OP3 Peeters model predicts a bigger peak than the OP3 model. This difference between the models would be expected due to the radical recycling from the Peeters mechanism (chapter 3.7).

Another factor that would be generating differences between the two models is the isoprene remaining at a higher than normal level after 18:00. During the nighttime chemistry phase isoprene will drop to concentrations in the region of 10 to 100 ppt, but on JDay 191 the concentration remains at near 500 ppt from 18:00 to 24:00. This added isoprene means that the OP3 Peeters model will be predicting more OH than the OP3 model, which in turn mean the OP3 Peeters model will also be predicting more HO_2 due to the radical recycling chemistry.

The values of OH from the two models show that the OP3 Peeters model shows constant higher values than the OP3 model. This is to be expected as it contains the added OH recycling system. The two models do contain the same trends in peaks in the predicted OH values.

The RO_2 predictions from the two models show a larger prediction from the OP3 Peeters model; this can be seen in figure 4.9 and table 4.2.1 where the values of RO_2 predicted by the OP3 Peeters model are much closer to the observed values than the OP3 model predictions. The average concentration values in table 4.2.1 indicate that's the OP3 Peeters model is more accurately predicting the concentrations of RO_2 than the OP3 model and that the daytime and midday predictions are much more accurate than the nighttime predictions.

The two sets of model predictions and the observations show a general diurnal pattern much like OH and HO_2. Even though there is similarity between overall diurnal shapes of the graphs there are factors in the RO_2 production that the model is not predicting. At 08:15 and 15:45 there are two sudden decreases in the observed concentrations of RO_2, with the decrease at 15:45 being much larger than the one at 08:15. At the same time as these decreases in the observations of RO_2 there are two peaks in the OH observations. Neither of the models predicts the decrease in RO_2 or the increase in OH at these points. At the same point there are no unusual fluctuations in the predictions or measurement of HO_2. Also there are no sudden changes in the concentrations of isoprene or the observed monoterpenes that coincides with both of these events. The simultaneous decrease of RO_2 and increase of OH would indicate that an unknown species is reacting with the RO_2 at these points to produce OH.

As discussed earlier there is an under prediction of an observed OH peak at just after 09:00. This occurs at the same point as both models predict a peak in the RO_2 concentration. The RO_2 observations show that there is a sudden increase in the concentration at this point, but also that the RO_2 peak is not as large as the model predict.

When the model results are compared to the measured values of OH and HO_2 the statistical error in the two methods must also be considered. Figure 4.2.14, displaying the modelled and measured values of OH on JDay 191 includes the instrumental error of the FAGE instrument when recording the values of OH of 28%(table 2.9). The systematic error of the two models is also included on the graph. The error bars are displayed every 15 minutes on the data points. When the sets of error bars from either of the models are compared with the model error, it displays that errors in either model cannot explain all the differences between the recorded and measured results.

The HO_2 modelled and measured results were also compared with statistical error from the FAGE HO_2 detection device (table 2.9). As previously described in figure 4.2.15 and table 4.2.2 there is a large discrepancy between the measured values of HO_2 and the predicted values from the OP3 model and the OP3 Peeters model. When the statistical error bars are applied to the results there is still a large discrepancy during the period between 06:00 and 18:00. The error is a systematic error with the models constantly over predicting the recorded values and the lowest point of the negative error bar still being much higher than observed values of HO_2 and the upper limit of the positive error from the FAGE detection device.

4.2.3 Day 192 (11th July 2008)

The air mass trajectory arriving at the Bukit Atur field site was predicted using the NOAA Hysplit model (fig 4.2.17). The NOAA model shows that the air mass arises to the South East of the field site over sea, but further south than the other two days. The majority of the time the air mass is travelling to the field site is spent over sea, before it travels over the forest to the south east of the field site for the final 18 hours. Figure 4.2.17 shows that the air mass was travelling slowly once it reached Borneo. The air mass travels northwest over Sulawesi island and the Celebes sea before reaching Borneo.

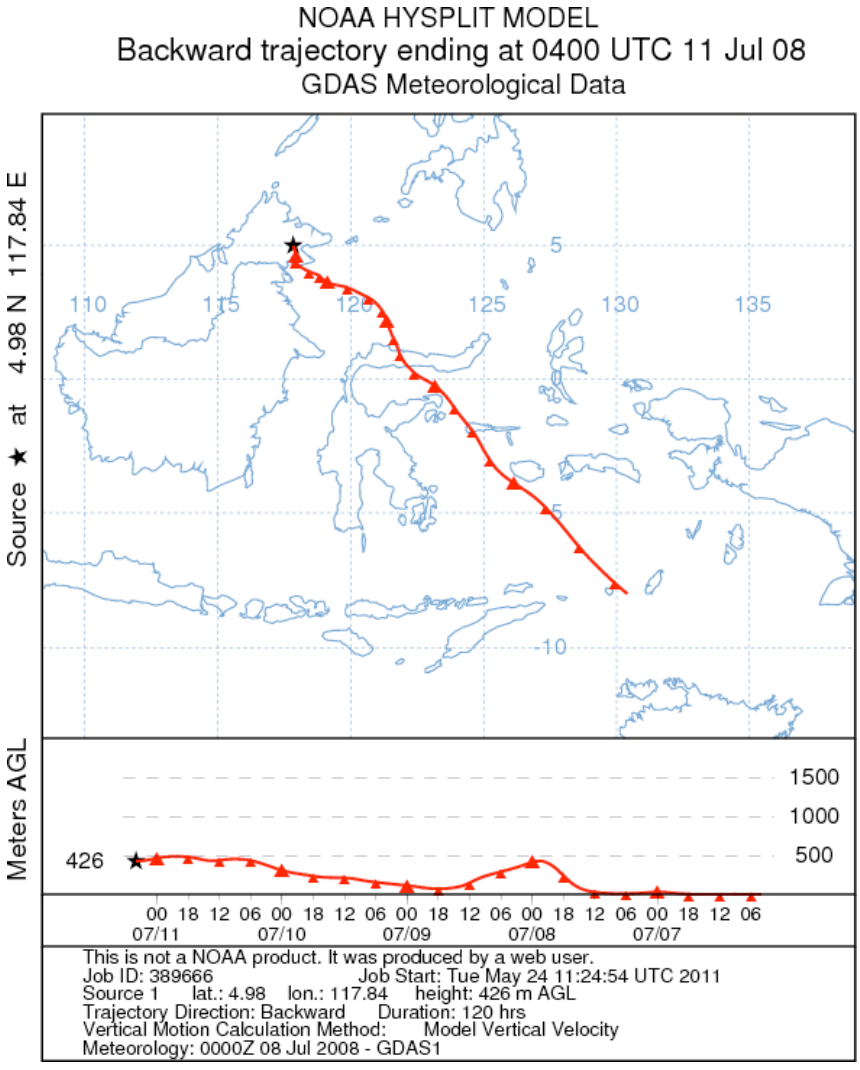

Figure 4.2.17 Air mass trajectory for 5 day arriving at the field site at 1200 hours (local time) on 11th July (JDay 192) The upper plot shows the path taken by the airmass travelling to the field site, for the 5 days previous to measurements being taken. The lower plot shows the altitude of the airmass for the 5 day period before arriving at the field site.

Figure 4.2.18 shows the concentrations of NO and NO_2 as examples, with occasional peaks from traffic along the logging road near to the field site.

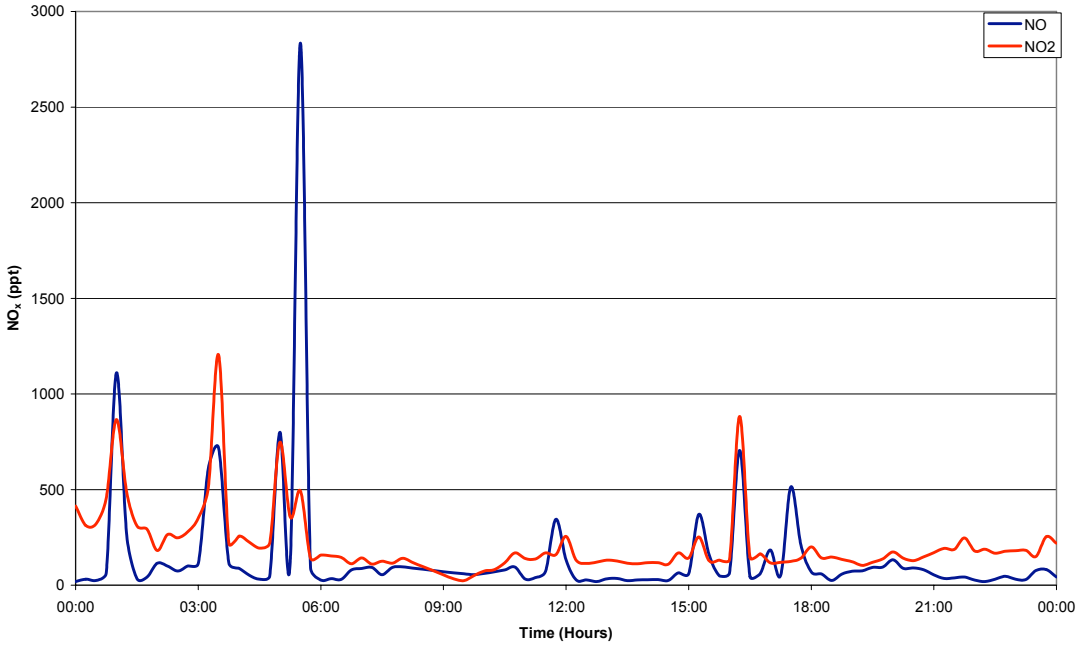

Figure 4.2.18 NO and NO_2 concentrations recorded at Bukit Atur on JDay 192 (11th July 2008)

As for the last two days the diurnal variation in the isoprene and monoterpene species shown in figures 4.2.19 and 4.2.20 indicates that the observed monoterpenes are generated locally at the site, by sources that are affected by temperature and sunlight levels (Hewitt et al., 2009).

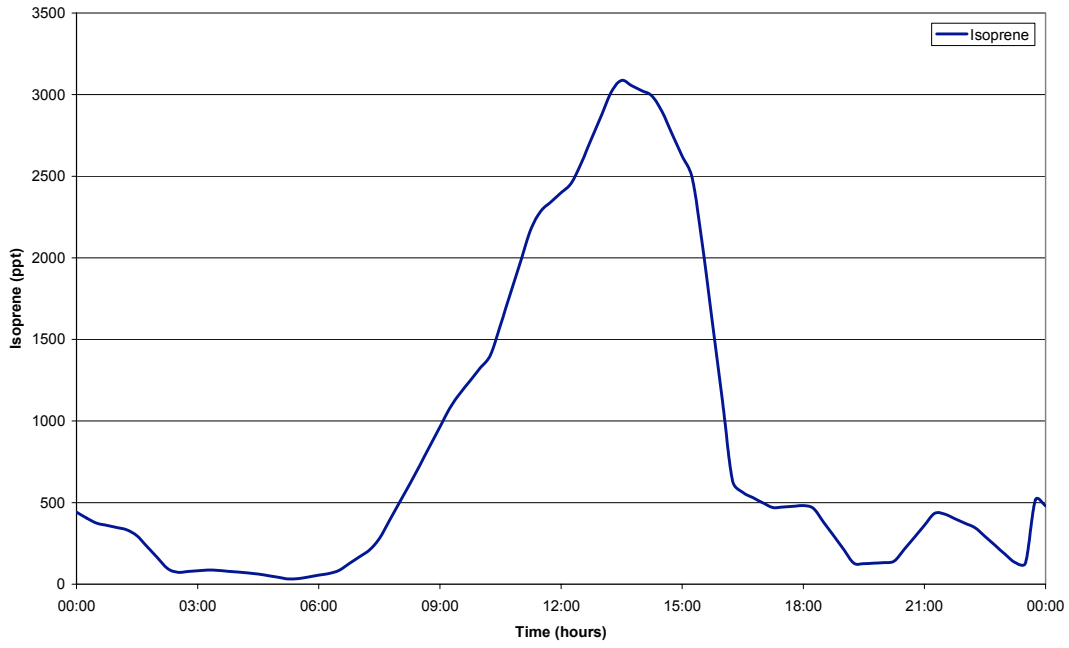

Figure 4.2.19 Isoprene concentrations recorded at Bukit Atur on JDay 192 (11th July 2008)

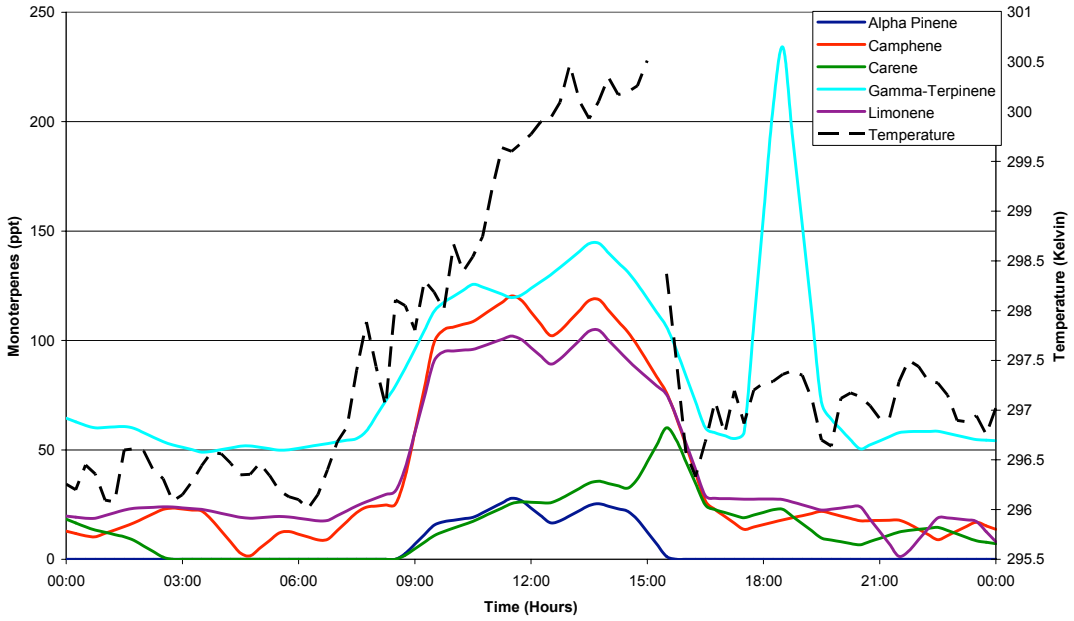

Figure 4.2.20 Monoterpene concentrations recorded at Bukit Atur on JDay 192 (11th July 2008)

The recorded value of j($O(^1D)$) at noon is 3.5 x 10^{-5} s^{-1} close to the theoretical of 4.0 x 10^{-5} and 3.6 x 10^{-5} respectively for day 192, as discussed in chapter 3.4. Clouds affected the site on this day particularly late morning. In addition, a heavy shower at 16:00 produced 20mm of rain in an hour.

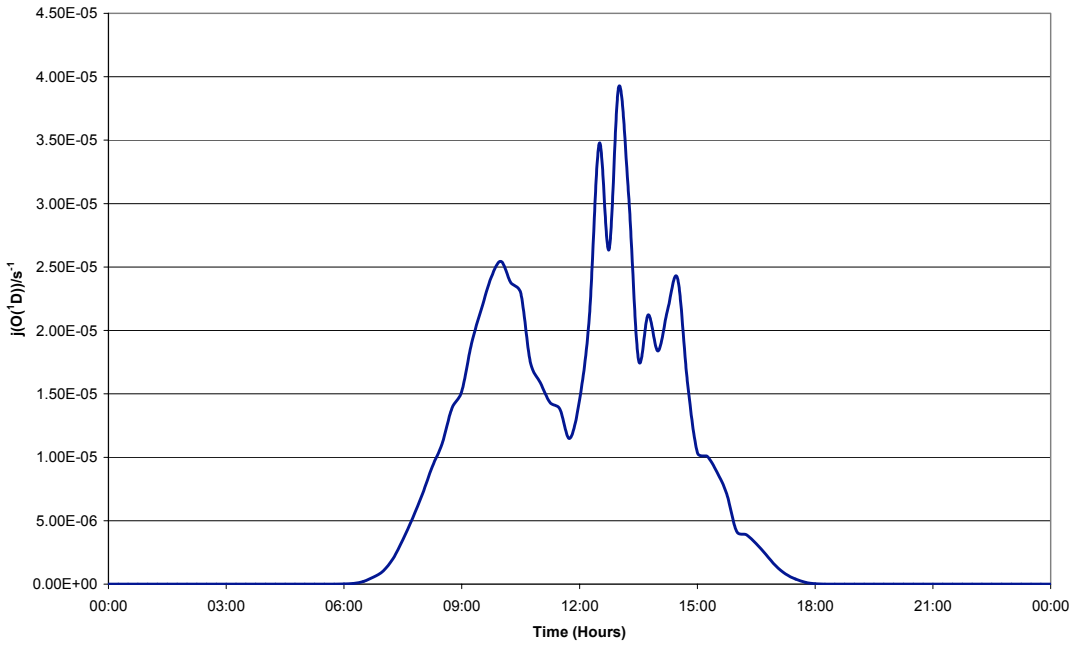

Figure 4.2.21 J(O^1D) observations recorded at Bukit Atur on JDay 192 (11th July 2008)

The concentrations predicted by the OP3 model and the OP3 Peeters model are displayed in figures 4.2.22, 4.2.23 and 4.2.24 along with the measured concentrations for OH, HO_2 and RO_2 respectively. The OP3 Peeters model predicted higher concentrations than the OP3 model for all three species, but particularly for HO_2(Table 4.2.3).

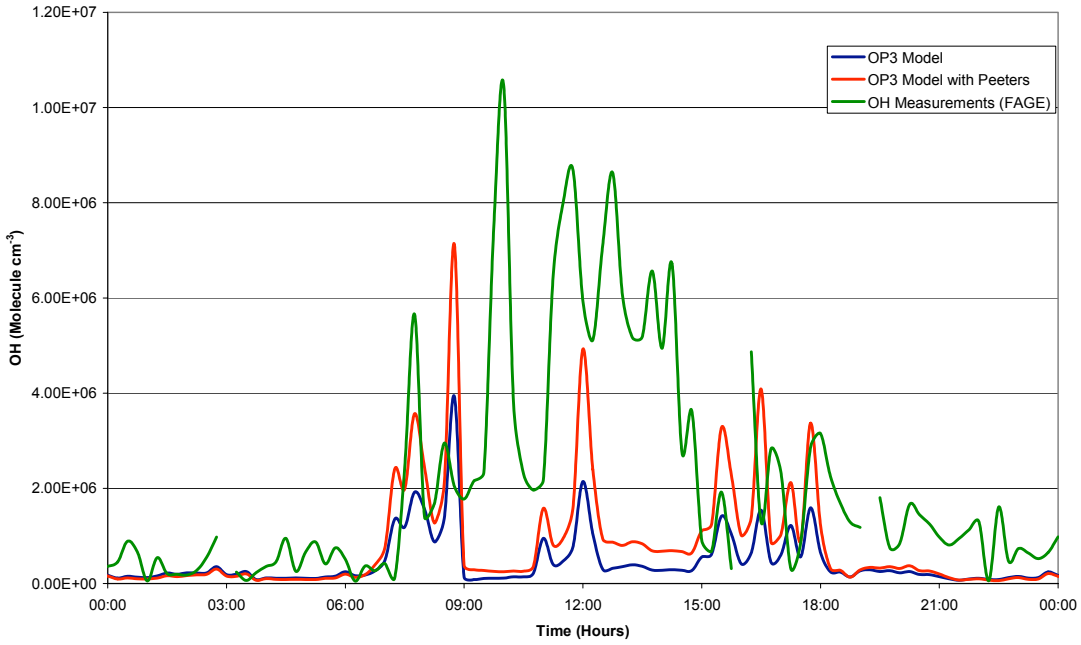

Figure 4.2.22 Model-measurement comparison of [OH] for day 192 (11th July 2008)

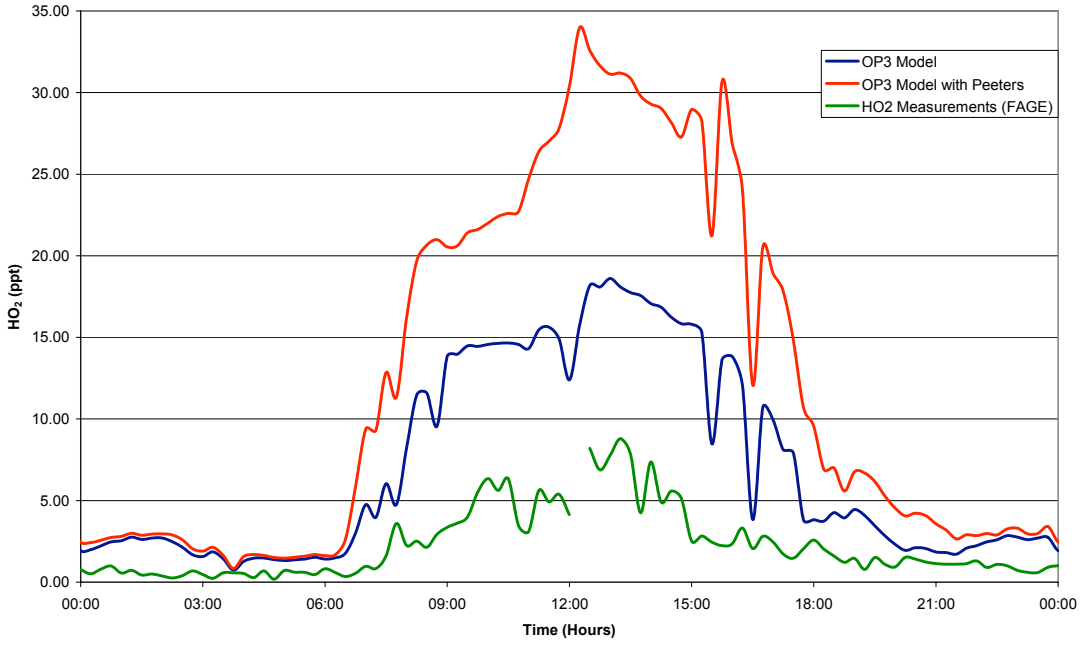

Figure 4.2.23 Model-measurement comparison of [HO_2] for day 192 (11th July 2008)

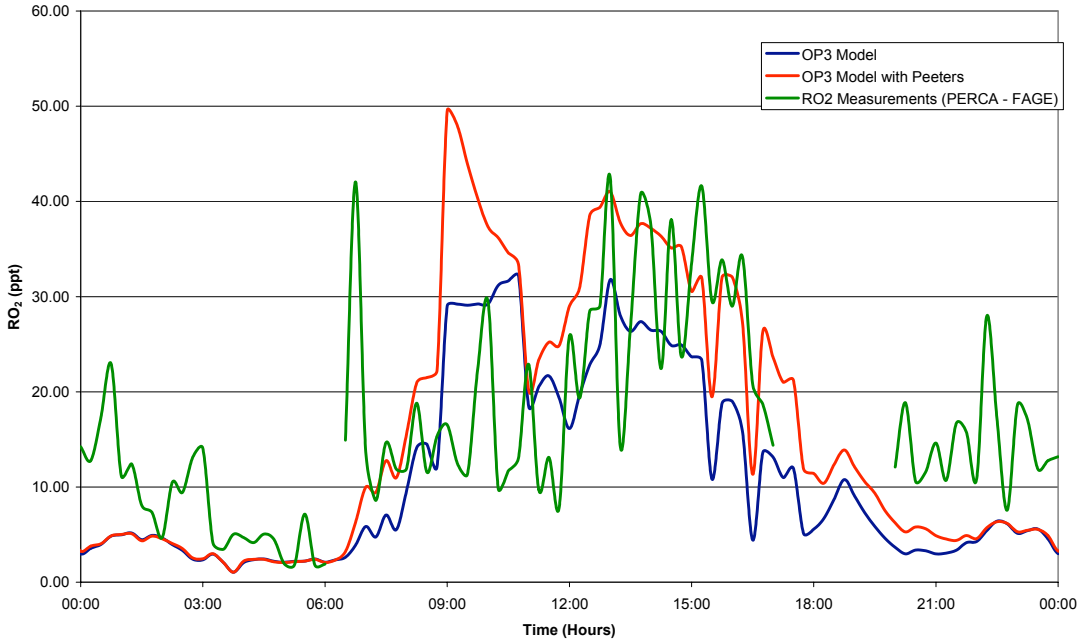

Figure 4.2.24 Model-measurement comparison of [RO_2] for day 192 (11th July 2008)

Table 4.2.3 Average concentrations of OH, HO_2 and RO_2 at Bukit Atur on JDay 192 (11^{th} July 2008) for the whole day, daytime (06:00 – 18:00), nighttime (00:00 – 06:00 and 18:00 – 24:00) and midday (11:00 -15:00).

		OH (Molecules cm^{-3})	HO_2 (ppt)	RO_2 (ppt)
OP3	Daily Average	4.4×10^5	7.0	11.1
	Daytime Average	7.1×10^5	11.7	17.9
	Nighttime Average	1.8×10^5	2.3	4.1
	Average between 11:00 and 15:00	5.5×10^5	16.3	23.7
OP3 Peeters	Daily Average	7.9×10^5	12.3	15.7
	Daytime Average	1.4×10^6	21.2	26.3
	Nighttime Average	1.8×10^5	3.2	5.1
	Average between 11:00 and 15:00	1.2×10^5	29.4	32.8
Measurements	Daily Average	2.0×10^5	2.2	14.2
	Daytime Average	3.3×10^6	3.6	19.2
	Nighttime Average	7.7×10^5	0.8	8.7
	Average between 11:00 and 15:00	5.5×10^6	5.4	25.6

One of the most noticeable trends in the HO_2 profile occurs at midday (figure 4.2.23) and is only seen in the original OP3 model and not detected by the OP3 Peeters model. There is a sudden decline in the concentration in the HO_2 measurements and the predicted values in the OP3 model. During this period where there is a decline in observed and predicted HO_2 there is an increase in the measured and predicted values of OH. The increase in OH is observed in both models, but the decline in HO_2 is only seen in one. This suggests that in the OP3 model the HO_2 is being converted to OH. This change in HO_2 and OH is observed shortly after an observed increase in NO concentrations.

Throughout day 192 there are periods where both models are able to predict the trends seen in the observed values of OH. These are most noticeably 06:00 to 09:00 and 15:00 to 18:00. However, between these two periods both models under predict the concentration of OH (table 4.2.3) and do not predict the fluctuations of OH seen at the field site. The values of OH from the two models show that the OP3 Peeters model shows constant higher values than the OP3 model. This is to be expected as it contains the added OH recycling system. The two models do contain the same trends in peaks in the predicted OH values. One reason the model might not be able to

predict the trends and accurately calculate the concentrations of OH from 09:00 is due to missing NO and NO_2 data.

The RO_2 predictions from the two models show a larger prediction from the OP3 Peeters model; this can be seen in figure 4.2.24 and table 4.2.3 where the values of RO_2 predicted by the OP3 Peeters model are much closer to the observed values than the OP3 model predictions. The average concentration values in table 4.2.3 indicate that's the OP3 Peeters model is more accurately predicting the concentrations of RO_2 than the OP3 model. From midday to 18:00 the OP3 Peeters model predicts the overall shape of the RO_2 concentration profile and accurately predicts the concentrations observed whereas the OP3 model largely under predicts the concentrations throughout this period.

4.2.4 Day 193 (12th July 2008)

The air mass trajectory arriving at the Bukit Atur field site was predicted using the NOAA Hysplit model (fig 4.2.25). The air mass arises to the South East of the field site over sea, as seen in previous days. The majority of the time the air mass is travelling to the field site is spent over sea, before it travels over the forest to the south of the field site for the final 6 to12 hours. The air mass passes over Sulawesi and the Celebes sea over before reaching the field site, just as observed on the previous days.

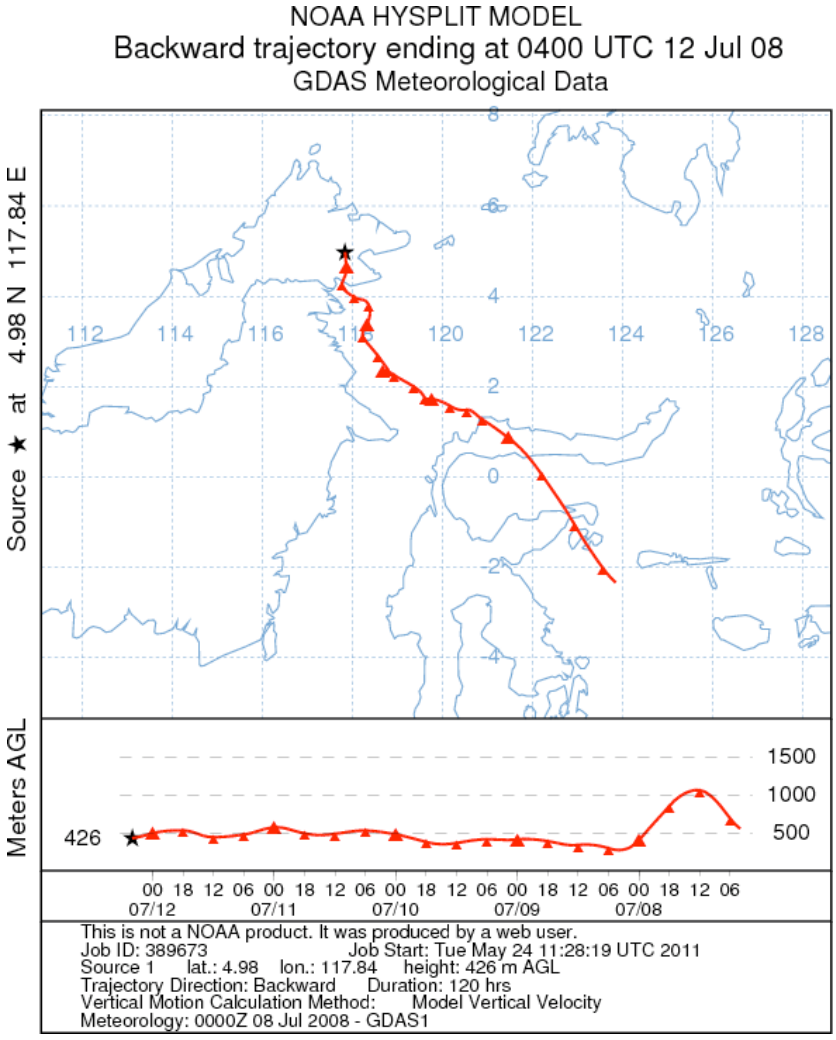

Figure 4.2.25 Air mass trajectory for 5 day arriving at the field site at 1200 hours (local time) on 12th July (JDay 193) The upper plot shows the path taken by the airmass travelling to the field site, for the 5 days previous to measurements being taken. The lower plot shows the altitude of the airmass for the 5 day period before arriving at the field site.

Figure 4.2.26 shows the concentrations of NO and NO_2 as examples. The larger peaks coincide with when vehicles were driven to the top of Bukit Atur and brought close to the observation point.

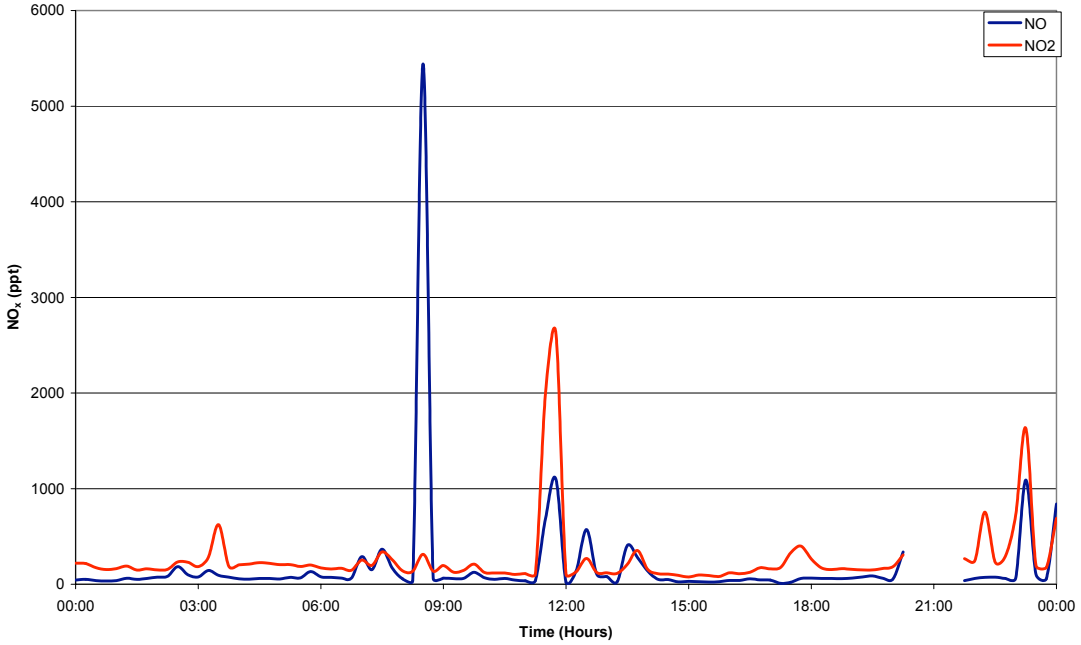

Figure 4.2.26 NO and NO_2 concentrations recorded at Bukit Atur on JDay 193 (12th July 2008)

The air mass moves over the rainforest before arriving at the Bukit Atur field site, but the diurnal variation in the isoprene and monoterpene species shown in figures 4.2.27 and 4.2.28 indicates that the observed monoterpenes are generated locally at the site.

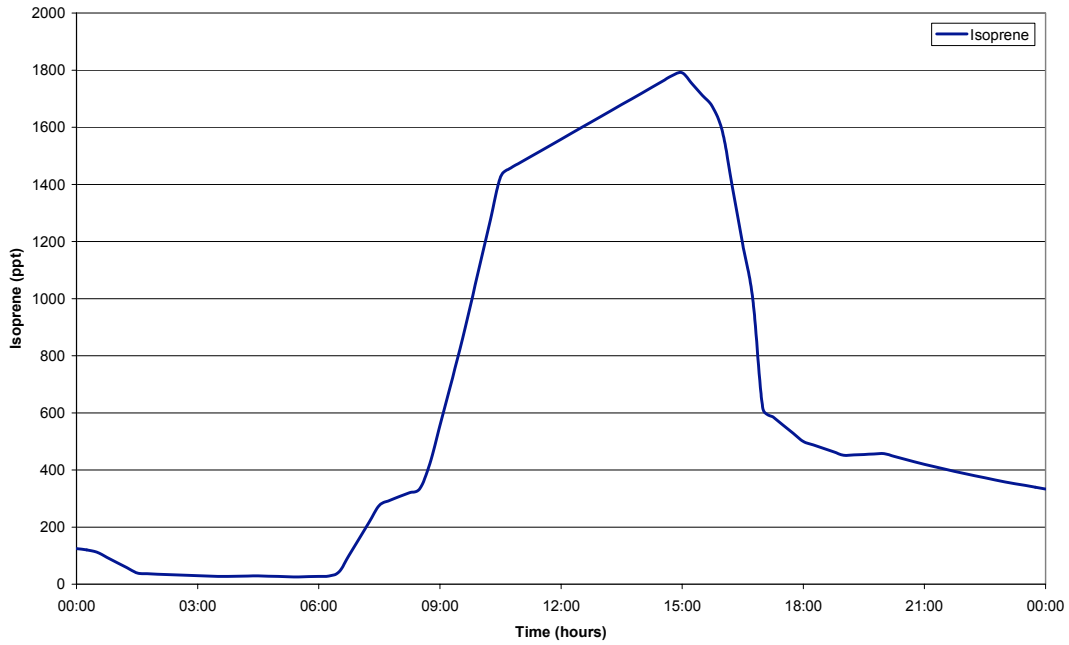

Figure 4.2.27 Isoprene concentrations recorded at Bukit Atur on JDay 193 (12th July 2008)

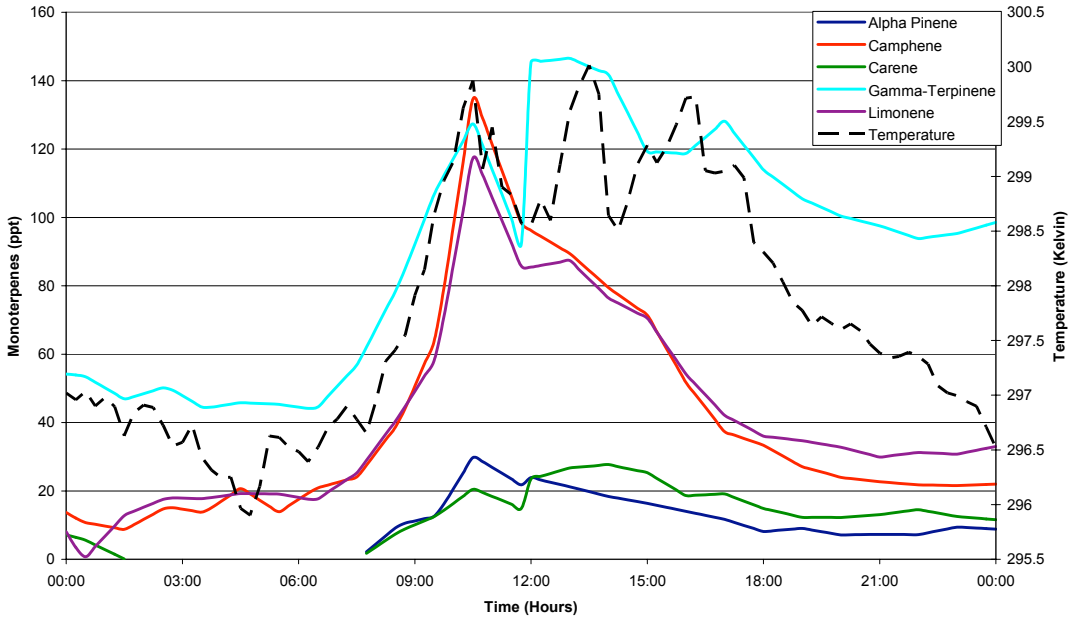

Figure 4.2.28 Monoterpene concentrations recorded at Bukit Atur on JDay 193 (12th July 2008)

The recorded value of j($O(^1D)$) at noon is 3.5 x 10^{-5} s^{-1} compared with the theoretical maximum value of 4.0 x 10^{-5} and 3.6 x 10^{-5} respectively for day 193, as discussed in chapter 3.4. There are a few clouds passing over the site and rainfall occurred at the site during the afternoon period at 12:00, 13L00 and 14:00 hours.

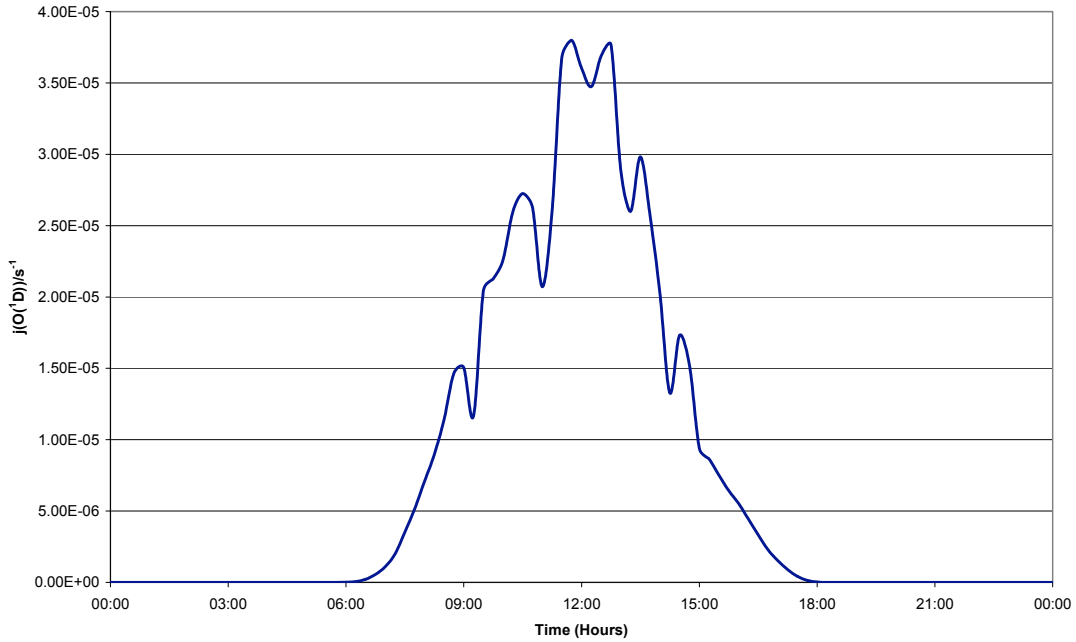

Figure 4.2.29 J(O^1D) observations recorded at Bukit Atur on JDay 193 (12th July 2008)

The results predicted by the OP3 model and the OP3 model containing the proposed Peeters scheme (OP3 Peeters) are displayed in figures 4.2.30, 4.2.31 and 4.2.32 along with the measured concentrations. The three species all show similar diurnal behaviour with the lowest values being predicted and measured during the nighttime periods and the highest values occurring during the daytime with maximum values tend to occur near solar noon. The OP3 Peeters model predicted higher concentrations than the OP3 model for all three species, but particularly for HO_2 (Table 4.2.4). This is to be expected given the recycling of radical discussed in chapter 3.7

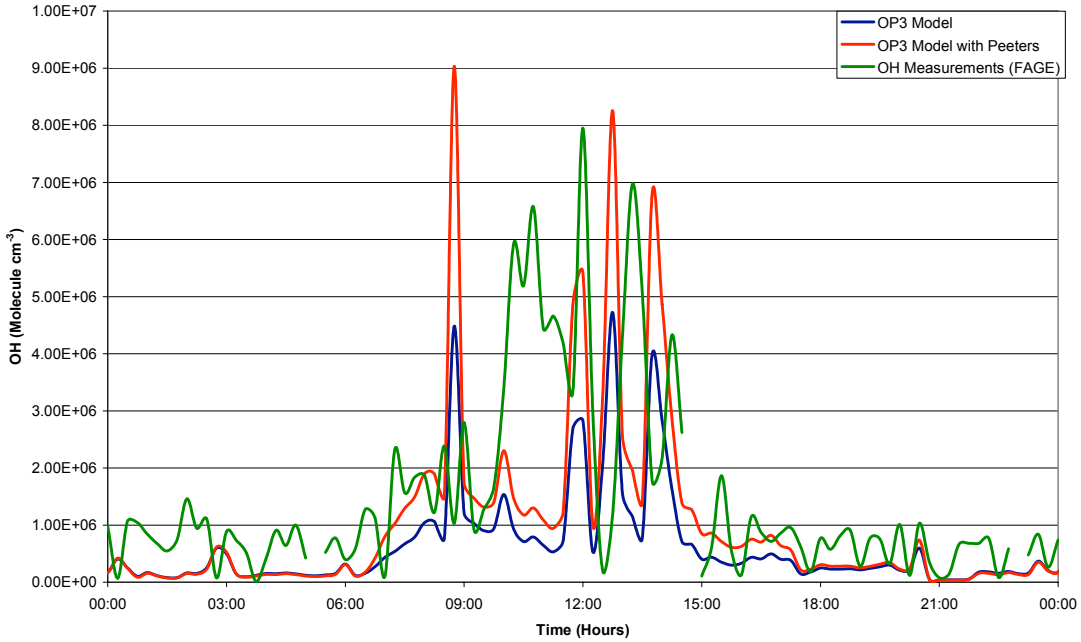

Figure 4.2.30 Model-measurement comparison of [OH] for day 193 (12th July 2008)

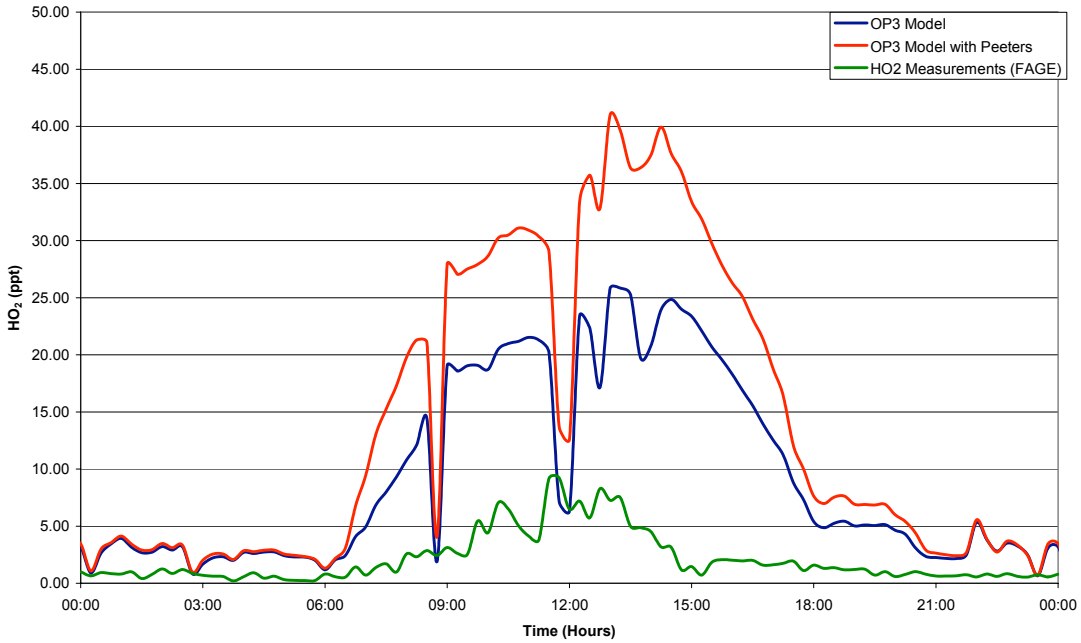

Figure 4.2.31 Model-measurement comparison of [HO_2] for day 193 (12th July 2008)

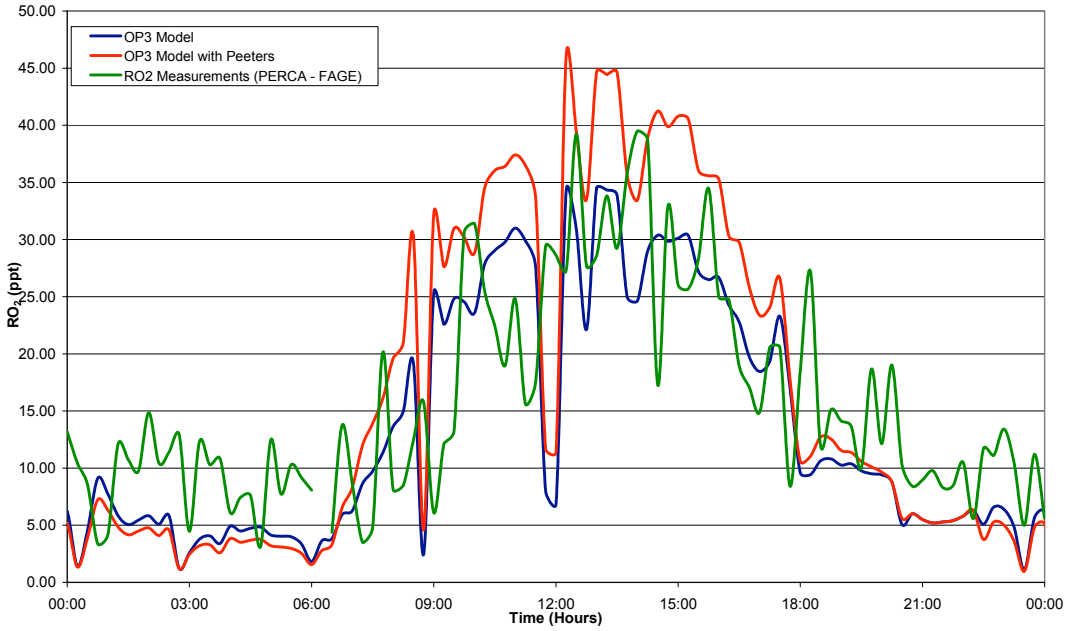

Figure 4.2.32 Model-measurement comparison of [RO_2] for day 193 (12th July 2008)

Table 4.2.4 Average concentrations of OH, HO_2 and RO_2 at Bukit Atur on JDay 193 (12th July 2008) for the whole day, daytime (06:00 – 18:00), nighttime (00:00 – 06:00 and 18:00 – 24:00) and midday (11:00 -15:00).

		OH (Molecule cm^{-3})	HO_2 (ppt)	RO_2 (ppt)
OP3	Daily Average	6.2×10^5	9.3	15.4
	Daytime Average	1.0×10^6	15.5	21.1
	Nighttime Average	1.9×10^5	3.1	9.5
	Average between 11:00 and 15:00	1.6×10^6	20.7	27.2
OP3 Peeters	Daily Average	1.0×10^6	13.8	18.5
	Daytime Average	1.8×10^6	23.9	27.4
	Nighttime Average	2.0×10^5	3.6	9.2
	Average between 11:00 and 15:00	2.9×10^6	32.7	36.0
Measurements	Daily Average	1.4×10^6	2.1	15.6
	Daytime Average	2.2×10^6	3.4	20.7
	Nighttime Average	5.9×10^5	0.7	10.6
	Average between 11:00 and 15:00	3.3×10^6	5.4	28.9

Two of the most noticeable trends in the HO_2 prediction profiles occur at 09:00 and 12:00 (figure 4.2.31). There is a sudden decline in the concentration in the HO_2 predictions from both models. This sudden decline coincides with a peak in the measurements of NO and NO_2. There is a sudden large pulse of NO and a smaller peak in measured NO at 12:00. The extra NO in the system removes HO_2 to form OH. The removal of the HO_2 in the predictions by reaction with NO lowers the predicted values of HO_2 close to the observed concentrations at 09:00 and 12:00. The reaction of NO and HO_2 in the model produced large peaks in OH occurring at 09:00 and 12:00, coinciding with the NO peaks and decline in HO_2. These decreases in HO_2 concentrations appear to be reproduced in the measurements.

The values of OH from the two models show that the OP3 Peeters model shows constant higher values than the OP3 model. This is to be expected as it contains the added OH recycling system. The two models do contain the same trends in peaks in the predicted OH values (4.2.30).

The highest observed value of OH seen on day 193 was recorded at 12:00; at this point the models both predict a large peak in OH concentration, but under predicts the observed values at this stage. The largest peak in the predicted values of OH occurs

at 09:00, but there is a large over prediction calculated by the model at this point. Between the two large predicted peaks at 09:00 and 12:00 there is a period of under prediction from the model, there is no factors in the input data that would indicate this under predicted phase. This indicates that during this period the chemistry taking place at the site is not included in the model.

Figure 4.2.32 and table 4.2.4 where the values of RO_2 predicted by the OP3 Peeters model are much closer to the observed values than the OP3 model predictions. The average concentration values in table 4.2.4 indicate that the OP3 Peeters model is more accurately predicting the concentrations of RO_2 than the OP3 model and that the daytime and midday predictions are much more accurate than the nighttime predictions.

The two sets of model predictions and the observations show a general diurnal pattern from 06:00 through to 21:00. Even though there is similarity between overall diurnal shapes of the graphs there are factors in the RO_2 production that the model is not predicting. At 09:00 and 12:00 there are two sudden decreases in the observed concentrations of RO_2, which coincides with the observations in NO_x peaks and the changes in the predictions of OH and HO_2.

4.2.5 Day 194 (13th July 2008)

The air mass trajectory arriving at the Bukit Atur field site was predicted using the NOAA Hysplit model (fig 4.2.33). The trajectory model shows that the air mass arises to the South East of the field site over sea. The majority of the time the air mass is travelling to the field site is spent over sea, before it travels over the forest to the south of the field site for the final 6 hours. 24 hours before reaching the field site the air mass slows down and spends a long time sat over the sea, this comes after passing over Sulawesi and the Celebes Sea to the south east of Borneo.

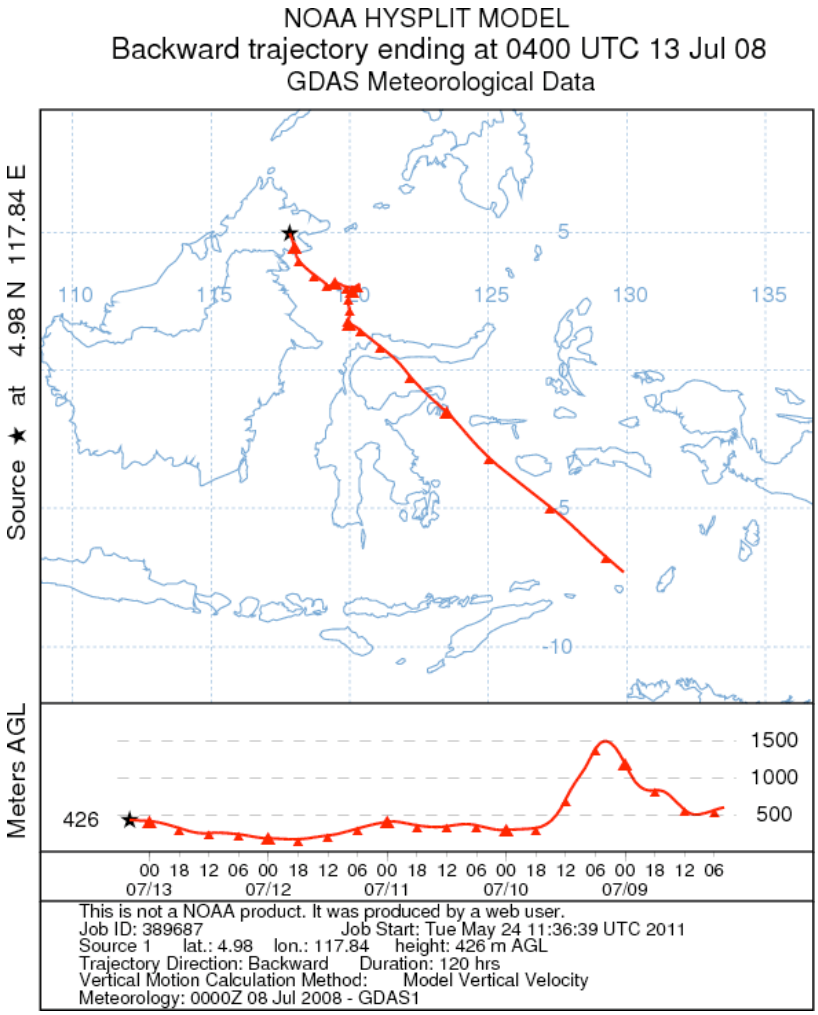

Figure 4.2.33 Air mass trajectory for 5 day arriving at the field site at 1200 hours (local time) on 13th July (JDay 194) The upper plot shows the path taken by the airmass travelling to the field site, for the 5 days previous to measurements being taken. The lower plot shows the altitude of the airmass for the 5 day period before arriving at the field site.

Figure 4.2.34 shows the concentrations of NO and NO_2 as examples. The profile of NO and NO_2 is slightly different on this day compared to the previous days. The back ground concentrations are higher showing NO_2 being photolysed.

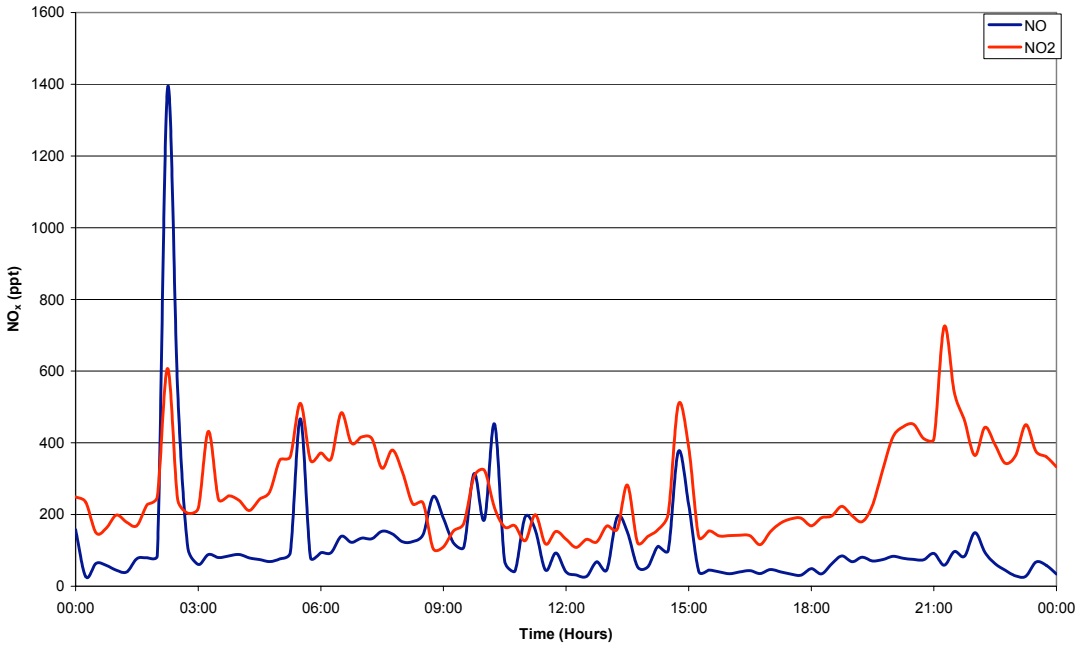

Figure 4.2.34 NO and NO_2 concentrations recorded at Bukit Atur on JDay 194 (13th July 2008)

Figures 4.2.35 and 4.2.36 again indicate that the observed monoterpenes are generated locally at the site, by sources that are effected by temperature and sunlight levels (Hewitt et al., 2009).

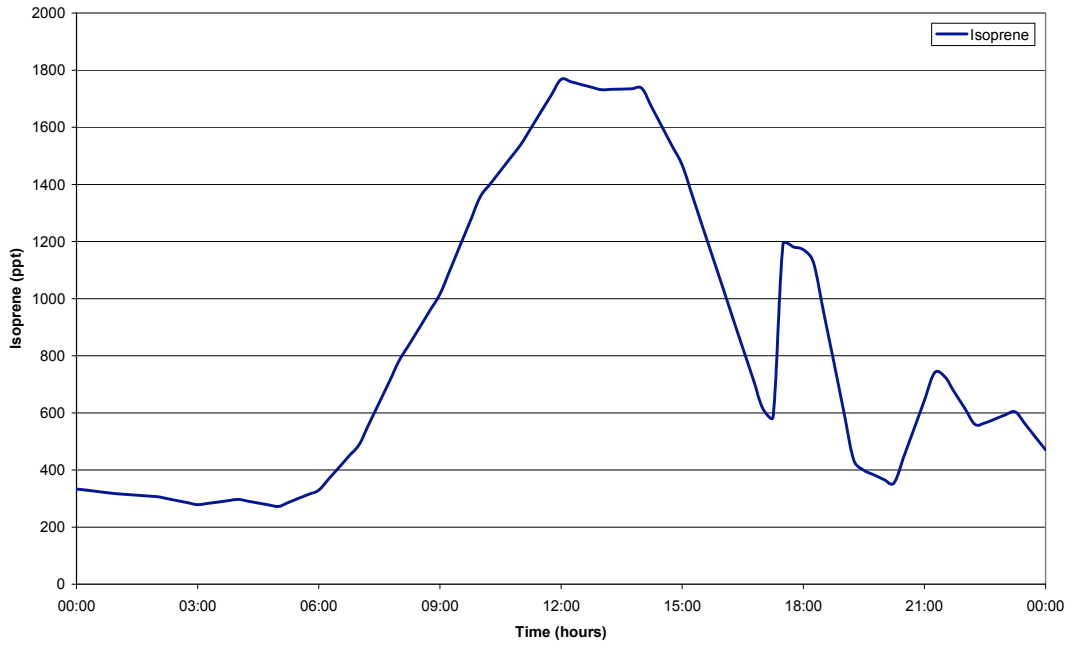

Figure 4.2.35 Isoprene concentrations recorded at Bukit Atur on JDay 194 (13th July 2008)

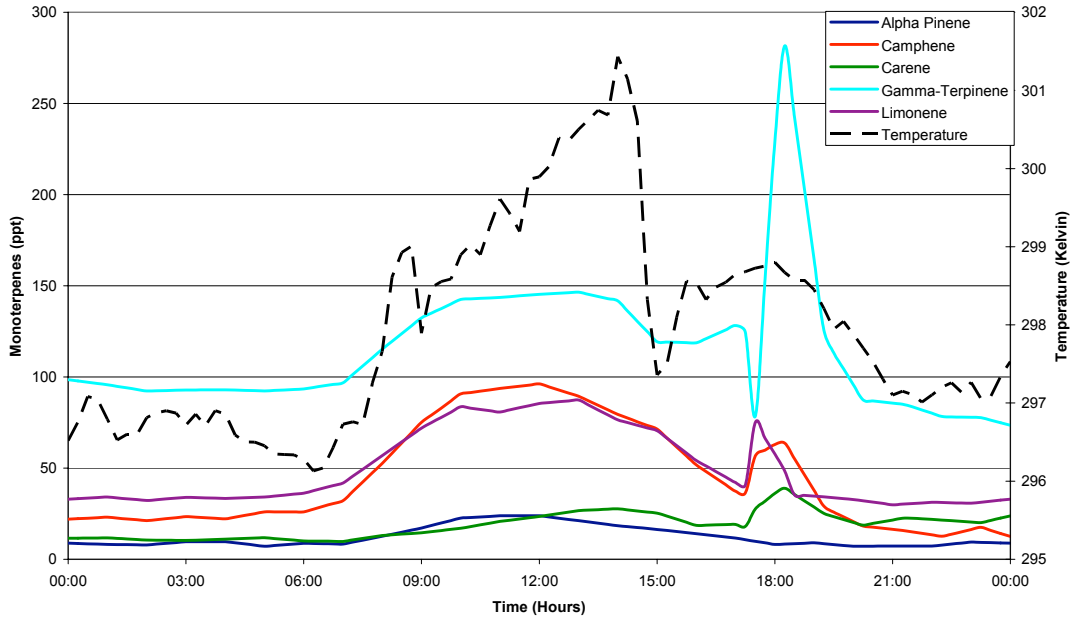

Figure 4.2.36 Monoterpene concentrations recorded at Bukit Atur on JDay 194 (13th July 2008)

The recorded value of j($O(^1D)$) at noon is 2.0 x 10^{-5} s^{-1} and the theoretical maximum value was of 4.0 x 10^{-5} . The discrepancy here could be a factor of clouds passing over the field site preventing the sunlight reaching the field site being at full intensity. Shortly after noon a value of 3.9 x 10^{-5} s^{-1} was recorded, much nearer to the theoretical maximum values indicating what was preventing the maximum light intensity reaching the field site had now passed.

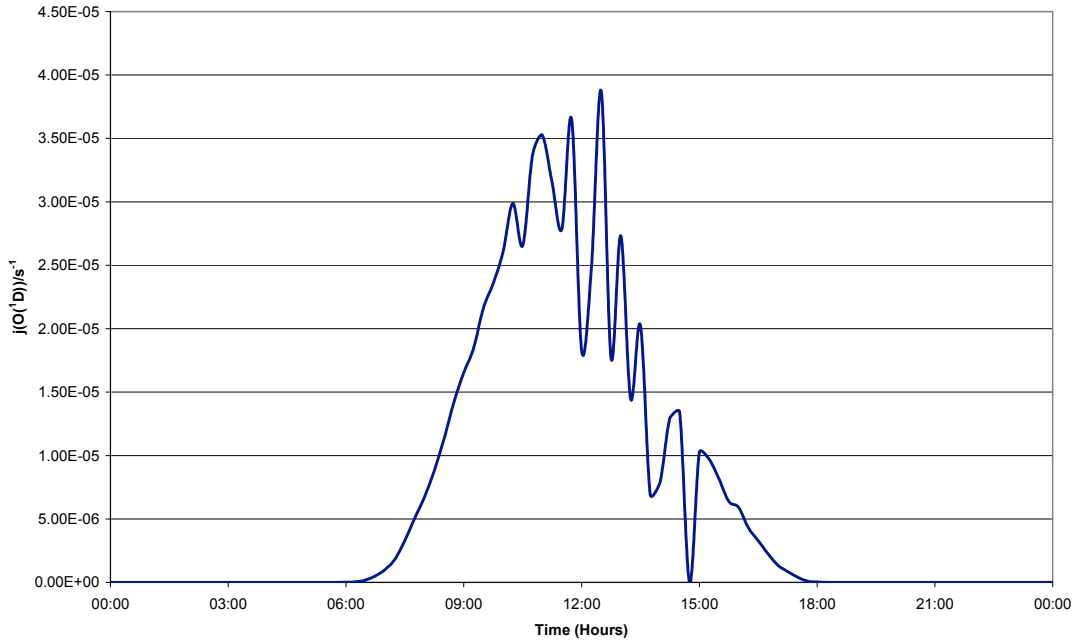

Figure 4.2.37 J(O^1D) observations recorded at Bukit Atur on JDay 194 (13th July 2008)

The results predicted by the OP3 model and the OP3 model containing the proposed Peeters scheme (OP3 Peeters) are displayed in figures 4.2.38, 4.2.39 and 4.2.40 along with the measured concentrations.

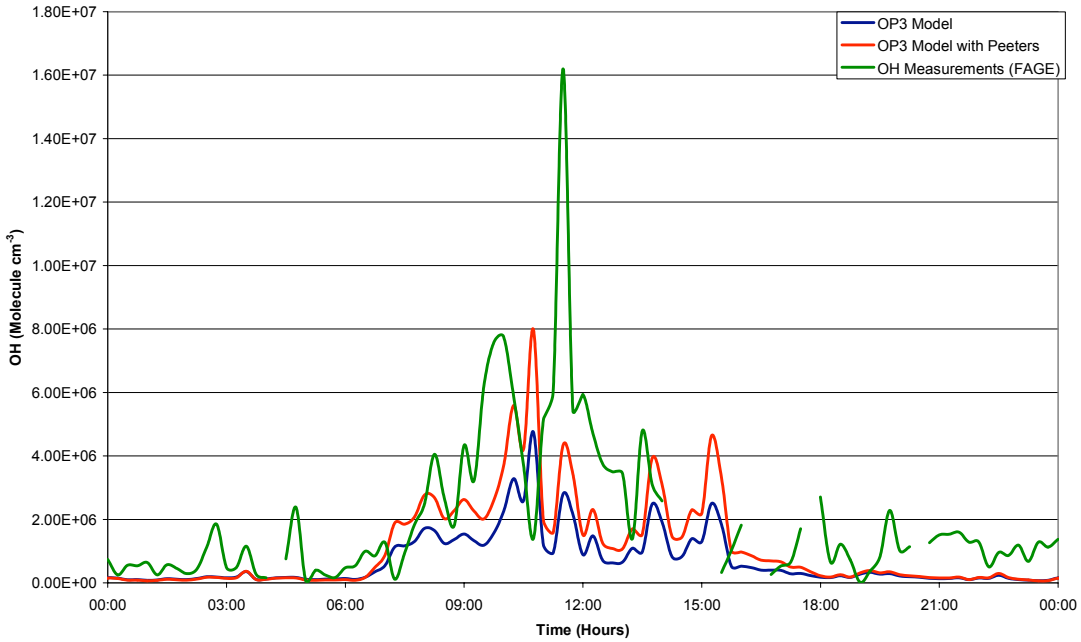

Figure 4.2.38 Model-measurement comparison of [OH] for day 194 (13th July 2008)

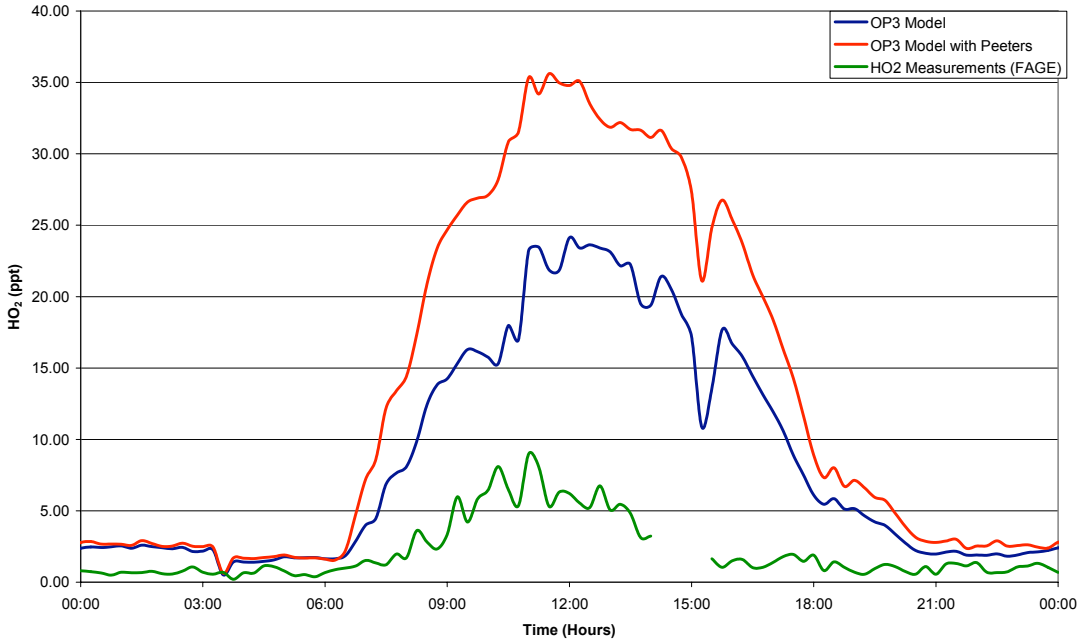

Figure 4.2.39 Model-measurement comparison of [HO_2] for day 194 (13th July 2008)

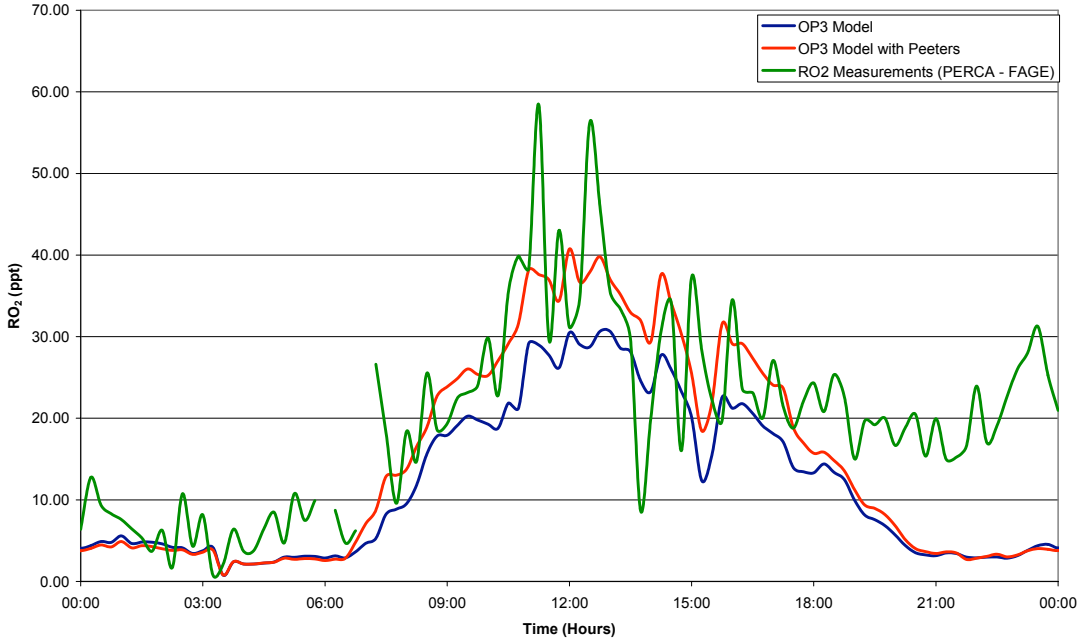

Figure 4.2.40 Model-measurement comparison of [RO_2] for day 194 (13th July 2008)

Table 4.2.5 Average concentrations of OH, HO_2 and RO_2 at Bukit Atur on JDay 194 (13th July 2008) for the whole day, daytime (06:00 – 18:00), nighttime (00:00 – 06:00 and 18:00 – 24:00) and midday (11:00 -15:00).

		OH (Molecule cm^{-3})	HO_2 (ppt)	RO_2 (ppt)
OP3	Daily Average	6.9×10^5	8.6	11.8
	Daytime Average	1.2×10^6	14.6	18.8
	Nighttime Average	1.5×10^5	2.5	4.7
	Average between 11:00 and 15:00	1.3×10^6	21.7	27.2
OP3 Peeters	Daily Average	1.1×10^6	13.2	14.8
	Daytime Average	2.0×10^6	23.1	24.8
	Nighttime Average	1.6×10^5	3.2	4.8
	Average between 11:00 and 15:00	2.1×10^6	32.5	35.0
Measurements	Daily Average	1.9×10^6	2.0	19.6
	Daytime Average	3.1×10^6	3.1	25.7
	Nighttime Average	8.2×10^5	0.8	13.5
	Average between 11:00 and 15:00	5.0×10^6	4.3	34.2

One of the most noticeable trends in the HO_2 profile occurs just before midday (figure 4.2.39). There is a sudden decline in the concentration in the HO_2 measurements and both sets of predicted values.

The values of OH from the two models show that the OP3 Peeters model shows constant higher values than the OP3 model. This is to be expected as it contains the added OH recycling system. The two models do contain the same trends in peaks in the predicted OH values (4.2.38). The highest observed value of OH seen on day 194 was recorded at 11:45; at this point the models both predict a small peak in OH concentration, but under predict this peak. The input data does not show any factors in concentrations of the constrained species or the physical data as to why this large peak occurs at this point. Another distinct difference between the OH predictions and observations is at 11:00 where both models over predict a peak in OH, which coincides with a peak in NO observations, but a decrease in concentration is observed in the measurements.

The RO_2 predictions again show that OP3 Peeters model is much closer to the observed values than the OP3 model. The average concentration values in table 4.2.5 indicate that's the OP3 Peeters model is more accurately predicting the concentrations

of RO_2 than the OP3 model and that the daytime and midday predictions are much more accurate than the nighttime predictions.

At 14:00 there is a sudden decrease in the observed concentrations of RO_2 and two large peaks in the observed values of RO_2 at 11:30 and 12:15. The models do not predict either of the peaks or the sudden decline in RO_2 and there is no information in the input data to explain why the observed changes happen.

4.2.6 Day 195 (14th July 2008)

The air mass trajectory arriving at the Bukit Atur field site was predicted using the NOAA Hysplit model (fig 4.2.41). The NOAA model shows that the air mass arises to the South East of the field site over sea. The majority of the time the air mass is travelling to the field site is spent over sea, before it travels over the forest to the south east of the field site for the final 12 hours. The air mass that reaches the field site on this day also passes over Pulau Taliabu first and then Sulawesi (Inodnesia) and slows down after doing this before reaching Borneo.

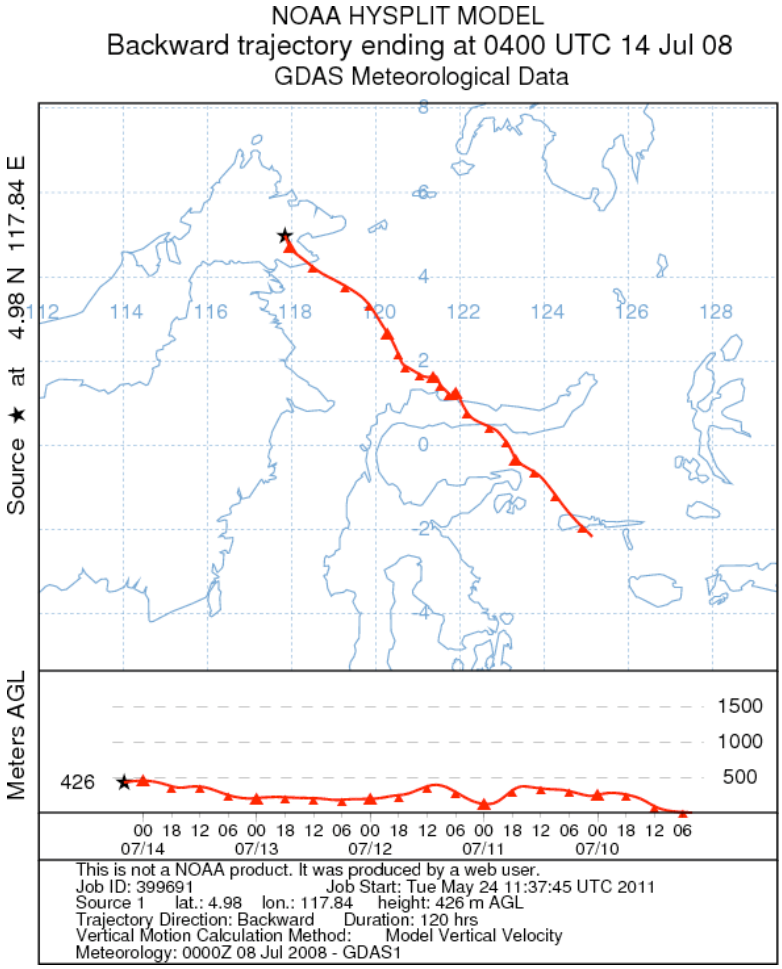

Figure 4.2.41 Air mass trajectory for 5 day arriving at the field site at 1200 hours (local time) on 14th July (JDay 195) The upper plot shows the path taken by the airmass travelling to the field site, for the 5 days previous to measurements being taken. The lower plot shows the altitude of the airmass for the 5 day period before arriving at the field site.

Figure 4.2.42 shows the concentrations of NO and NO_2. The peaks through out the day are caused by NO_x emissions from traffic passing along the logging road near the field site. The larger peaks are associated to vehicles arriving at the field site. On this day the back ground concentrations of NO and NO_2 were higher that on days 190 to 193.

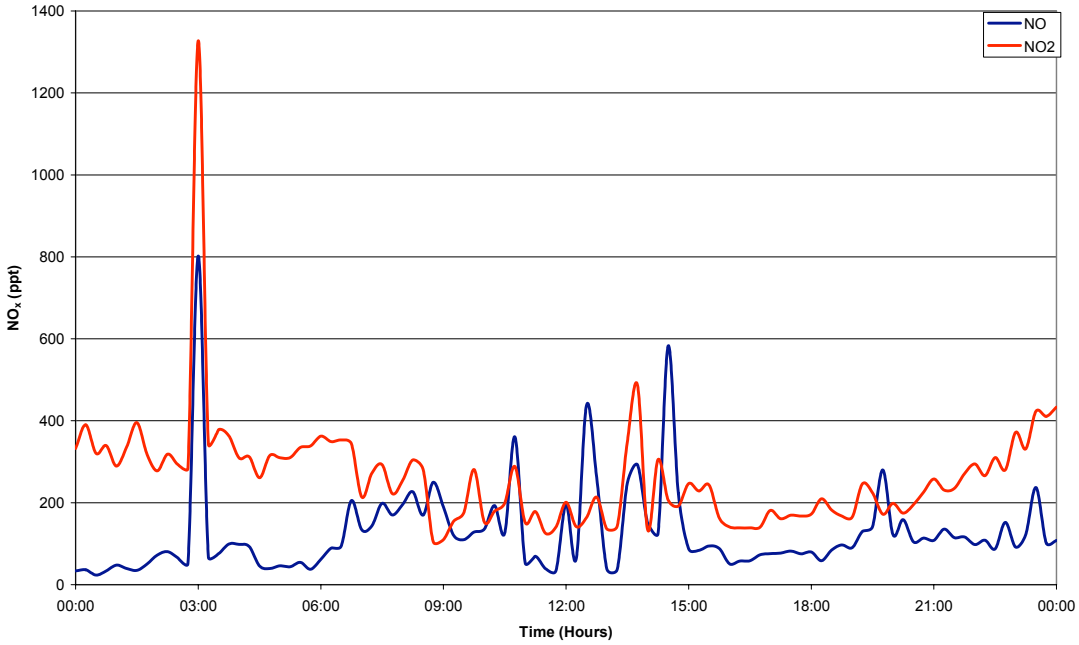

Figure 4.2.42 NO and NO_2 concentrations recorded at Bukit Atur on JDay 195 (14th July 2008)

The air mass moves over the rainforest before arriving at the Bukit Atur field site, but the diurnal variation in the isoprene and monoterpene species shown in figures 4.2.43 and 4.2.44 indicate that the observed monoterpenes are generated locally at the site.

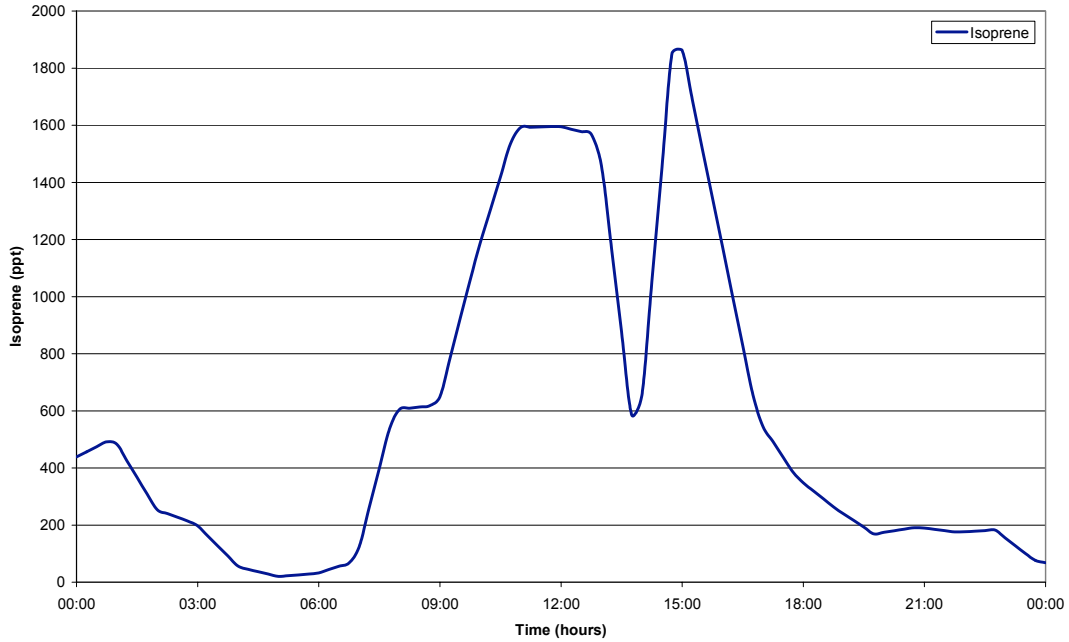

Figure 4.2.43 Isoprene concentrations recorded at Bukit Atur on JDay 195 (14th July 2008)

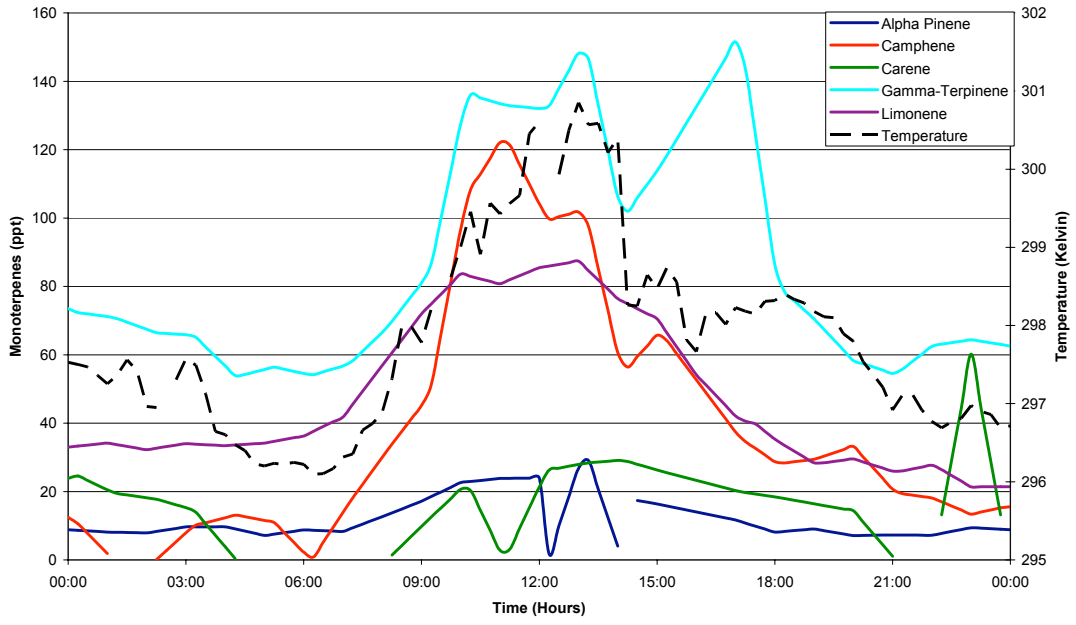

Figure 4.2.44 Monoterpene concentrations and temperature recorded at Bukit Atur on JDay 195 (14th July 2008)

The recorded value of $j(O(^1D))$ at noon is 3.7 x 10^{-5} s^{-1} compared to the theoretical maximum of 4.0 x 10^{-5} (3.4). Again, clouds affected the site particularly in the afternoon and rainfall was observed at 15:00 hours.

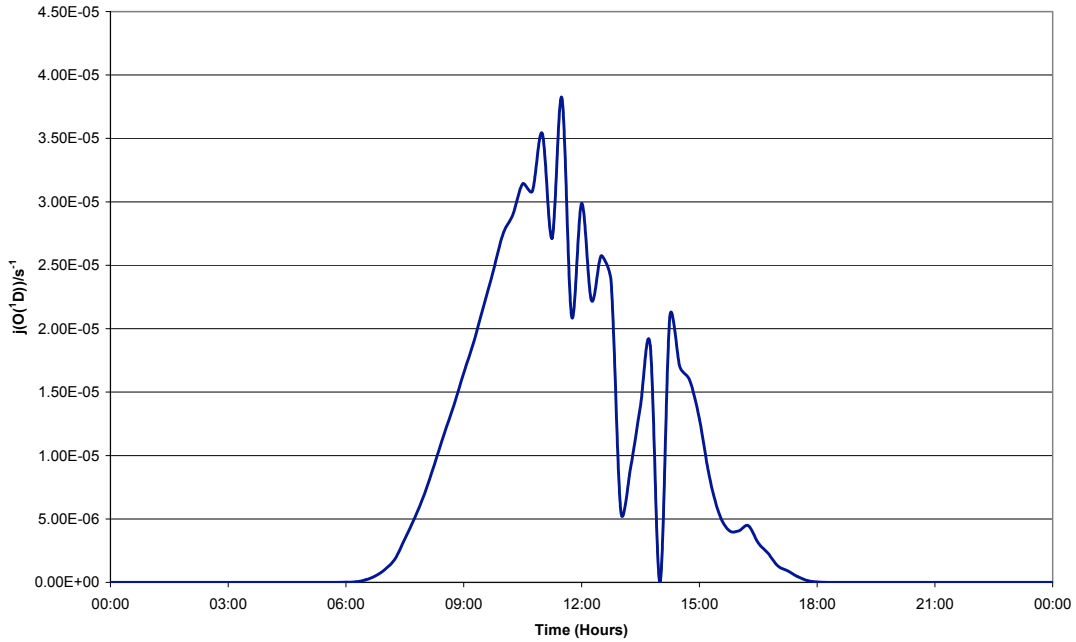

Figure 4.2.45 J(O^1D) observations recorded at Bukit Atur on JDay 195 (14th July 2008)

The results predicted by the OP3 model and the OP3 model containing the proposed Peeters scheme (OP3 Peeters) are displayed in figures 4.2.46, 4.2.47 and 4.48 along with the measured concentrations.

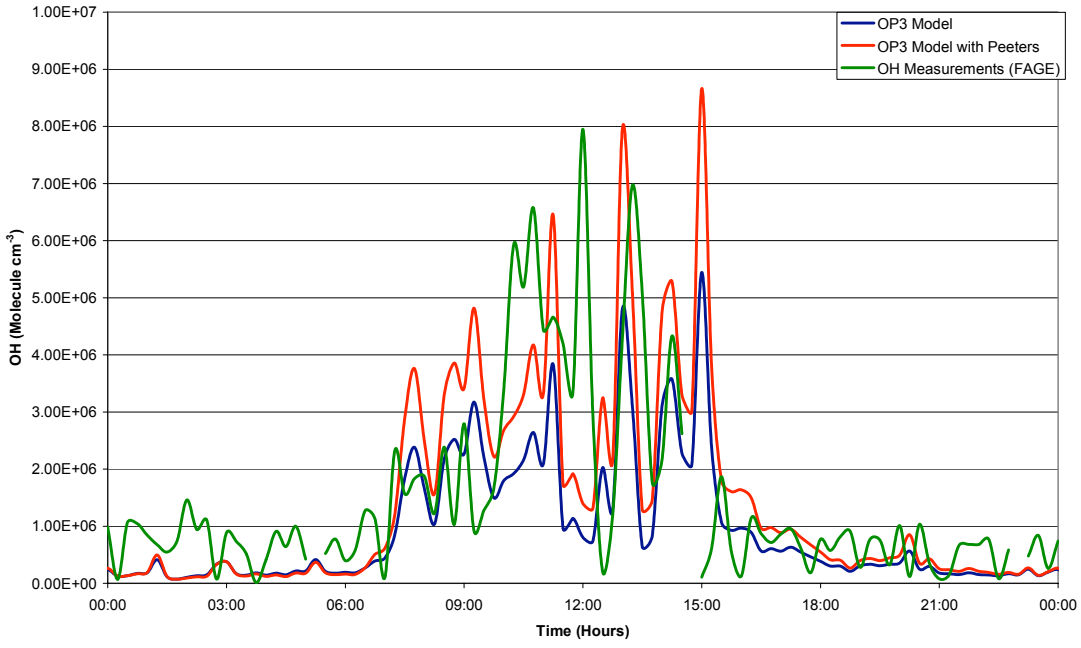

Figure 4.2.46 Model-measurement comparison of [OH] for day 195 (14th July 2008)

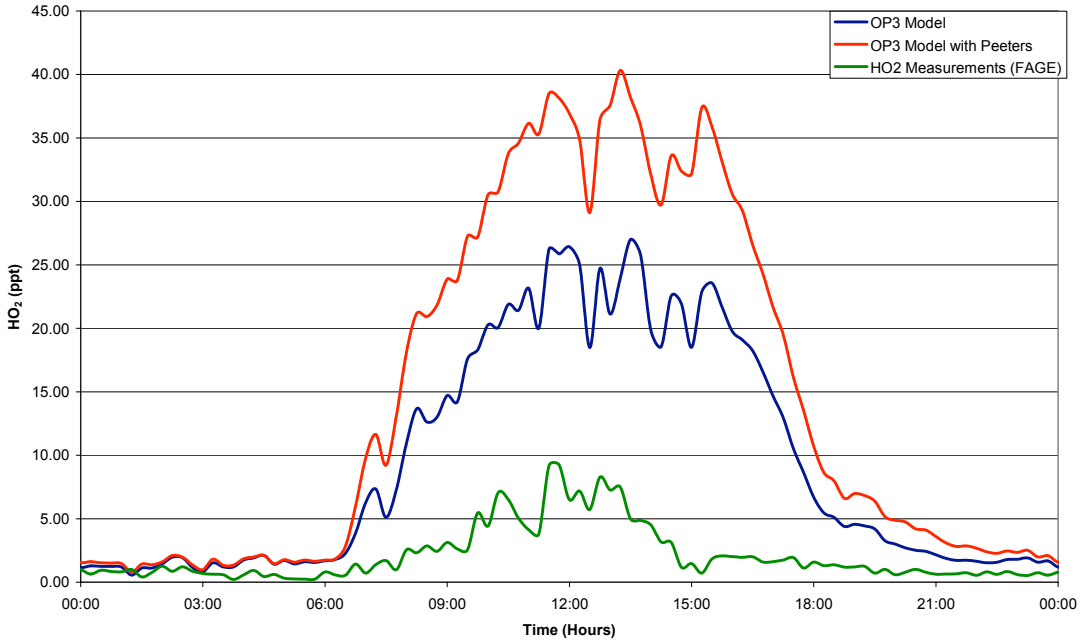

Figure 4.2.47 Model-measurement comparison of [HO_2] for day 195 (14th July 2008)

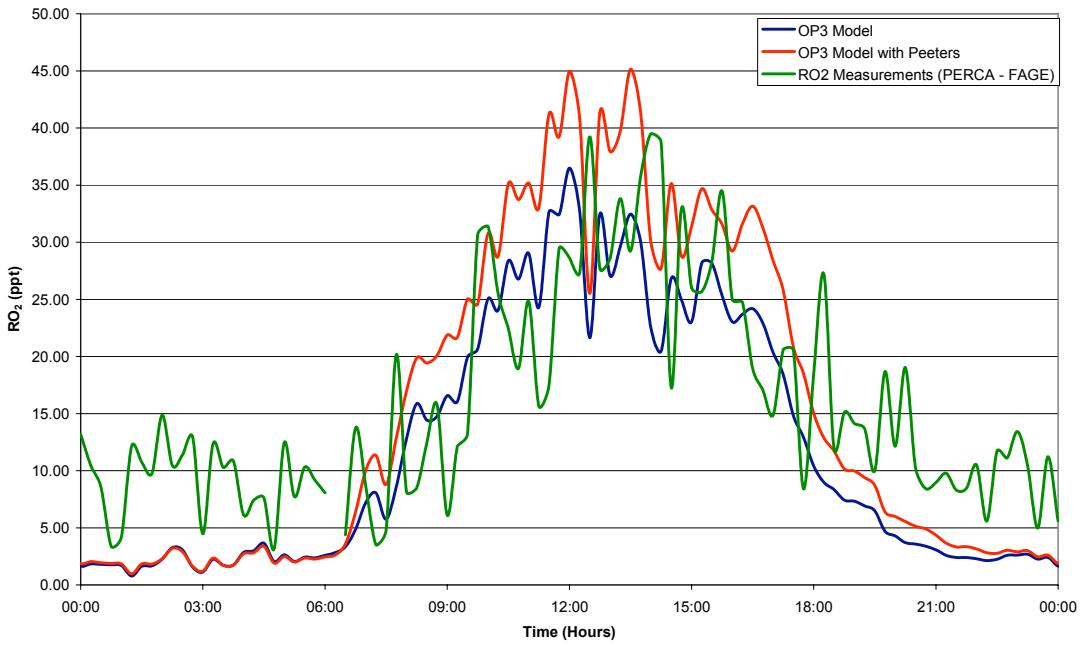

Figure 4.2.48 Model-measurement comparison of [RO_2] for day 195 (14th July 2008)

Table 4.2.6 Average concentrations of OH, HO_2 and RO_2 at Bukit Atur on JDay 195 (14th July 2008) for the whole day, daytime (06:00 – 18:00), nighttime (00:00 – 06:00 and 18:00 – 24:00) and midday (11:00 -15:00).

		OH (Molecules cm^{-3})	HO_2 (ppt)	RO_2 (ppt)
OP3	Daily Average	9.3×10^5	9.4	11.9
	Daytime Average	1.6×10^6	16.7	20.6
	Nighttime Average	2.2×10^5	2.1	3.2
	Average between 11:00 and 15:00	2.2×10^6	22.8	28.1
OP3 Peeters	Daily Average	1.4×10^6	14.4	15.3
	Daytime Average	2.5×10^6	25.8	26.6
	Nighttime Average	2.5×10^5	2.9	3.9
	Average between 11:00 and 15:00	3.6×10^6	35.1	36.3
Measurements	Daily Average	1.4×10^6	2.1	15.6
	Daytime Average	2.2×10^6	3.4	20.7
	Nighttime Average	5.9×10^5	0.7	10.6
	Average between 11:00 and 15:00	3.3×10^6	5.4	28.9

The highest observed value of OH seen on day 195 was recorded at 12:00; at this point the models both predict only a small peak in OH concentration. Just after 12:15 there is a small peak followed by a large peak in the OH concentrations, the models predict the large peak but not the small peak. This coincides with a similar shaped peak at the same time in the NO observations (figure 4.2.42). These coinciding peaks in NO and OH are also at 09:00 and 15:00 in both the models and observations of OH. However, the event predicted at 15:00 only sees one peak in the observations where as the model predicts two. At the same points as the OH/NO interactions are see in the model output and the observations, similar changes occur in the HO_2 prediction profiles (4.2.47). At 09:00, 12:15 and 15:00 there are small declines seen in the over predicted values of HO_2.

The two sets of model RO_2 predictions and the observations show a general diurnal pattern much like OH and HO_2. Even though there is similarity between overall diurnal shapes of the graphs there are factors in the RO_2 production that the model is not predicting. At 12:00 and there is a decrease in the modelled concentrations of RO_2, where as the observations show an increase in the concentration at this point. The decline in the model occurs at the same point as the model predicts a decline in HO_2 and an increase in OH from an increase in the observed value of NO. The chemistry in the model would lead to a decrease in RO_2 from increased reactions with NO.

4.2.7 Day 198 (17th July 2008)

The air mass trajectory arriving at the Bukit Atur field site was predicted using the NOAA Hysplit model (fig 4.2.49). The NOAA model shows that the air mass arises to the South East of the field site over sea. The majority of the time the air mass is travelling to the field site is spent over sea. However, 2 days before reaching the field site it travels over the coast and more inland parts of the Indonesian half of Borneo and then finally over the forest to the south of the field site.

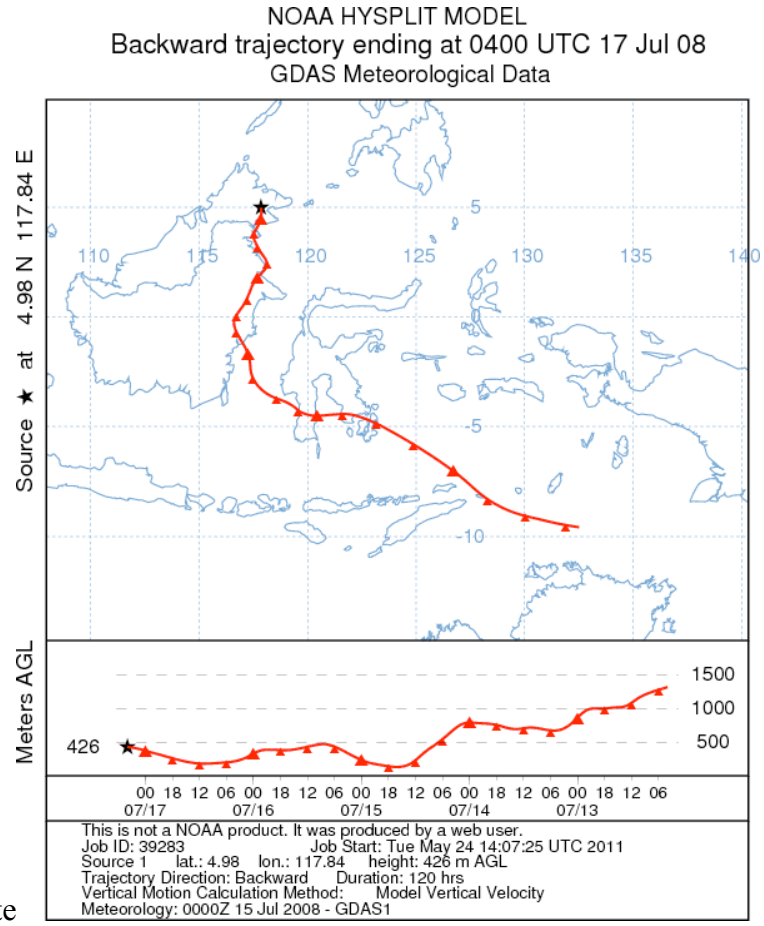

site

Figure 4.2.49 Air mass trajectory for 5 day arriving at the field site at 1200 hours (local time) on 17th July (JDay 198) The upper plot shows the path taken by the airmass travelling to the field site, for the 5 days previous to measurements being taken. The lower plot shows the altitude of the airmass for the 5 day period before arriving at the field site.

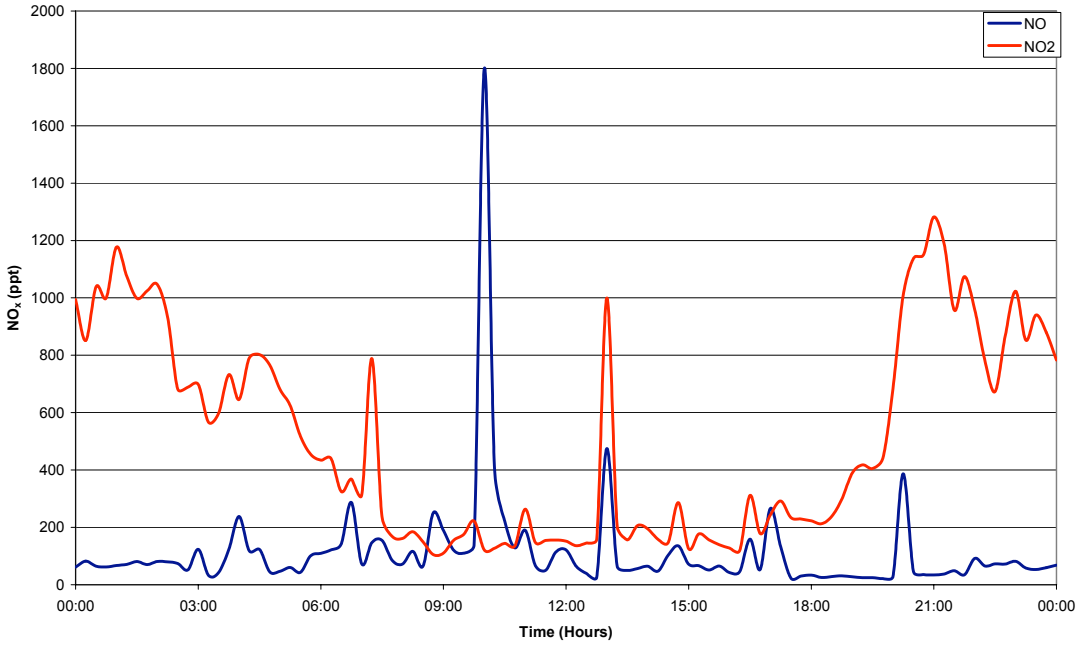

Figure 4.2.50 NO and NO_2 concentrations recorded at Bukit Atur on JDay 198 (17th July 2008)

The air mass moves over the rainforest before arriving at the Bukit Atur field site, but the diurnal variation in the isoprene and monoterpene species shown in figures 4.2.51 and 4.2.52 indicates that the observed monoterpenes are generated locally at the site, by sources that are affected by temperature and sunlight levels (Hewitt et al., 2009).

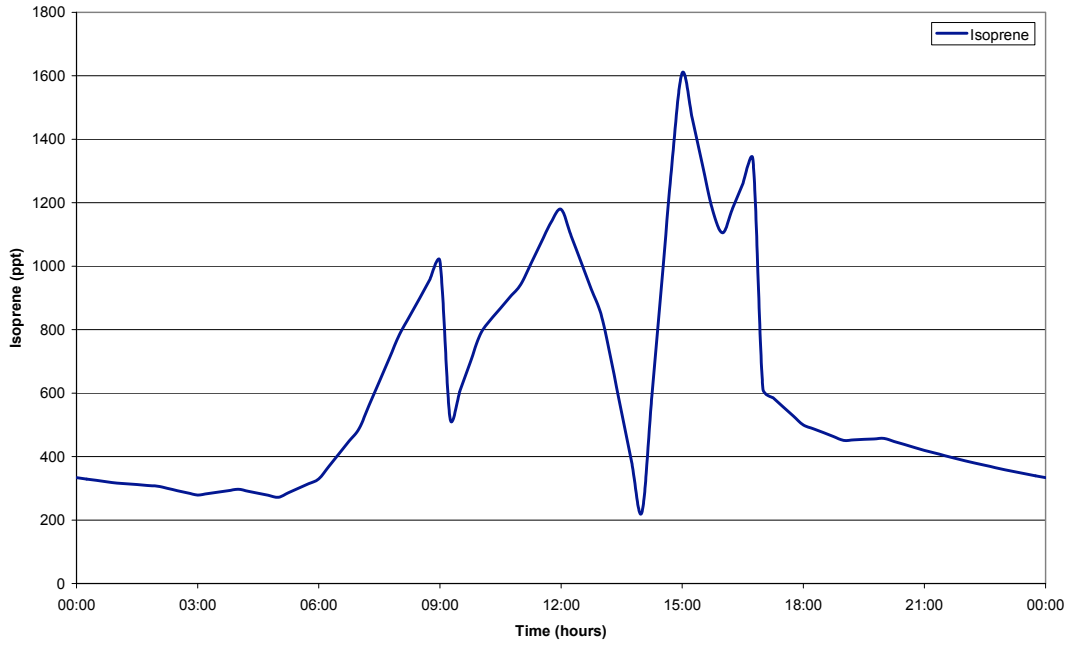

Figure 4.2.51 Isoprene concentrations recorded at Bukit Atur on JDay 198 (17th July 2008)

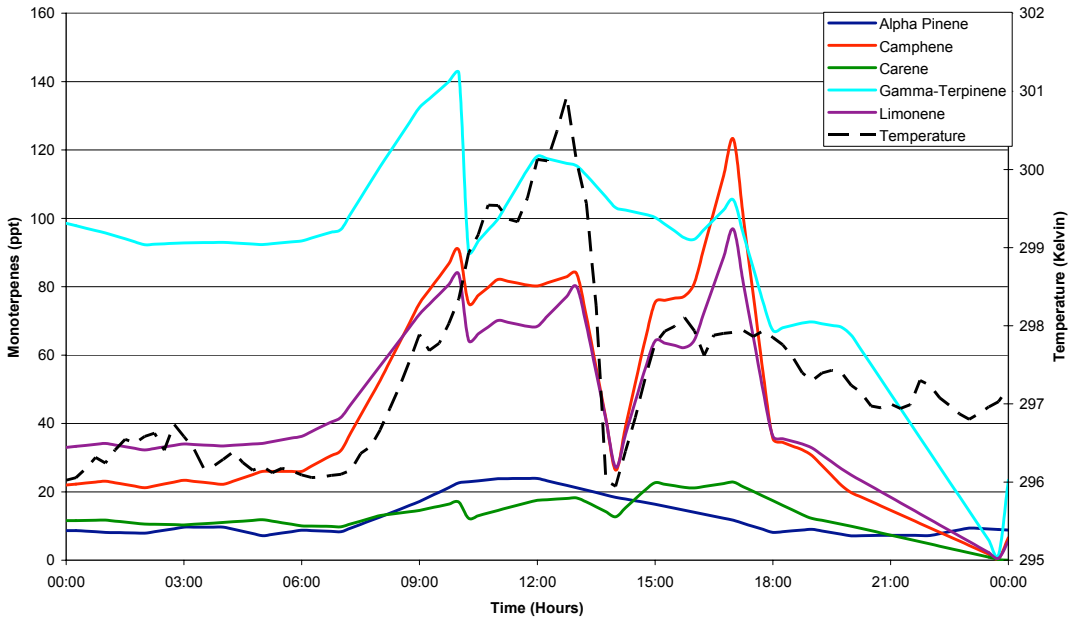

Figure 4.2.52 Monoterpene concentrations recorded at Bukit Atur on JDay 198 (17th July 2008)

The measurements of j($O(^1D)$), the rate of the photochemical breakdown of O_3 to O_2 and an O^1D radical, were also recorded at the site on a minute by minute basis. The diurnal profile for this on JDay 198 is shown in figure 4.2.53. The diurnal plot shows that the value of j($O(^1D)$), starts to be measured at 06:00 when the sun rises at the field site. The value continues to rise until approximately 12:00 and then begins to decline until it stops being detectable at 18:00 when the sunsets at the field site. The diurnal plot is not one smooth curve as might be expected for the change in intensity of sunlight, but there parts of the graph that shows areas where the sunlight intensity unexpectedly declines. These parts of the graph can attributed to points in the day where there was some degree of cloud cover lowering the intensity of the light reaching the photometer.

The recorded value of j($O(^1D)$) at noon is 1.5×10^{-5} s^{-1} compared to the theoretical maximum value at this point of 4.0×10^{-5}. There was rainfall at 15:00 hours, but cloud obviously affected the site for much of the day.

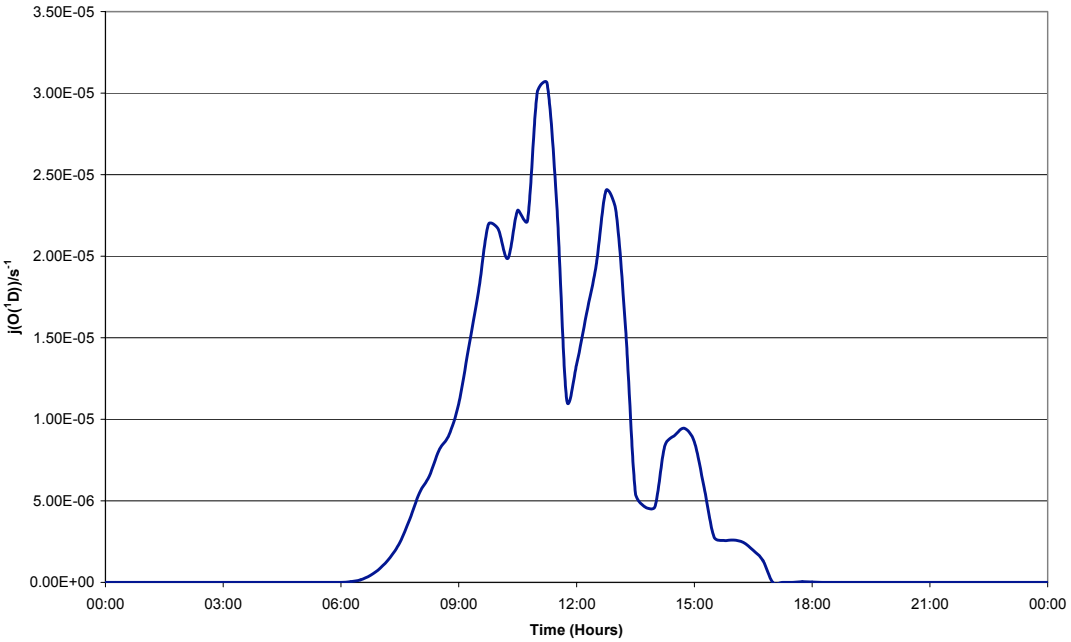

Figure 4.2.53 JO^1D observations recorded at Bukit Atur on JDay 198 (17th July 2008)

The results predicted by the OP3 model and the OP3 model containing the proposed Peeters scheme (OP3 Peeters) are displayed in figures 4.2.54, 4.2.55 and 4.2.56 along with the measured concentrations.

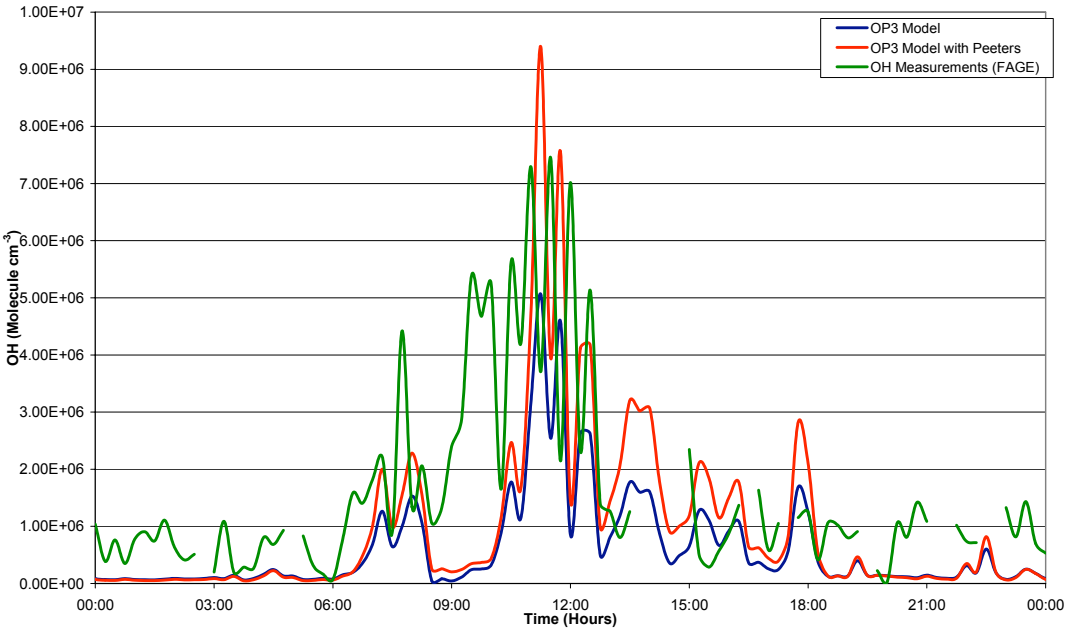

Figure 4.2.54 Model-measurement comparison of [OH] for day 198 (17th July 2008)

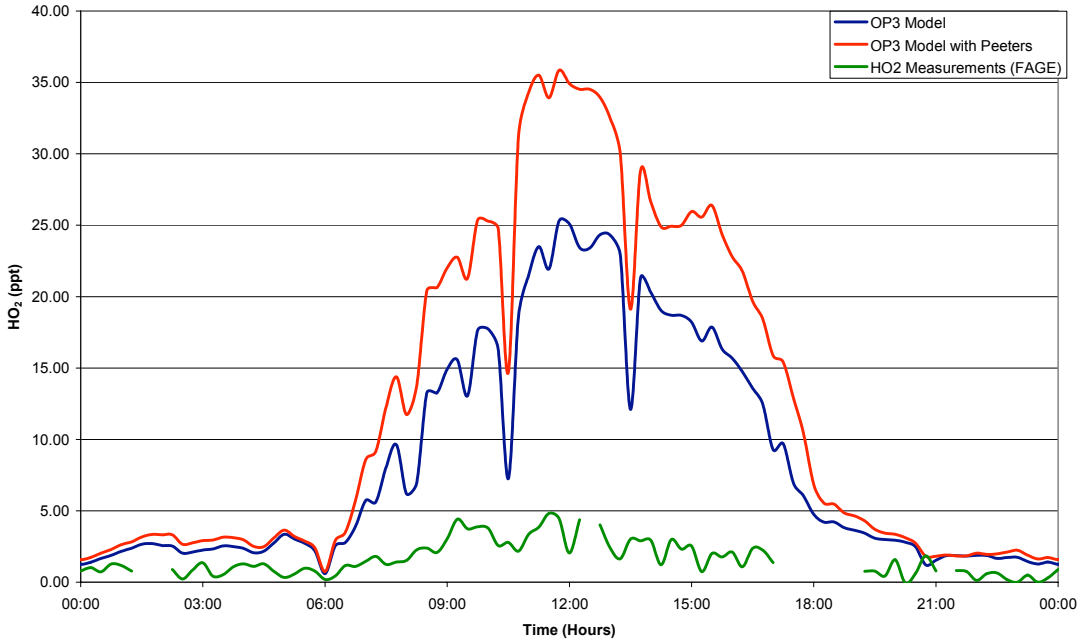

Figure 4.2.55 Model-measurement comparison of [HO_2] for day 198 (17th July 2008)

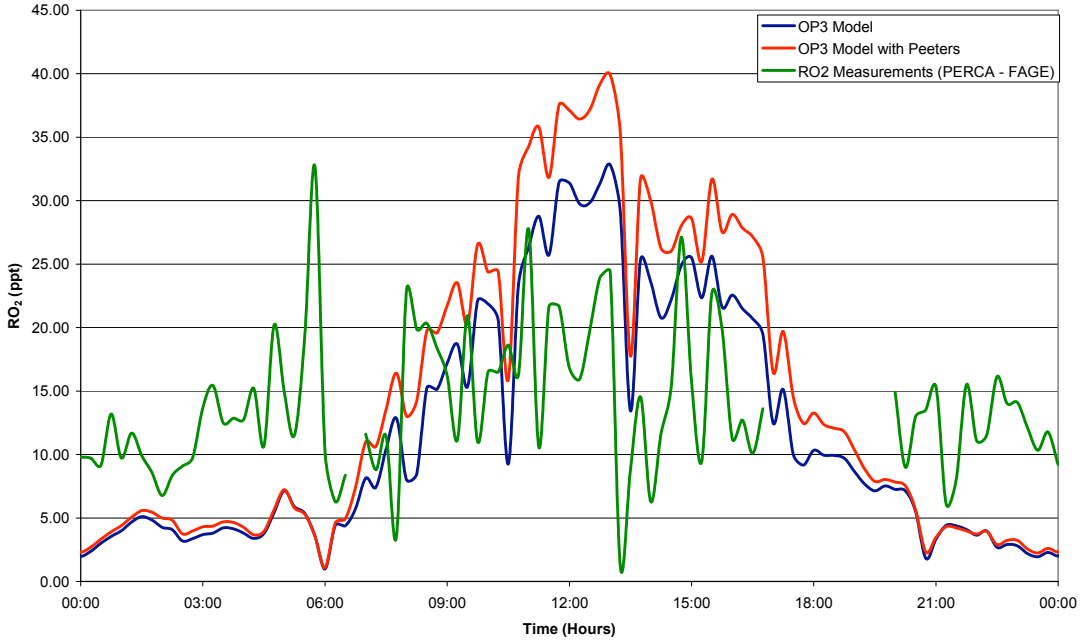

Figure 4.2.56 Model-measurement comparison of [RO_2] for day 198 (17th July 2008)

Table 4.2.7 Average concentrations of OH, HO_2 and RO_2 at Bukit Atur on JDay 198 (17th July 2008) for the whole day, daytime (06:00 – 18:00), nighttime (00:00 – 06:00 and 18:00 – 24:00) and midday (11:00 -15:00).

		OH (Molecules cm^{-3})	HO_2 (ppt)	RO_2 (ppt)
OP3	Daily Average	8.5×10^5	8.4	11.7
	Daytime Average	1.5×10^6	14.4	18.6
	Nighttime Average	1.8×10^5	2.3	4.6
	Average between 11:00 and 15:00	1.5×10^6	21.4	26.6
OP3 Peeters	Daily Average	1.2×10^6	12.1	14.3
	Daytime Average	2.3×10^6	21.3	23.4
	Nighttime Average	1.8×10^5	2.8	5.1
	Average between 11:00 and 15:00	2.3×10^6	30.3	32.5
Measurements	Daily Average	1.5×10^6	1.4	11.9
	Daytime Average	2.2×10^6	2.1	13.2
	Nighttime Average	8.3×10^5	0.6	10.4
	Average between 11:00 and 15:00	2.8×10^6	2.8	16.6

The highest observed value of OH (figure 4.2.54) seen on day 198 was recorded at 15:00 and not closer to midday as would often be expected, due to the lower levels of sunlight from the cloud cover. At this point neither of the models predicts a peak in OH concentration. The largest predicted peak in OH occurs at 10:30 where there is a very large peak in NO. At this point the HO_2 predicted concentrations observe a decline (figure 4.2.55). This indicates that in the model at this point the HO_2 is reacting with the large levels of NO, reducing the predicted values of HO_2 and generating OH.

During the nighttime (18:00 to 24:00) both models over predict the concentrations of HO_2 and under predict the concentration of OH. One fluctuation that the model does predict is between at 21:00 when there was a sudden increase in the NO, at the same point there is an observed peak in the OH measurements and predictions. The increase in the NO allows more reaction with the HO_2 to form more OH. Even though the models both predict the peak in OH at 20:15, they both predict only half the observed concentration, with the OP3 Peeters model predicting slightly more than the OP3 model. At the same point in the model the HO_2 predictions increase, whereas the HO_2 observations decrease.

4.2.8 Day 199 (18th July 2008)

The air mass trajectory arriving at the Bukit Atur field site was predicted using the NOAA Hysplit model (fig 4.2.56). The NOAA model shows that the air mass arises to the South East of the field site over sea. The majority of the time the air mass is travelling to the field site is spent over sea, before it travels over the forest to the south east of the field site for the final 6 hours. The air mass that reaches the field site on this day also passes over Sulawesi (Indonesia) and slows down after doing this.

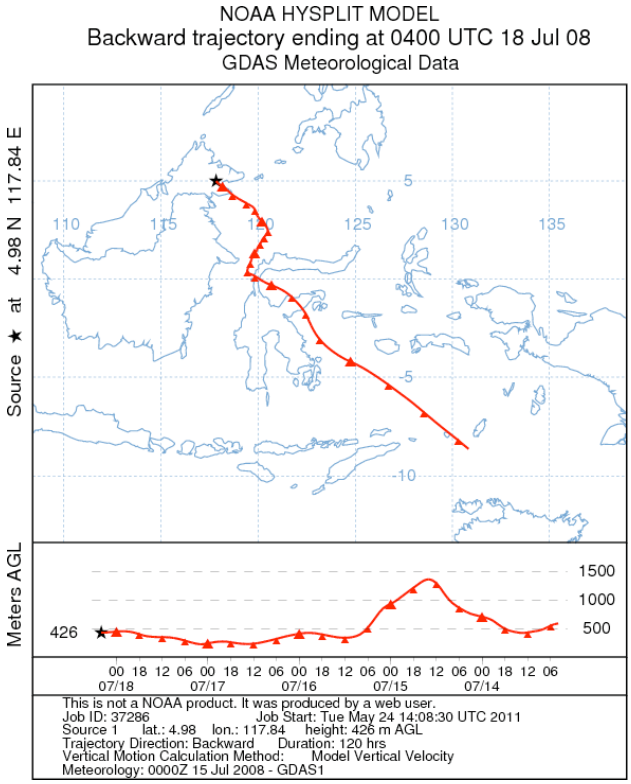

Figure 4.2.57 Air mass trajectory for 5 day arriving at the field site at 1200 hours (local time) on 18th July (JDay 199) The upper plot shows the path taken by the airmass travelling to the field site, for the 5 days previous to measurements being taken. The lower plot shows the altitude of the airmass for the 5 day period before arriving at the field site.

There is no uniform diurnal variation in the NO and NO_2 concentrations, which remain steady except for some peaks that can be attributed to along the logging road near to the field site. The larger peaks coincide with when vehicles were driven to the top of Bukit Atur and brought close to the observation point.

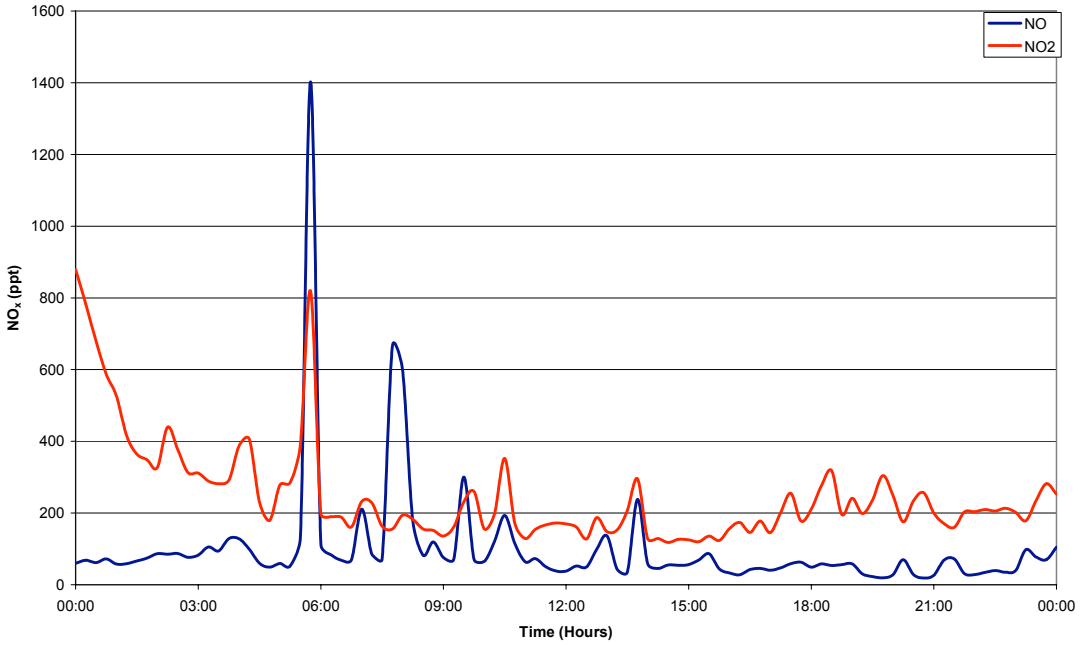

Figure 4.2.58 NO and NO_2 concentrations recorded at Bukit Atur on JDay 199 (18^{th} July 2008)

Figures 4.2.59 and 4.2.60 indicates that the observed monoterpenes are generated locally at the site.

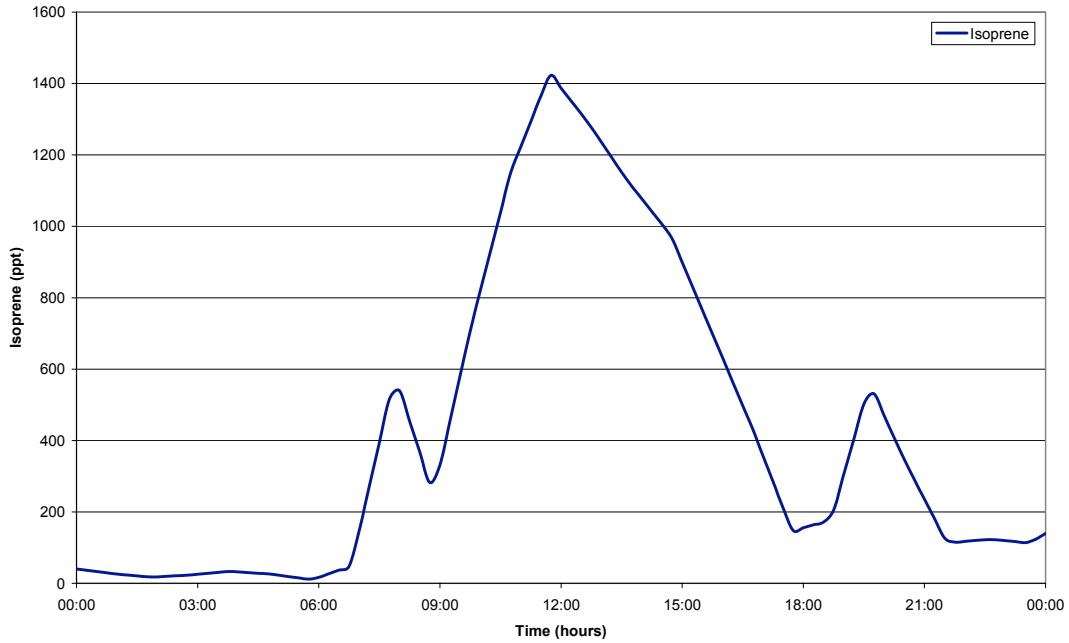

Figure 4.2.59 Isoprene concentrations recorded at Bukit Atur on JDay 199 (18^{th} July 2008)

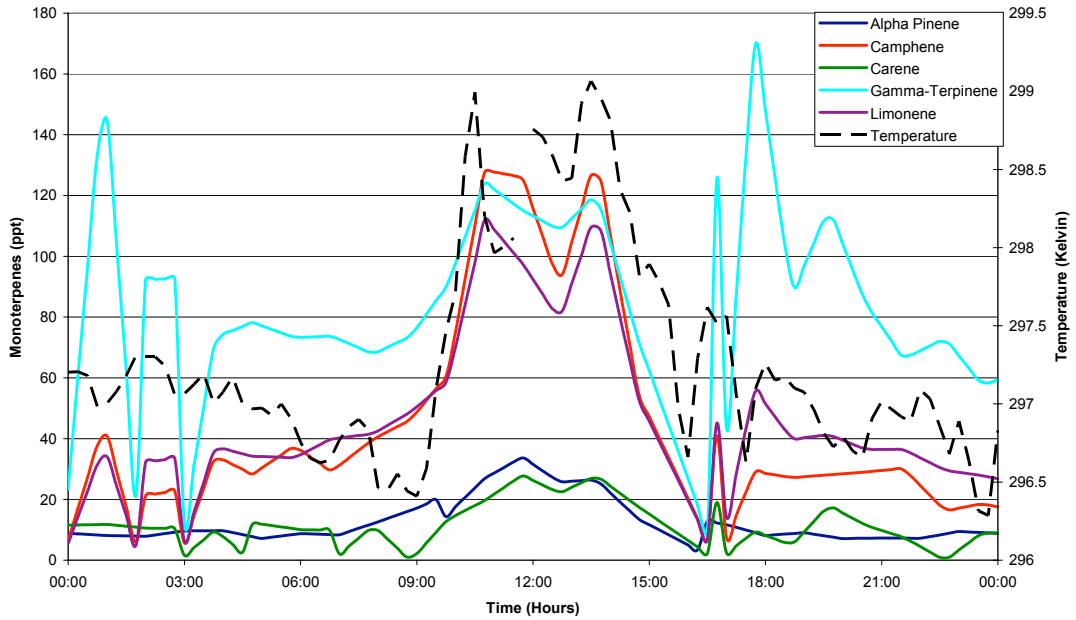

Figure 4.2.60 Monoterpene concentrations recorded at Bukit Atur on JDay 199 (18th July 2008)

The recorded value of j($O(^1D)$) at noon is 3.1 x 10^{-5} s^{-1} compared to the theoretical maximum value at this 4.0 x 10^{-5} and 3.6 x 10^{-5} respectively for day 199 (chapter 3.4). The site was affected by slight cloudiness and no rain was recorded on this day also no rain was recoded on this day.

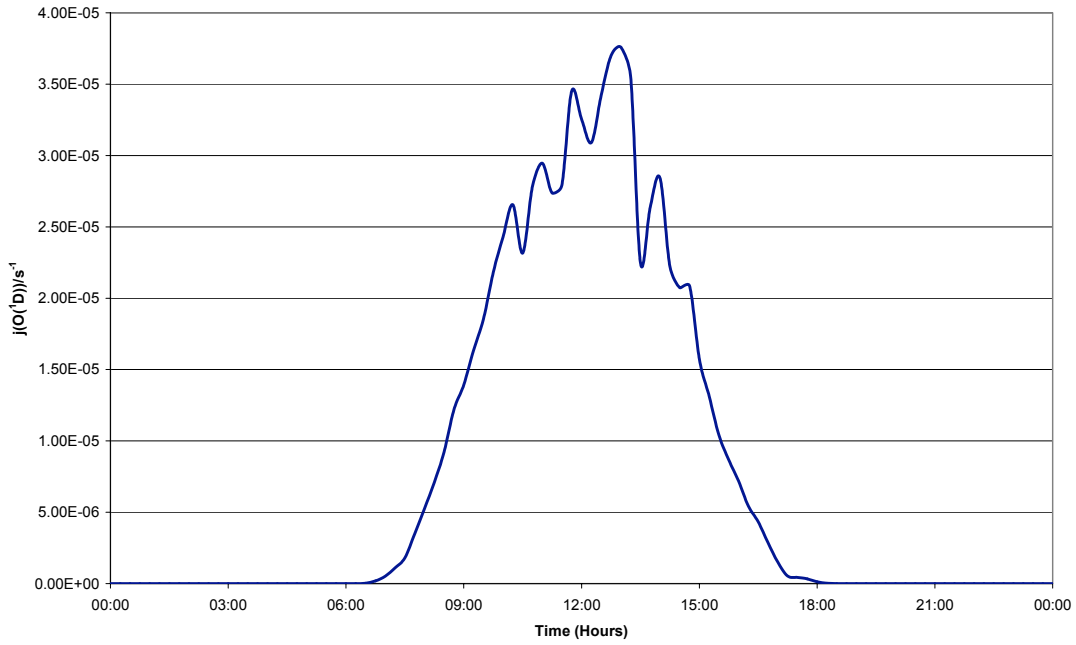

Figure 4.2.61 J(O^1D) observations recorded at Bukit Atur on JDay 199 (18th July 2008)

The results predicted by the OP3 model and the OP3 model containing the proposed Peeters scheme (OP3 Peeters) are displayed in figures 4.2.62, 4.2.63 and 4.2.64 along with the measured concentrations.

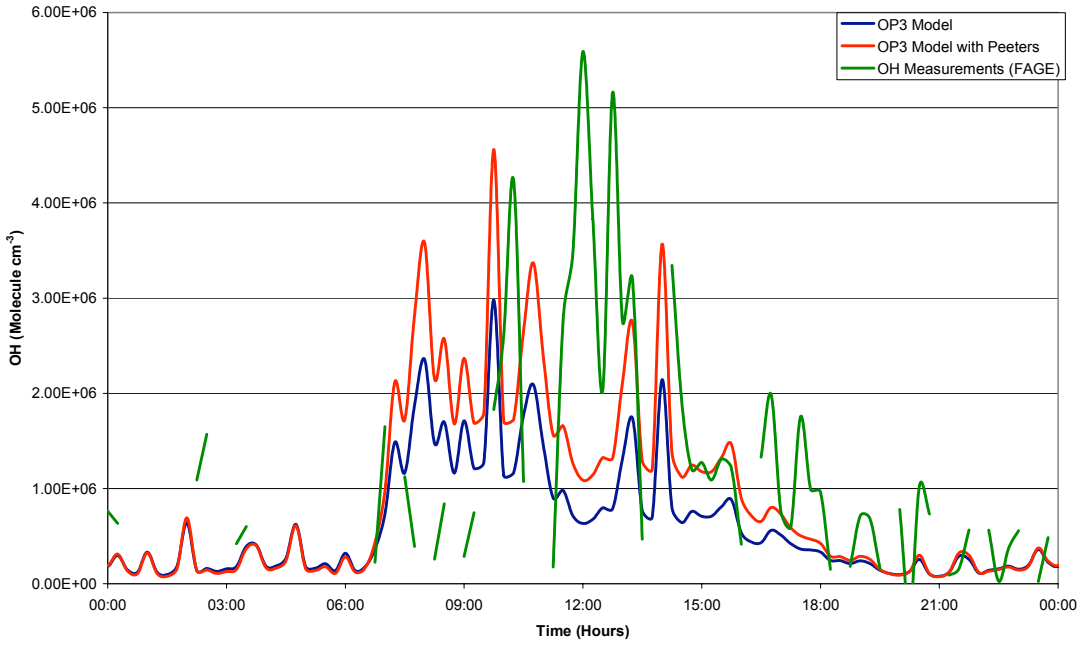

Figure 4.2.62 Model-measurement comparison of [OH] for day 199 (18th July 2008)

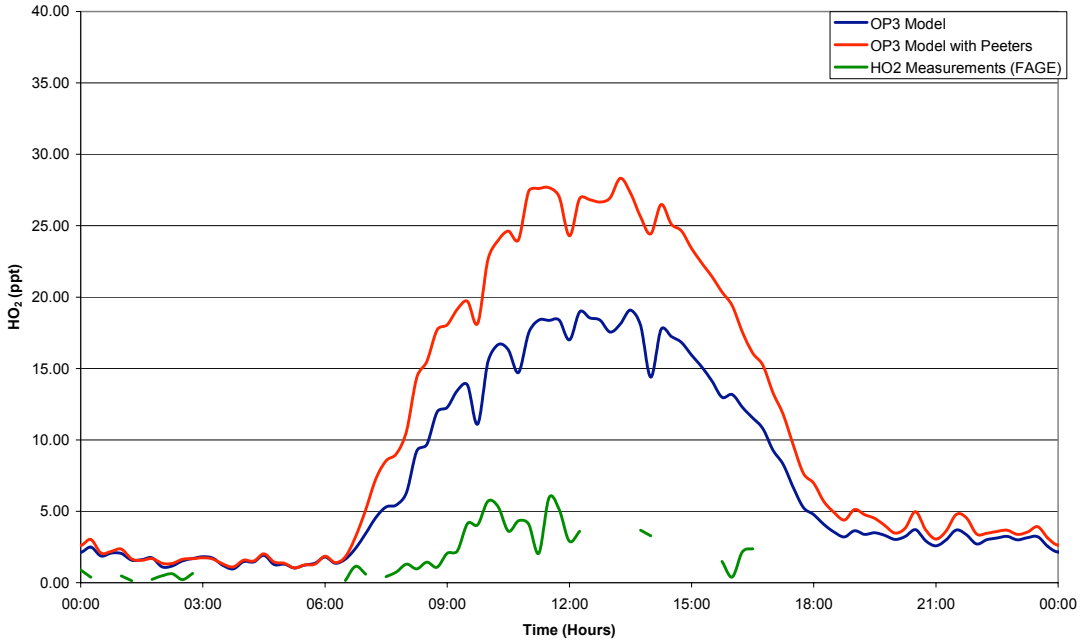

Figure 4.2.63 Model-measurement comparison of [HO_2] for day 199 (18th July 2008)

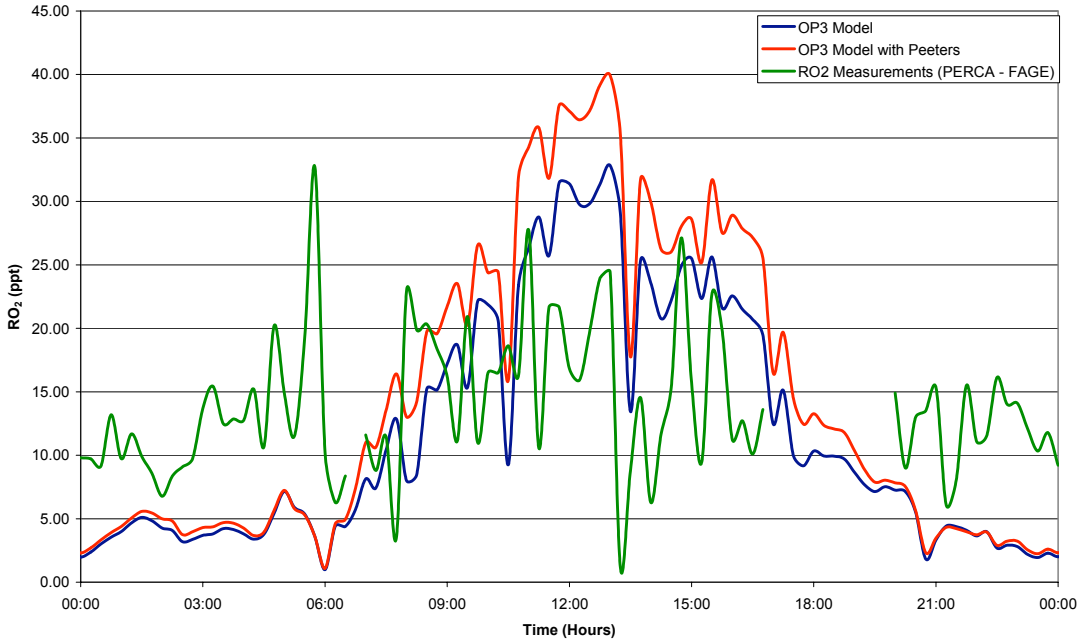

Figure 4.2.64 Model-measurement comparison of [RO_2] for day 199 (18th July 2008)

Table 4.2.8 Average concentrations of OH, HO_2 and RO_2 at Bukit Atur on JDay 199 (18th July 2008) for the whole day, daytime (06:00 – 18:00), nighttime (00:00 – 06:00 and 18:00 – 24:00) and midday (11:00 -15:00).

		OH (Molecules cm^{-3})	HO_2 (ppt)	RO_2 (ppt)
OP3	Daily Average	6.1×10^5	7.3	11.1
	Daytime Average	1.0×10^6	12.2	17.2
	Nighttime Average	2.1×10^5	2.4	4.9
	Average between 11:00 and 15:00	9.7×10^5	17.6	25.6
OP3 Peeters	Daily Average	8.8×10^5	10.6	13.6
	Daytime Average	1.5×10^6	18.2	21.8
	Nighttime Average	2.1×10^5	2.9	5.3
	Average between 11:00 and 15:00	1.6×10^6	26.2	32.1
Measurements	Daily Average	1.2×10^6	1.9	21.5
	Daytime Average	1.7×10^6	2.5	25.5
	Nighttime Average	5.4×10^5	0.4	17.4
	Average between 11:00 and 15:00	2.6×10^6	3.8	28.2

On JDay 199 the highest values from both models for the concentration of OH is predicted at 9:45, where as the highest observed value is seen at 12:00. The models both over predict the values of OH from sunrise (06:00) until 11:15, after this point the predicted values decline and the observed values increase. At midday when the expected maximum value of OH is observed there is a decline in the prediction of OH.

The peak in the prediction of OH concentration coincides with a peak in NO and NO_2 concentrations and a decline in the predicted HO_2 concentration. There is a second predicted peak in OH that occurs at 10:45, this also coincides with a decline in HO_2 and peaks in NO and NO_2. During both of the predicted OH peaks there are no peaks in observed OH concentrations, but there is an observed peak in OH that occurs at 10:15 between the two predicted peaks.

When the OH reaches its highest observed value for JDay 199 the predicted values of OH from both models are declining. At this stage there is a decline in the observed NO concentrations. The concentrations for other species being observed shows no fluctuations that would indicate the peak occurring at this point, except the photolysis rates reaching one of the highest values for JDay 199.

At 13:15 and 14:15 there are observed peaks in the concentrations of OH which coincide with predicted peaks being generated by the models. The peak at 13:15 occurs at the same time as a peak in NO and NO_2 and a small decline in HO_2 predicted concentrations.

4.2.9 Summary of individual day data.

Table 4.2.9 contains the data for OH production for two models and the measured data from the FAGE instrument, but also contains data for the concentration of NO, NO_2, VOCs and $J(O^1D)$. The table also contains details of the model to measurement ratio for OH concentration.

The results displayed in the table reflect that the OP3 model containing the Peeters mechanism consistently produced closer values of OH to the measurement than the OP3 model. This can be seen in the model to measured ratios with the OP3 The days where the measured value of OH is at its highest (above 5 x 10^6 molecules cm^{-3}) are JDay 192 and 194, these two days have the lowest ratios of modelled to measured results and two of the lowest concentrations of NO_x.

The days where the measured concentration of OH is lower the model to measured ratio is higher. The ratio is closest to one on the days where the measured concentration is bellow 4x10^6 molecules cm^{-3} and the observed NO_x concentration is higher.

Table 4.2.19 shows that when the measured values of NO_x were at their highest, the difference between the modelled factors of OH was closer to the measured value of OH. This relationship was seen in both the OP3 and OP3 Peeters models, but with the OP3 Peeters values being closer to the measured concentrations of OH.

Table 4.2. 9 Average modelled and measured values between 11:00 and 15:00 during the second phase of the OP3 campaign.

JDay	OH Concentrations (molecule cm^{-3})			NO (ppt)	NO_2 (ppt)	Isoprene (ppt)	$J(O^1D)$ (s^{-1})	VOC (ppbC)	Model / Measured	Model Peeters / Measured	$VOC:NO_x$
	Measured	Model	Model With Peeters								
190	4.0×10^6	9.2×10^5	1.7×10^6	85.4	161.0	1645.5	2.9×10^{-5}	12.0	0.23	0.42	48.6
191	3.1×10^6	1.2×10^6	2.1×10^6	138.6	159.3	1430.2	3.0×10^{-5}	11.0	0.39	0.70	37.1
192	5.5×10^6	5.6×10^5	1.2×10^6	60.2	139.3	2613.9	2.1×10^{-5}	17.3	0.10	0.22	86.5
193	3.3×10^6	1.7×10^6	3.0×10^6	222.9	400.7	1638.3	2.8×10^{-5}	11.2	0.51	0.89	18.0
194	5.1×10^6	1.3×10^6	2.1×10^6	104.9	176.3	1131.0	2.2×10^{-5}	9.6	0.26	0.42	34.0
195	3.3×10^6	2.3×10^6	3.7×10^6	189.0	209.2	1372.9	2.1×10^{-5}	10.4	0.69	1.11	26.2
198	2.9×10^6	1.6×10^6	2.3×10^6	105.6	223.6	914.1	1.6×10^{-5}	7.6	0.54	0.80	23.2
199	2.7×10^6	9.7×10^5	1.6×10^6	69.9	158.9	1195.0	2.9×10^{-5}	9.9	0.37	0.61	43.1

Table 4.2.10 contains values for the HO_2 modelled predictions and the measured values as well as the model to measured comparison ratios. The model to measured ratios show an over prediction for all days in the second phase of the field campaign. The ratios also show that this over prediction is worse on the days when the HO_2 measurements were observed at their lowest concentration. The model to measured ratio recorded its best agreement on day 192 with a value of 3 for the OP3 model and 5.7 for the OP3 Peeters model. The worst agreement was observed on day 198 with values of 7.4 and 10.6 for the OP3 and OP3 Peeters model respectively.

A difference that can be observed between the OH and HO_2 results in tables 4.2.9 and 4.2.10 is that where the OH model to measured ratio is at its worst on day 192, the HO_2 model to measured ratio is at its best. This indicates that there maybe some factor that links the two species that is not present in the model. Results from previous studies such as SOAPEX and NAMBLEX have raised the question of HO_2 to OH recycling mechanisms being present that has not been accounted for.

Table 4.2.10 Average modelled and measured values between 11:00 and 15:00 during the second phase of the OP3 campaign.

Jday	HO_2 Concentrations (ppt)			NO (ppt)	NO_2 (ppt)	Isoprene (ppt)	$J(O^1D)$ (s^{-1})	VOC (ppbC)	Model / Measured	Model Peeters / Measured	$VOC:NO_x$
	Measured	Model	Model With Peeters								
190	4.4	17.5	27.1	85.4	161.0	1645.5	2.9×10^{-5}	12.0	4.0	6.2	48.6
191	5.1	18.7	28.9	138.6	159.3	1430.2	3.0×10^{-5}	11.0	3.7	5.7	37.1
192	5.4	16.4	29.4	60.2	139.3	2613.9	2.1×10^{-5}	17.3	3.0	5.4	86.5
193	5.4	20.8	32.7	222.9	400.7	1638.3	2.8×10^{-5}	11.2	3.8	6.0	18.0
194	4.4	21.7	32.6	104.9	176.3	1131.0	2.2×10^{-5}	9.6	5.0	7.5	34.0
195	5.4	22.9	35.2	189.0	209.2	1372.9	2.1×10^{-5}	10.4	4.2	6.5	26.2
198	2.9	21.4	30.3	105.6	223.6	914.1	1.6×10^{-5}	7.6	7.4	10.5	23.2
199	3.8	17.7	26.3	69.9	158.9	1195.0	2.9×10^{-5}	9.9	4.6	6.8	43.1

Table 4.2.11 contains the measured and modelled results for the RO_2 concentrations during the eight days that were analysed in the second phase of the field campaign. Unlike OH and HO_2 where one version of the model consistently had the better model to measured ratio, the RO_2 model to measured ratio varies between the OP3 model and OP3 Peeters model. Out of the eight days analysed the OP3 model had values closest to 1 five times and the OP3 Peeters model three times.

The day that observed the worst model to measure agreement for RO_2 in both models was also the day the worst observed HO_2 model to measured agreement was recorded (day 198). The days where the RO_2 model to measured ratio showed good agreement for both models was the days where the HO_2 model to measured ratio was also recorded at its best agreement (days 192 and 193).

Table 4.2.11 Average modelled and measured values between 11:00 and 15:00 during the second phase of the OP3 campaign.

Jday	RO_2 Concentrations (ppt)			NO (ppt)	NO_2 (ppt)	Isoprene (ppt)	$J(O^1D)$ (s^{-1})	VOC (ppbC)	Model / Measured	Model Peeters / Measured	VOC:NO_x
	Measured	Model	Model With Peeters								
190	28.6	27.8	33.5	85.4	161.0	1645.5	2.9×10^{-5}	12.0	1.0	1.2	48.6
191	35.9	27.2	34.2	138.6	159.3	1430.2	3.0×10^{-5}	11.0	0.8	1.0	37.1
192	25.6	23.7	32.9	60.2	139.3	2613.9	2.1×10^{-5}	17.3	0.9	1.3	86.5
193	29.0	27.2	36.1	222.9	400.7	1638.3	2.8×10^{-5}	11.2	0.9	1.2	18.0
194	34.2	27.3	35.1	104.9	176.3	1131.0	2.2×10^{-5}	9.6	0.8	1.0	34.0
195	29.0	28.2	36.4	189.0	209.2	1372.9	2.1×10^{-5}	10.4	1.0	1.3	26.2
198	16.7	26.6	32.5	105.6	223.6	914.1	1.6×10^{-5}	7.6	1.6	2.0	23.2
199	28.2	25.6	32.1	69.9	158.9	1195.0	2.9×10^{-5}	9.9	0.9	1.1	43.1

The results in tables 4.2.9 to 4.2.11 indicate that the discrepancies of the values generated by the models are not a uniform under or over prediction. The differences in what are considered key factors of the input data and the interactions of the species have important effects on the output of the radical species from the model.

As VOC and NO_x concentrations and the ratio of these species to each other can affect the OH concentration (Sillman., 1995), the modelled to measured OH concentration was plotted against the VOC:NO_x ratio for each day and for both models (figures 42.65 and 4.2.66 for OP3 Peeters model and OP3 model respectively).

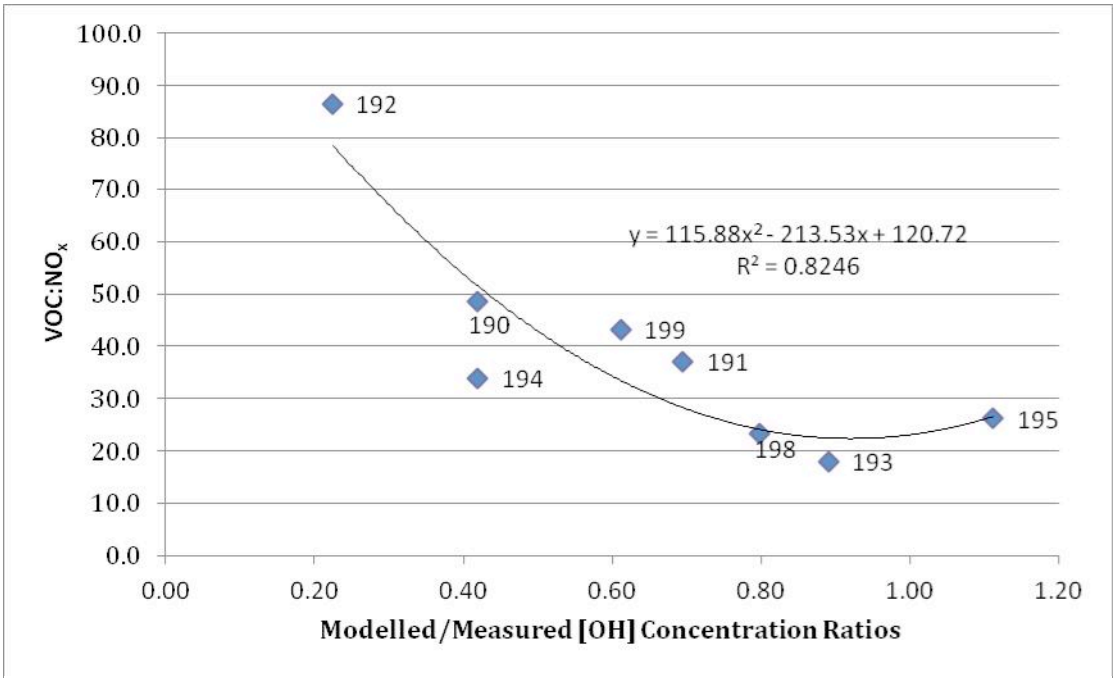

Figure 4.2.65 Average modelled (OP3 Peeters) to measured ratios of OH from 11:00 to 15:00 plotted against the ratio of VOCs (ppbC) to total NO_x during the second phase of the field campaign at Bukit Atur. The individual days are identified by data labels.

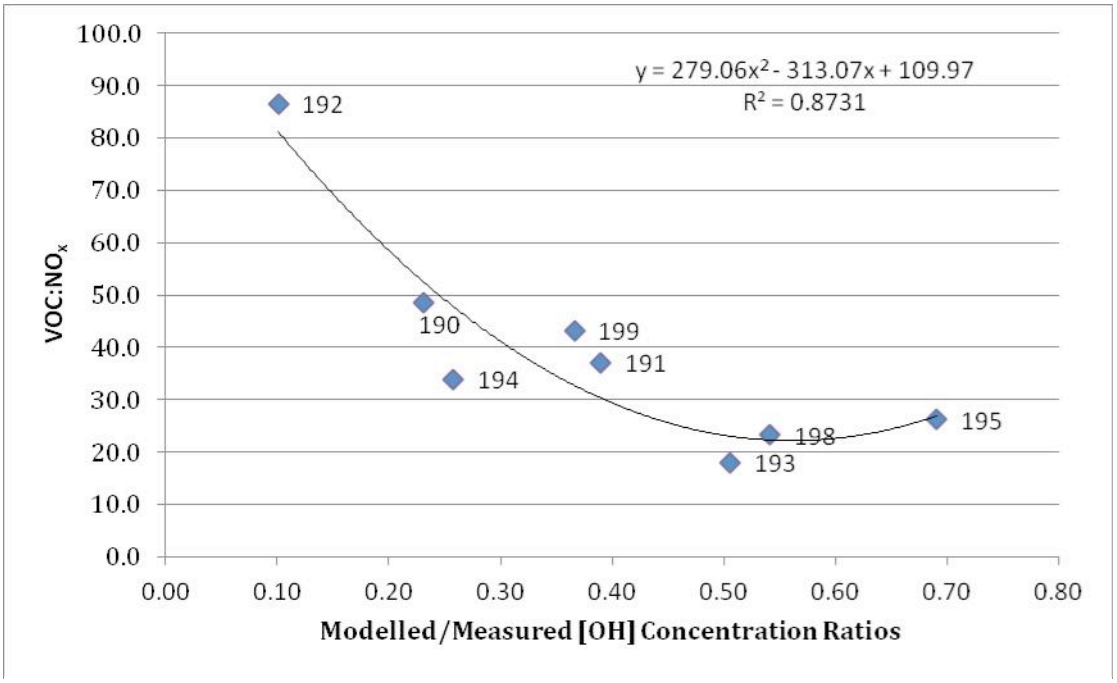

Figure 4.2.66 Average modelled (OP3) to measured ratios of OH from 11:00 to 15:00 plotted against the ratio of VOCs (ppbC) to total NO_x during the second phase of the field campaign at Bukit Atur. The individual days are identified by data labels.

In general, there is better agreement between model and measurement when the VOC:NO_x ratio is lower (figures 4.2.66 and 4.2.67). This relationship is observed in comparisons of both the OP3 model and OP3 model containing the Peeters Scheme. However, it is more noticeable in the OP3 Peeters model results. This indicates two potential factors that are at work in the model; the first being that NO_x chemistry plays an important part in controlling OH concentrations, the second being that the model can replicate the chemistry of the atmosphere in the area better when it is less complicated.

Figure 4.2.67 shows the relationship between VOC:NO_x and the model to measured ratio for each 15 minute data point. When the model predictions and measurements are compared in more detail instead of a daily average the relationship is less clear. However, when the VOC to NO_x ratio is highest, values the level of under prediction in the model is worse. Table 4.2.11 shows the worst daily average model to measurement comparison is observed on day 192 where the VOC concentrations in ppbC were highest and the value of NO_x was one of the lowest recorded for the campaign. Many of the highest values of VOC:NO_x and lowest model/measured

values were recorded on day 192, 190 and 194. However, figure 4.2.68 also indicates that for these days when the values of VOC:NO_x become lower, the model/measured value moves close to 1 indicating better model to measurement agreement.

The next worst days after 192 for model to measured ratios, were days 190 and 194 (table 4.2.9). These days both have similar values for their model to measured ratio and both have high values of VOC to NO_x ratios. This is in contrast to Days 193, 195 and 198 that have the three model to measured ratios closest to 1 and the lowest VOC:NO_x values.

The results of the comparison for the model to measured values for the OP3 model without the proposed Peeters mechanism (figure 4.2.68) shows similar behaviour to the OP3 Peeters model. The poorer degree of OH replication through the models where the VOC:NO_x is high, further indicates that the models may perform better in less complicated systems. Previous work has show that similar models behave well in very clean conditions (NAMBLEX (Sommariva etal., 2006), SOAPEX (Sommariva et al., 2004)), also very polluted conditions when NO_x dominates radical chemistry (PUMA(Emmerson et al., 2005), TORCH (Emmerson et al., 2007)). However, at intermediate regions such as OP3 with moderate NO_x and relatively high VOC the chemistry appears more complex and less well represented in the models.

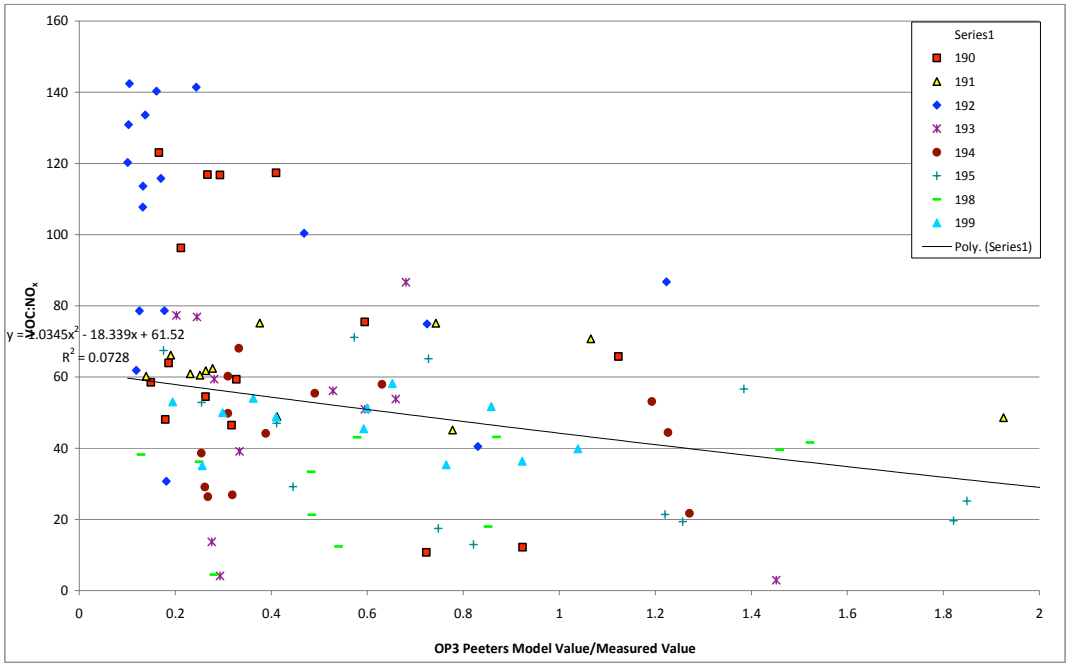

Figure 4.2.67 Modelled (Peeters) to measured ratios of OH from 11:00 to 15:00 plotted against the ratio of VOCs to total NO_x during the second phase of the field campaign at Bukit Atur.

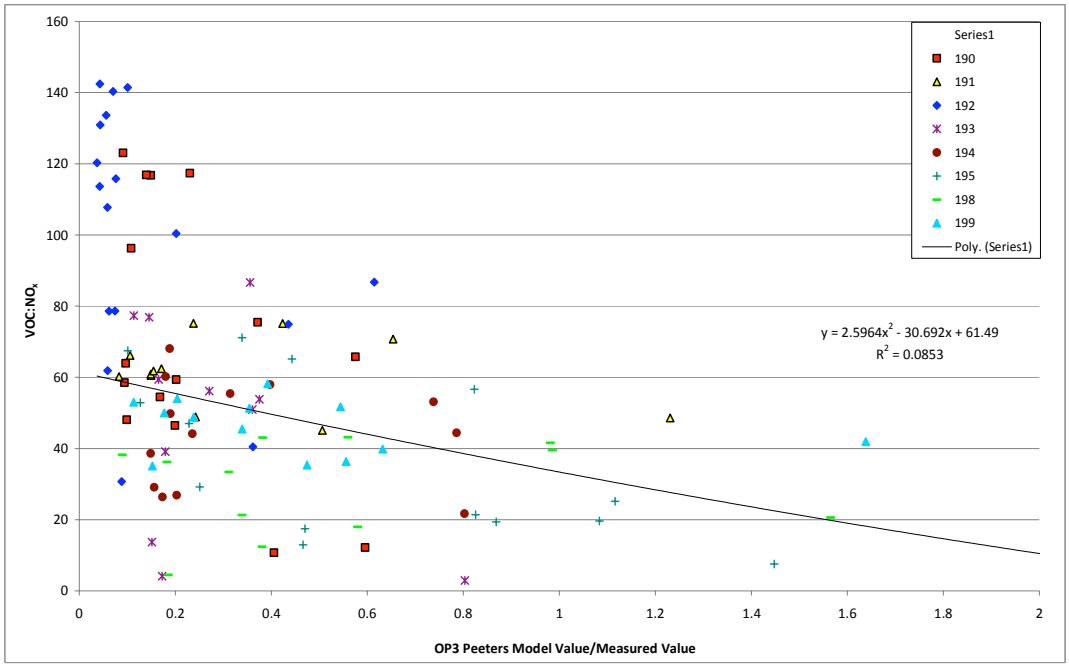

Figure 4.2.68 Modelled (without Peeters) to measured ratios of OH from 11:00 to 15:00 plotted against the ratio of VOCs to total NO_x during the second phase of the field campaign at Bukit Atur.

In such a complex system, the chemical scheme in the model is likely to be incomplete; there were likely many more organic species emitted by vegetation at the site and present in the atmosphere that could not be sampled or detected (Jones et al., 2011). If these undetected VOCs behave like other species included in the model it is likely that they would have had a large effect on days when the measured VOC are higher: the highest VOC concentrations were recorded on day 192 when model:measured [OH] was only 0.22.

A final test was carried out to further explore the impact of NO_x concentrations of the $[HO_2]$:[OH] ratio (figure 4.2.69). Such a test has been shown previously to demonstrate that modelled and measured ratios exhibit different behaviour with respect to NO_x concentrations (Emmerson et al., 2007). The general trend for both models is that the ratio of $[HO_2]$:[OH] concentrations is higher when the concentration of NO is lower. This is because as the [NO] increases, more HO_2 is converted to OH, so $[HO_2]$:[OH] decreases. However, the measured ratio shows a much lower dependence on NO_x concentrations.

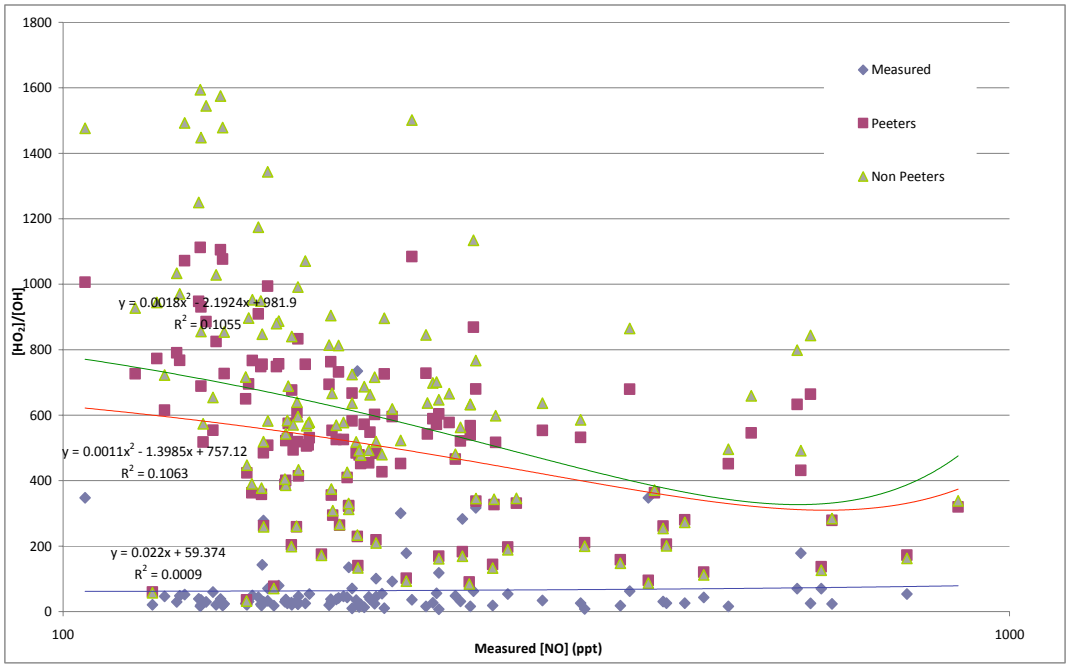

Figure 4.2.69 Modeled and measured values of HO_2/OH plotted against the concentration of measured NO during the second phase of the field campaign at Bukit Atur.

Other projects in the past have investigated the relationship between [HO_2]:[OH] and [NO] (TORCH, PUMA, BERLIOZ). These projects all found the HO_2 to OH ratio decreased as NO concentrations increased. The higher concentrations of NO along with higher concentrations of HO_2 leads to reactions between these species causing OH regeneration, this in return gives a higher concentration of OH and a lower HO_2 to OH ratio at higher NO concentrations (Emmerson et al., 2007; Ren et al., 2003; Stevens et al., 1997). However, in these previous campaigns there was an observed relationship between measured [HO_2]:[OH] with [NO_x] which is not present here. This indicates that in the OP3 model the NO_x chemistry has too great an influence on the model. Ren et al. (2005) concluded that [HO_2]:[OH] as a function of [NO] was not well captured by their model which was the same conclusion as Emmerson et al. (2007) found. Neither study could find an obviously apparent reason for this discrepancy, but sited that further study into the issue was required. The lack of relationship found in the OP3 models between measured and modelled [HO_2]:[OH] with respect to [NO] supports the idea for further study into the problem.

4.3.1 Rate of Production Analysis (ROPA)

The rate of production analysis (ROPA) for the second phase of the field campaign was conducted for the average day data for the second phase of the field campaign. The ROPA was used to study the rate at which the OH, HO_2 and RO_2 radicals were being formed, terminated and undergoing reactions to form other radical species (table 4.3.1 and 4.3.2).

Table 4.3.1. A summary of the rate of production analysis for radicals being predicted by the OP3 Peeters Model during the second phase of the campaign at Bukit Atur, July 2007 between 11:00 and 15:00 hours.

	190 Peeters	191 Peeters	192 Peeters	193 Peeters	194 Peeters	195 Peeters	198 Peeters	199 Peeters
OH Initiation s^{-1}	59.8	57.5	61.8	71.2	52.2	72.4	45.9	73.3
OH Termination s^{-1}	8.0	14.3	6.4	27.3	11.7	25.6	13.8	18.6
HO_2 Initiation s^{-1}	106.3	124.1	109.5	200.8	150.1	196.5	162.4	186.6
HO_2 Termination s^{-1}	172.0	158.7	161.0	236.6	189.5	236.3	182.3	237.0
RO_2 Initiation s^{-1}	40.1	37.8	45.9	55.7	43.2	55.6	45.6	54.9
RO_2 Termination s^{-1}	68.9	71.4	64.4	101.6	78.8	102.0	77.2	100.0
OH-HO_2 s^{-1}	35.5	50.5	27.0	103.0	60.9	129.1	65.0	85.0
HO_2-OH s^{-1}	140.6	172.3	107.5	339.8	170.2	375.1	173.2	268.0
OH-RO_2 s^{-1}	170.1	135.6	123.4	242.4	129.1	256.7	124.9	209.1
RO_2-HO_2 s^{-1}	2.4	1.8	2.1	2.5	2.1	2.4	1.5	2.2
Initiation s^{-1}	360.8	340.9	334.2	500.7	391.9	505.7	377.6	493.4
Termination s^{-1}	366.7	346.7	340.3	514.7	400.1	511.0	385.4	500.2
% Difference	-1.6	-1.7	-1.8	-2.8	-2.1	-1.0	-2.1	-1.4
VOC (ppb)	2.0	1.9	3.2	2.0	1.7	1.8	1.3	1.8
VOC (ppbC)	12.0	11.0	17.3	11.2	9.6	10.4	7.6	9.9
NO_2 (ppb)	0.2	0.2	0.1	0.4	0.2	0.2	0.2	0.2
NO (ppb)	0.1	0.1	0.1	0.2	0.1	0.2	0.1	0.1
NO_x (ppb)	0.3	0.3	0.2	0.6	0.3	0.4	0.3	0.3
O_3 (ppb)	6.2	6.7	4.7	5.4	5.0	7.7	7.9	6.5
$J(O^1D)$ s^{-1}	$2.95x10^5$	$2.95x10^5$	$2.11x10^5$	$2.76x10^5$	$2.16x10^5$	$2.09x10^5$	$1.59x10^5$	$2.85x10^5$

Table 4.3.2. A summary of the rate of production analysis for radicals being predicted by the OP3 Model during the second phase of the campaign at Bukit Atur, July 2007 between 11:00 and 15:00 hours.

	190 OP3	**191 OP3**	**192 OP3**	**193 OP3**	**194 OP3**	**195 OP3**	**198 OP3**	**199 OP3**
OH Initiation s^{-1}	14.4	18.8	10.3	16.6	16.6	18.2	16.6	16.1
OH Termination s^{-1}	4.2	7.0	2.2	20.7	13.0	20.8	17.9	18.2
HO_2 Initiation s^{-1}	61.1	75.8	56.7	163.9	178.2	191.2	178.2	160.4
HO_2 Termination s^{-1}	70.1	74.8	56.7	118.9	122.4	131.6	128.0	120.2
RO_2 Initiation s^{-1}	14.2	22.3	16.8	60.2	68.9	69.8	68.9	61.2
RO_2 Termination s^{-1}	35.2	40.2	29.0	107.0	108.3	122.5	121.7	110.2
OH-HO_2 s^{-1}	10.2	20.0	7.5	67.6	71.8	109.4	71.8	69.4
HO_2-OH s^{-1}	60.2	96.1	53.3	287.7	280.7	372.3	280.7	277.7
OH-RO_2 s^{-1}	70.8	76.8	50.8	185.0	185.8	227.5	186.6	190.1
RO_2-HO_2 s^{-1}	0.3	0.3	0.2	0.8	0.8	0.9	0.9	0.8
Initiation s^{-1}	118.4	153.1	107.1	316.8	349.9	370.3	349.9	333.2
Termination s^{-1}	120.3	156.0	109.5	327.3	315.3	362.3	355.0	340.1
% Difference	-1.6	-1.9	-2.2	-3.3	9.9	2.2	-1.5	-2.1
VOC (ppb)	2.0	1.9	3.2	2.0	1.7	1.8	1.3	1.8
VOC (ppbC)	12.0	11.0	17.3	11.2	9.6	10.4	7.6	9.9
NO_2 (ppb)	0.2	0.2	0.1	0.4	0.2	0.2	0.2	0.2
NO (ppb)	0.1	0.1	0.1	0.2	0.1	0.2	0.1	0.1
NO_x (ppb)	0.3	0.3	0.2	0.6	0.3	0.4	0.3	0.3
O_3 (ppb)	6.2	6.7	4.7	5.4	5.0	7.7	7.9	6.5
$J(O^1D)$ s^{-1}	$2.95x10^5$	$2.95x10^5$	$2.11x10^5$	$2.76x10^5$	$2.16x10^5$	$2.09x10^5$	$1.59x10^5$	$2.85x10^5$

The percentage difference between the total values of initiation and termination are for both models are below 10%. This low percentage difference in both models indicates that the majority of fluxes controlling the predicted concentrations of radicals are included in the mechanisms of both models. The OP3 Peeters model has a smaller percentage difference (table 4.3.1) than the original OP3 model (table 4.3.2), particularly day 194.

One of the largest and most significant differences between the two models is the OH initiation step. OH initiation is more important in the Peeters model, than without the extended scheme. OH initiation also becomes more important than termination in the

Peeters scheme whereas without it, initiation and termination are much more balanced. This difference is reflected in the higher concentration of OH being predicted by the OP3 Peeters model. The increase in the OH formation in the model with the addition of the Peeters scheme was expected due to the OH regeneration chemistry in the Peeters scheme (Peeters et al, 2009).

There are differences in other fluxes concerning the OH radical in the two models: The increase in the OH formation in the model with the addition of the Peeters scheme was expected due to the OH regeneration chemistry in the Peeters scheme (Peeters et al, 2009). The Peeters Scheme also leads to an increased generation of HO_2 on most days, which is reflected in the larger predicted concentrations of HO_2 and the higher rate of initiation of HO_2 in the OP3 Peeters model compare to the OP3 model (table 4.3.1). The rates of propagation of other radical species and form HO_2 are also higher in the OP3 Peeters model, for similar reasons.

The RO_2 fluxes in the ROPA show a difference in the chemistry surrounding the initiation and termination of RO_2 radicals between the OP3 model and the OP3 Peeters Model. The alterations made to the chemistry in the mechanism of the model by adding the Peeters reaction scheme changed the behavior of isoprene in the mechanism leading to the production of different intermediate products from Isoprene oxidation leading to the formation of different RO_2 species (Peeters et al 2009). The initiation is sometimes higher with the Peeters Scheme (190-192) and sometimes higher without it (193-198), but there is still a higher concentration of RO_2 predicted by the OP3 Peeters model compared to the OP3 model. On these latter four days, RO_2 formation rates are higher, as the fluxes from OH-RO_2.

One factor that can cause a difference in between the two models in the rate of production analysis is the changes that were made to the Criegee chemistry by adding the Peeters reaction mechanism. By adding in the new isoprene degradation chemistry with different

The ROPA can be looked at in more detail; figure 4.3.1 displays the details of individual key reactions in the initiation and termination of radical species for day 192 when the agreement between model and measurements was worst, and day 193 when

the measured to modeled ratio was good. Also it contains values comparing the rate of production on day 193 between the OP3 model and the OP3 model with the Peeters scheme.

One area of the chemistry where there is a notable difference is in reactions with NO_x. The two days being analysed have very different concentrations of NO_x, with day 193 having an average NO_x concentration of 0.4 ppb between 11:00 and 15:00 which is 4 times higher than that of day 192. In section 4.2 it was stated that days with higher concentrations of NO_x were observed to have greater model to measurement agreement and in figure 4.3.1 this can be seen where day 193 has much larger reaction rates in the initiation and termination steps of the OH chemistry. The production of OH from reactions of HONO and HNO_3 and the loss of OH from reactions of NO and, NO_2 and HO_2NO_2 are an order of magnitude higher. Such a large difference in the rates between two days is not seen in other reactions in the ROPAs. The large difference between the two days NO_x chemistry occurs when there is a three time increase in the concentration of observed NO_x. This indicates that the mechanism of the model maybe too reliant on the NO_x chemistry.

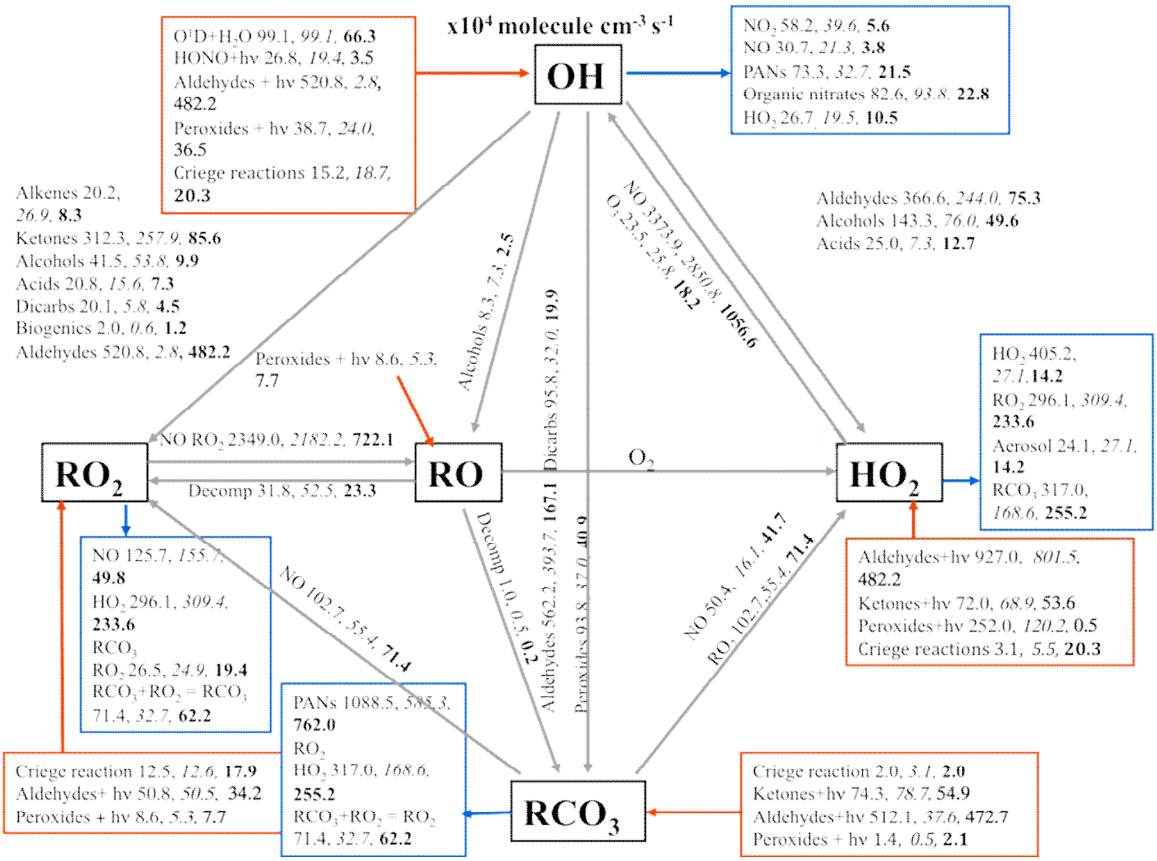

Figure 4.3.1 Rate of production analysis between 11:00 and 15:00 hours for day 193 (Peeters model), *193 (OP3 model),* **192 (Peeters model)**

When the ROPAs for the different models on day 193 are compared, the rates of formation of radicals are greater for the OP3 model containing the Peeters Scheme except for production of radicals through the reaction of the Criegees. This is observed in the initiation of OH, HO_2, RO_2 and RCO_3 production. The mechanistic changes made to the model through the addition of the Peeters scheme reduce the rate of production of radicals through the Criegee reactions. However, the model containing the Peeters scheme predicts a much higher rate of production of RO_2 from the reaction of OH and aldehydes. The rate of production is two orders of magnitude greater from the model containing the Peeters scheme, which agrees with the findings reported by Archibald et al., (2010).

Chapter 5. April Campaign

5.1 Introduction

5.1.1 General Summary

The second phase of the OP3 field campaign was conducted from the 7th April 2008 through to 4th May 2008 (JDay 98 to 125). Typically this is the driest period of the year in the tropical rainforests in Borneo (Hewitt et al., 2009). At this time of year the area is affected by the northeast monsoon and experiences a change to the southeast monsoon (Bidin and Chappell 2006). This period of change the area experiences makes the rainfall at the site more erratic and much harder to predict (Hewitt etl ., 2009).

5.1.2 Data Coverage

In order to replicate the measurements from the field campaign through the use of the OP3 model only day with sufficient data for each constrained variable can be used. The data were analysed and any substantial gaps of 2 hours or more in the measurements that could not be removed through interpolating the surrounding data was noted (table 5.1.1)

Table 5.1.1 Data coverage for the second phase of the field campaign. ✓ indicates species that have a full days worth of cover and x indicates species where a whole days worth of data coverage is not present.

Jday	111	112	113	114	115	116	117	118	119	120	121
Isoprene	✓	✓	✓	✓	✓	✓	✓	✓	✓	✓	✓
Alpha-Pinene	X	X	X	X	X	X	X	X	✓	✓	✓
Limonene	X	X	X	X	X	X	X	X	✓	✓	✓
Camphene	X	X	X	X	X	X	X	X	✓	✓	✓
Carene	X	X	X	X	X	X	X	X	✓	✓	✓
Gamma-Terpinene	X	X	X	X	X	X	X	X	✓	✓	✓
Ethene	X	X	X	X	X	X	X	X	✓	✓	✓
O_3	✓	✓	✓	✓	✓	✓	✓	✓	✓	✓	✓
NO	✓	✓	✓	✓	✓	✓	✓	X	X	✓	X
NO_2	✓	✓	✓	✓	✓	✓	✓	X	X	✓	X
CO	✓	✓	✓	✓	✓	✓	✓	✓	✓	✓	✓
Temperature	✓	✓	✓	✓	✓	✓	✓	✓	✓	✓	✓
H_2O	✓	✓	✓	✓	✓	✓	✓	✓	✓	✓	X
M	✓	✓	✓	✓	✓	✓	✓	✓	✓	✓	✓

From table 5.1.1 it is possible to see that only there was only data available to run one days worth of models for phase 1 of the OP3 campaign due to the lack of VOC data (day 120). In order too attempt to model more of the first phase of the campaign VOC data was required for days 111 t0 118. To provide this data for the model an average daily profile of VOCs was built using the available VOC data from days 119 to 121, obviously leading to considerable uncertainty in model predictions for this campaign.

Another factor affecting data coverage in the first phase of the campaign is the absence of HO2 measured data. As there is no HO_2 to compare the model to, during the first phase of the campaign the measured $RO_2 + HO_2$ from the PERCA instrument is used to compare the sum of the modelled RO_2 and HO_2 concentrations. However, due to the over prediction of HO_2 during phase 2 of the OP3 campaign, the modelled values of HO_2 are normalised by dividing them by the average model to measured ratios (7) for HO_2 observed in phase 2 in order to avoid adding an extra degree of over prediction to the results.

In summation the days selected to be studied and modelled from the first phase of the campaign were days 111 to 117 and 120. Note that only day 120 had a complete data set and that it's own VOC data was used a opposed to the average VOC profile in days 111 to 117.

5.2 Results

5.2.1 Day 111 (11th April 2008)

The air mass trajectory arriving at the Bukit Atur field site was predicted using the NOAA Hysplit model (figure 5.2.1). The NOAA model shows that the air mass arises over the sea to the northeast of the island, as would be expected at this time of year (Hewitt et al., 2009), then moves southwesterly passing over Mindanao (Southern Island of the Philippines). There is a period of over a day between the air mass arriving at Borneo and the field site at Bukit Atur, travelling from a northeast direction.

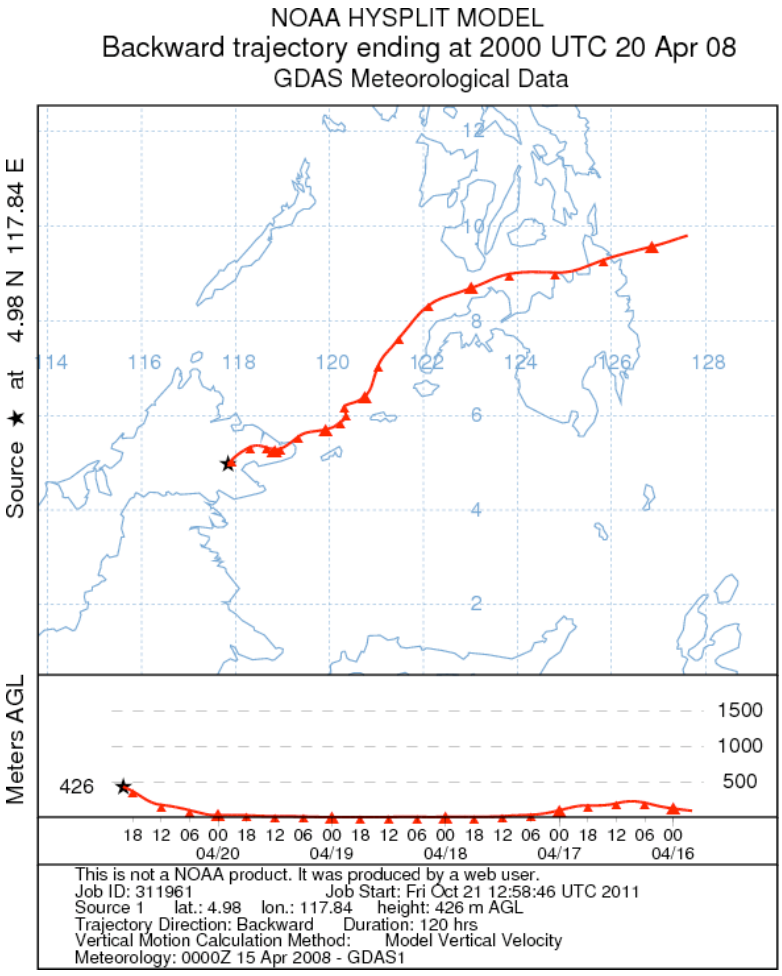

Figure 5.2.1 Air mass back trajectory for 5 day arriving at the field site at 1200 hours (local time) on 11th April (JDay 111) The upper plot shows the path taken by the airmass travelling to the field site, for the 5 days previous to measurements being taken. The lower plot shows the altitude of the airmass for the 5 day period before arriving at the field site.

The air mass moves over few populated areas. There would likely be few anthropogenic organic species contained in the airmass and low concentrations of NO_x and CO would be expected as a consequence. Figure 5.2.2 shows the concentrations of NO and NO_2 as an example. The concentration of NO builds through out the day until 12:00 and then begins to decline. The NO_2 concentrations are highest in the morning and then decline between 08:00 and 11:00, there is another peak 12:00 before the NO_2 cocnetration declines again and then builds up after sunset at 18:00. The larger peaks coincide with when vehicles were driven to the top of Bukit Atur and brought close to the observation point or when logging vehicles were observed on the road at the foot of Bukit Atur. The largest peaks occur when the vehicles were closest to the inlets at the field site.

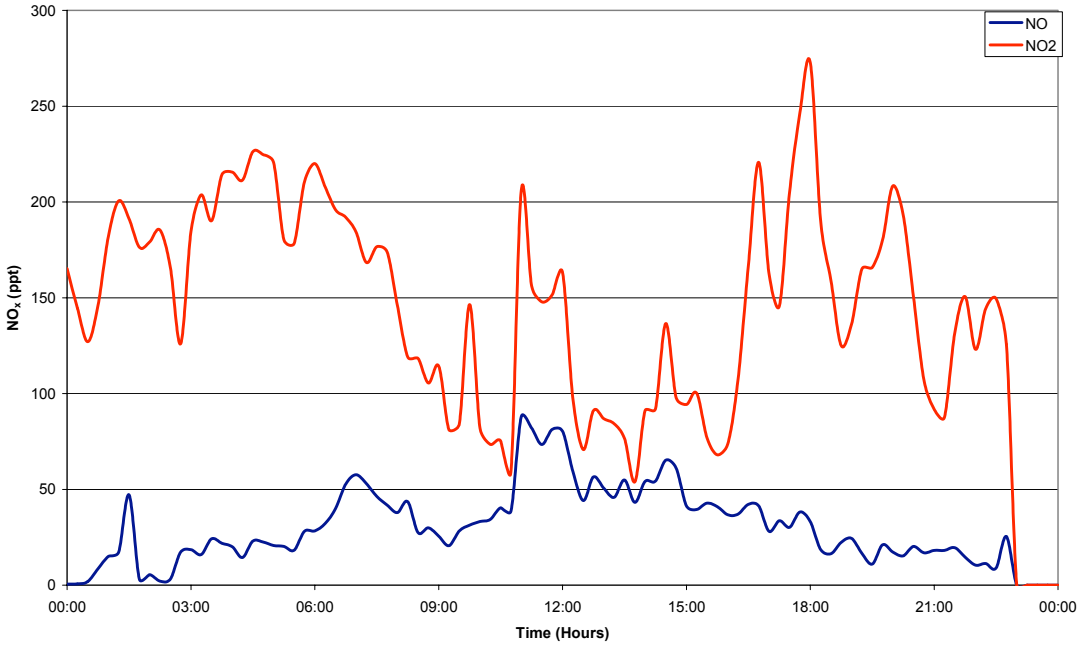

Figure 5.2.2 NO and NO_2 concentrations recorded at Bukit Atur on JDay 111 (11th April 2008)

The air mass moves over the rainforest before arriving at the Bukit Atur field site, but the diurnal variation in the isoprene and monoterpene species shown in figures 5.2.3 indicates that it is generated locally at the site, by sources that are affected by temperature and sunlight levels (Hewitt et al., 2009).

The concentrations of monoterpenes and ethene used in the model for this day were the average values for this period of the campaign, as there were no values available

for this day. The diurnal profile of VOCs used is shown in figure 5.2.4 as well as the temperature profile for the day.

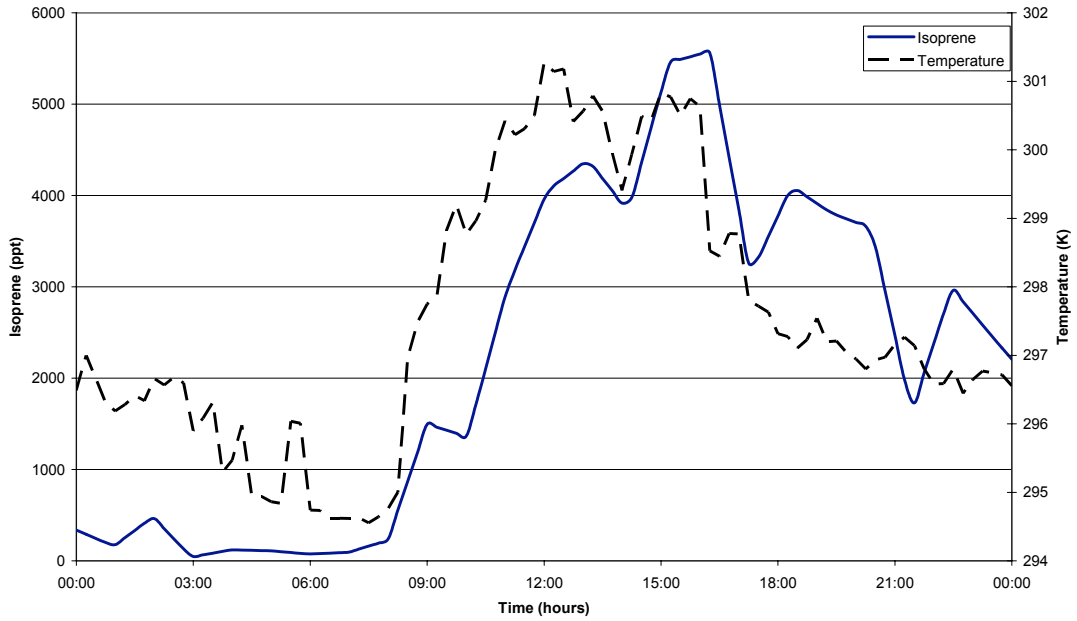

Figure 5.2.3 Isoprene concentrations recorded at Bukit Atur on JDay 111 (11th April 2008)

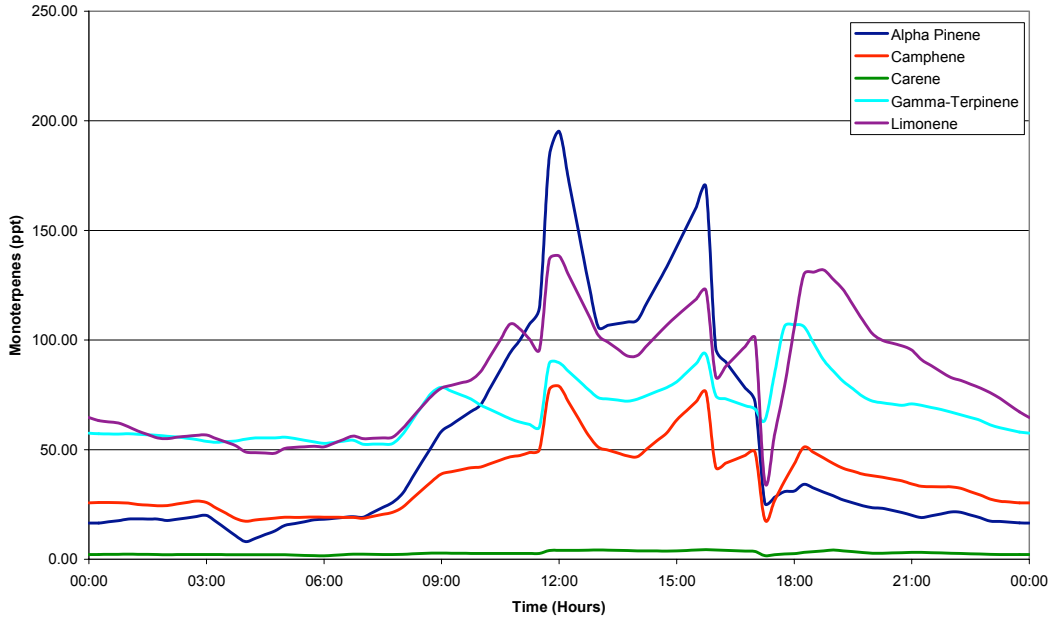

Figure 5.2.4 Average monoterpene concentrations from Bukit Atur used to model JDay 111 (11th April 2008) with the recorded temperatures.

The measurements of j($O(^1D)$), were also recorded at the site on a minute by minute basis (figure 5.2.5). The diurnal plot shows that the value of j($O(^1D)$), increases at 06:00 when the sun rises at the field site. The value continues to rise until approximately 12:00 and then begins to decline until it becomes negligible at 15:00 indicating a period of cloud cover. The diurnal plot is not a smooth curve, but demonstrates there was some degree of cloud cover during the day lowering the intensity of the light reaching the photometer.

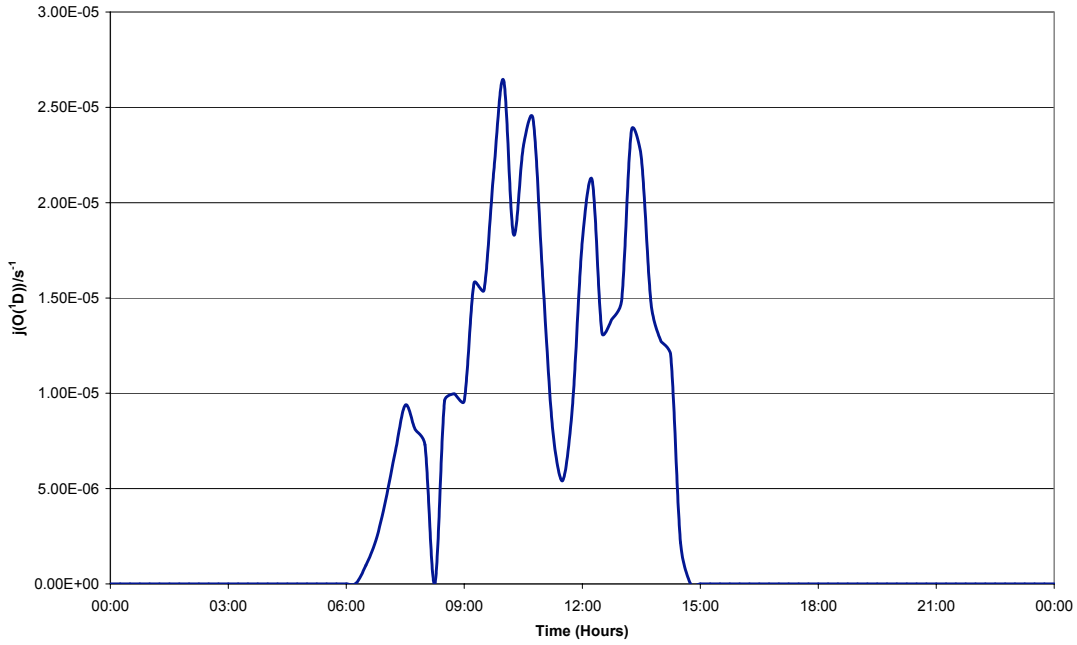

Figure 5.2.5 J(O^1D) observations recorded at Bukit Atur on JDay 111 (11^{th} April 2008)

The results predicted by the OP3 model and the OP3 model containing the proposed Peeters scheme (OP3 Peeters) are displayed in figures 5.2.6 and 5.2.7 along with the measured concentrations for OH and $RO_2 + HO_2$ respectively. The three species all show similar diurnal behaviour with the lowest values being predicted and measured during the nighttime periods and the highest values occurring during the daytime with maximum values tending to occur near solar noon. The OP3 Peeters model predicted higher concentrations than the OP3 model for OH, but lower concentrations for $HO_2 + RO_2$ (Table 5.2.1).

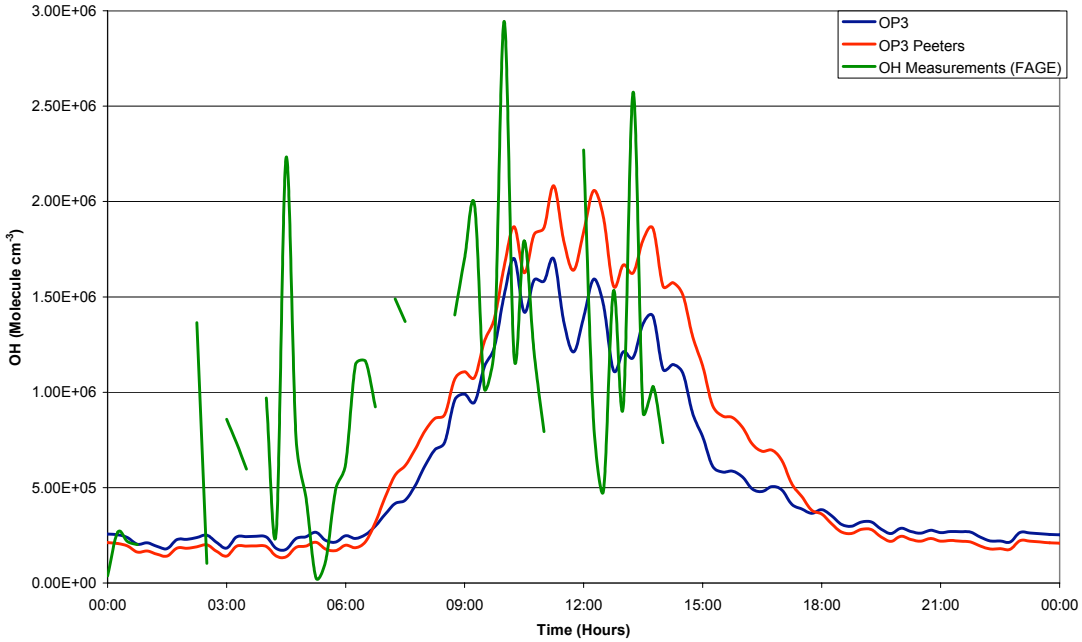

Figure 5.2.6 Model-measurement comparison of [OH] for day 111 (11th July 2008)

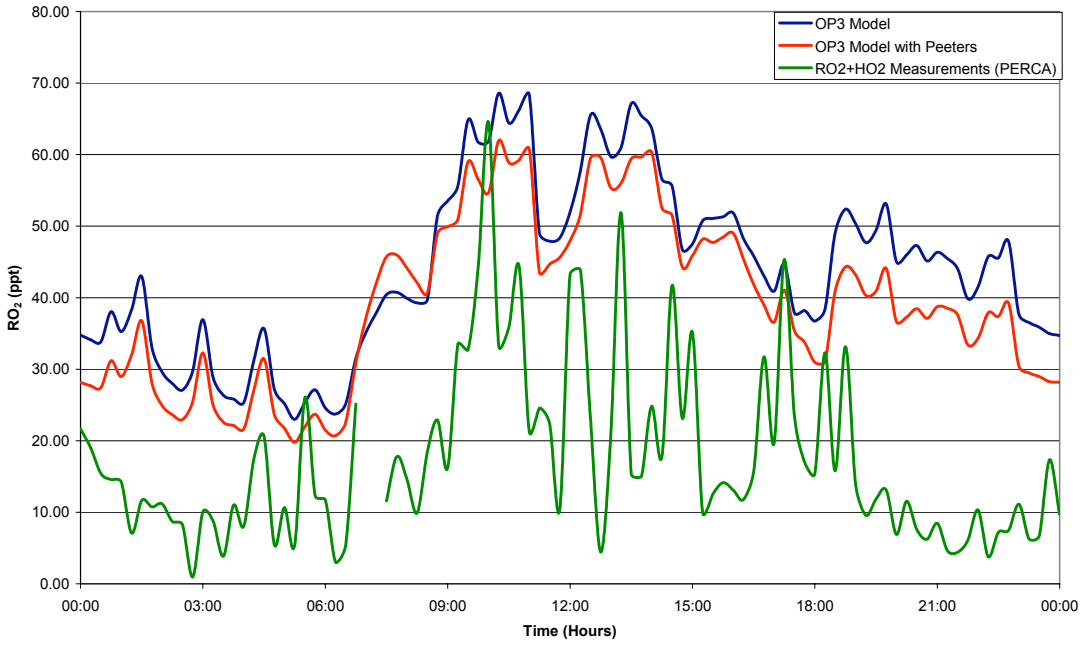

Figure 5.2.7 Model-measurement comparison of [$HO_2 + RO_2$] for day 111 (11th July 2008)

Table 5.2.1 Average concentrations of OH and $RO_2 + HO_2$ at Bukit Atur on JDay 111 (11th July 2008) for the whole day, daytime (06:00 – 18:00), nighttime (00:00 – 06:00 and 18:00 – 24:00) and midday (11:00 -15:00).

		OH (Molecule cm^{-3})	$RO_2 + HO_2$ (ppt)
OP3 Model	Daily Average	$5.7X10^5$	43.8
	Daytime Average	$8.9X10^5$	49.9
	Nighttime Average	$2.5X10^5$	37.3
	Average between 11:00 and 15:00	$1.3X10^6$	57.4
OP3 Peeters	Daily Average	$6.7X10^5$	39.1
	Daytime Average	$1.1X10^6$	46.7
	Nighttime Average	$2.1X10^5$	31.2
	Average between 11:00 and 15:00	$1.7X10^6$	52.8
Measurements	Daily Average	$1.0X10^6$	17.5
	Daytime Average	$1.4X10^6$	23.7
	Nighttime Average	$5.8X10^5$	11.5
	Average between 11:00 and 15:00	$1.3X10^6$	25.8

The results in table 5.2.1 indicates that the OP3 model predicts the concentration of OH very closely to the measured values during the midday period, where the OP3 Peeters predictions are higher than the values observed at this point. However, there is incomplete coverage of the measured OH data on this day, and also lots of large peaks in the measurements that are hard to understand. The gaps in data are due to technical problems, indicating there may be issues with the remaining data.

The measured and modelled comparison of $HO_2 + RO_2$ indicates that there is an over prediction of $HO_2 + RO_2$ from the model during the day.

5.2.2 Day 112 (12th April 2008)

The air mass trajectory arriving at the Bukit Atur field site was predicted using the NOAA Hysplit model (figure 5.2.8). The NOAA model shows that the air mass arises over the sea to the northeast of the island, as would be expected at this time of year (Hewitt et al., 2009), then moves south-westerly passing over no other landmass before reaching Borneo. There is a period of 12 hours between the air mass arriving at Borneo and the field site at Bukit Atur, approaching from the south east of the field site.

.

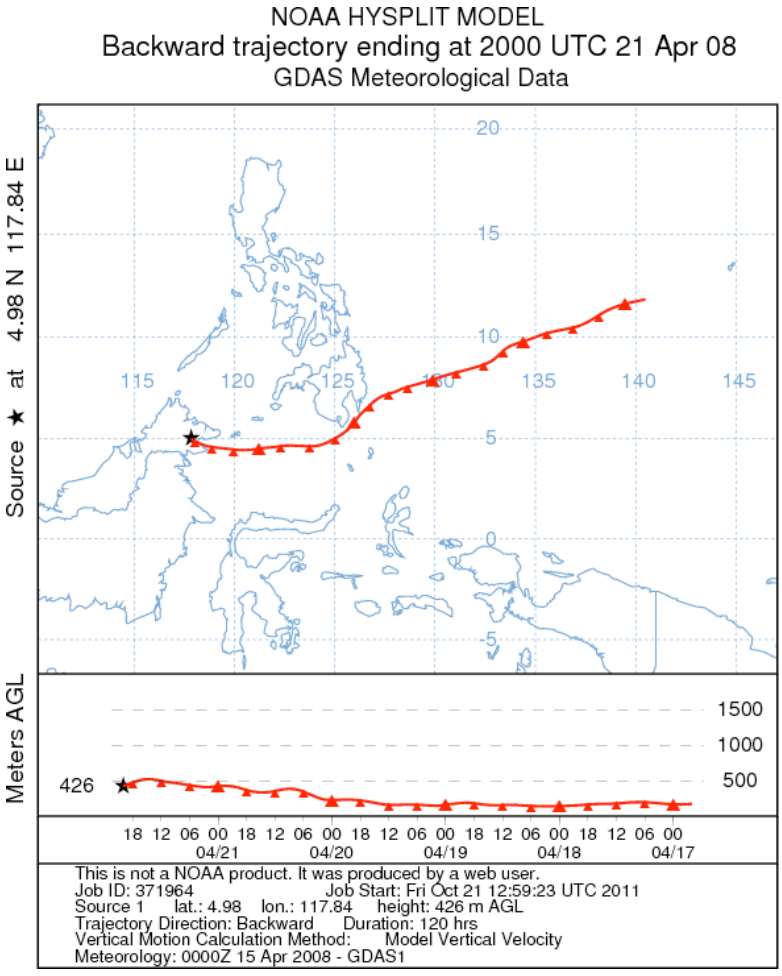

Figure 5.2.8 Air mass back trajectory for 5 day arriving at the field site at 1200 hours (local time) on 12th April (JDay 112) The upper plot shows the path taken by the airmass travelling to the field site, for the 5 days previous to measurements being taken. The lower plot shows the altitude of the airmass for the 5 day period before arriving at the field site.

Figure 5.2.9 shows the concentrations of NO and NO_2 measured at the field site. There is no uniform diurnal variation in the NO and NO_2 concentrations, which remain steady except for some peaks that can be attributed to traffic along the logging road near to the field site. The larger peaks coincide with when vehicles were driven to the top of Bukit Atur and brought close to the observation point or when logging vehicles were observed on the road at the foot of Bukit Atur. The largest peaks occur when the vehicles were closest top the inlets at the field site such as the peaks observed at 10:30, 14:45 and 18:00. The largest peak in the observed values of NO_2 occurs at 18:00, but the coinciding NO peak is much smaller in comparison.

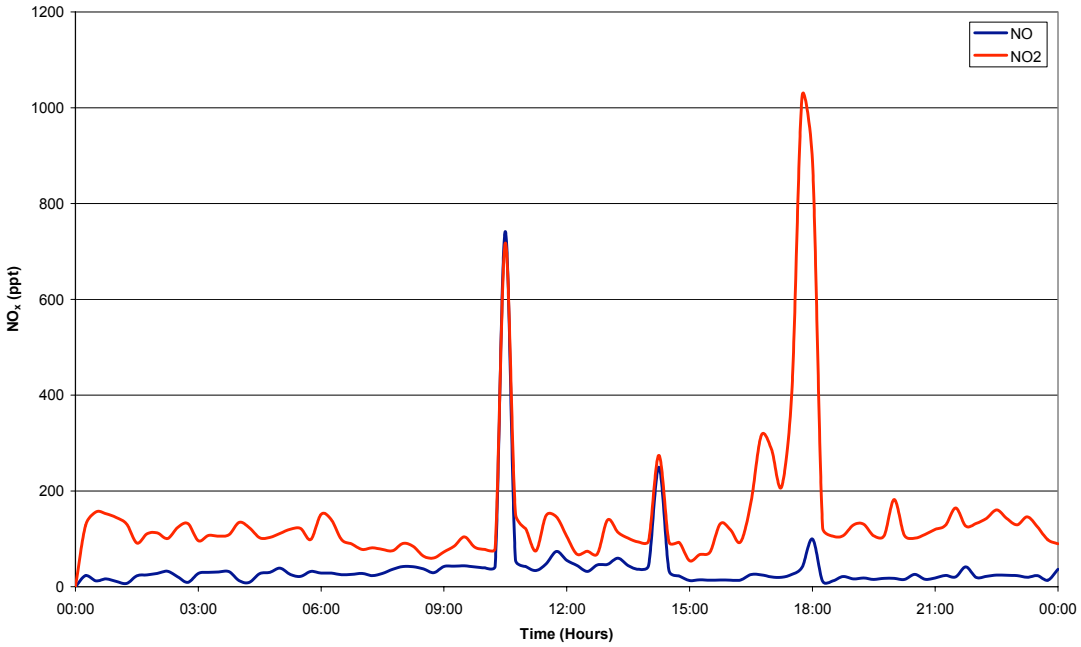

Figure 5.2.9 NO and NO_2 concentrations recorded at Bukit Atur on JDay 112 (12^{th} April2008)

The isoprene component of the air mass is generated locally at the site by sources that are affected by temperature and sunlight levels (Hewitt et al., 2009), as shown in figure 5.2.10 along with the temperature profile for day 112. The monoterpenes used in the model on this day were taken from the average monoterpene profile generated on other days see figure 5.2.4.

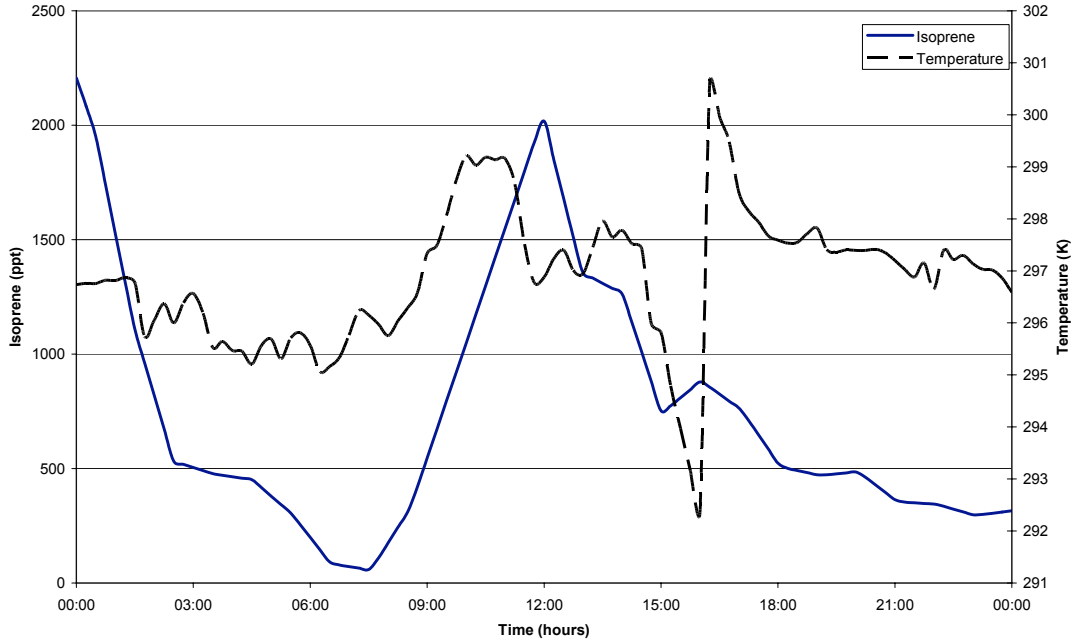

Figure 5.2.10 Isoprene concentrations recorded at Bukit Atur on JDay 112 (12th April 2008)

The measurements of j($O(^1D)$) for day 112 are displayed in figure 5.2.11. The observed values are negligible before sunrise and after sunset, but heavy cloud cover at other points in the day reduce the observed values of j(O^1D) on this day. The maximum value observed on this day was observed at midday.

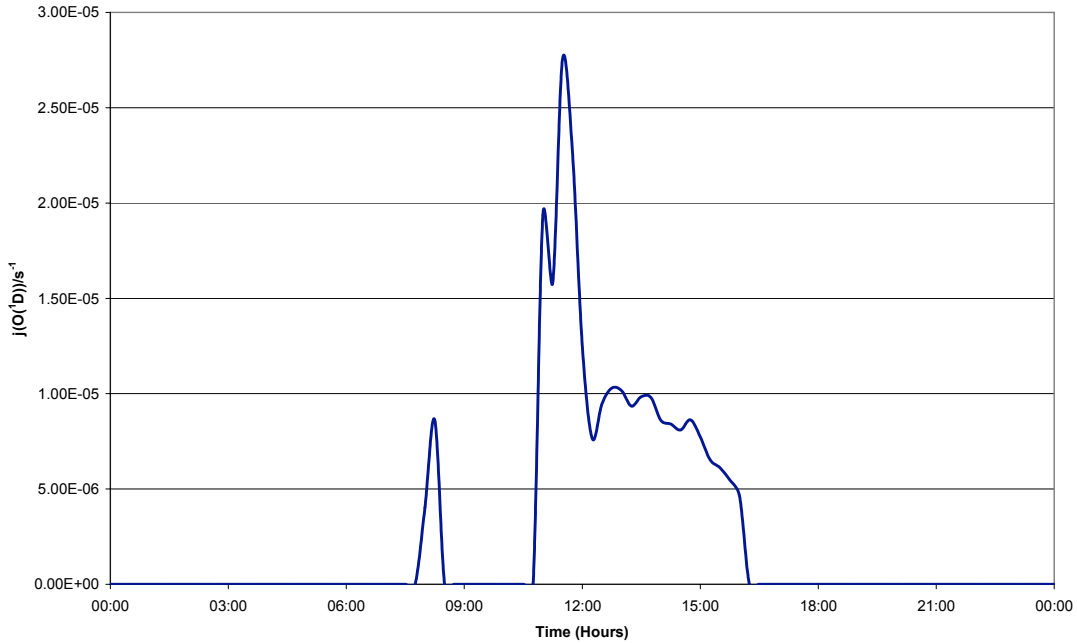

Figure 5.2.11 JO^1D observations recorded at Bukit Atur on JDay 112 (12th April 2008)

The results predicted by the OP3 model and the OP3 model containing the proposed Peeters scheme (OP3 Peeters) are displayed in figures 5.2.12 and 5.2.13 along with the measured concentrations for OH and RO_2 + HO_2 respectively. The three species all show similar diurnal behaviour with the lowest values being predicted and measured during the nighttime periods and the highest values occurring during the daytime. The OP3 Peeters model predicted higher concentrations than the OP3 model for OH, but lower concentrations for HO_2 + RO_2 (Table 5.2.2).

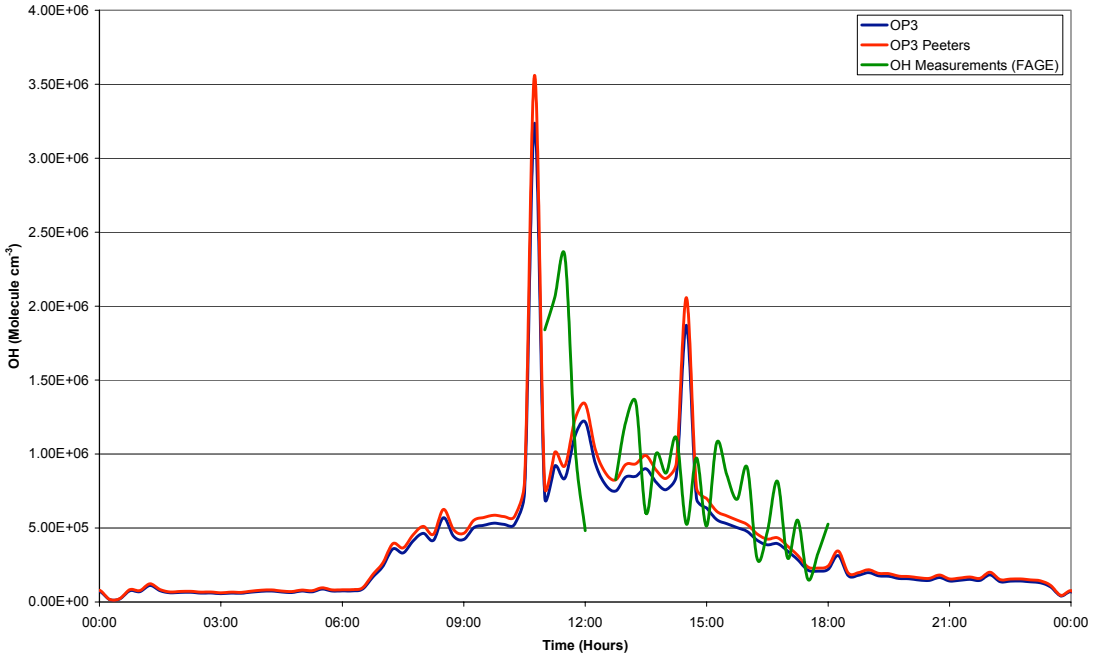

Figure 5.2.12 Model-measurement comparison of [OH] for day 112 (12th April 2008)

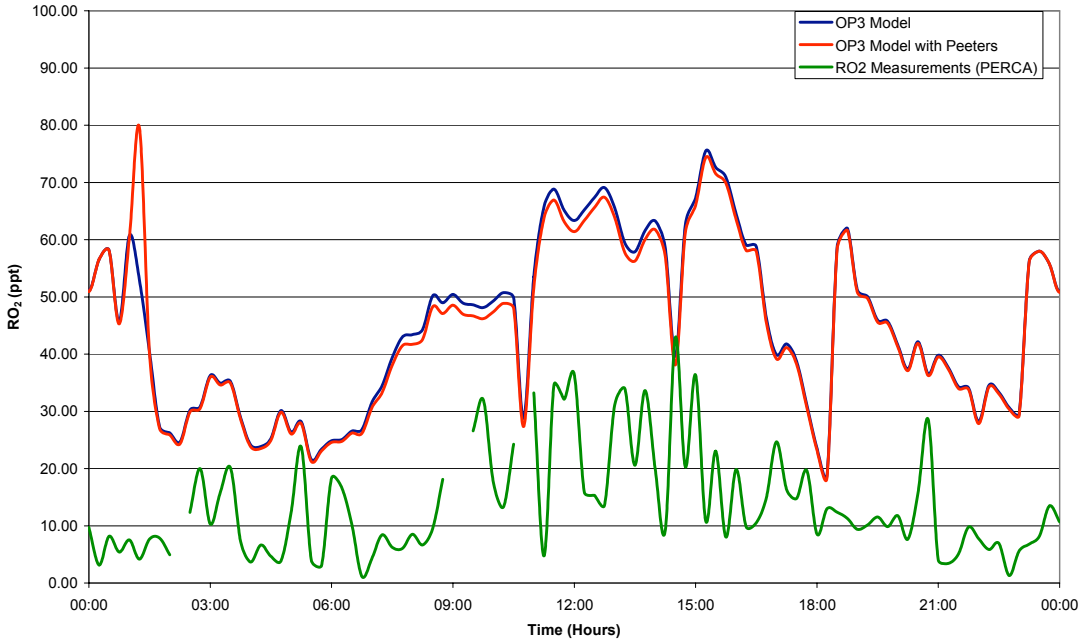

Figure 5.2.13 Model-measurement comparison of [HO_2 + RO_2] for day 112 (12th April 2008)

Table 5.2.2 Average concentrations of OH and RO_2 + HO_2 at Bukit Atur on JDay 112 (12th April 2008) for the whole day, daytime (06:00 – 18:00), nighttime (00:00 – 06:00 and 18:00 – 24:00) and midday (11:00 -15:00).

		OH (Molecule cm^{-3})	RO_2 + HO_2 (ppt)
OP3 Model	Daily Average	$3.7X10^5$	44.8
	Daytime Average	$6.3X10^5$	49.9
	Nighttime Average	$1.1X10^5$	37.3
	Average between 11:00 and 15:00	$9.1X10^5$	57.4
OP3 Peeters	Daily Average	$4.1X10^5$	44.3
	Daytime Average	$6.9X10^5$	49.5
	Nighttime Average	$1.2X10^5$	38.3
	Average between 11:00 and 15:00	$1.0X10^6$	60.3
Measurements	Daily Average	$8.8X10^5$	13.8
	Daytime Average	$8.8X10^5$	18.3
	Nighttime Average	$5.3X10^5$	9.5
	Average between 11:00 and 15:00	$1.1X10^6$	25.5

On day 112 there were limited OH measurements from the FAGE instrument to compare the OH predictions to. The results in figure 5.2.13 show that the two models predicted similar values to those observed. However, the models fail to identify the peaks in OH at 11:45 and 13:00. The values in table 5.2.2 shows that both models both predict the observed OH close to the observations between 11:00 and 15:00, with the OP3 Peeters model performing slightly better.

The HO_2+RO_2 data in figure 5.1.14 indicates a large over prediction from both models, with predictions twice as large as the observed values between 11:00 and 15:00.

5.2.3 Day 113 (13th April 2008)

The air mass trajectory arriving at the Bukit Atur field site was predicted using the NOAA Hysplit model (figure 5.2.14). The NOAA model shows that the air mass arises over the sea to the northeast of the island, as would be expected at this time of year (Hewitt et al., 2009), then moves from south-west passing over no other landmass before reaching Borneo. There is a period 14 hours between the air mass arriving at Borneo and the field site at Bukit Atur, approaching from the south east of the field site

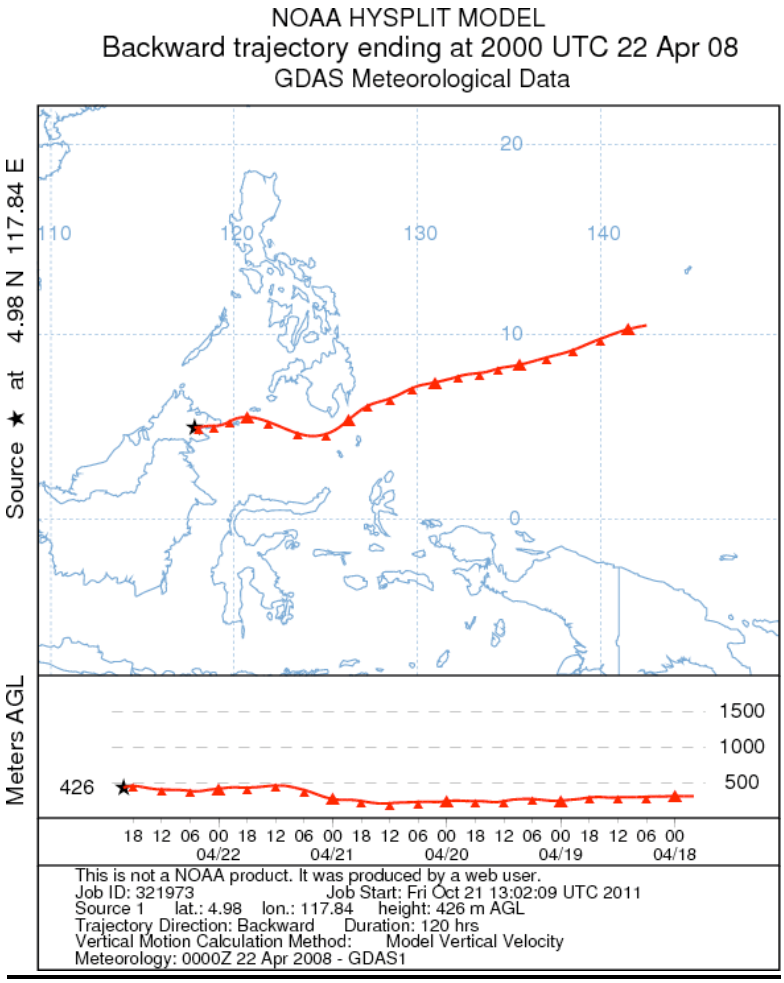

Figure 5.2.14 Air mass back trajectory for 5 day arriving at the field site at 1200 hours (local time) on 13th April (JDay 113) The upper plot shows the path taken by the airmass travelling to the field site, for the 5 days previous to measurements being taken. The lower plot shows the altitude of the airmass for the 5 day period before arriving at the field site.

Figure 5.2.15 shows the concentrations of NO and NO_2 measured at the field site. Again, peaks can be attributed to traffic along the logging road near to the field site. The largest peaks occur when the vehicles were closest to the inlets at the field site, such as those observed at 9:00, 16:00 and 18:00. The largest peak in the observed values of NO_2 occurs at 16:00, with the largest NO peak being observed at the same point.

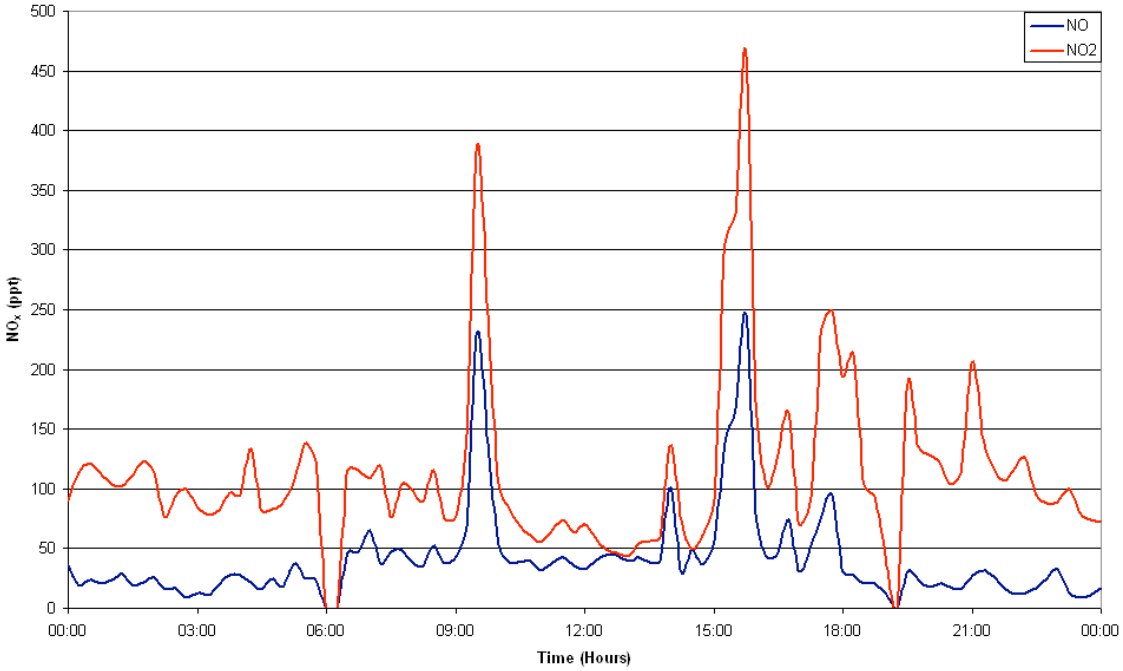

Figure 5.2.15 NO and NO_2 concentrations recorded at Bukit Atur on JDay 113 (13th April 2008)

The isoprene component of the air mass is generated locally at the site by sources that are affected by temperature and sunlight levels (Hewitt et al., 2009), this is shown in figure 5.2.16 as well as the daily temperature profile. The monoterpenes used in the model on this day were taken from the average monoterpene profile generated on other days as seen in figure 5.2.4

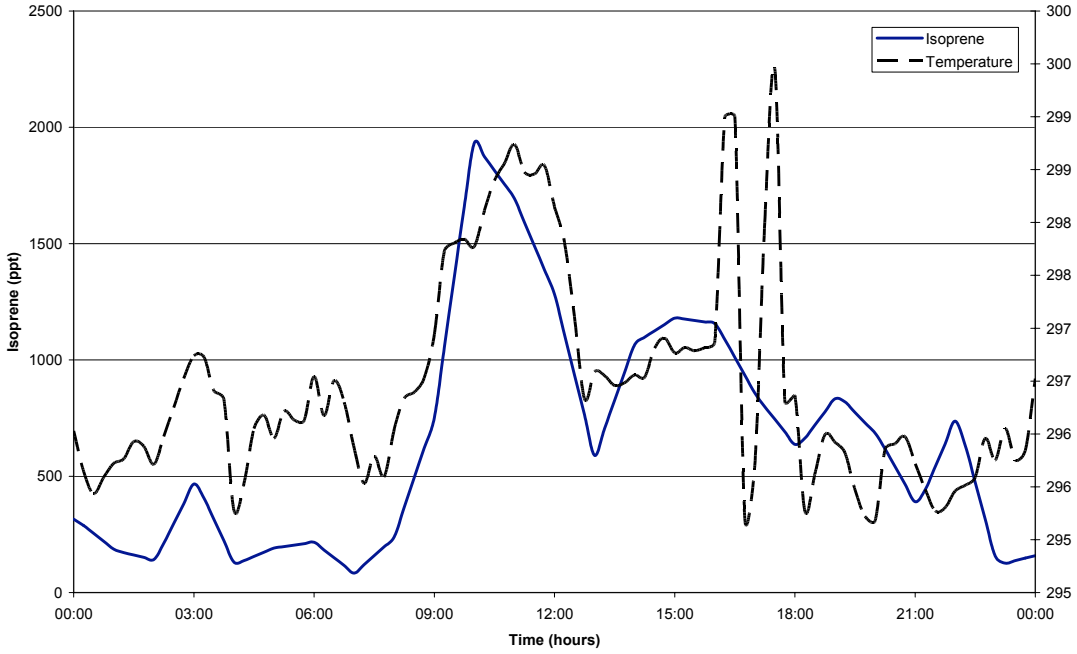

Figure 5.2.16 Isoprene concentrations recorded at Bukit Atur on JDay 113 (13th April 2008)

The measurements of j($O(^1D)$) for day 113 are displayed in figure 5.2.17. The observed values are negligible before sunrise and after sunset, but heavy cloud cover at other points in the day reduce the observed values of j(O^1D). The maximum value observed on this day was seen at 10:30, rather than solar noon as would be expected.

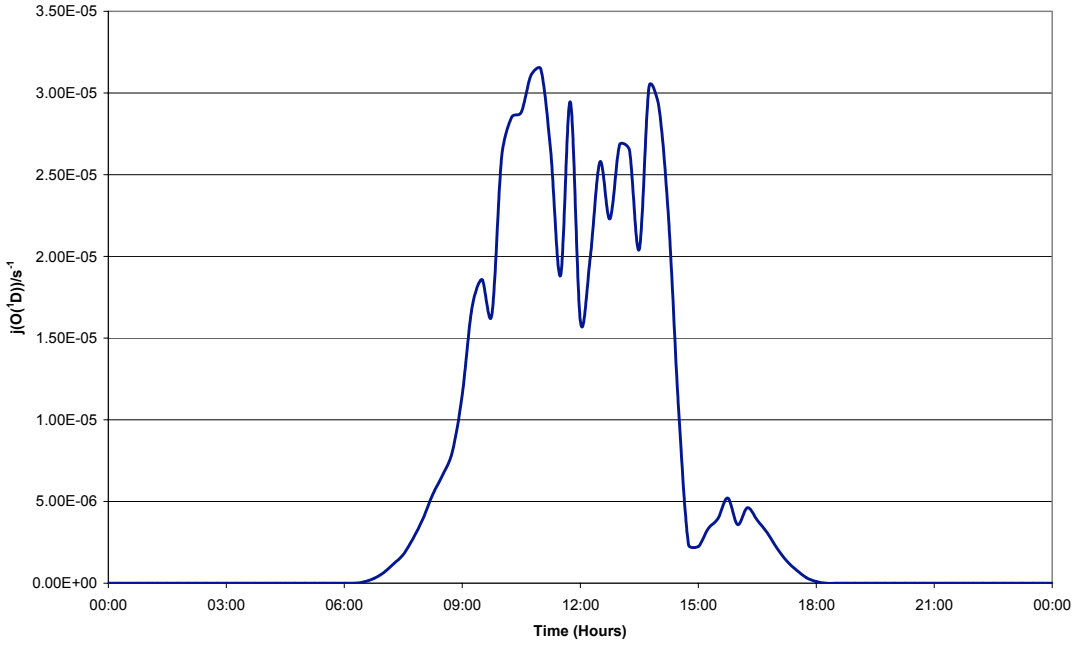

Figure 5.2.17 J(O^1D) observations recorded at Bukit Atur on JDay 113 (13th April 2008)

The results predicted by the OP3 model and the OP3 model containing the proposed Peeters scheme (OP3 Peeters) are displayed in figures 5.2.18 and 5.2.19 along with the measured concentrations for OH and HO_2 + RO_2 respectively. The three radicals display similar diurnal behaviour with the lowest values being predicted and measured during the nighttime periods. The highest values occurring during the daytime, with maximum values tend to occur near solar noon for HO_2 + RO_2. The OP3 Peeters model predicted higher concentrations than the OP3 model for OH, but lower concentrations for HO_2 + RO_2 (Table 5.2.3).

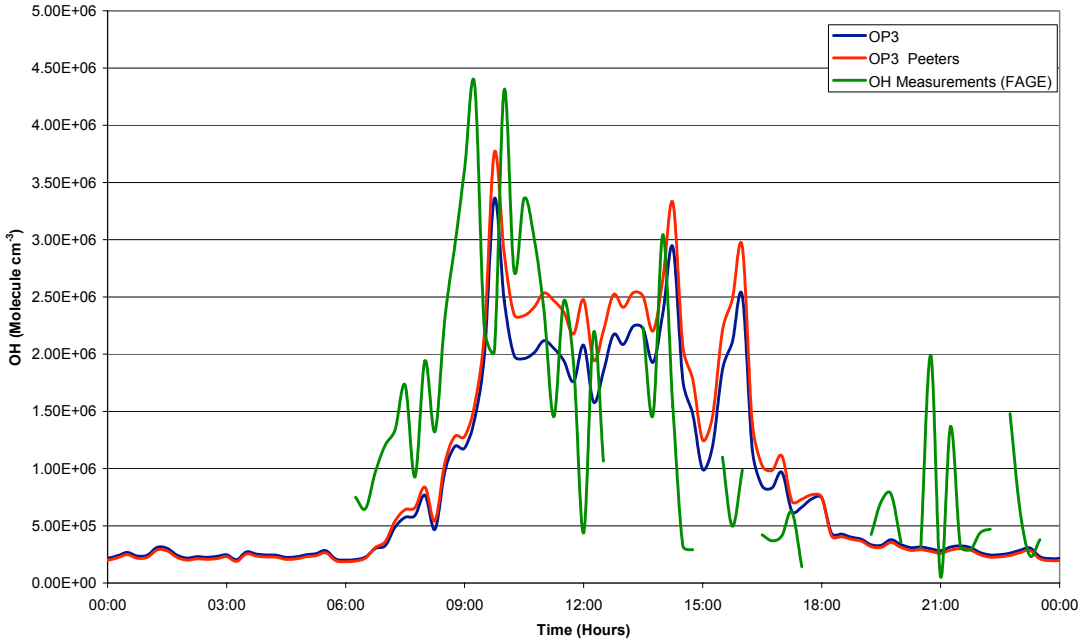

Figure 5.2.18 Model-measurement comparison of [OH] for day 113 (13th April 2008)

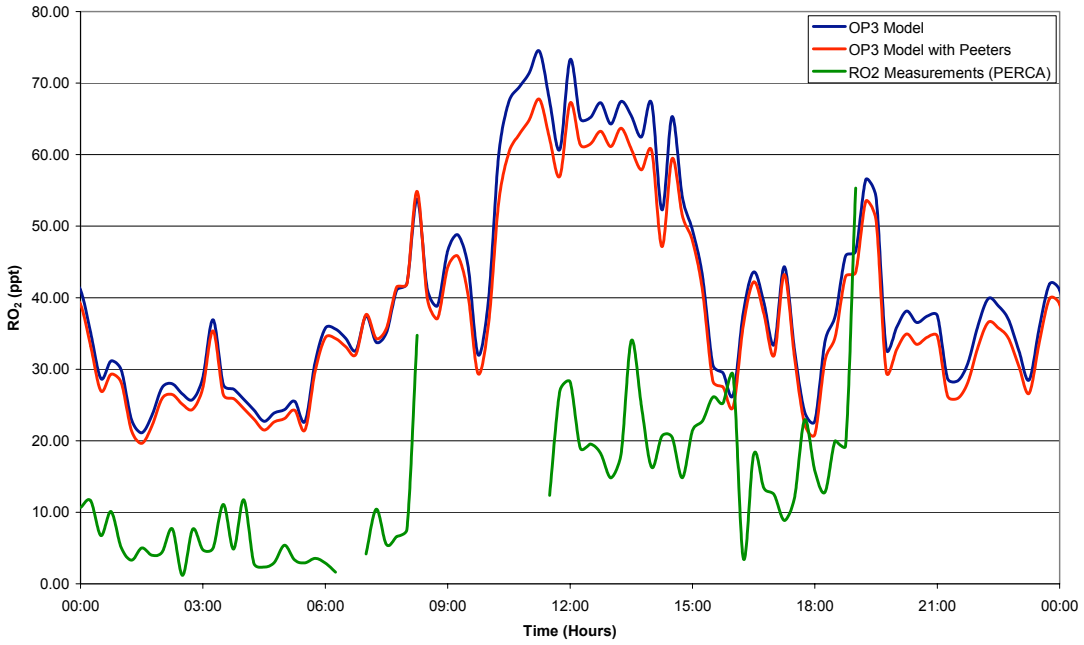

Figure 5.2.19 Model-measurement comparison of [HO_2 + RO_2] for day 113 (13th April 2008)

The OH results displayed in figure 5.2.18 have limited measurements from FAGE to compare the model predictions to. The models predict a large peak in the concentration of OH at just after 09:00 which coincides with a large peak in the observed values of OH. This point also fits with a large peak in the observed values

of NO_x though FAGE measurements appear to peak somewhat earlier. There is also a smaller peak in NO_x measurements at 14:45 which coincides with observed and predicted peaks in the concentration of OH.

The HO_2+RO_2 predictions in figure 5.2.19 show an over prediction when compared to the PERCA measurements that were available.

Table 5.2.3 Average concentrations of OH and RO_2 + HO_2 at Bukit Atur on JDay 113 (13th April 2008) for the whole day, daytime (06:00 – 18:00), nighttime (00:00 – 06:00 and 18:00 – 24:00) and midday (11:00 -15:00).

		OH (Molecule cm^{-3})	HO_2 + RO_2 (ppt)
OP3 Model	Daily Average	$8.6X10^5$	40.7
	Daytime Average	$1.4X10^6$	48.4
	Nighttime Average	$2.9X10^5$	32.7
	Average between 11:00 and 15:00	$2.0X10^6$	64.3
OP3 Peeters	Daily Average	$9.7X10^5$	39.1
	Daytime Average	$1.7X10^6$	46.7
	Nighttime Average	$2.7X10^5$	31.2
	Average between 11:00 and 15:00	$2.3X10^6$	52.8
Measurements	Daily Average	$1.3X10^6$	13.3
	Daytime Average	$1.7X10^6$	17.0
	Nighttime Average	$6.0X10^5$	8.8
	Average between 11:00 and 15:00	$1.6X10^6$	20.6

During the period of 11:00 to 15:00 both models over predict the concentrations of OH and HO_2+RO_2 (table 5.2.3). The OP3 Peeters model predicts higher OH than the OP3 model during this period and both models over predict the measured OH. The HO_2+RO_2 values generated by both models are over two times larger than the observed values, with the OP3 Peeters model predicting closer values to the measurements than the OP3 model.

5.2.4 Day 114 (14th April 2008)

The air mass trajectory arriving at the Bukit Atur field site was predicted using the NOAA Hysplit model (figure 5.2.20). The NOAA model shows that the air mass arises over the sea to the northeast of the island, then moves in a south-westerly passing over no other landmass before reaching Borneo. There is a period of 18 hours between the air mass arriving at Borneo and the field site at Bukit Atur, approaching from the south east of the field site

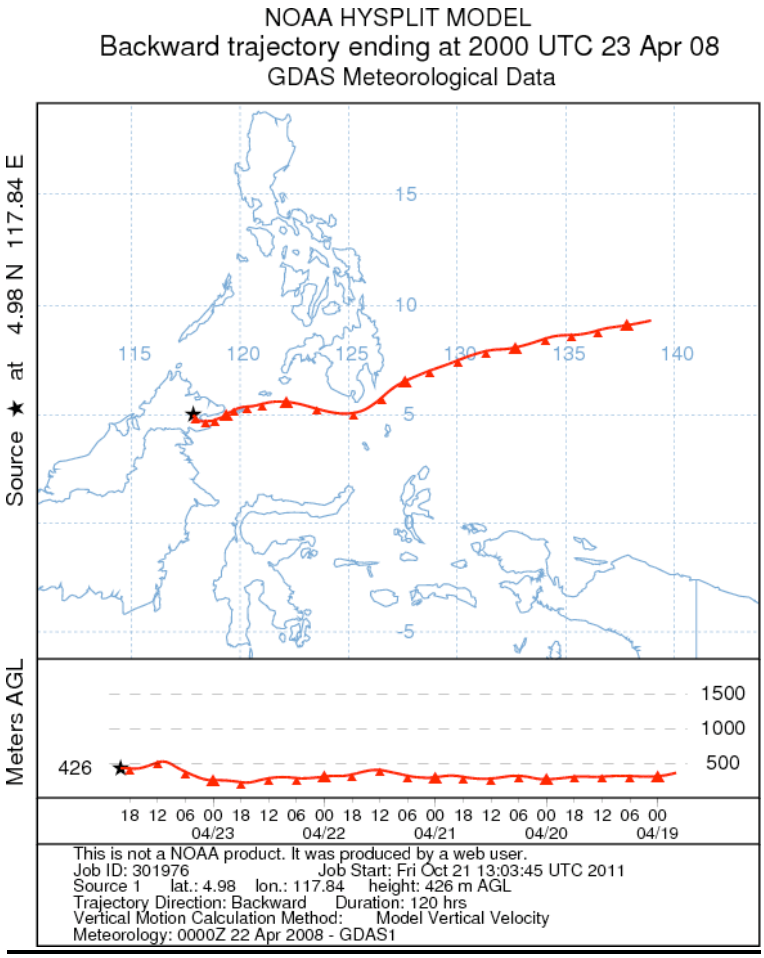

Figure 5.2.20 Air mass back trajectory for 5 day arriving at the field site at 1200 hours (local time) on 14th April (JDay 114) The upper plot shows the path taken by the airmass travelling to the field site, for the 5 days previous to measurements being taken. The lower plot shows the altitude of the airmass for the 5 day period before arriving at the field site.

Figure 5.2.21 shows the concentrations of NO and NO_2 measured at the field site. Peaks in the daily profile can again be attributed to traffic along the logging road near to the field site, with larger peaks coinciding with when vehicles were driven to the top of Bukit Atur and brought close to the observation. The largest peak in NO_2 is seen at 14:30 with a peak in NO shortly after. There is a smaller peak in NO and NO_2 seen at 16:00.

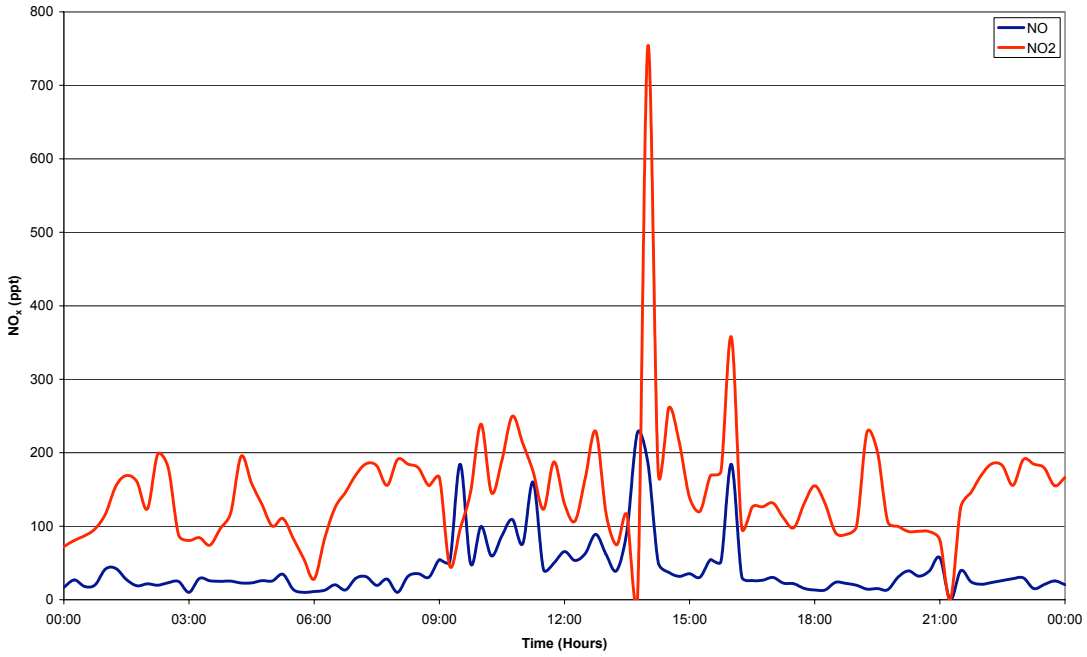

Figure 5.2.23 NO and NO_2 concentrations recorded at Bukit Atur on JDay 114 (14th April 2008)

The isoprene is again generated locally at the site as is shown in figure 5.2.24 along with the daily temperature profile. The monoterpenes used in the model on this day were taken from the average monoterpene profile generated on other days shown in Figure 5.2.4.

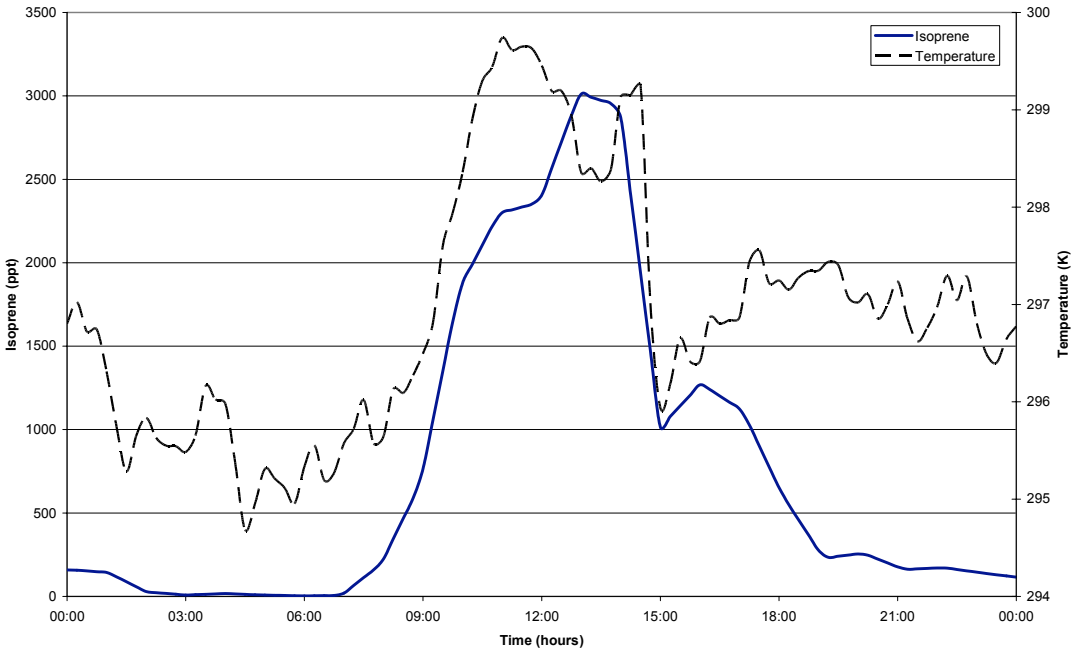

Figure 5.2.22 Isoprene concentrations recorded at Bukit Atur on JDay 114 (14th April 2008)

The measurements of j($O(^1D)$) for day 114 are displayed in figure 5.2.23. The maximum value observed on this day was recorded at 11:00, then heavy cloud cover obscured the sunlight for several hours.

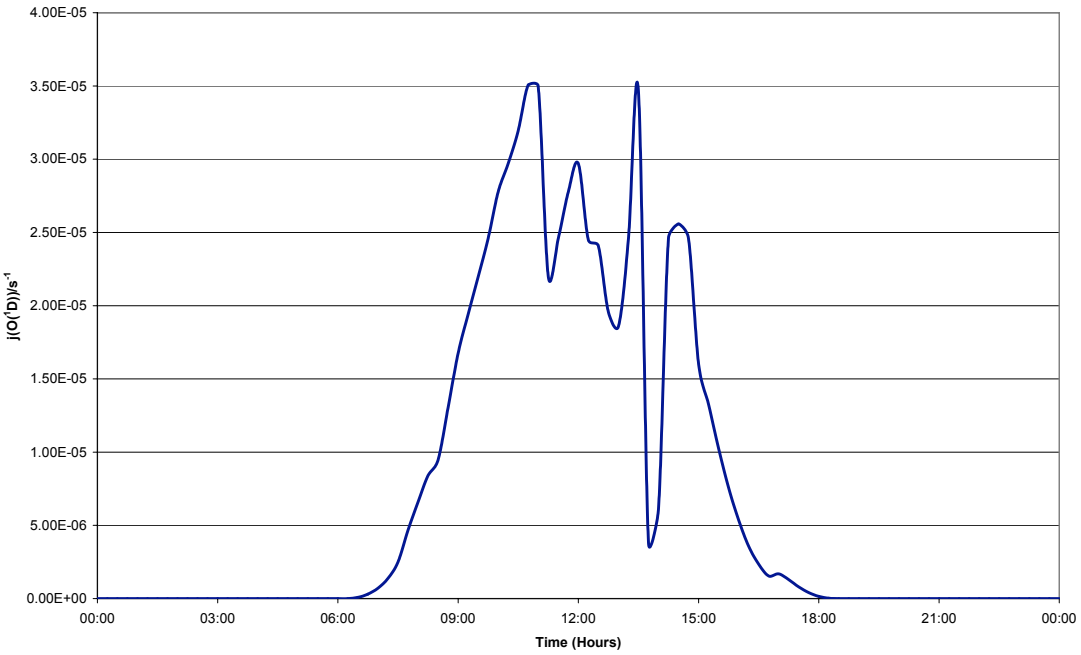

Figure 5.2.23 J(O^1D) observations recorded at Bukit Atur on JDay 114 (14th April 2008)

The results predicted by the OP3 model and the OP3 model containing the proposed Peeters scheme (OP3 Peeters) are displayed in figures 5.2.27 and 5.2.28 along with the measured concentrations for OH and $HO_2 + RO_2$ respectively. The radical species all display the lowest values being predicted and measured during the nighttime periods and the highest values during the daytime. The OP3 Peeters model predicted higher concentrations than the OP3 model for OH, but lower concentrations for $HO_2 + RO_2$ (Table 5.2.4).

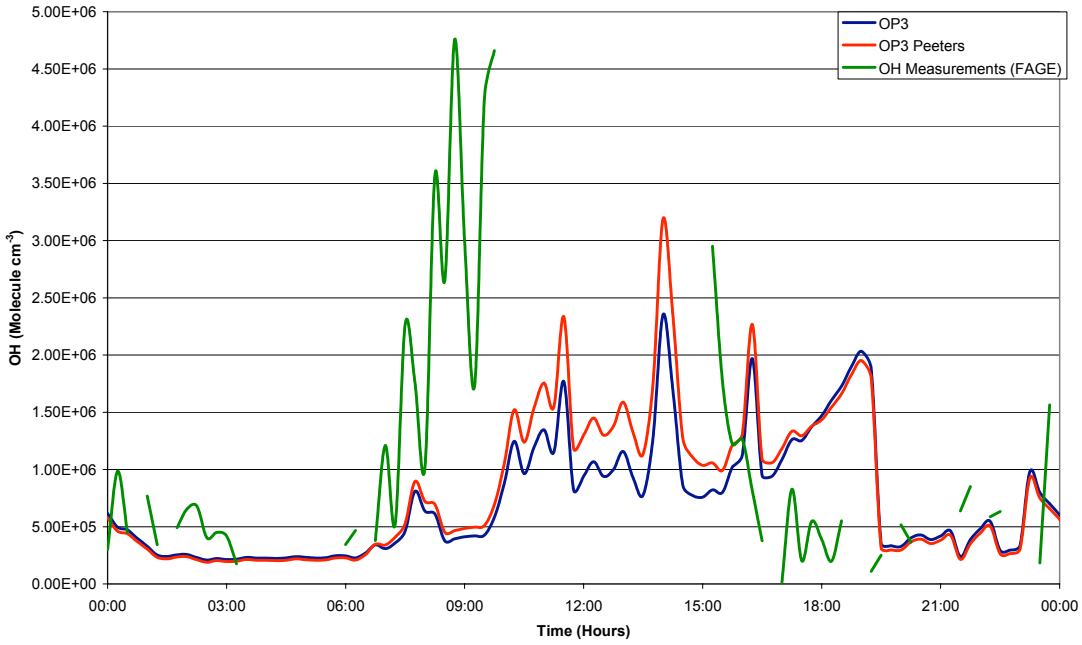

Figure 5.2.24 Model-measurement comparison of [OH] for day 114 (14th April 2008)

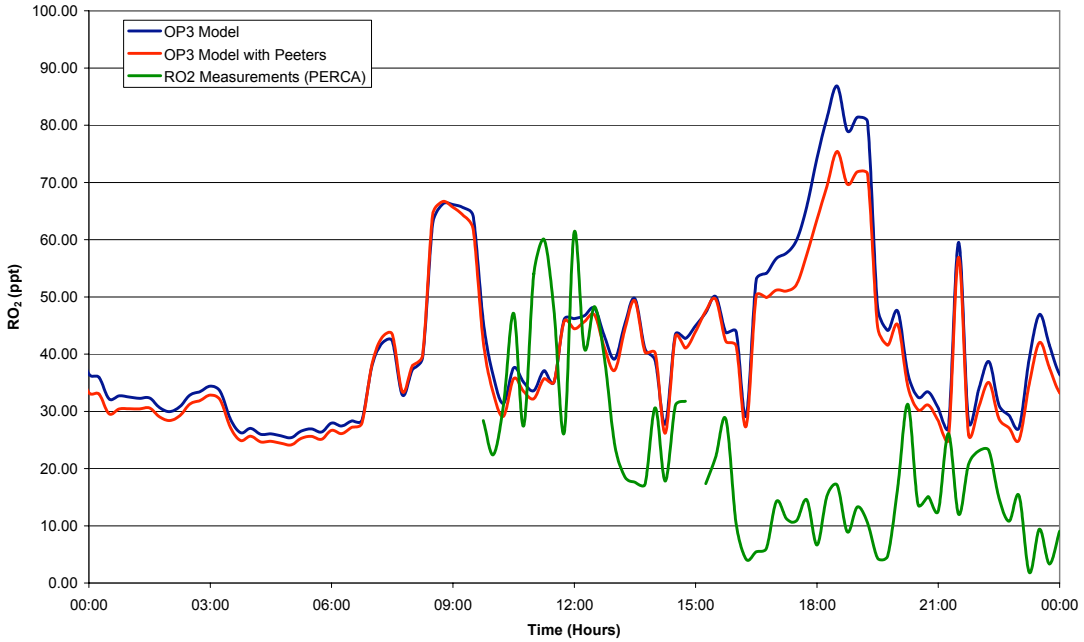

Figure 5.2.25 Model-measurement comparison of [HO_2 + RO_2] for day 114 (14th April 2008)

There are limited OH measurements from the FAGE instrument in figure 5.2.24. From the limited measurements, it is possible to see that both models are under predicting the concentrations of OH for this day. Both of the models predict a peak in the concentrations in OH at 14:30, which coincides with the largest observed peak in NO and NO_2 during day 114.

From the limited observations of HO_2+RO_2 concentrations it is possible to see that both models tend to over predict the concentrations on this day. Table 5.2.4 also shows the over prediction of HO_2+RO_2 from both models.

Table 5.2.4 Average concentrations of OH and $RO_2 + HO_2$ at Bukit Atur on JDay 114 (14/04/2008) for the whole day, daytime (06:00 – 18:00), nighttime (00:00 – 06:00 and 18:00 – 24:00) and midday (11:00 -15:00).

		OH (Molecule cm^{-3})	$RO_2 + HO_2$ (ppt)
OP3 Model	Daily Average	$7.2X10^5$	41.7
	Daytime Average	$9.2X10^5$	44.9
	Nighttime Average	$5.3X10^5$	39.0
	Average between 11:00 and 15:00	$1.2X10^6$	41.7
OP3 Peeters	Daily Average	$8.1X10^5$	39.3
	Daytime Average	$1.1X10^6$	43.2
	Nighttime Average	$4.9X10^5$	35.8
	Average between 11:00 and 15:00	$1.6X10^6$	40.7
Measurements	Daily Average	$1.1X10^6$	21.2
	Daytime Average	$1.7X10^6$	26.5
	Nighttime Average	$5.0X10^5$	13.6
	Average between 11:00 and 15:00	No Data Available	35.4

5.2.5 Day 115 (15th April 2008)

The air mass trajectory arriving at the Bukit Atur field site was predicted using the NOAA Hysplit model (figure 5.2.6). The NOAA model shows that the air mass arises over the sea to the northeast of the island, then moves over Mindanao (Southern Island of the Philippines). There is a period of 16 hours between the air mass arriving at Borneo and the field site at Bukit Atur, travelling from a northeast direction.

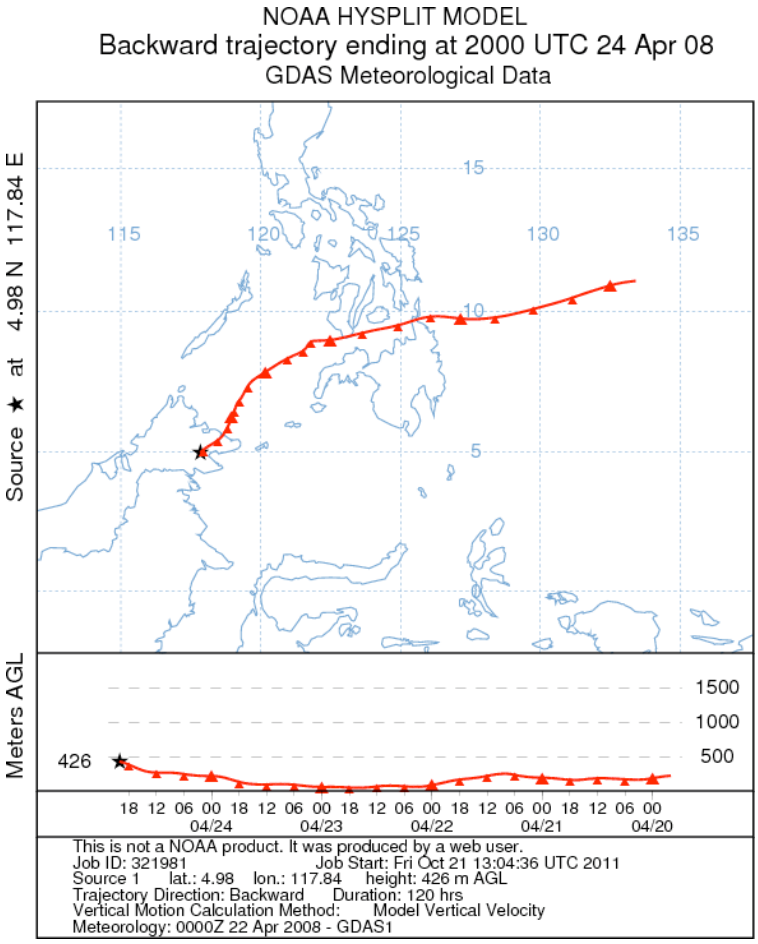

Figure 5.2.26 Air mass back trajectory for 5 days arriving at the field site at 1200 hours (local time) on 15th April (JDay 115) The upper plot shows the path taken by the airmass travelling to the field site, for the 5 days previous to measurements being taken. The lower plot shows the altitude of the airmass for the 5 day period before arriving at the field site.

Figure 5.2.27 shows the concentrations of NO and NO_2 measured at the field site. During the day the largest peaks in NO occur at 08:45, 13:15 and 16:30, the largest peak in NO_2 also occurs at 16:30 with other noticeable peaks occurring at 08:45 and 13:15.

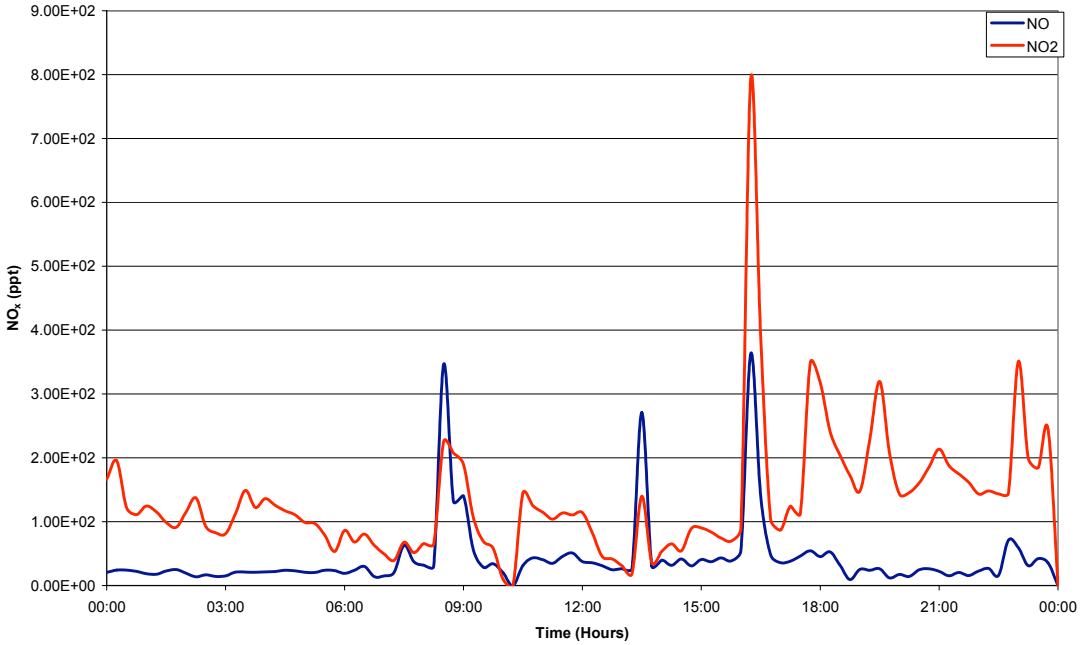

Figure 5.2.27 NO and NO_2 concentrations recorded at Bukit Atur on JDay 115 (15th April 2008)

The isoprene and temperature profiles are shown in figure 5.2.28. The monoterpenes used in the model on this day were taken from the average monoterpene profile generated on other days. Figure 5.2.4 displays the monoterpene concentrations that were input into the mode.

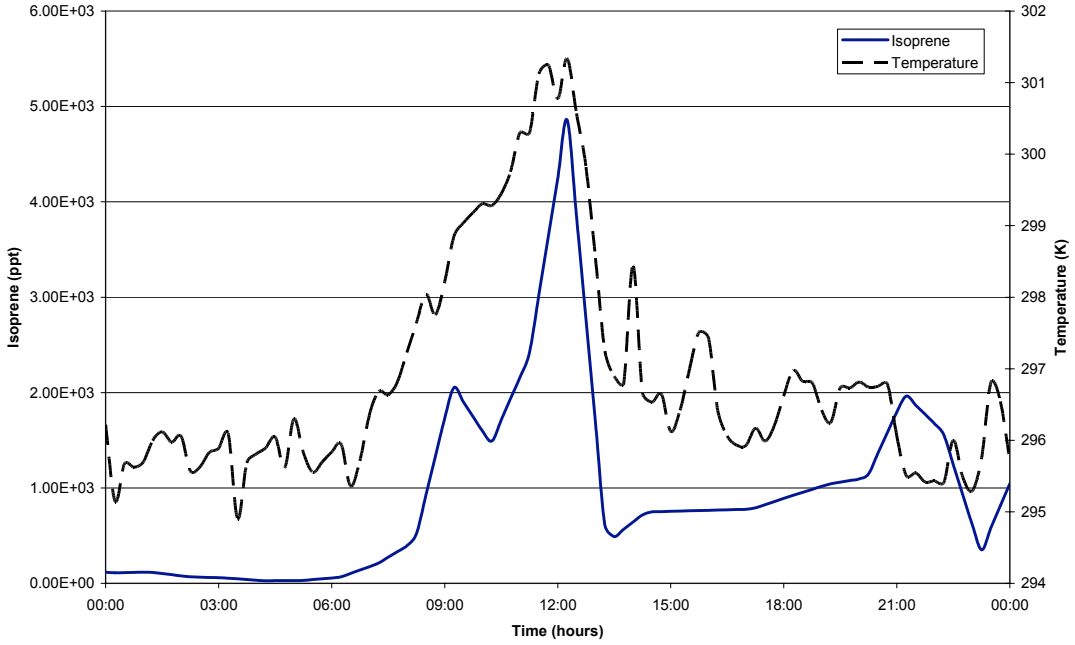

Figure 5.2.28 Isoprene concentrations recorded at Bukit Atur on JDay 115 (15th April 2008)

The measurements of j($O(^1D)$) for day 115 are displayed in figure 5.2.29. The observed values are negligible at the times before sunrise and after sunset, although there is some cloud cover during the morning, from midday the skies are clearer.

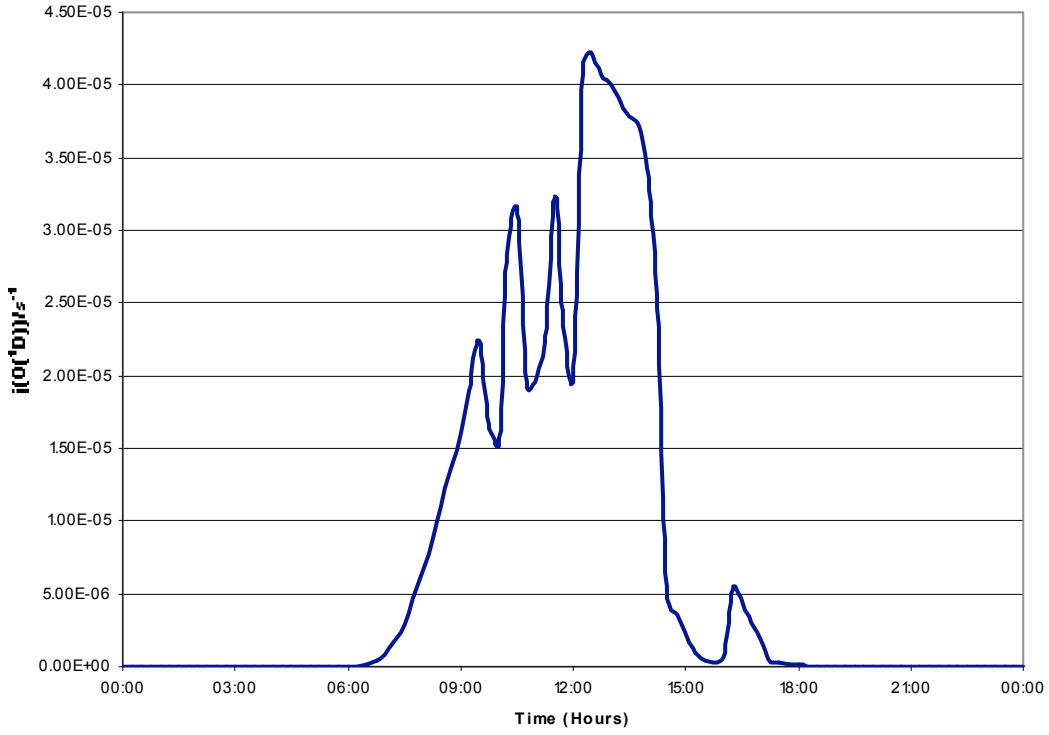

Figure 5.2.29 J(O^1D) observations recorded at Bukit Atur on JDay 115 (15th April 2008)

The results predicted by the OP3 model and the OP3 model containing the proposed Peeters scheme (OP3 Peeters) are displayed in figures 5.2.30 and 5.2.31 along with the measured concentrations for OH and $RO_2 + HO_2$ respectively. The radical species all show similar diurnal behaviour with the lowest values being predicted and measured during the nighttime periods and the highest values occurring during the daytime with maximum values tend to occur near solar noon. The OP3 Peeters model predicted higher concentrations than the OP3 model for OH, but lower concentrations for $HO_2 + RO_2$ (Table 5.2.5).

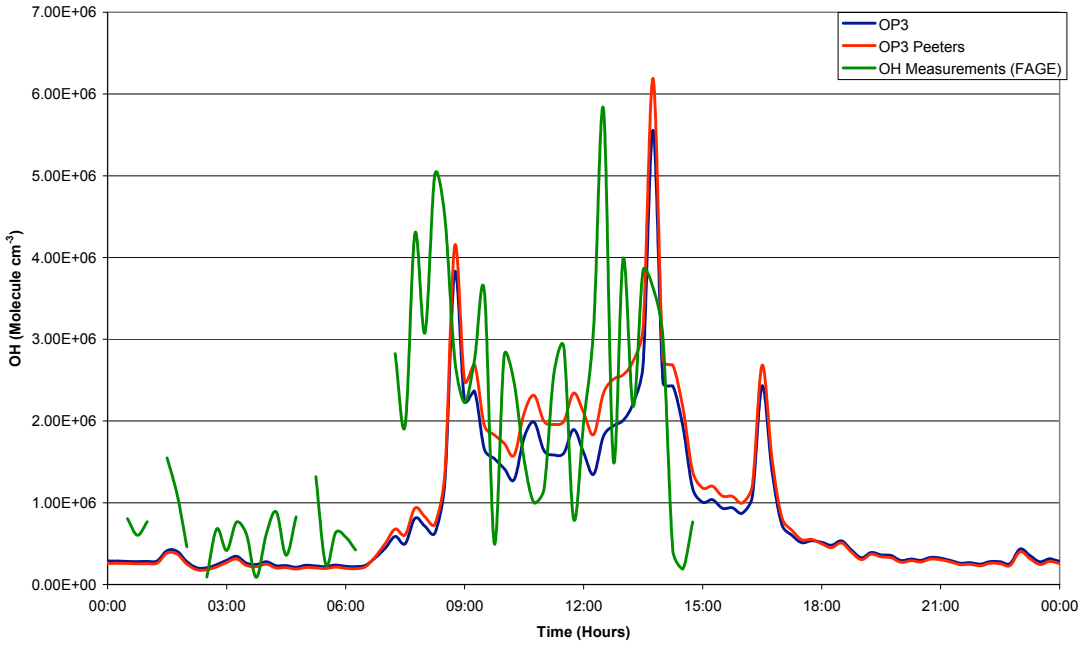

Figure 5.2.30 Model-measurement comparison of [OH] for day 115 (15th April 2008)

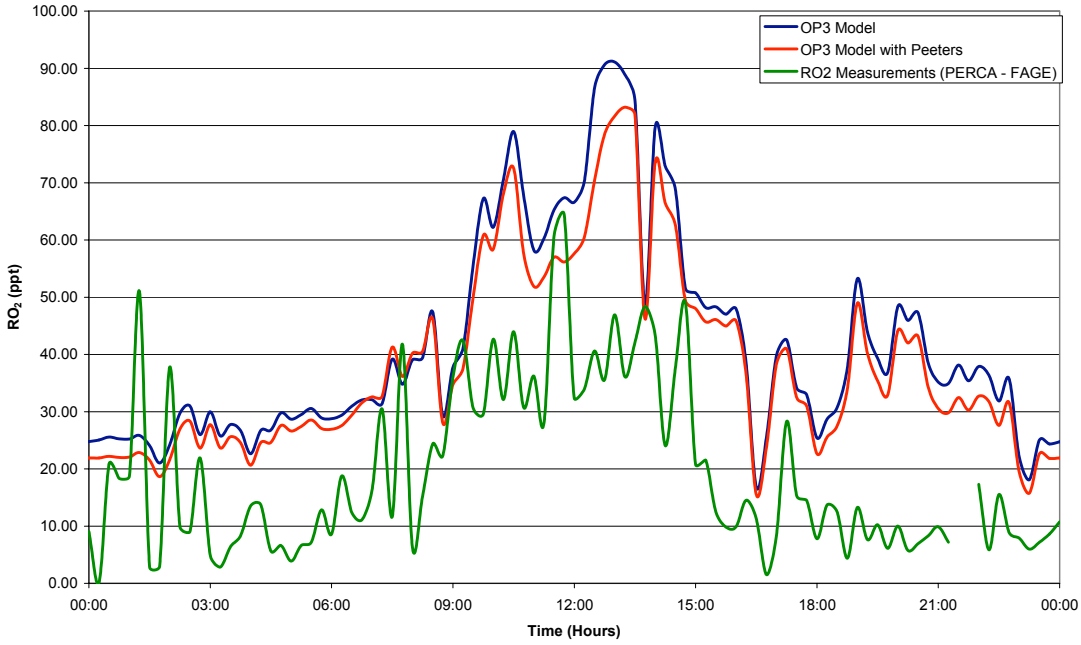

Figure 5.2.31 Model-measurement comparison of [HO_2 + RO_2] for day 115 (15th April 2008)

Figure 5.2.30 shows the limited observed concentrations of OH in comparison to the modelled values from the OP3 and OP3 Peeters models. There are observed and predicted peaks in OH around 09:00 which is the same point at which the first large peaks of NO and NO_2 occur on day 115. Other peaks in the predicted OH concentration occur at 14:00 which coincides with an observed peak, but both models over predict this. The models also predict a peak in OH concentration at 16:30 when there is a large peak in NO and NO_2, but there are no data from the FAGE to support the existence of an observed OH peak at this point.

The HO_2+RO_2 model and measured profile shows that both models and the measurements predict and observe a diurnal variation in the concentration for this day, and also, some of the instrumental peaks.

Table 5.2.5 Average concentrations of OH and $RO_2 + HO_2$ at Bukit Atur on JDay 115 (16th April 2008) for the whole day, daytime (06:00 – 18:00), nighttime (00:00 – 06:00 and 18:00 – 24:00) and midday (11:00 -15:00).

		OH (Molecule cm^{-3})	$RO_2 + HO_2$ (ppt)
OP3 Model	Daily Average	$8.8X10^5$	41.6
	Daytime Average	$1.4X10^6$	51.9
	Nighttime Average	$3.0X10^5$	30.9
	Average between 11:00 and 15:00	$2.1X10^6$	70.7
OP3 Peeters	Daily Average	$9.8X10^5$	38.1
	Daytime Average	$1.7X10^6$	48.1
	Nighttime Average	$2.8X10^5$	27.8
	Average between 11:00 and 15:00	$2.5X10^6$	63.4
Measurements	Daily Average	$1.8X10^6$	19.4
	Daytime Average	$2.4X10^6$	27.4
	Nighttime Average	$6.7X10^5$	10.7
	Average between 11:00 and 15:00	$2.4X10^6$	40.0

The average concentrations displayed in table 5.2.5 demonstrate that from 11:00 to 15:00 the OP3 Peeters model slightly over predicts the OH concentration while the OP3 model under predicts, with the OP3 Peeters model prediction being closer to the observed values. The values in table 5.2.5 also show that both models over predict the concentration of $HO_2 + RO_2$ with the OP3 Peeters model over predicting by less than the OP3 model.

5.2.6 Day 116 (16th April 2008)

The air mass trajectory arriving at the Bukit Atur field site was predicted using the NOAA Hysplit model (figure 5.2.32). The NOAA model shows that the air mass arises over the land south of the field site in Indonesia Borneo. The vastly different trajectory to the other days during this phase of the field campaigns indicates that the Island could be experiencing a change in the monsoon that affects the climate of Borneo.

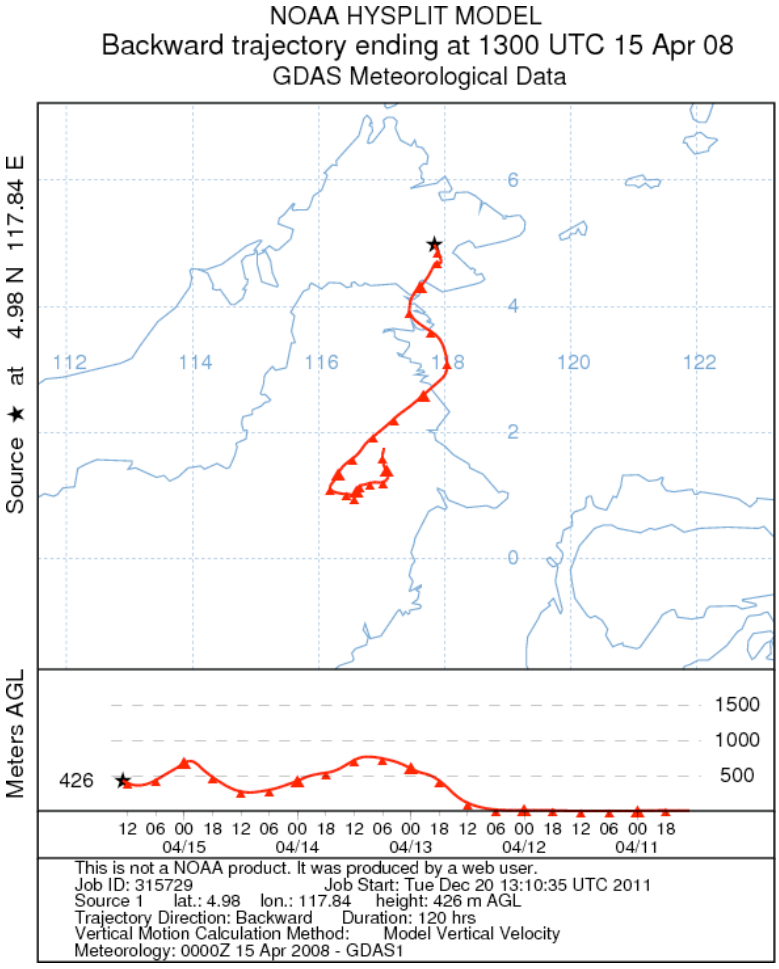

Figure 5.2.32 Air mass back trajectory for 5 day arriving at the field site at 1200 hours (local time) on 16th April (JDay 116) The upper plot shows the path taken by the airmass travelling to the field site, for the 5 days previous to measurements being taken. The lower plot shows the altitude of the airmass for the 5 day period before arriving at the field site.

Figure 5.2.33 shows the concentrations of NO and NO_2 measured at the field site. The concentration of NO remains is reasonablyconstant through out day 116, where as there are three very large peaks in the NO2 concentration,as well as many smaller fluctuations. Most peaks in the daily profile can be attributed to traffic along the logging road near to the field site.

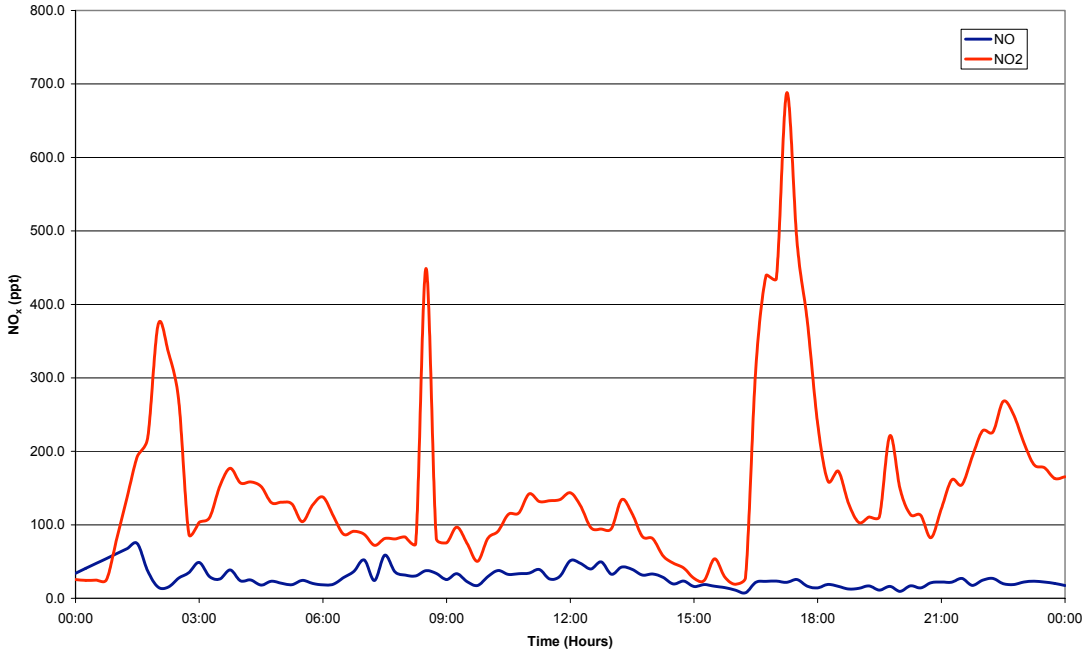

Figure 5.2.33 NO and NO_2 concentrations recorded at Bukit Atur on JDay 116 (16^{th} April 2008)

The isoprene concentration and temperature profiles are shown in figure 5.2.34. The monoterpenes used in the model on this day were taken from the average monoterpene profile generated on other days (figure 5.2.4).

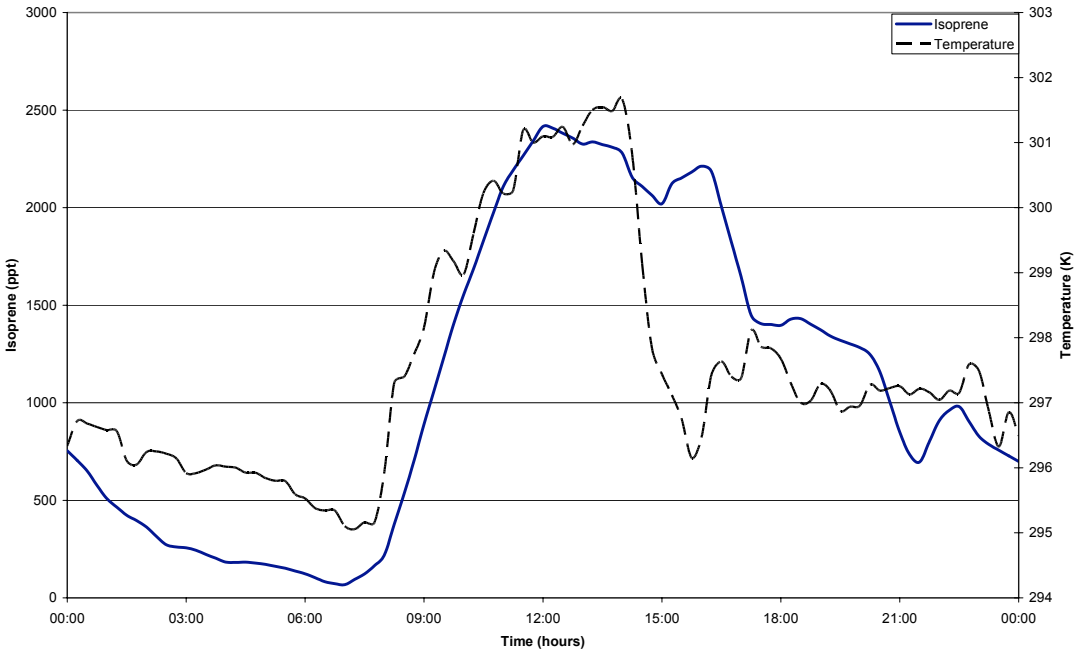

Figure 5.2.34 Isoprene concentrations recorded at Bukit Atur on JDay 116 (16th April 2008)

The measurements of j($O(^1D)$) for day 116 are displayed in figure 5.2.35. The maximum value observed on this day was seen close to 12:00 as would be expected, due to sunlight being at its most intense at this time. The profile of j($O(^1D)$) shows a diurnal pattern with few unexpected decreases in light intensity, indicating a relatively cloud free day.

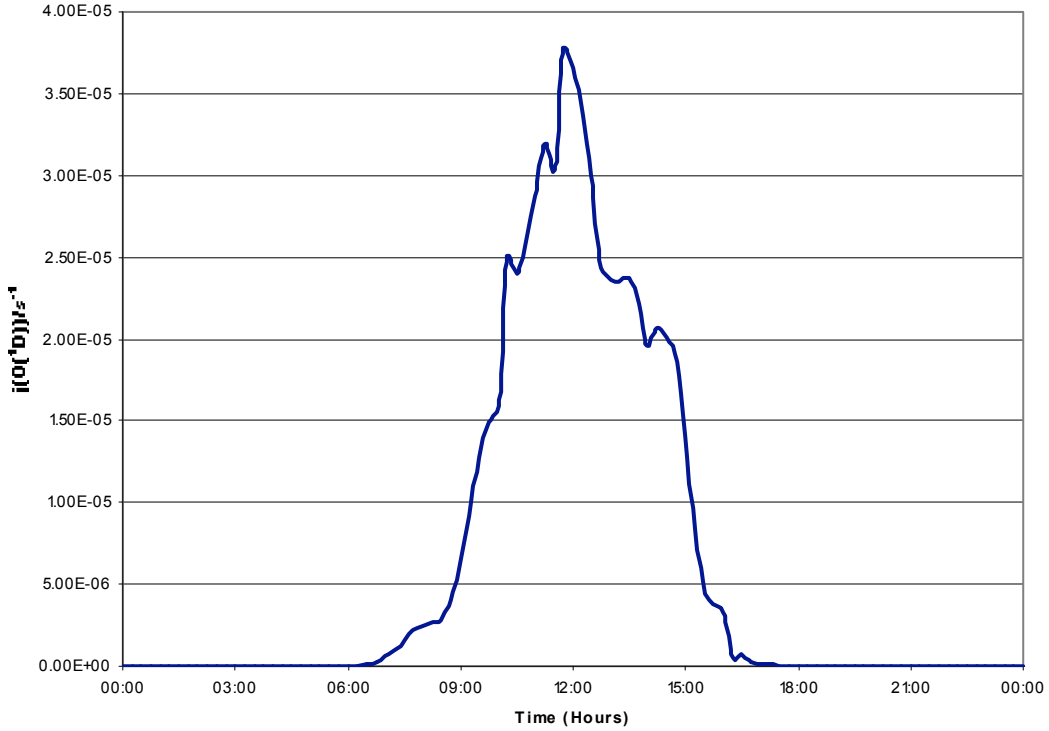

Figure 5.2.35 J(O^1D) observations recorded at Bukit Atur on JDay 116 (16th April 2008)

The results predicted by the OP3 model and the OP3 model containing the proposed Peeters scheme (OP3 Peeters) are displayed in figures 5.2.41 and 5.2.42 along with the measured concentrations for OH and HO_2 + RO_2 respectively. The three species all show similar diurnal behaviour with the lowest values being predicted and measured during the nighttime periods and the highest values occurring during the daytime with maximum values tend to occur near solar noon. The OP3 Peeters model predicted higher concentrations than the OP3 model for OH, but lower concentrations for HO_2 + RO_2 (Table 5.2.7).

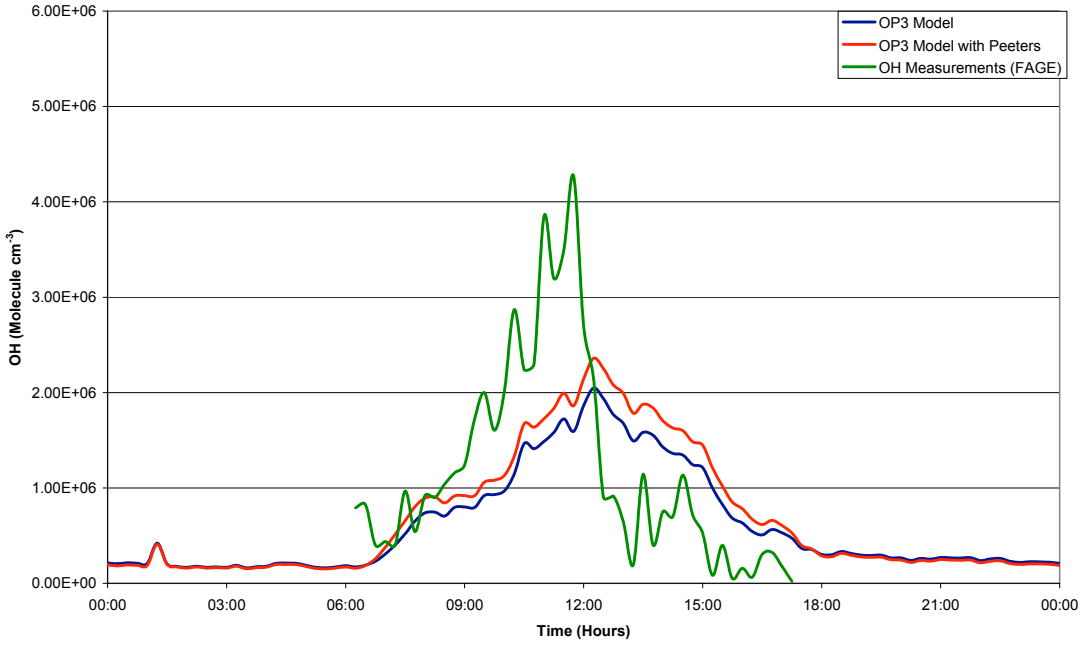

Figure 5.2.36 Model-measurement comparison of [OH] for day 116 (16th April 2008)

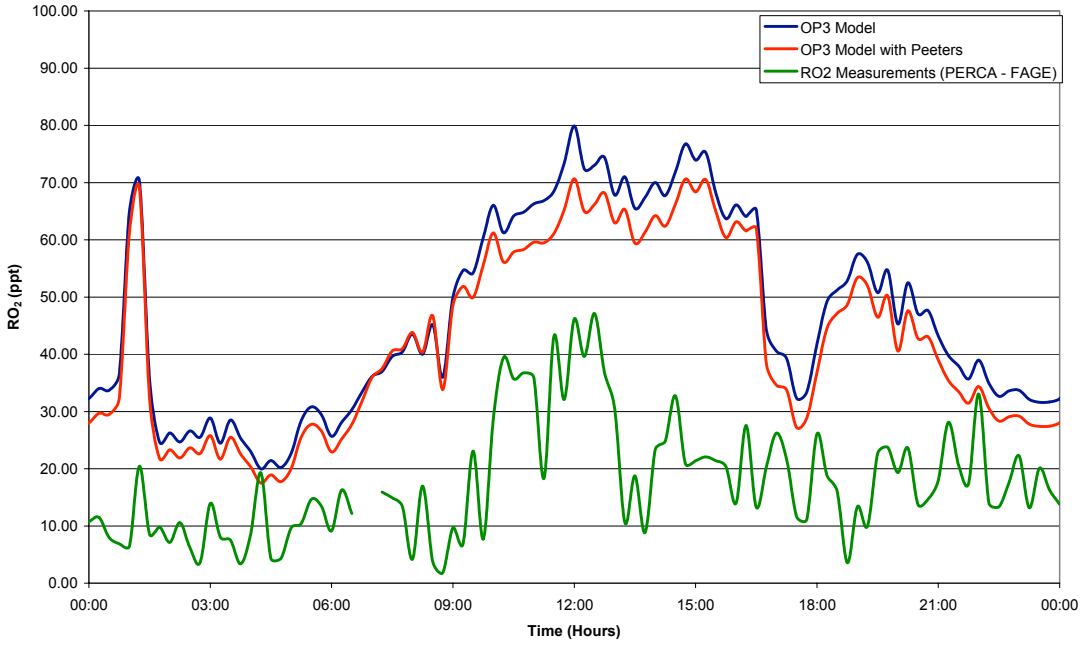

Figure 5.2.37 Model-measurement comparison of [RO_2 + HO_2] for day 116 (16th April 2008)

Figure 5.2.36 indicates that before 12:00 both models under predict the concentration of OH, but after 12:00 both models are over predicting the OH concentrations observed at the site.

The profiles of HO_2 + RO_2 displays the maximum values of predicted and observed values at 12:00 (figure 5.2.42). Both the models and the observations follow a diurnal pattern. However, the models predict a large peak occurring at 01:30 which coincides with a peak in the observed values of HO_2+RO_2. These peaks occur at the same point as an observed large peak in NO_2 concentrations.

Table 5.2.6 Average concentrations of OH and RO_2 + HO_2 at Bukit Atur on JDay 116 (16^{th} April 2008) for the whole day, daytime (06:00 – 18:00), nighttime (00:00 – 06:00 and 18:00 – 24:00) and midday (11:00 -15:00).

		OH (Molecule cm^{-3})	RO_2 + HO_2 (ppt)
OP3 Model	Daily Average	$6.1X10^5$	46.5
	Daytime Average	$9.8X10^5$	56.2
	Nighttime Average	$2.3X10^5$	36.6
	Average between 11:00 and 15:00	$1.6X10^6$	71.0
OP3 Peeters	Daily Average	$6.8X10^5$	42.6
	Daytime Average	$1.1X10^6$	51.9
	Nighttime Average	$2.1X10^5$	32.9
	Average between 11:00 and 15:00	$1.9X10^6$	64.5
Measurements	Daily Average	$1.2X10^6$	17.7
	Daytime Average	$1.2X10^6$	21.8
	Nighttime Average	No Data Available	13.8
	Average between 11:00 and 15:00	$1.6X10^6$	28.9

The values in table 5.2.6 show that despite the under prediction of OH before 12:00, the OP3 model correctly predicts the average concentration between 11:00 and 15:00 and OP3 Peeters model over predicts the OH concentration at this point.

5.2.7 Day 117 (17th April 2008)

The air mass trajectory arriving at the Bukit Atur field site was predicted using the NOAA Hysplit model (figure 5.2.38). The NOAA model shows that the air mass arises over the sea to the northeast of the island, between Borneo and Mindanao (Southern Island of the Philippines). There is a period of over two days between the air mass arriving at Borneo and the field site at Bukit Atur, travelling from a northeast direction. The airmass moves to the northwest of the field site before passing back and approaching the field site from the east.

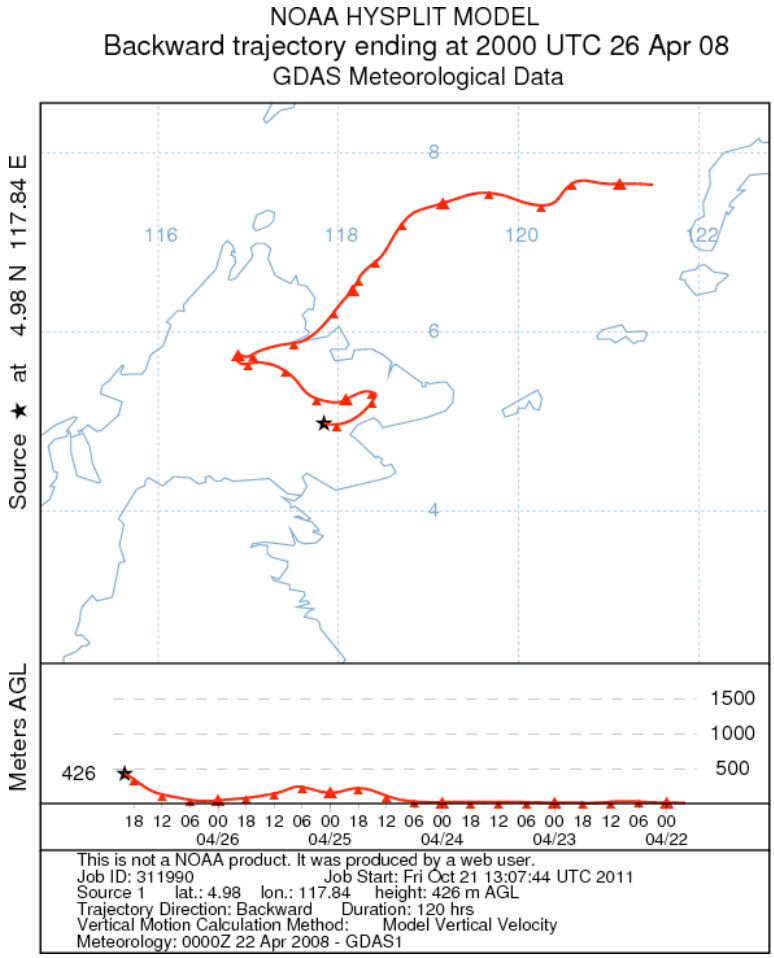

Figure 5.2.38 Air mass back trajectory for 5 day arriving at the field site at 1200 hours (local time) on 17th April (JDay 117) The upper plot shows the path taken by the airmass travelling to the field site, for the 5 days previous to measurements being taken. The lower plot shows the altitude of the airmass for the 5 day period before arriving at the field site.

Figure 5.2.39 shows the concentrations of NO and NO_2 measured at the field site. The values of NO remain reasonably constant, except for a large peak observed at 08:45, where a large peak is also observed in the NO_2 concentration.

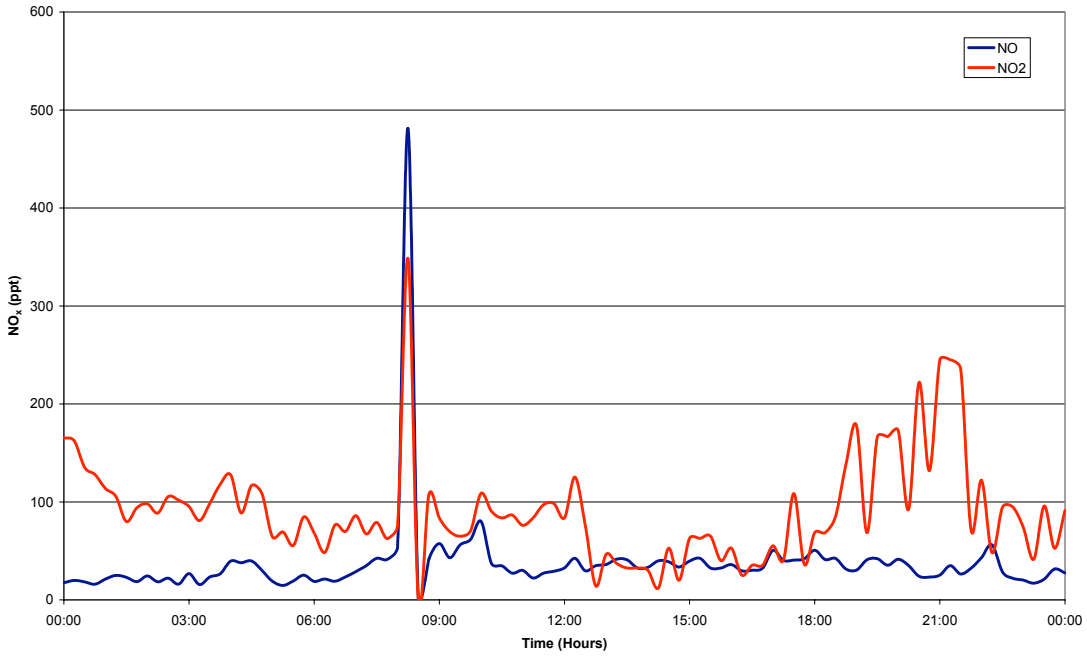

Figure 5.2.39 NO and NO_2 concentrations recorded at Bukit Atur on JDay 117 (17^{th} April 2008)

The isoprene concentrations and temperature profile are shown in figure 5.2.40. The monoterpenes used in the model on this day were taken from the average monoterpene profile generated on other days (figure 5.2.4).

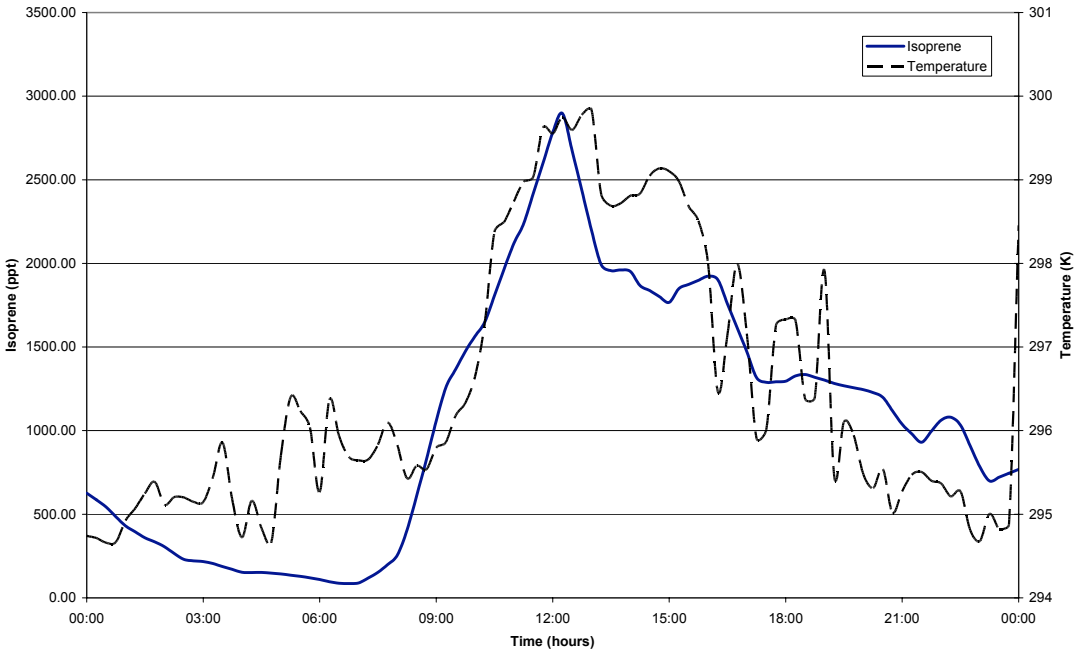

Figure 5.2.40 Isoprene concentrations recorded at Bukit Atur on JDay 117 (17th April 2008)

The measurements of $j(O(^1D))$ for day 117 are displayed in figure 5.2.41. The observed values are negligible at the times before sunrise and after sunset. The maximum value observed on this day was seen close to 12:00 as would be expected, but decreases in $j(O(^1D))$ which can be attributed to periods of cloud cover.

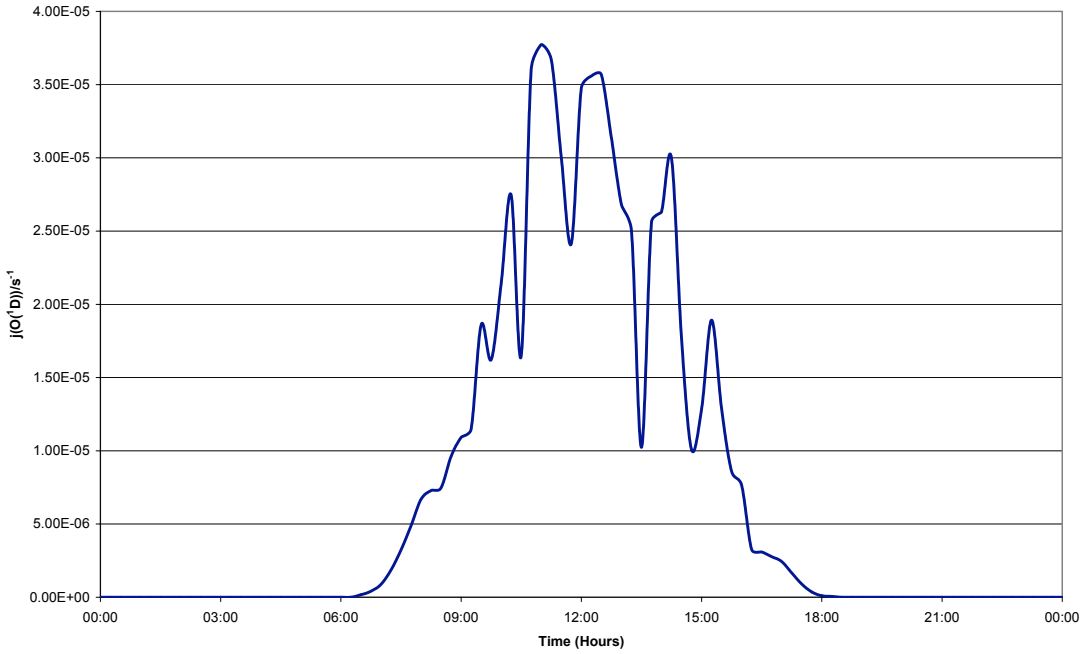

Figure 5.2.41 J(O^1D) observations recorded at Bukit Atur on JDay 117 (17th April 2008)

The results predicted by the OP3 model and the OP3 model containing the proposed Peeters scheme (OP3 Peeters) are displayed in figures 5.2.42 and 5.2.43 along with the measured concentrations for OH and HO_2 + RO_2 respectively. The OP3 Peeters model predicted higher concentrations than the OP3 model for OH, but lower concentrations for HO_2 + RO_2 (Table 5.2.7).

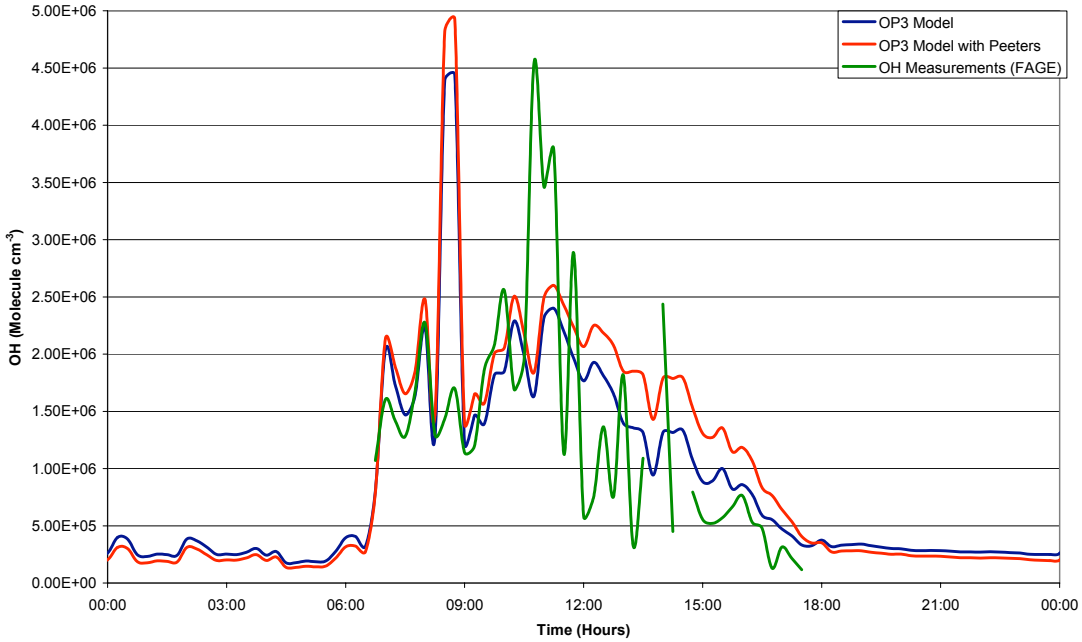

Figure 5.2.42 Model-measurement comparison of [OH] for day 117 (17/04/2008)

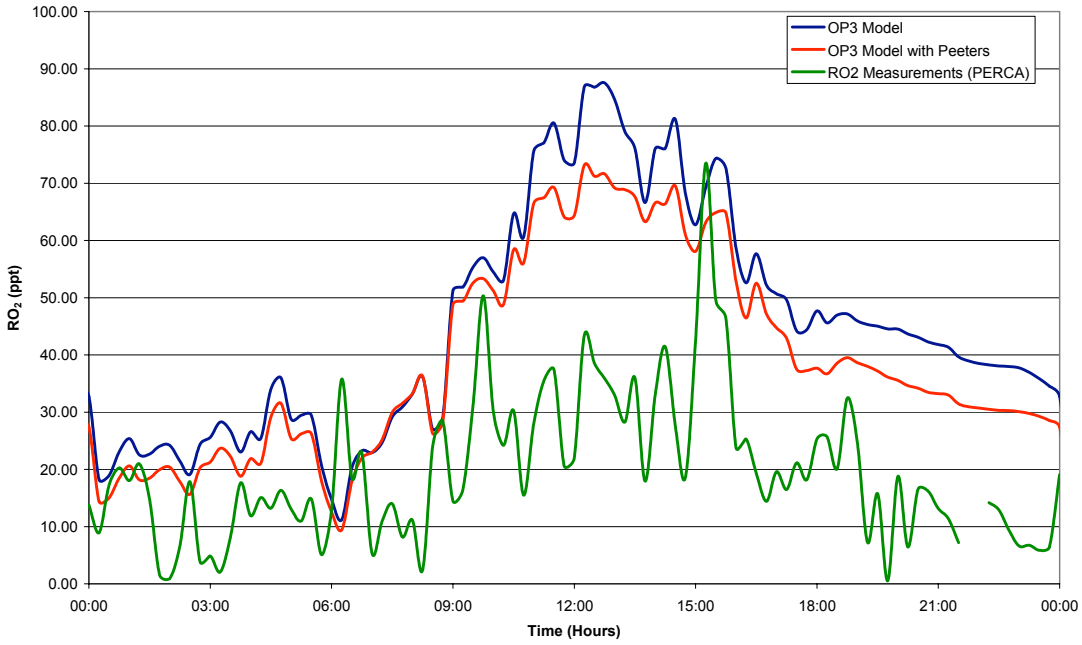

Figure 5.2.43 Model-measurement comparison of [$RO_2 + HO_2$] for day 117 (17/04/2008)

The OH profiles from both models shown in figure 5.2.42 display a reasonably typical diurnal pattern with the exception of a large peak in OH that both models predict at 08:45, coinciding with a large peak in NO and NO_2. There appears to be a smaller peak in the FAGE data at around 08:45 when compared to the model. Similarly the peak in measurements at 11:00 is not reproduced by the models.

The profiles of HO_2+RO_2 in figure 5.2.43 show a distinct diurnal profile and the observed values from the PERCA also observe a diurnal variation in the concentrations. The models both over predict the concentrations of HO_2+RO_2, including during late afternoon/evening, when concentrations are sustained in the model but not in the atmosphere..

Table 5.2.7 Average concentrations of OH and RO_2 + HO_2 at Bukit Atur on JDay 117 (17/04/2008) for the whole day, daytime (06:00 – 18:00), nighttime (00:00 – 06:00 and 18:00 – 24:00) and midday (11:00 -15:00).

		OH (Molecule cm^{-3})	RO_2 + HO_2 (ppt)
OP3 Model	Daily Average	$8.5X10^5$	44.7
	Daytime Average	$1.4X10^6$	55.9
	Nighttime Average	$2.8X10^5$	33.2
	Average between 11:00 and 15:00	$1.6X10^6$	77.2
OP3 Peeters	Daily Average	$9.5X10^5$	38.7
	Daytime Average	$1.7X10^6$	49.9
	Nighttime Average	$2.3X10^5$	27.2
	Average between 11:00 and 15:00	$2.0X10^6$	67.0
Measurements	Daily Average	$1.4X10^6$	19.7
	Daytime Average	$1.4X10^6$	26.5
	Nighttime Average	No Data Available	12.8
	Average between 11:00 and 15:00	$1.5X10^6$	31.7

Table 5.2.7 contains average values of OH and HO_2+RO_2 concentrations from both models and the observed values. The OH data displayed indicates that both the OP3 models over predict the concentration of OH from 11:00 to 15:00, with the OP3 model predicting closer to the average observed values. The values of HO_2+RO_2 in table 5.2.7 display the over prediction of both models especially during the period of 11:00 to 15:00, but the OP3 Peeters model over predicts to a lesser extent.

5.2.8 Day 120 (20th April 2008)

The air mass trajectory arriving at the Bukit Atur field site was predicted using the NOAA Hysplit model (figure 5.2.44). The NOAA model shows that the air mass arises over the sea to the northwest of the island, indicating that there is a change in the meteorology around Borneo. This indicates that the area maybe experiencing a change in the monsoon that influences the weather on the island, this change usually happens at this time of year (Hewitt et al., 2009). The airmass then moves from west to east, passing over Singapore, before circling round and approaching the field site from the southeast. There is a period of over 18 hours between the air mass arriving at Borneo and the field site at Bukit Atur, travelling from a northeast direction.

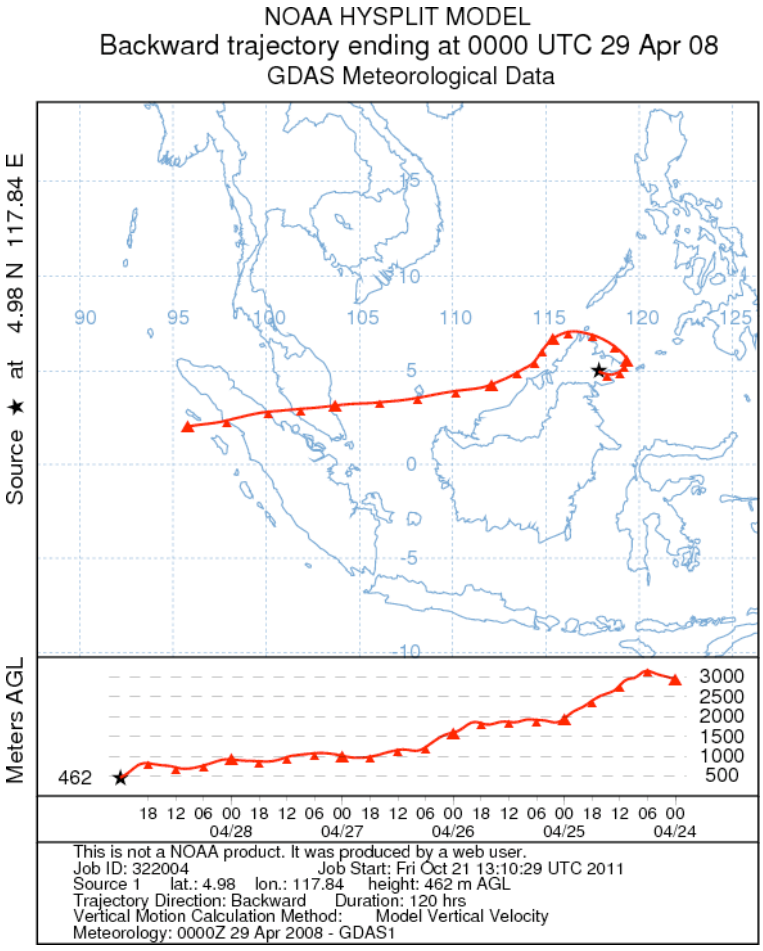

Figure 5.2.44 Air mass trajectory for 5 day arriving at the field site at 1200 hours (local time) on 20th April (JDay 120) The upper plot shows the path taken by the airmass travelling to the field site, for the 5 days previous to measurements being taken. The lower plot shows the altitude of the airmass for the 5 day period before arriving at the field site.

Figure 5.2.45 shows the concentrations of NO and NO_2 measured at the field site. The values of NO remain at a near constant value, except for a large peak observed at 06:00, where a large peak is also observed in the NO_2 concentration. There are also large peaks in NO_2 at 03:00 and 20:00.

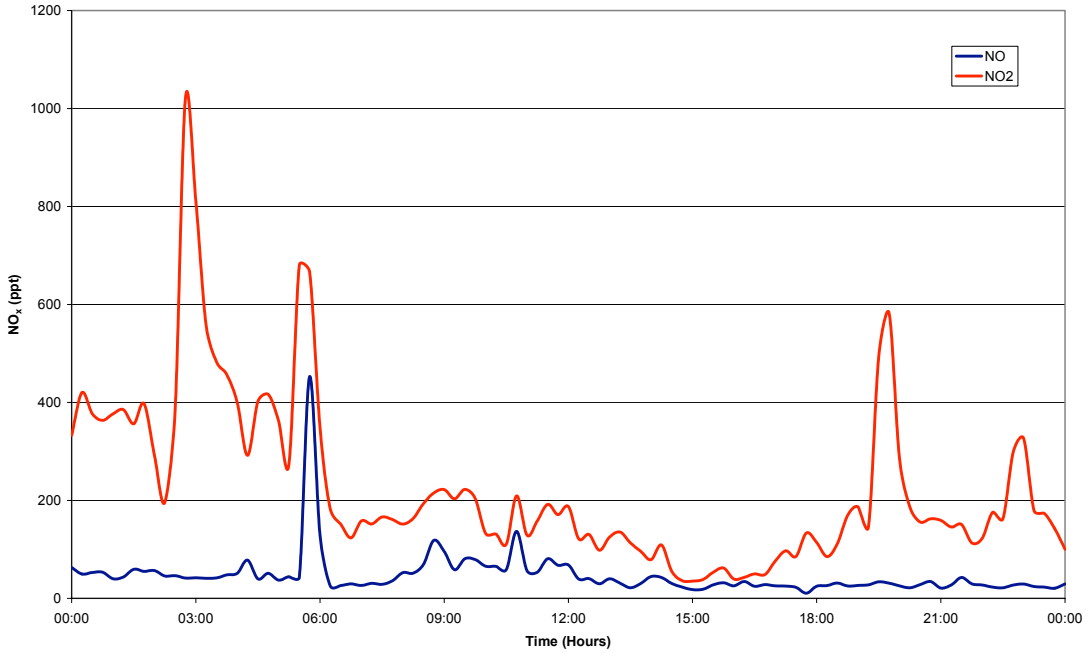

Figure 5.2.45 NO and NO_2 concentrations recorded at Bukit Atur on JDay 120 (20th April 2008)

The isoprene and temperature profile are shown in figure 5.2.46. Figure 5.2.47 displays the monoterpene concentrations, which were measured on this day using a GCMS, that were input into the model.

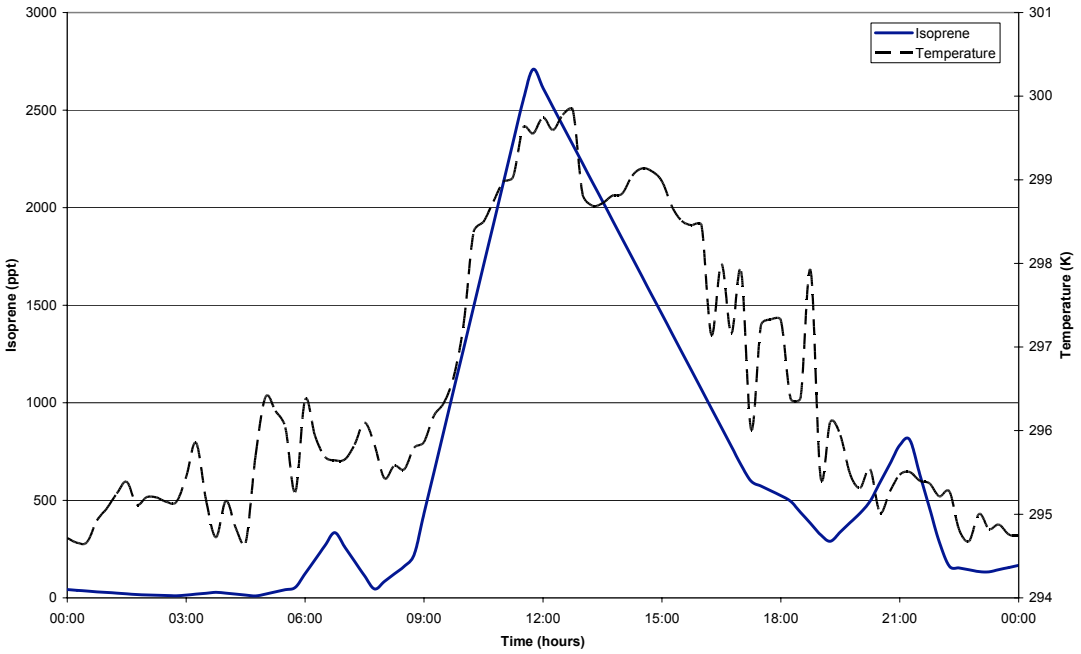

Figure 5.2.46 Isoprene concentrations recorded at Bukit Atur on JDay 120 (20th April 2008)

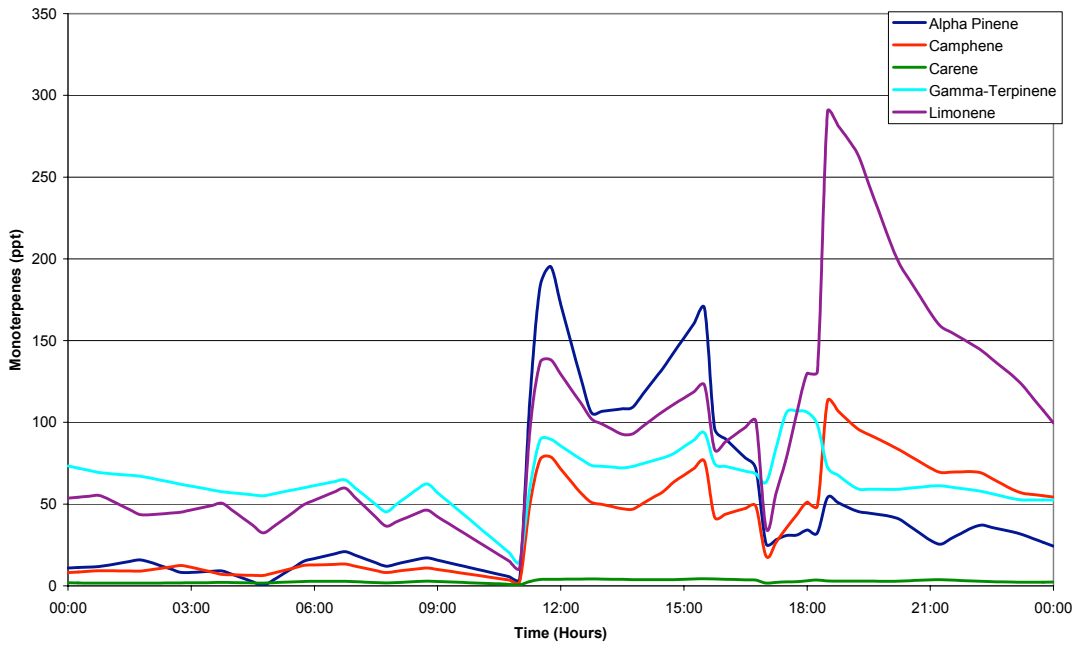

Figure 5.2.47 Average monoterpene concentrations from Bukit Atur used to model JDay 120 (20th April 2008) with the recorded temperatures.

The measurements of j($O(^1D)$) for day 120 are displayed in figure 5.2.54. The maximum value observed on this day was seen close to 12:00 as would be expected, but there is also significant cloud cover throughout the afternoon..

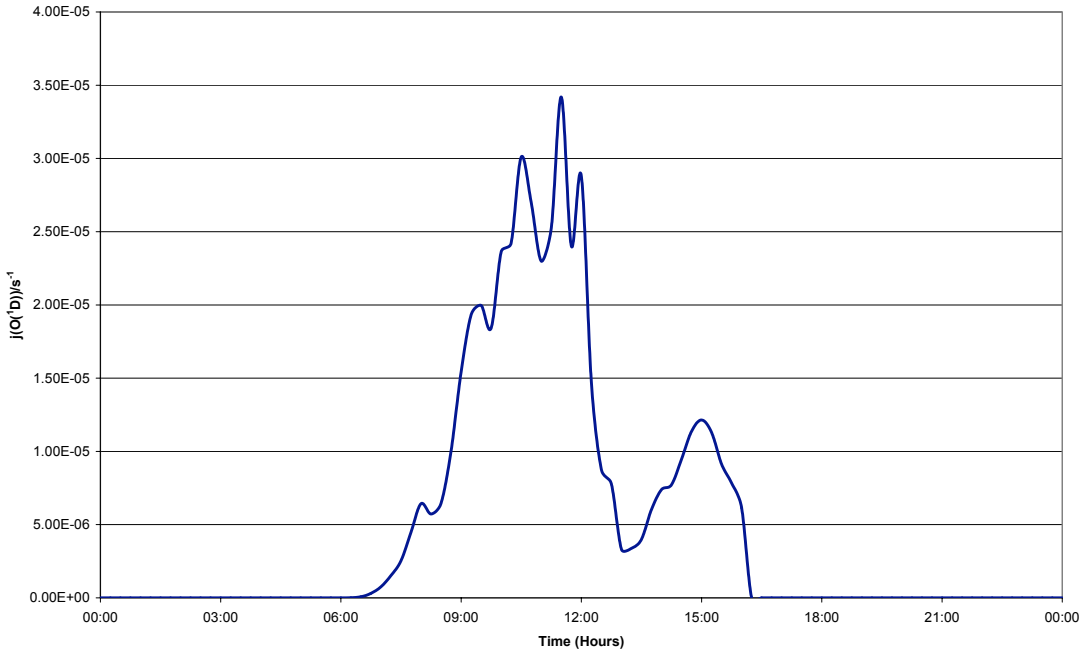

Figure 5.2.48 J(O^1D) observations recorded at Bukit Atur on JDay 120 (20th April 2008)

The results predicted by the OP3 model and the OP3 model containing the proposed Peeters scheme (OP3 Peeters) are displayed in figures 5.2.40 and 5.2.50 along with the measured concentrations for OH and HO_2 + RO_2 respectively. The OP3 Peeters model predicted higher concentrations than the OP3 model for OH, but lower concentrations for HO_2 + RO_2 (Table 5.2.8).

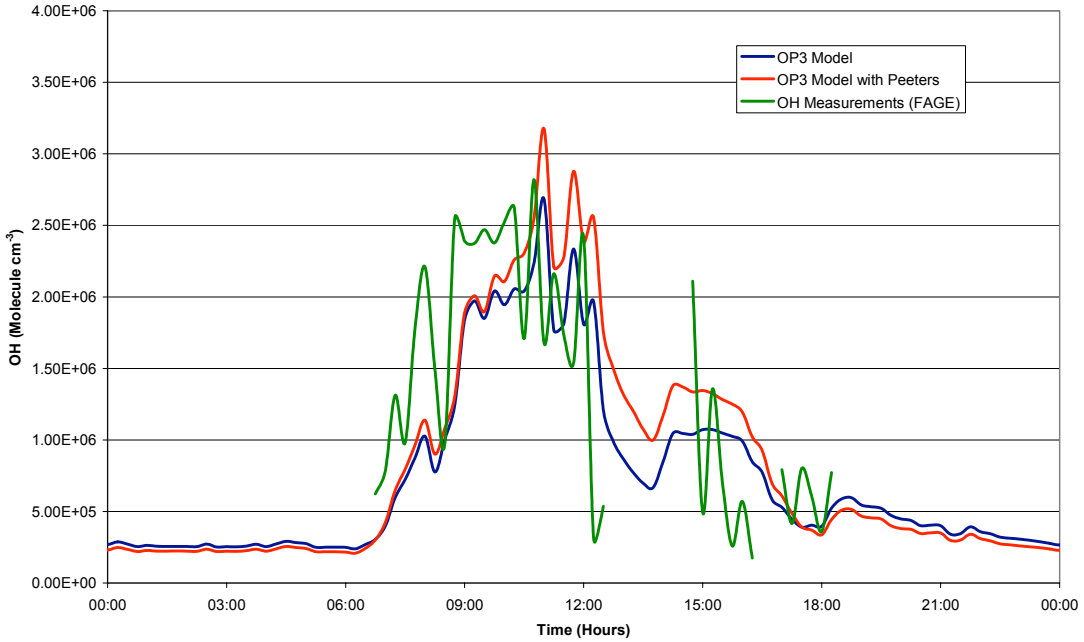

Figure 5.2.49 Model-measurement comparison of [OH] for day 120 (20/04/2008)

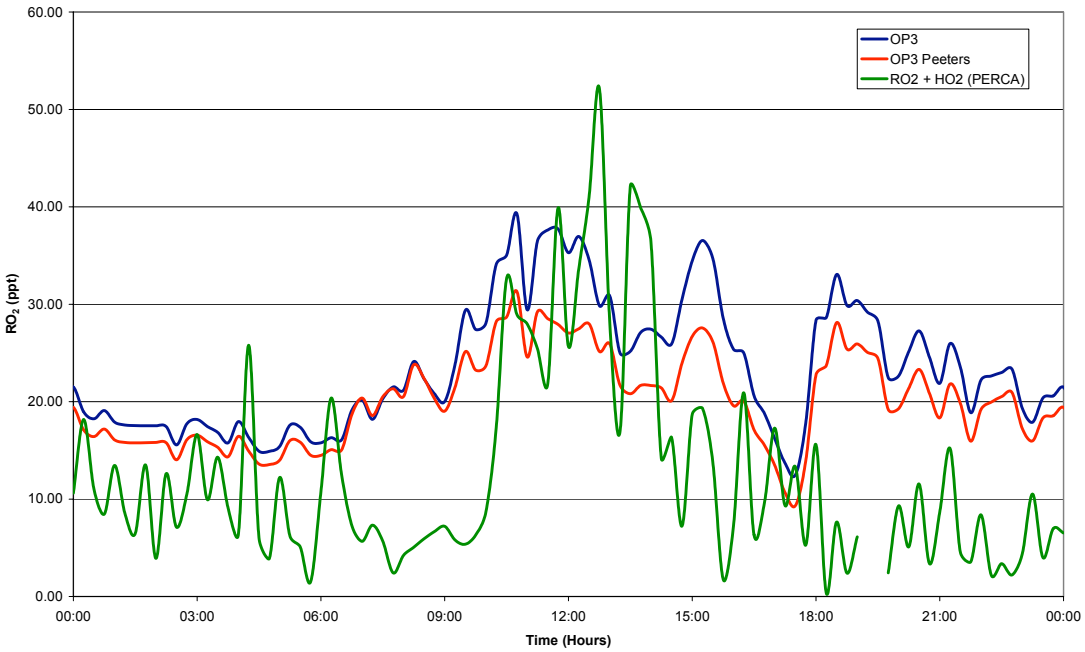

Figure 5.2.50 Model-measurement comparison of [HO_2 + RO_2] for day 120 (20/04/2008)

The predicted values of OH concentration are displayed in figure 5.2.49 with the limited observed OH data from FAGE. The two models and the observed concentrations increase from 06:30 until close to 12:00 when both suddenly decline. There are peaks in the observed concentration of OH at 08:00, 11:00 and 11:30 that both models also predict.

Table 5.2.8 Average concentrations of OH and $RO_2 + HO_2$ at Bukit Atur on JDay 120 (20/04/2008) for the whole day, daytime (06:00 – 18:00), nighttime (00:00 – 06:00 and 18:00 – 24:00) and midday (11:00 -15:00).

		OH (Molecule cm^{-3})	$RO_2 + HO_2$ (ppt)
OP3 Model	Daily Average	$7.3X10^5$	23.5
	Daytime Average	$1.1X10^6$	26.2
	Nighttime Average	$3.3X10^5$	20.8
	Average between 11:00 and 15:00	$1.3X10^6$	31.2
OP3 Peeters	Daily Average	$8.2X10^5$	20.1
	Daytime Average	$1.3X10^6$	21.9
	Nighttime Average	$2.9X10^5$	18.3
	Average between 11:00 and 15:00	$1.8X10^6$	24.8
Measurements	Daily Average	$1.4X10^6$	14.5
	Daytime Average	$1.4X10^6$	19.6
	Nighttime Average	$5.7X10^5$	9.5
	Average between 11:00 and 15:00	$1.4X10^6$	24.7

The average values in table 5.2.8 displays that the OP3 model over predicts the concentration of OH at 11:00 to 15:00, but the OP3 model under predicts the concentration at this stage. The OP3 model predicts the value of OH closer to the observed value at this time.

The average values of HO2+RO2from the models displayed in table 5.2.8 shows that both models over predict the concentration at 11:00 to 15:00. However, the OP3 Peeters model predicts the average HO_2+RO_2 closer to the observed values.

5.2.9 Summary of individual day data.

Table 5.2.9 contains the data for the OH concentration for the two models and the measured data from the FAGE instrument, but also contains data for the concentrations of NO, NO_2, VOCs and $J(O^1D)$. The table also contains details of the model to measured ratio for the OH concentration.

The results in table 5.2.9 illustrate that neither model consistently over predicted or under predicted the concentration of OH in the first phase of the campaign between 11:00 and 15:00. Also neither model consistently predicted concentrations closer to the observed values, unlike the second phase of the campaign where the OP3 Peeters model consistently predicted concentrations closest to the observed values. During the first phase of the campaign the day with the highest observed concentration of OH was day 115, where the observed concentration of OH was $2.4x10^6$ molecules cm^{-3}. This day also saw the closest replication of this concentration from both models with model/measured ratios of 0.9 and 1.0 for the OP3 and OP3 Peeters models respectively.

The results in table 5.2.10 displays similar behaviour to the results for HO_2+RO_2 to those seen in OH in table 5.2.9 with no one model having a better model to measured relationship. When the model to measured ratios are compared with the VOC:NO_X ratios there are no obvious trends, with some days where VOC:NO_X is low having good model to measurement agreement, and other days having very poor model to measurement agreement despite similar VOC:NO_X ratios.

The use of averaged VOC data for much of the first phase of the field campaign means that less confidence can be placed in these results compared to the second phase of the campaign. Only day 120 contains a full suite of the required input data. Further the, the absence of HO_2 measurements adds uncertainty to the predictions, particularly given that assumptions made regarding modelled HO_2 concentrations, in order to provide a modelled HO_2 + RO_2 concentration compared with measurements.

Table 5.2.9 Average modelled and measured values of OH between 11:00 and 15:00 during the first phase of the OP3 campaign.

	OH Concentrations (molecules cm^{-3})			NO (ppt)	NO_2 (ppt)	NO_x (ppt)	Isoprene (ppt)	$J(O^1D)$ (s^{-1})	VOC (ppbC)	Model / Measure	Model Peeters / Measured	VOC: NOx
JDay	Measured	Model	Model With Peeters									
111	$1.3X10^6$	$1.3X10^6$	$1.7X10^6$	60.9	111.6	172.5	4045.3	$1.2X10^{-5}$	24.3	1.0	1.3	140.9
112	$1.1X10^6$	$9.1X10^5$	$1.0X10^6$	54.3	109.6	163.9	1431.8	$1.2X10^{-5}$	11.1	0.8	0.9	67.8
113	$1.6X10^6$	$2.0X10^6$	$2.3X10^6$	43.7	65.2	108.9	1114.1	$2.1X10^{-5}$	9.5	1.2	1.4	86.9
114	No Data Available	$1.2X10^6$	$1.6X10^6$	80.1	186.9	267.0	2441.9	$3.6X10^{-6}$	16.1	NA	NA	60.4
115	$2.4X10^6$	$2.1X10^6$	$2.5X10^6$	49.4	76.7	126.1	1996.7	$2.7X10^{-5}$	13.9	0.9	1.0	109.8
116	$1.6X10^6$	$1.6X10^6$	$1.9X10^6$	34.4	99.1	133.5	1773.0	$2.6X10^{-5}$	15.2	1.0	1.1	113.8
117	$1.5X10^6$	$1.6X10^6$	$2.0X10^6$	27.0	60.2	87.2	3862.4	$2.7X10^{-5}$	14.9	1.1	1.3	170.4
120	$1.4X10^6$	$1.3X10^6$	$1.8X10^6$	42.2	116.0	158.2	2126.7	$1.4X10^{-5}$	14.3	0.9	1.2	90.4

Table 5.2.10 Average modelled and measured values of HO_2+RO_2 between 11:00 and 15:00 during the first phase of the OP3 campaign.

	RO_2 + HO_2 Concentrations (ppt)			NO (ppt)	NO_2 (ppt)	NO_x (ppt)	Isoprene (ppt)	$J(O^1D)$ (s^{-1})	VOC (ppbC)	Model/ Measure	Model Peeters / Measured	VOC: NOx
JDay	Measured	Model	Model With Peeters									
111	10.7	57.4	52.8	60.9	111.6	172.5	4045.3	$1.2X10^{-5}$	24.3	5.4	5.0	140.9
112	9.8	57.4	60.3	54.3	109.6	163.9	1431.8	$1.2X10^{-5}$	11.1	5.9	6.2	67.8
113	4.6	64.3	52.8	43.7	65.2	108.9	1114.1	$2.1X10^{-5}$	9.5	13.9	11.4	86.9
114	No Data Available	41.7	40.7	80.1	186.9	267.0	2441.9	$3.6X10^{-6}$	16.1	NA	NA	60.4
115	9.4	70.7	63.4	49.4	76.7	126.1	1996.7	$2.7X10^{-5}$	13.9	7.5	6.8	109.8
116	10.2	71.0	64.5	34.4	99.1	133.5	1773.0	$2.6X10^{-5}$	15.2	7.0	6.3	113.8
117	13.4	77.2	67.0	27.0	60.2	87.2	3862.4	$2.7X10^{-5}$	14.9	5.7	5.0	170.4
120	7.1	31.2	24.8	42.2	116.0	158.2	2126.7	$1.4X10^{-5}$	14.3	4.4	3.5	90.4

5.3 Rate Of Production Analysis (ROPA) for Phase 1

A rate of production analysis (ROPA) study was performed for day 120 during the first phase of the campaign. This day was chosen as it contained the most complete coverage of data through out this period of the field campaign. The results of the ROPA test display the difference between the OP3 model and the OP3 Peeters model (table 5.3.1). The comparison between the OP3 and OP3 Peeters model for day 120 shows the higher rates of initiation and termination in OH, HO_2 and RO_2. This is to be expected as the OP3 Peeters model predicts a larger concentration of OH than the OP3 model.

Another difference between the two models run for day 120 is that the OP3 Peeters model predicts a larger rate of HO_2 termination than initiation, which is the opposite of what is seen in the OP3 model. This is reflected in the model output, where the OP3 model predicts higher concentrations of HO_2+RO_2 than the OP3 Peeters model.

Table 5.3.1 ROPA data from the OP3 Peeters and OP3 model between 11:00 and 15:00 for day 120.

	120 OP3 Peeters	120 OP3
OH Initiation	61.5	18.1
OH Termination	22.6	12.8
HO2 Initiation	137.6	123.5
HO2 Termination	164.3	113.6
RO2 Initiation	67.0	53.4
RO2 Termination	54.1	48.3
OH-HO2	18.5	11.4
HO2-OH	96.2	18.5
OH-RO2	80.4	54.4
RO2-HO2	$9.7x10^{-4}$	$1.7x10^{-4}$
Initiation	354.9	232.7
Termination	334.7	220.3
% Difference	5.7	5.3
VOC (ppbC)	14.3	14.3
NO2 (ppb)	0.1	0.1
NO (ppb)	0.0	0.0
NOx (ppb)	0.2	0.2
JO1D	$1.4x10^{-5}$	$1.4x10^{-5}$

The individual components of the ROPA analysis of day 120 are displayed in figure 5.3.1. The higher rates of initiation and termination of OH, HO_2 and RO_2 seen through the photolysis reactions of the VOCs.

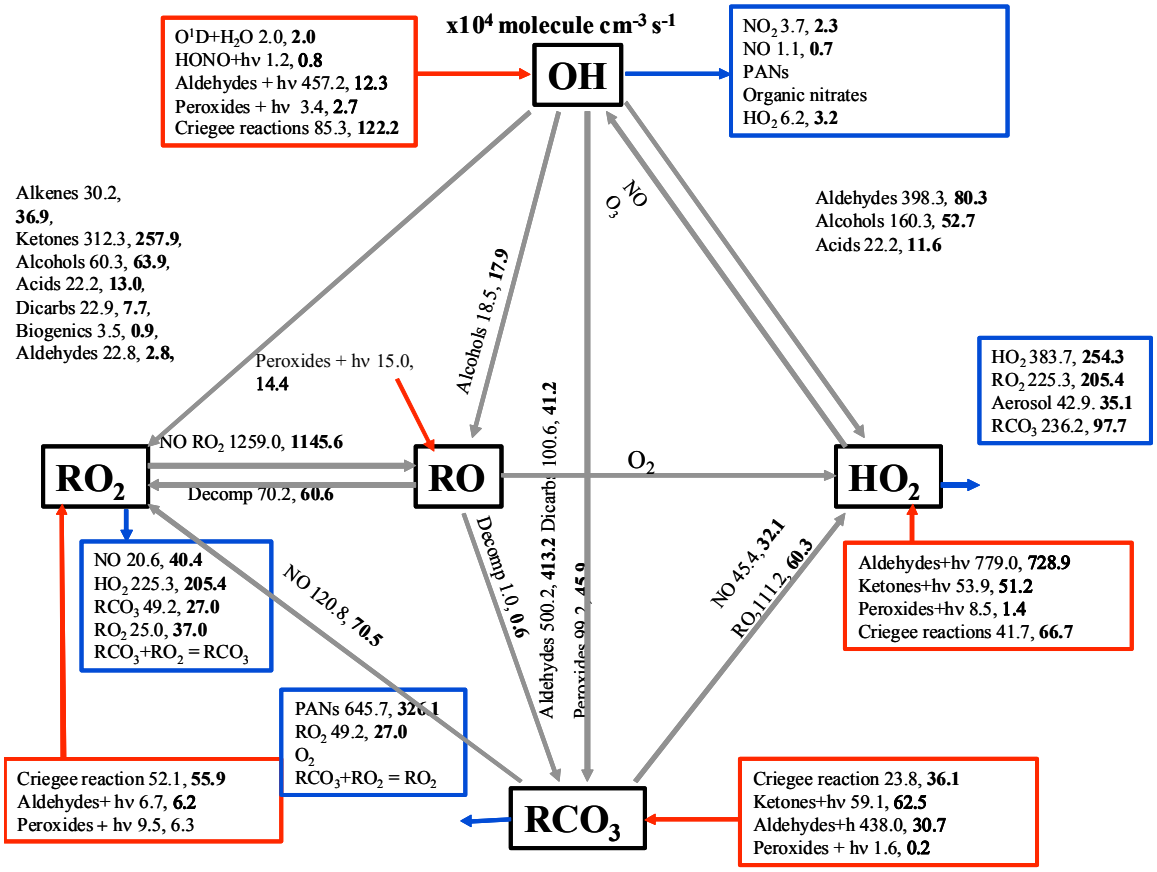

Figure 5.3.1 ROPA study of day 120 (11:00 to 15:00) for the OP3 Peeters model and **OP3 model**

The results of the ROPA study display similar results to the ROPA described in Chapter 4.3 for phase 2 of the field campaign. The addition of the Peeters mechanism leads to an increase in initiation by chemical reactions for all the radical sources, except the Criegee reactions where the OP3 model has higher rates of initiation. The aldehydes photolysis reactions in phase 1 show the same change as those observed in phase 2, with the OP3 Peeters model predicting a far greater rate of radical production through the photolysis of aldehydes species. This increase was expected, as previous theoretical work by Archibald et al. (2010) predicted that the rate of production of OH using the theoretical Peeters mechanism would be two orders of magnitude higher than with the existing MCM chemistry.

The ROPA from phase 1 demonstrates similar behaviour to that conducted for phase 2. In both phases the OP3 Peeters model displays much higher rates of radical initiation and termination than the OP3 model. Another similarity between the two phases of the campaign is that the OP3 Peeters model predicts a higher rate of HO_2 termination than initiation, which is the opposite of what is observed in the predictions from the OP3 model.

Chapter 6. Comparisons and Conclusions

6.1 Summary of Modelled Results from the Two Field Campaigns

The results from predicting the radical concentrations observed in the two phases of the Bukit Atur Field campaigns in April and July, described in chapters 4 and 5, produced similar results to other projects in forested regions, where models have been used to predict radical concentrations. The under prediction of OH and over prediction of HO_2 was also observed the AEROBIC (Carslaw et al., 2000).

This chapter aims to summarise how our understanding has developed from before OP3 and what needs to be studied in the future. Since the AEROBIC campaign data in 1999, the master chemical mechanism used to investigate field campaigns has undergone a number of updates. These have included both mechanism updates (branching ratios, pathways), but also rate coefficients. In particular, there are now detailed degradation schemes for beta-pinene and limonene that were not available in 1999. Therefore, this chapter first investigates the effect of using an updated mechanism on the AEROBIC data. The OP3 model and OP3 model with Peeters mechanism are both used for this purpose.

As well as comparing the model results for the two phases of the field campaign to the measured radical concentrations, the model to measurement agreement was examined relative to various input parameters, to attempt to discover the source of the discrepancy. The relationship of the model/measured ratio when compared to the VOC:NO_x ratio various field campaigns is investigated and compared to the results from the OP3 campaign, to see if different atmospheric conditions for other field studies cause a different relationship between VOC:NO_x and model/measured ratios.

Finally, to further investigate the reasons why there is an under prediction of OH and over prediction of HO_2 the OP3 and OP3 Peeters model results were subjected to various sensitivity tests. The results for these tests are discussed, and then final conclusions are drawn.

6.2 Impact of new model mechanism and results from the AEROBIC campaign

Previous field campaigns investigating radical chemistry in the atmosphere have also attempted to model the chemical processes leading to the production of OH, HO_2 and RO_2. One such campaign was the AEROBIC campaign based in north-west Greece during 1997 (Carslaw et al., 2001). In order to investigate the effect of an updated model mechanism, measured data from the AEROBIC data were run through the original AEROBIC model, the OP3 model and the OP3 Peeters model. These data represented the average concentrations over the course of the field campaign as reported in Carslaw et al., (2001)

The NO_X concentrations for the AEROBIC campaign were between 1 ppb and 1.5 ppb than those experienced during the OP3 project, especially around 08:00 (2.5 ppb higher) when the rush hour traffic in nearby towns and villages, led to peak in the observed concentrations of NO and NO_2 (figure 6.2.1). Compared to the OP3 field campaign, a wider range of biogenic species were measured during the AEROBIC campaign (figure 6.2.2). Concentrations and profiles were quite different for the two campaigns. Higher daytime O_3 during the AEROBIC campaign (60 ppb compared to 6 ppb) ensured that monoterpene concentrations were suppressed during the day and concentrations peaked at nighttime. Alpha-pinene was the monoterpene concentrations, and gamma-terpinene was much less important compared to OP3. Finally isoprene concentrations peaked much later in the day for AEROBIC compared to OP3 with maximum concentrations of 2.3 ppb, compared to 240 ppt.

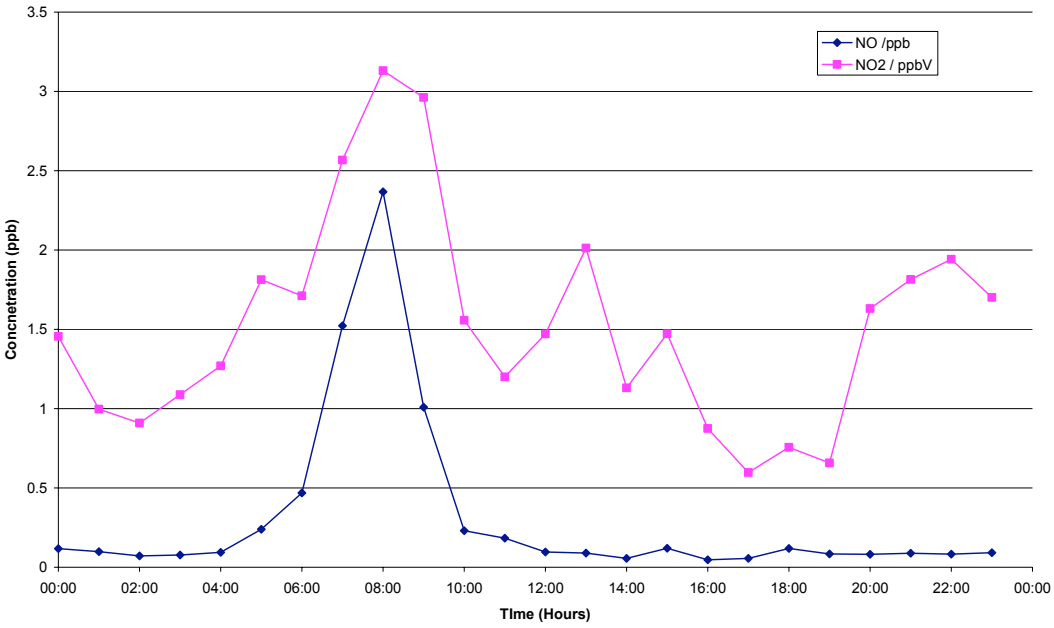

Figure 6.2.1 NO and NO_2 concentrations for an average day during the AEROBIC field campaign.

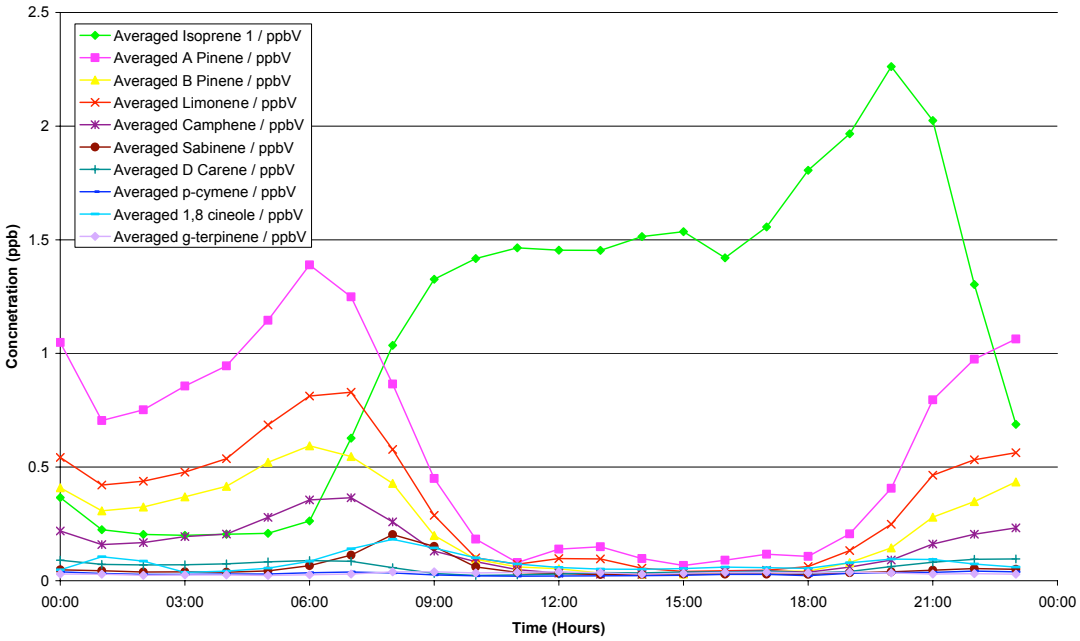

Figure 6.2.2 VOC concentrations for an average day during the AEROBIC field campaign.

The results of the model comparison for the AEROBIC field data are displayed in figures 6.2.3, 6.2.4 and 6.2.5 displaying the predicted concentrations for OH, HO_2 and RO_2 respectively.

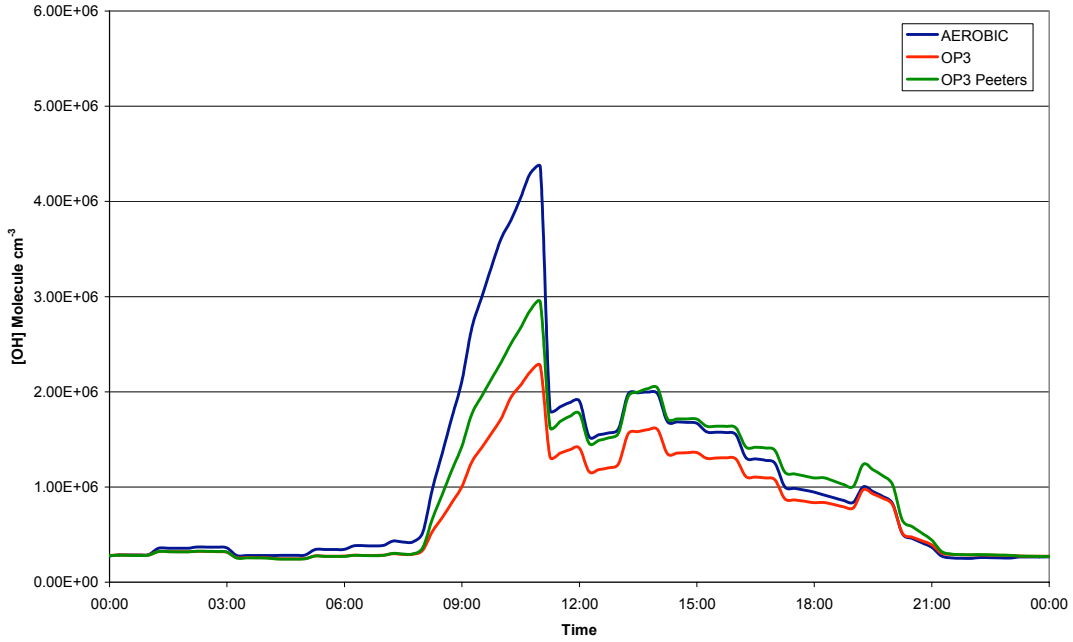

Figure 6.2.3 OH concentration from the AEROBIC average data predicted using the AEROBIC, OP3 and OP3 Peeters models.

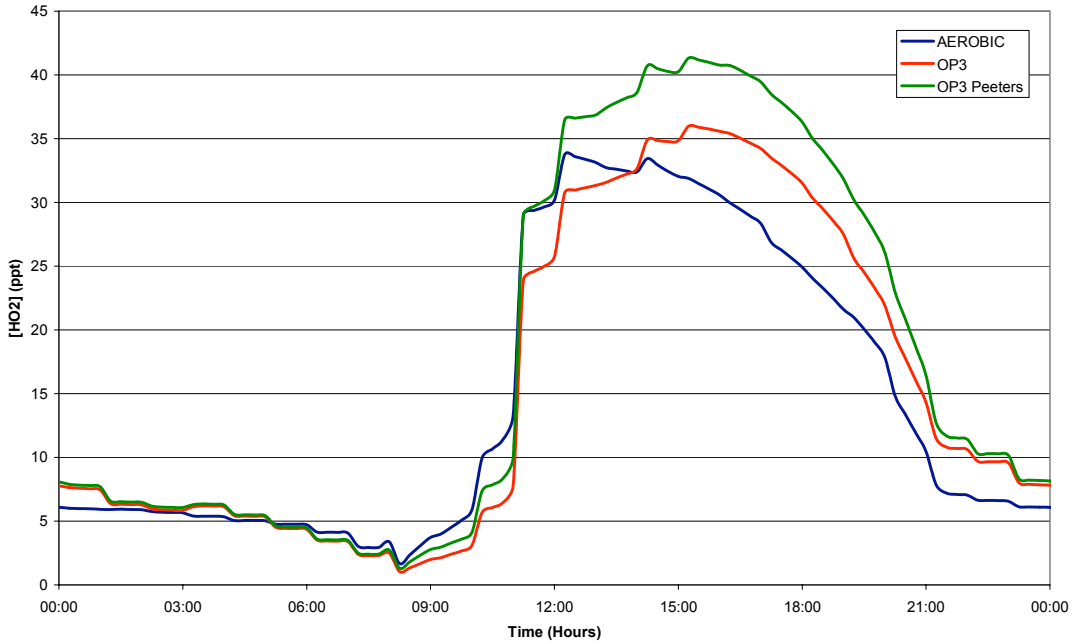

Figure 6.2.4 HO_2 concentration from the AEROBIC average data predicted using the AEROBIC, OP3 and OP3 Peeters models.

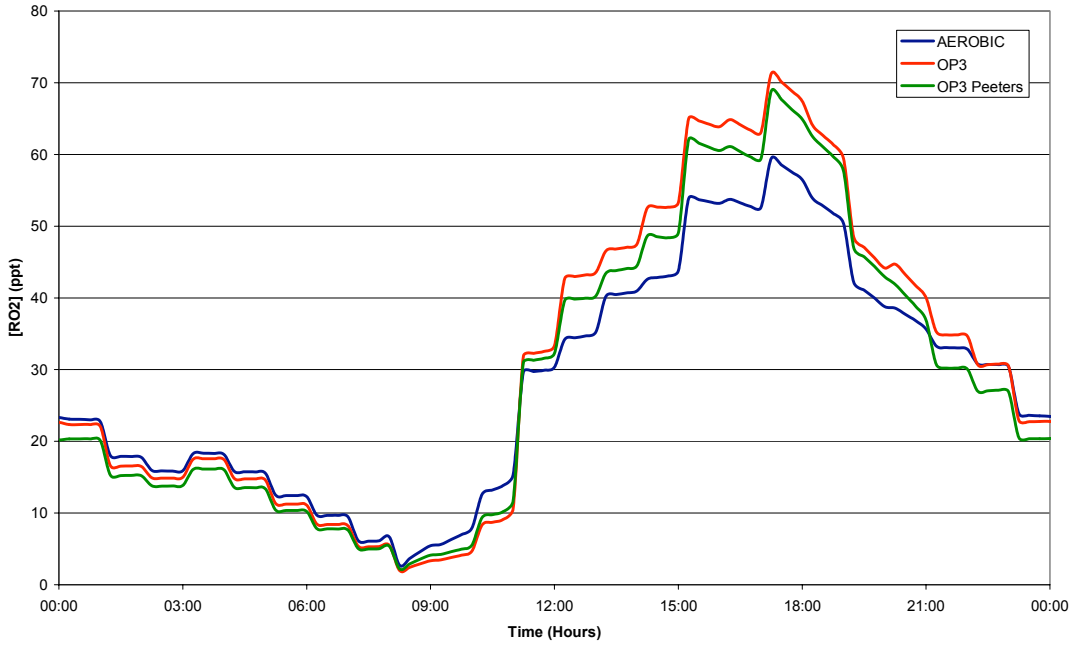

Figure 6.2.5 RO_2 concentration from the AEROBIC average data predicted using the AEROBIC, OP3 and OP3 Peeters models.

The profiles for all three species generated from the three models all show the same general profile throughout the average day, with all three models predicting highest peaks at the same point. The predicted maximum values for OH and RO_2 concentrations are predicted at the same time by all three models. The predicted OH concentration maximum values are at 11:00 (figure 6.2.4). The concentrations begins to increase at 08:00 in all three models when the value of $J(O(^1D))$ begins to increase, leading to the start of photochemical processes. This increase continues until 11:00, when there is a sudden decline in the concentrations predicted in all three models. This high predicted concentration of OH up until 11:00 is influenced by the presence of elevated NO_x and CO early in the morning from road traffic affecting the field site. The HO_2 profile for the AEROBIC average day data shows a slight difference between the AEROBIC and two OP3 models in the timing of the prediction of the maximum value of HO_2. The AEROBIC model predicts the maximum value at 11:00 and the OP3 model and OP3 Peeters model at 15:15. This indicates a difference in the production route of HO_2 between the AEROBIC and OP3 models in the mechanisms, probably linked to the more detailed biogenic species degradation mechanisms in the latter models. Also the HO_2 concentration is suppressed until late mainly by the rush hour NO concentration. This early suppression of peroxyradicals can also be seen in the RO_2 concentrations in figure 6.2.5

The values of the average concentrations for the three species are displayed in table 6.2.1, along with the observed values of OH and HO_2 from the field campaign (note that RO_2 measurements weren't made during this field campaign). In the original model runs, there was an under prediction of OH concentrations and an over prediction of HO_2 concentrations. The same trend was observed with the OP3 and OP3 Peeters model both for AEROBIC and OP3.

Table 6.2.1 Radical concentrations predicted by the AEROBIC, OP3 and OP3 Peeters models and measurements between 11:00 and 15:00 (using average data from the AEROBIC campaign)

Model	OH (molecules cm^{-3})	HO_2 (ppt)	RO_2 (ppt)
AEROBIC	$1.9x10^6$	31.0	35.8
OP3	$1.4x10^6$	29.3	41.9
OP3 Peeters	$1.8x10^6$	34.7	39.3
Measurements	$4.1x10^6$	15.6	

Table 6.1.1 indicates that the OP3 and OP3 Peeters models lead to a larger under prediction of OH than the original AEROBIC model compared to the AEROBIC model. However, the OP3 model predicts a slightly lower concentration of HO_2, compared to the AEROBIC model, whilst the OP3 Peeters model causes a larger over prediction of HO_2.

In summary, the use of more detailed chemical degradation mechanism for the biogenic species has made little difference to the overall radical predictions, and certainly cannot explain the discrepancy discovered in this original forested campaign.

6.3 Previous Campaign Comparisons of VOC : NO_x vs. OH Model : Measured Results

As described in chapter 4, the model/measured ratio for OH is found to be closer to 1 at lower values of VOC:NO_x for the OP3 campaign 2nd campaign. This section aims to investigate the same conclusion can be drawn for other campaigns, and to that end, results from the TORCH, AEROBIC and SOAPEX campaigns have also been studied (figure 6.3.1). The SOAPEX (Southern Ocean Atmospheric Chemistry Experiment) campaign was a very clean campaign in Tazmania, and modelled to measured results

have been discussed in Sommariva et al., (2004). Two very clean days with NO concentrations less than 10 ppt have been included on figure 6.3.1. The TORCH campaign was semi-polluted and six days are available for comparison on figure 6.3.1, along with four days from the AEROBIC campaign.

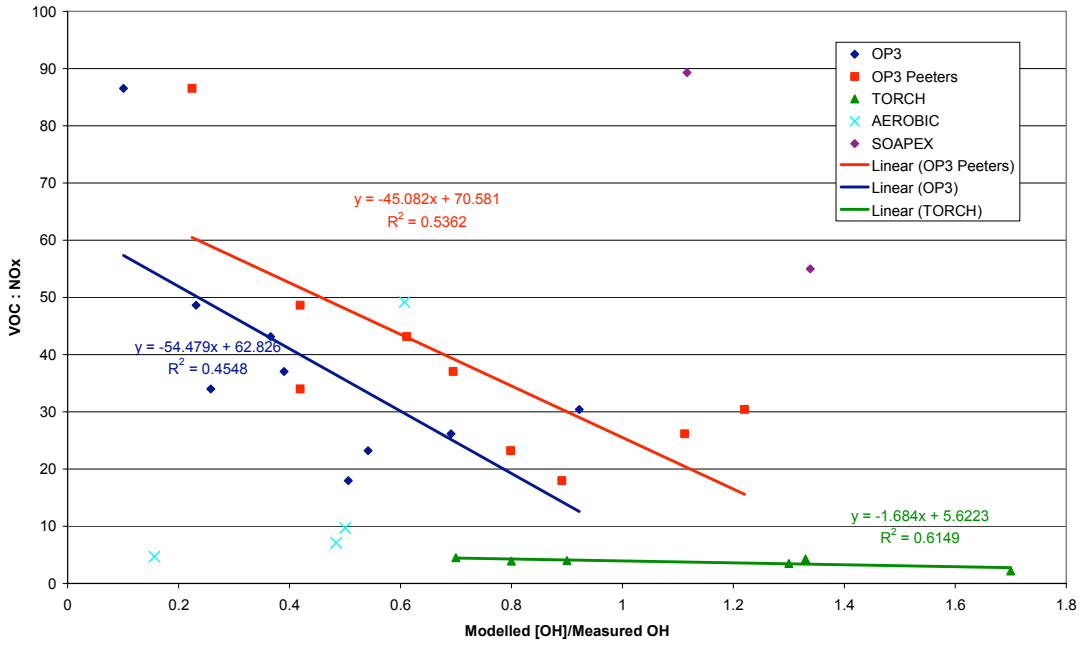

Figure 6.3.1. Modelled/Measured OH against VOC:NO_x ratios for OP3, TORCH, AEROBIC and SOAPEX field campaigns averages for 11:00 to 15:00

The field campaigns illustrated in figure 6.3.1 were conducted in different areas of the world with different atmospheric compositions. The results from SOAPEX were under high values of VOC:NO_x due to the low concentrations of NO. For the AEROBIC campaign lower values of VOC:NO_x becauseof the high concentrations of observed NO_x. The TORCH campaign had relatively low concentrations of NO_x and VOC giving the lower VOC:NO_x ratio. Figure 6.3.1 shows the results definitely improve as VOC:NO_X ratio decreases. The results from the other campaigns are less clear for TORCH the results are very flat (VOC:NO_X is very invariant), and for AEROBIC, results are very scattered, though some close to those for OP3. The SOAPEX data are at a much higher VOC:NO_X ratio du to the much lower NO concentration. For SOAPEX, a higher VOC:NO_x ration has better modelled measured agreement.

The VOC:NO_X is not the only issue that determines the measured:modelled agreement. High VOC:NO_x ratios are possible through high VOC or low NO_x and the same ratio could indicate very different chemical conditions. In particular, the proportion of biogenic VOC is an issue, especially given the uncertainties of biogenic VOC is an issue in their degradation mechanisms.

6.4 Sensitivity Analysis

The over prediction of HO_2 and under prediction of OH in the OP3 and OP3 Peeters models could be a result of incomplete chemistry or unmeasured species, in the models. It is already know that not all organic species at the site could be measured to provide data for constraining in the OP3 models. In order to explore the possible influence of these species on the chemistry in the models and the potential effects on the outputs of OH, HO_2 and RO_2, the models were run using increased levels of the most reactive and influential species already constrained in the models. These species were isoprene, limonene, gamma terpinene and camphene. In effect increasing the concentrations of these species acts as a surrogate for biogenic species present in the atmosphere at Bukit Atur, but not measured. It is likely, that a missing biogenic species would have behaved in a similar manner to those measured (in terms of maximum and minimum concentrations), if not in absolute terms through its chemical degradation in the atmosphere. The effect of increasing the concentration of NO was also investigated to explore the possibility of an unknown species with chemical properties similar to NO influencing the site and not being observed.

The results of the predictions from the model runs with doubled concentrations of monoterpenes, isoprene and NO were compared to the original OP3 (figures 6.4.1, 6.4.2, 6.4.3) and OP3 Peeters models and the measured values (figures 6.4.4, 6.4.5, 6.4.6). In order to perform the theoretical model runs, the data used was the average day data from the second phase of the field campaign.

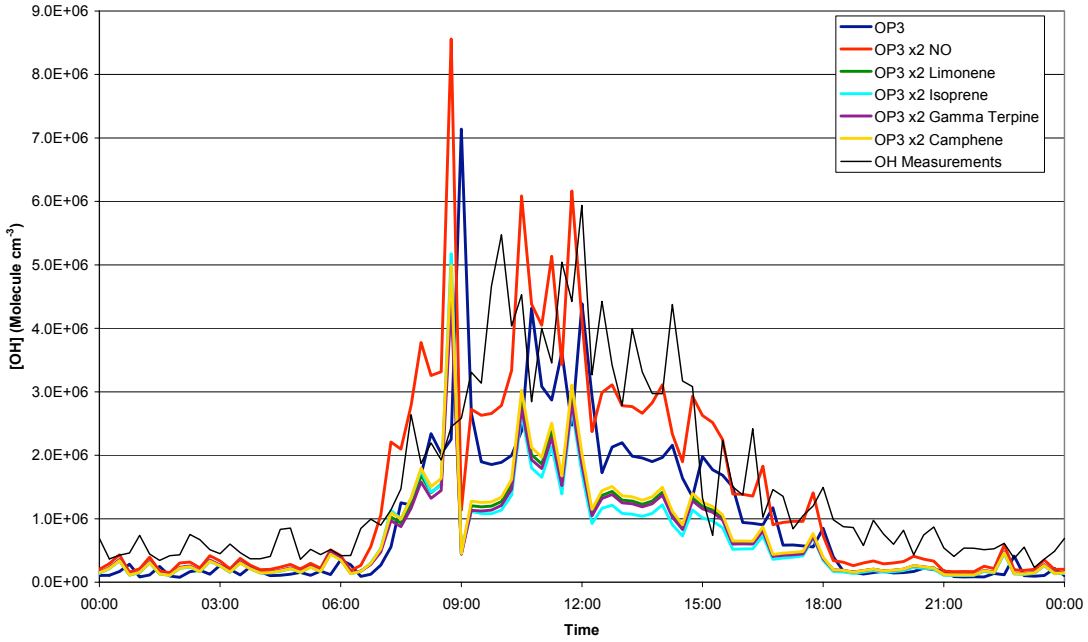

Figure 6.4.1 Predicted average OH profile from second phase of the OP3 field campaign at Danum Valley introducing increased VOC and NO concentrations to represent missing chemical species using the OP3 model.

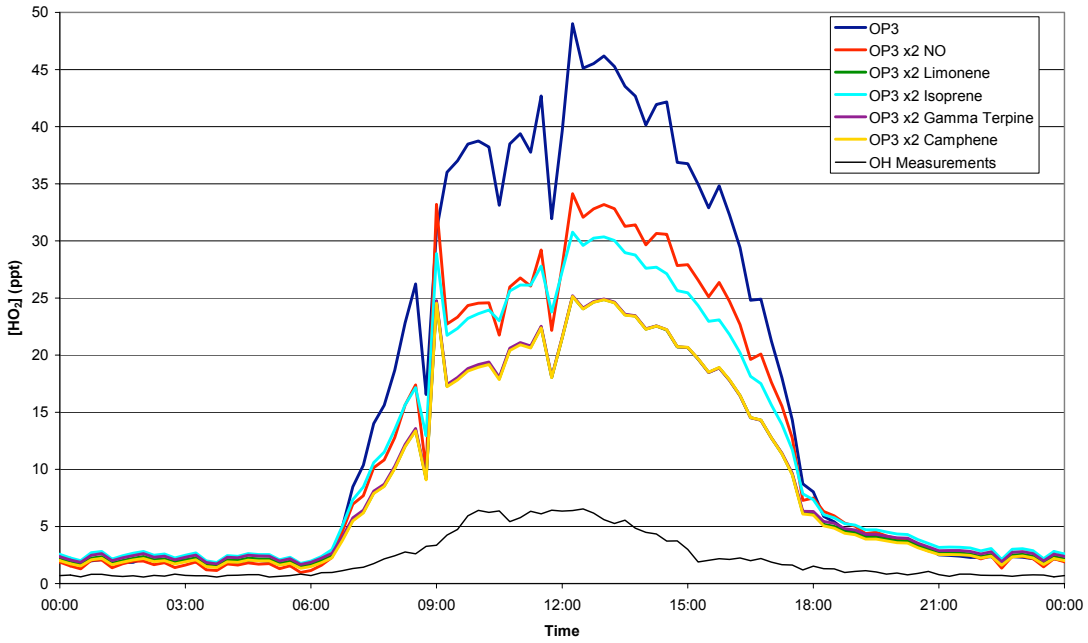

Figure 6.4.2 Predicted average HO_2 profile from second phase of the OP3 field campaign at Danum Valley introducing increased VOC and NO concentrations to represent missing chemical species using the OP3 model.

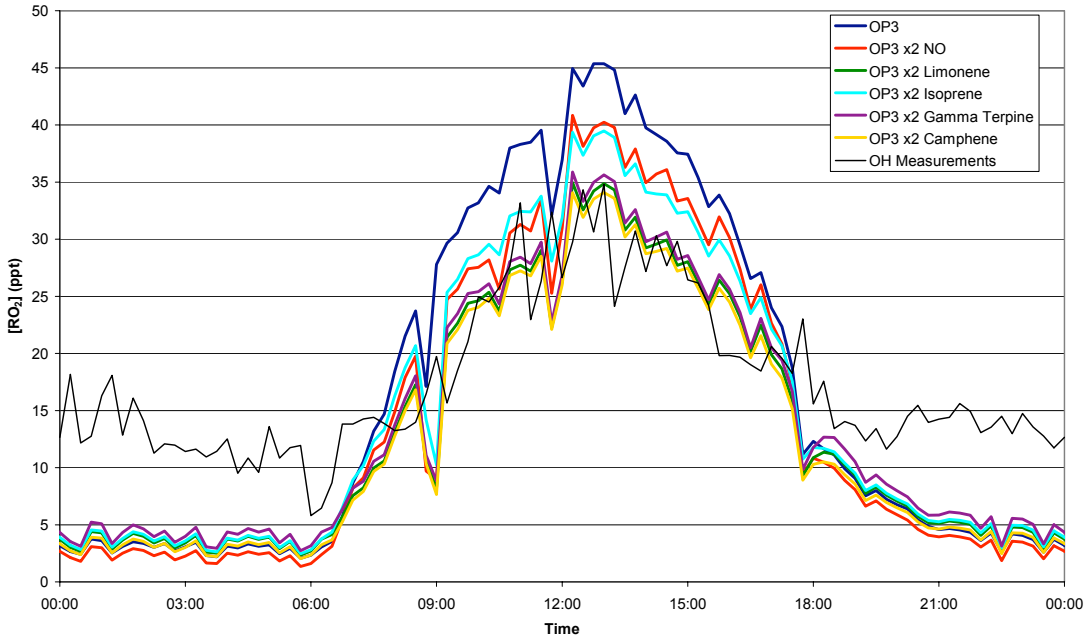

Figure 6.4.3 Predicted average RO_2 profile from second phase of the OP3 field campaign at Danum Valley introducing increased VOC and NO concentrations to represent missing chemical species using the OP3 model.

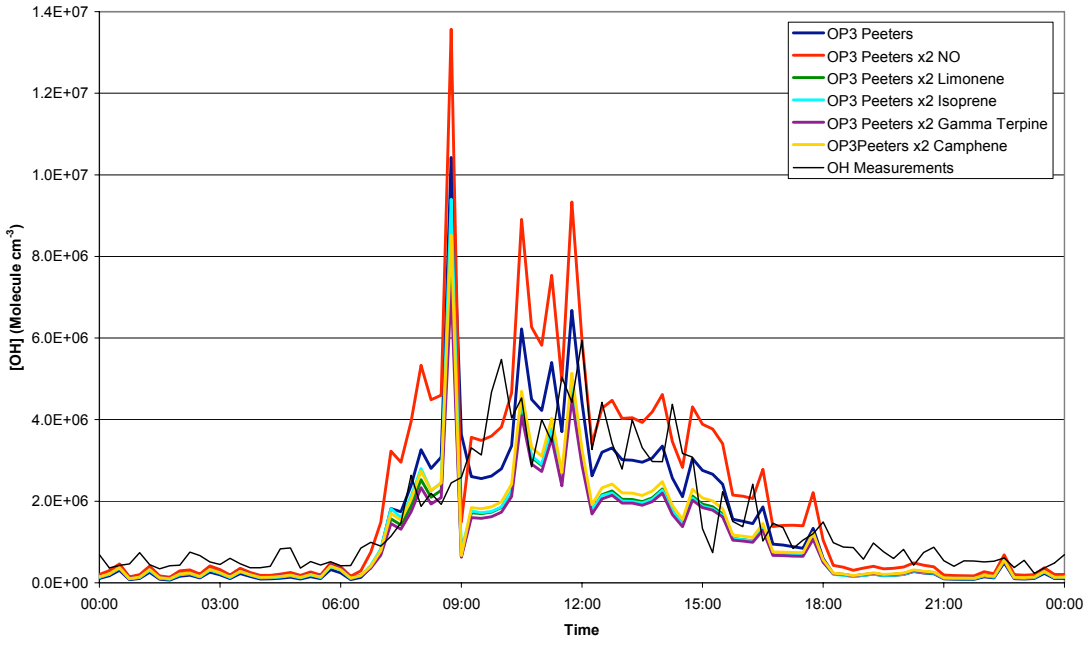

Figure 6.4.4 Predicted average OH profile from second phase of the OP3 field campaign at Danum Valley introducing increased VOC and NO concentrations to represent missing chemical species using the OP3 model.

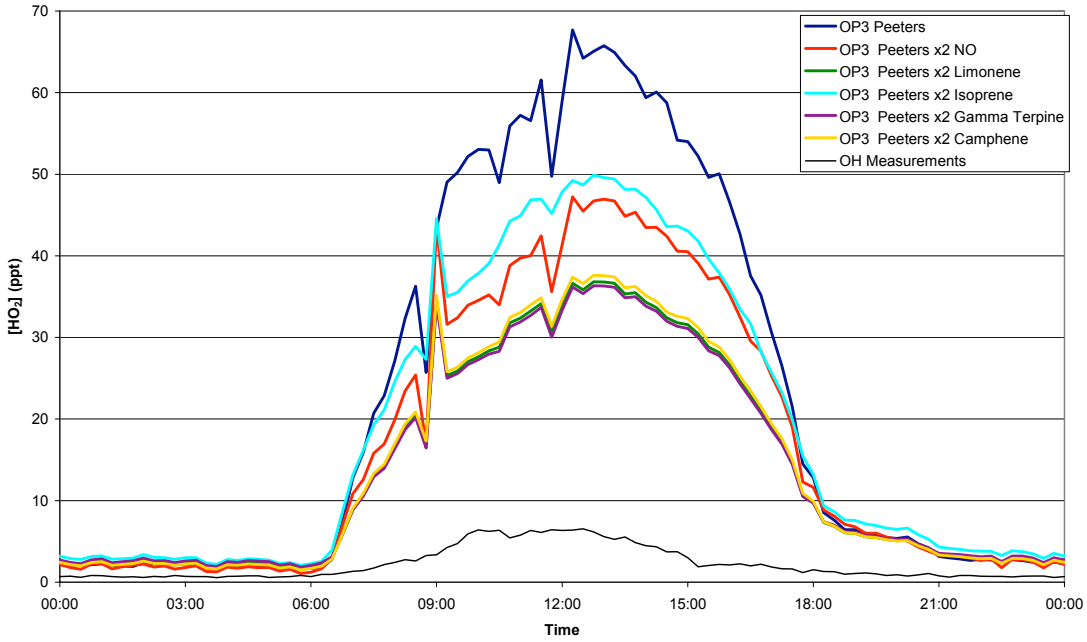

Figure 6.4.5 Predicted average HO_2 profile from second phase of the OP3 field campaign at Danum Valley introducing increased VOC and NO concentrations to represent missing chemical species using the OP3 model.

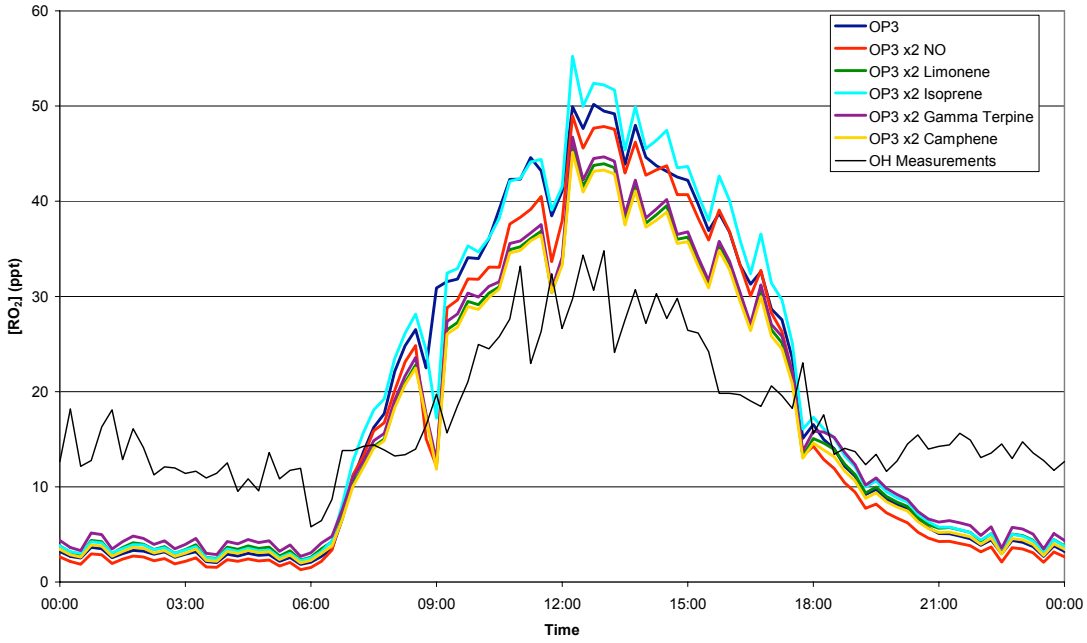

Figure 6.4.6 Predicted average RO_2 profile from second phase of the OP3 field campaign at Danum Valley introducing increased VOC and NO concentrations to represent missing chemical species using the OP3 model.

The effect of the addition of a doubled NO concentration to the output of OH can be seen in figures 6.4.1 and 6.4.4 for the OP3 model and OP3 Peeters model

respectively. The doubling of NO leads to an increase in OH concentrations from both models during the 11:00 to 15:00 phase of the chemistry. In figures 6.4.1 and 6.4.4 it can be observed that the effect of doubling any of the VOC concentrations leads to a reduction in the predicted concentration of OH during the reactive period. The predicted concentrations of HO_2 for the OP3 model and OP3 Peeters model (figures 6.4.2 and 6.4.5) observe a decline through the doubling of any VOC concentration being doubled or the NO concentration being doubled. In both models the monoterpene concentrations being doubled has the largest effect on reducing the predicted concentrations of HO_2, particularly those of limonene and gamma terpinene. There were differences in the effects of doubling the concentrations of isoprene and NO in the OP3 and OP3 Peeters models. In the OP3 model, isoprene had a greater influence on reducing the predicted concentration of HO_2 whereas in the OP3 model, the effect of NO was greater in reducing the predicted values of HO_2 (table 6.4.1).

Table 6.4.1. Predicted concentrations of OH, HO_2 and RO_2 between 11:00 and 15:00 using the average day data in the second phase of the OP3 campaign, with increased concentrations of NO and VOCs.

		OH (Molecule cm^{-3})	HO_2 (ppt)	RO_2 (ppt)
Original Data	OP3 Model	$2.3x10^6$	39.6	38.9
	OP3 Peeters Model	$3.6x10^6$	59.0	44.3
x2 NO	OP3 Model	$3.2x10^6$	28.8	34.3
	OP3 Peeters Model	$4.8x10^6$	42.6	42.4
x2 Limonene	OP3 Model	$1.5x10^6$	21.8	29.3
	OP3 Peeters Model	$2.4x10^6$	33.6	38.2
x2 Isoprene	OP3 Model	$1.3x10^6$	26.9	33.8
	OP3 Peeters Model	$2.4x10^6$	46.2	46.1
x2 Gamma Terpinene	OP3 Model	$1.4x10^6$	21.9	30.0
	OP3 Peeters Model	$2.3x10^6$	33.1	38.8
x2 Camphene	OP3 Model	$1.6x10^6$	21.8	28.7
	OP3 Peeters Model	$2.6x10^6$	34.4	37.7
Measurements		$3.6x10^6$	5.3	29.1

Similarly to the effect on HO_2, the doubling of the monoterpene concentrations caused the largest reduction in the predicted concentrations of RO_2 in the OP3 (figure 6.4.3) and OP3 Peeters model (figure 6.4.6). Differences were observed between the two models under the influence of doubled isoprene and NO concentrations. In the OP3 model, by doubling the concentration of isoprene or NO, the predicted concentrations of RO_2 decreased in both cases. In the OP3 Peeters model, the addition of NO caused a decrease in predicted RO_2 concentrations whereas isoprene caused an increase in the predicted RO_2 concentrations.

The best agreement for OH is the original OP3 Peeters model: all sensitivity tests make the level of agreement worse. However, doubling the NO concentration brings the OP3 model into better agreement with the measurements. For HO_2, the best agreement was between the measurements and the OP3 model with doubled limonene, gamma-terpinene or camphene concentrations. Doubling the limonene or camphene also bought RO_2 into better agreement with the measurements for the OP3 model.

The addition of an increased concentration of one species in the models did not singularly rectify the problems with modelling the chemistry at Bukit Atur. The influence of additional monoterpene concentrations reducing HO_2 predictions demonstrates that potentially missing VOC species could be leading to an over prediction of HO_2. However, the introduction of extra monoterpenes and other VOCs would have a negative influence on the prediction of OH concentrations (figures 6.4.1, 6.4.4, and table 6.4.1), as the chemical mechanis, stands at the moment, and assuming the experimental data are correct.

The results of these experimental model runs indicate that a more complete profile of VOCs must be included in models when the system being replicated is complex, but also that there is still potentially a species missing from the system that will generate OH to compensate for the OH lost through reactions with the additional VOCs.

The theoretical Peeters mechanism was proposed as a novel, but theoretical, method of HOx regeneration following OH-initiated oxidation of isoprene (Peeters et al., 2009). The new reaction pathways aimed to explain the much higher measured than modelled concentrations of OH radicals in tropical forests (Nguyen et al., 2010), as observed in campaigns such as PROPHET (Tan et al., 2001), AEROBIC (Carslaw et

al., 2001) and GABRIEL (Lelieveld et al., 2008) (Tan et al., 2001; Thornton et al., 2002; Ren et al., 2008; Butler et al., 2008; Kubistin et al., 2010; Lelieveld et al., 2008; Martinez et al., 2010; Hofzumahaus et al., 2009; Pugh et al., 2010; Wolfe et al., 2011; Whalley et al., 2011)

The Peeters mechanism suggests new pathways to OH, HO_2 and highly photolabile aldehydes, which can lead to HO_x regeneration in forested area. However, the mechanism is theoretical at the moment and needs confirmation through laboratory experiments. In addition, there is currently debate over how much OH HPALDs can actually produce and further experimental work to determine the exact yield of OH would be beneficial

The OP3 work appears to show that the proposed Peeters mechanism does not explain the whole story of the chemistry in the atmosphere above forests. These conclusions are supported by Stone et al. (2011) who found that in line with previous work in tropical forests, the standard model based on MCM chemistry significantly under estimates the observed OH concentrations. Stone et al. (2011) also observed that of the current suggestions for improving isoprene degradation in mechanisms, none can simultaneously remove the bias from both OH and HO_2 simulations at the present time.

6.5 Conclusions

This thesis has reported model to measured comparisons for the OP3 campaign in Borneo 2008. Two campaigns were held in April and July that year, although data coverage was sparse. For the July campaign, OH concentrations were under predicted relative to measured values, whilst those for HO_2 were under predicted. The adoption of a new mechanism for isoprene degradation improved agreement for OH, but made model predictions worse for HO_2. The results of adding the isoprene degradation mechanism had varied effects on the predicted concentrations of RO_2 in comparison to observed vales. Clearly the OP3 campaign has not been able to answer all of the questions it aimed to address, though it has added to the evidence that shows we do not currently understand the atmospheric chemistry in areas that are strongly influenced by biogenic emissions.

What is required now is a suite of laboratory experiments that aim to: elucidate key features of isoprene degradation, including rate coefficients, reaction pathways (including photolysis rates. Also required is further research into dry deposition as the sensitivity studies discussed in chapter 3 displayed how sensitive models are to changes in the deposition rates..

Future field campaigns must include OH, HO_2 and preferably speciated RO_2 concentrations as this helps to elucidate the degradation pathways of VOCs. A full suite of biogenic VOCs, better sensitivity and a wider range of measurements. Also a wider range of secondary species (e.g HPALDs, organic nitrates and other carbonyls) as well as high quality ancillary measurements (NO_x O_3, CO and a wider range of photolysis rates.).

7. References

Alicke, B., Hebestreit, K., Stutz, J., Platt, U. 1999. Iodine oxide in the marine boundary layer. Nature. 397: 572–573

Archibald, A. T., Cooke, M. C., Utembe, S. R., Shallcross, D. E., Derwent, R. G., Jenkin, M. E.: Impacts of mechanistic changes on HOx formation and recycling in the oxidation of isoprene. Atmos. Chemistry and Physics. 2010. 10, 8097–8118

Archibald, A. T., Levine, J. G., Abraham, N. L., Cooke, M. C., Edwards, P. E., Heard, D. E., Jenkin, M. E., Pike, R. C., Monks, P., Shallcross, D. E., Teford, P. J., Whalley, L. K., Pyle, J. A. 2011. Impacts of HOx regeneration and recycling in the oxidation of isoprene: Consequences for the composition of past, present and future atmospheres, Geophysical Research. Letters. 38

Bloss, C., Wagne, V., Jenkin, M. E., Volkamer, R.,Bloss W. J., Lee, J. D., Heard, D. E., Wirtz, K., Martin-Reviejo, M.., Rea, G., Wenger, J. C., Pilling, M. J., 2005. Development of a detailed chemical mechanism (MCMv3.1) for the atmospheric oxidation of aromatic hydrocarbons. Atmospheric Chemistry and Physics 5(3): 641-664.

Bonn, B., Moorgat, G. K. 2002. New particle formation during a- and b-pinene oxidation by O3, OH and NO3, and the influence of water vapour: particle size distribution studies. Atmospheric Chemistry and Physics 2(3): 183-196.

Butler, T. M., Taraborrelli, D., Br¨uhl, C., Fischer, H., Harder, H., Martinez, M., Williams, J., Lawrence, M. G., and Lelieveld, J. 2008. Improved simulation of isoprene oxidation chemistry with the ECHAM5/MESSy chemistry-climate model: lessons from the GABRIEL airborne field campaign. Atmospheric Chemistry and Physics. 8,
4529–4546

Carslaw, N., Creasey, D. J., Harrison, D., Heard, D. E., Hunter, M. C., Jacobs, P. J., Jenkin, M. E., Lee, J. D., Lewis, A. C., Pilling, M. J., Saunders, S. M., and Seakins, P. W. 2001. OH and HO2 radical chemistry in a forested region of north western Greece. Atmospheric Environment 35: 4725-4737.

Chen, J., Griffin, R. J. 2005. Modelling secondary organic aerosol formation from oxidation of a-pinene, b-pinene and d-limonene. Atmospheric Environment 39: 7731-7744.

Claeys, M., Graham, B., Vas, G., Wang, W., Vermylen, R. Pashnyshka, V., Cafmeyer J., Guyon, P., Andreae, M., Artaxo, P., Maehutt, W. 2004. Formation of Secondary Organic Aerosols through Photooxidation of Isoprene. Science 303: 1173-1176

Da Silva, G., Graham, C., Wang, Z. 2009. Unicmolecular β-Hydroperoxy Radical Decomposition with OH Recycling in Photochemical Oxidation of Isoprene. Environmental Science and Technology. 44: 250-256

Emmerson, K. M., Carslaw, N., Carslaw., D. C., Lee, J. D., McFiggans, G., Bloss, W. J., Gravestock, T., Heard, D. E., Hopkins, J., Ingham, T., Pilling, M. J., Smith, S. C., Jacob, M. J., Monks, P .S. 2007. Free radical modelling studies during the UK TORCH Campaign in summer 2003. Atmospheric Chemistry and Physics 7(1): 167-181.

Faloona, I. (2001). "Nighttime observations of anomalously high levels of hydroxyl radicals above deciduous forest canopy." Journal of Geophysical Research 106: 24315-24333.

Griffin, R. J., Crocker, D. R., Seinfeld, J. H. 1999. Incremental Aerosol Reactivity: Application to Aromatic and Biogenic Hydrocarbons. Environmental Science and Technology 1999(33): 2403-2408.

Hasson, A. S., Tyndall, G. S., Orlando, J. J. 2004. A product yield study of the reaction of HO2 radicals with ethyl peroxy (C2H5O2), acetyl peroxy (CH3C(O)O2), and acetonyl peroxy (CH3C(O)CH2O2) radicals, Journal of Physical. Chemistry. 108: 5979–5989,

Heard, D. E., Pilling, M. J. 2003. Measurement of OH and HO2 in the Troposphere. Chemistry Review 103: 5163-5198.

Hewitt, C. N., Lee, J. D., MacKenzie, A. R., Barkley, M. P., Carslaw, N., Carver, G. D., Chappell, N. A., Coe, H., Collier, C., Commane, R., Davies, F., Davison, B., DiCarlo, P., Di Marco, C. F., Dorsey, J. R., Edwards, P. M., Evans, M. J., Fowler, D., Furneaux, K. L., Gallagher, M., Guenther, A., Heard, D. E., Helfter, C., Hopkins, J., Ingham, T., Irwin, M., Jones, C., Karunaharan, A., Langford, B., Lewis, A. C., Lim, S. F., MacDonald, S. M., Mahajan, A. S., Malpass, S., McFiggans, G., Mills, G., Misztal, P., Moller, S., Monks, P. S., Nemitz, E., Nicolas-Perea, V., Oetjen, H., Oram, D. E., Palmer, P. I., Phillips, G. J., Pike, R., Plane, J. M. C., Pugh, T., Pyle, J. A., Reeves, C. E., Robinson, N. H., Stewart, D., Stone, D., Whalley, L. K., Yin, X. 2010. Overview: oxidant and particle photochemical processes above a south-east Asian tropical rainforest (the OP3 project): introduction, rationale, location characteristics and tools. Atmospheric Chemistry and Physics. 10, 169–199

Hofzumahaus, A., Rohrer, F., Lu, K., Bohn, B., Brauers, T., Chang, C. C., Fuchs, H., Holland, F., Kita, K., Kondo, Y., Li, X., Lou, S., Shao, M., Zeng, L., Wahner, A., Zhang, Y. 2009.Amplified trace gas removal in the troposphere. Science. 324: 1702–1704,

Hurst, J. M. (2001). "Investigation of the nighttime decay of isoprene." Journal of Geophysical Research 106: 24335-24346.

Jenkin, M. E., Saunders, S. M., Wagner, V., Pilling, M. J. 2003. Protocol for the development of the Master Chemical Mechanism, MCMv3 (Part B): tropospheric degradation of aromatic volatile organic compounds. Atmospheric Chemistry and Physics 3(1): 181-193.

Johnson, D., Utembe, S. R., Jenkin, M. E., Derwent, R. G., Hayman, G .D., Alfarra, M. R., Coe, H., G. Mcfiggans, G. 2006. Simulating regional scale secondary organic

aerosol formation during the TORCH 2003 campaign in the southern UK. Atmospheric Chemistry and Physics 6(2): 403-418.

Jones, C. E., Hopkins, J. R., Lewis, A. C. 2011. In situ measurements of isoprene and monoterpenes within a South-East Asian tropical rainforest. Atmospheric Chemistry Physics. 11: 1189–1218,

Kanaya, Y., Matsumoto, J., Kato, S., Akimoto, J. 2001. Behaviour of OH and HO2 radicals during the Observation at a Remote Island of Okinawa (ORION99) field campaign: 1. Observation using a laser-induced fluorescence instrument. Journal of Geophysical Research 106: 24197-24208.

Kanaya, Y., Matsumoto, J., Kato, S., Akimoto, J. 2001. Behaviour of OH and HO2 radicals during the Observation at a Remote Island of Okinawa (ORION99) field campaign: 2. Comparison between observations and calculations. Journal of Geophysical Research 106: 24209-24223.

Kovacs, T. A., Brune, W. H., 2001. Total OH Loss Rate Measurement. Journal of Atmospheric Chemistry 39: 105-122.

Kroll, J. H., Ng, N., Murphy, S., Flagan, R., Seinfeld, J. H. 2006. Secondary Organic Aerosol Formation from Isoprene Photooxidation. Environmental Science and Technology 40(6): 1869-1877.

Kubistin, D., Harder, H., Martinez, M., Rudolf, M., Sander, R., Bozem, H., Eerdekens, G., Fischer, H., Gurk, C., Klpfel, T., Knigstedt, R., Parchatka, U., Schiller, C. L., Stickler, A., Taraborrelli, D., Williams, J., Lelieveld, J. 2010. Hydroxyl radicals in the tropical troposphere over the Suriname rainforest: comparison of measurements with the box model MECCA, Atmospheric. Chemistry. Physics. 10: 9705–9728

Kuhn, U., Andreae, M. O., Ammann, C., Araujo, A. C., Brancaleoni, E. Ciccioli, P., Dindorf., Frattoni., Gatti, L. V., Ganzeveld, L., Leleiveld, J., Lloyd, J., Meixner, F. X., Nobre, A. D., Poschl, U., Spirig, C., Stefani, P., Thielmann, A., Valentini, R., Kesselmeir, J. 2007. Isoprene and Monoterpene fluxes from Central Amazonian rainforest inferred from tower based and airboirne measurements, and implications on atmospheric chemistry and local carbon budget. Atmospheric Chemistry and Physics. &: 2855-2879

Lee, A., Goldstein, A., Keywood, M,. Gao, S., Varutbangkul, V., Bahreini, R., Ng, N., Flagan, R., Seinfeld, J. 2006. Gas-phase products and secondary aerosol yields from the ozonolysis of ten different terpenes. Journal of Geophysical Research 111.

Lelieveld, J., Butler, T. M., Crowley, J. N., Dillon, T. J., Fischer, H., Ganzeveld, L., Harder, H., Lawrence, M. G., Martinez, M., Taraborrelli, D., and Williams, J. 2008. Atmospheric oxidation capacity sustained by a tropical forest. Nature. 452: 737–740

Martinez, M. (2003). "OH and HO2 concentrations, sources, and loss rates during the Southern Oxidants Study in Nashville, Tennessee, summer 1999." Journal of Geophysical Research 108.

Mihele, C. M., Hastie, D. R. 2003. Radical Chemistry at a Forested Continental Site: Results from the PROPHET 1997 Campaign. Journal of Geophysical Research 108.

Monks, P. S. (2005). "Gas-phase radical chemistry in the troposphere." Chemical Society Reviews 34: 376-395.

Nguyen, T. L., Vereecken, L., Peeters. 2010. HO_X, Regeneration in Oxidation of Isoprene III,: Theoretical Study of the Key Isomerisation of the Z-δ-hydroxy-peroxy Isoprene Radicals. Chemical Physics Physical Chemistry. 11: 3996-4001.

Paulot, F., Crounse, J. D., Kjaergaard, H. G., Kurten, A., St. Clair, J. M., Seinfeld, J. H., and Wennberg, P. O. 2009. Unexpected Epoxide Formation in the Gas-Phase Photooxidation of Isoprene, Science. 325: 730–733

Peeters, J., Nguyen, T. L., Vereecken, L. 2009. HOx radical regeneration in the oxidation of isoprene, Physical Chemistry Chemical Physics 11(28): 5935–5939

Peeters, J., Muller, J. F. 2010. HO_X radical Regeneration in Isoprene Oxidation via Peroxy radical isomerisation. II: experimental evidence and global impact. Physical Chemistry Chemical Physics: 12, 14227-14235.

Pinho, P. G. Pio, C. A., Jenkin, M. E. 2004. Evaluation of Isoprene degradation in the detailed tropospheric chemical mechanism, MCM v3, using environmental chamber data. Atmospheric Environment 39: 1303-1322.

Ren, X., Brune, W. H, Cantrell, C. A, Edwards, G. D., Shirley, T., Metcalf, A., Lesher, R. L. 2005. Hydroxyl and Peroxy Radical Chemistry in a Rural Rea of Central Pennsylvania: Observations and Model Comparisons. Journal of Atmospheric Chemistry 52: 231-257.

Pugh, T. A. M., MacKenzie, A. R., Hewitt, C. N., Langford, B., Edwards, P. M., Furneaux, K. L., Heard, D. E., Hopkins, J. R., Jones, C. E., Karunaharan, A., Lee, J., Mills, G., Misztal, P., Moller, S., Monks, P. S., and Whalley, L. K. 2010. Simulating atmospheric composition over a South-East Asian tropical rainforest: performance of a chemistry box model. Atmospheric Chemistry and Physics., 10: 279–298

Saunders, S. M., Jenkin, M. E., Derwent, R. G., Pilling, M. J. 2003. Protocol for the development of the Master Chemical Mechanism, MCMv3 (Part A): tropospheric degradation of non-aromatic volatile organic compounds. Atmospheric Chemistry and Physics 3(1): 161-180.

Sillman, S. 1995. The use of NO_y, H_2O_2 and HNO_3 as indicators for ozone-NO_x hydrocarbon sensitivity in urban locations. Journal of Geophysical Research. 100: 14,175-14,186

Sillman, S., Carroll, M.A., Thornberry, T., Lamb, B.K., Westberg, H., Brune, W.H., Faloona, I., Tan, D., Shepson, P.B., Sumner, A.L., Hastie, D.R., Mihele, C.M., Apel, E.C., Riemer, D.D., Zika, R.G. 2002. Loss of isoprene and sources of nighttime OH

radicals at a rural site in the United States: Results from photochemical models. Journal of Geophysical Research 107.

D. Stone, D, Evans, M. J., Edwards, P. M., Commane, R., Ingham, T., Rickard, A. R., Brookes, D. M., Hopkins, J. M., Leigh, R. J., Lewis, A. C., Monks, P. S., Oram, D. R., Reeves, C. E., Stewart, D., Heard, D. E. 2011. Isoprene oxidation mechanisms: measurements and modelling of OH and HO_2 over a South-East Asian tropical rainforest during the OP3 field campaign. Atmospheric Chemistry and Physics 11, 6749–6771, 2011

Stavrakou, T., Peeters, J., Muller, J. F.,2010. Improved global modelling of HO_X recycling in isoprene oxidation: evaluation against GABRIEL and INTEX-A aircraft campaign.

Tan, D. (2001). HOx budgets in a deciduous forest: Results from the PROPHET summer 1998 campaign. Journal of Geophysical Research 106: 24407-24427.

Warneke, C. (2004). "Comparison of daytime and nighttime oxidation of biogenic and anthropogenic VOCs along the New England coast in summer during New England Air Quality Study 2002." Journal of Geophysical Research 109.

Whalley, L. K., Furneaux, K. L., Goddard, A., Lee, J. D., Mahajan, A., Oetjen, H., Read, K. A., Kaaden, N., Carpenter, L. J., Lewis, A. C., Plane, J. M. C., Saltzman, E. S., Wiedensohler, A., Heard, D. E. 2010. The chemistry of OH and HO2 radicals in the boundary layer over the tropical Atlantic Ocean, Atmospheric Chemistry and Physics. 10: 1555–1576

Wolfe, G. M., Thornton, J. A., Bouvier-Brown, N. C., Goldstein, A. H., Park, J.-H., McKay, M., Matross, D. M., Mao, J., Brune, W. H., LaFranchi, B. W., Browne, E. C., Min, K.-E., Wooldridge, P. J., Cohen, R. C., Crounse, J. D., Faloona, I. C., Gilman, J. B., Kuster, W. C., de Gouw, J. A., Huisman, A., Keutsch, F. N. 2011. The Chemistry of Atmosphere-Forest Exchange (CAFE) Model – Part 2: Application to BEARPEX-2007 observations. Atmospheric Chemistry and Physics., 11, 1269–1294